AD-A250 520

COMPOSITE FAILURE ANALYSIS HANDBOOK
VOL I - PROGRAM OVERVIEW

R.J. Kar
Northrop Corporation
One Northrop Avenue
Hawthorne, California   90250-3277

February 1992

U.S. Department
of Transportation

Federal Aviation
Administration

Final Report for Period January 1987 - October 1990

Approved for public release; distribution unlimited.

DTIC
ELECTE
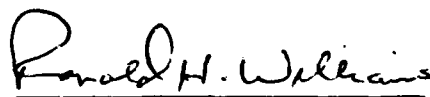MAY 07 1992
S B D

92-12347

92

NOTICE

When Government drawings, specifications, or other data are used for any purpose other than in connection with a definitely Government-related procurement, the United States Government incurs no responsibility or any obligation whatsoever. The fact that the Government may have formulated or in any way supplied the said drawings, specifications, or other data, is not to be regarded by implication, or otherwise in any manner construed, as licensing the holder, or any other person or corporation; or as conveying any rights or permission to manufacture, use, or sell any patented invention that may in any way be related thereto.
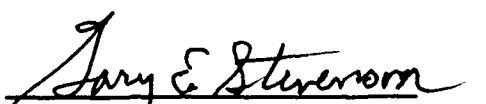
This report is releasable to the National Technical Information Service (NTIS). At NTIS, it will be available to the general public, including foreign nations.

This technical report has been reviewed and is approved for publication.

PATRICIA L. STUMPFF
Project Engineer
Materials Integrity Branch

RONALD H. WILLIAMS
Technical Manager
Structural and Electronic
Failure Analysis

FOR THE COMMANDER

GARY E. STEVENSON, Actg Br Chf
Materials Integrity Branch
Systems Support Division

If your address has changed, if you wish to be removed from our mailing list, or if the addressee is no longer employed by your organization please notify WL/MLSA, WPAFB, OH 45433-6533 to help us maintain a current mailing list.

Copies of this report should not be returned unless return is required by security considerations, contractual obligations, or notice on a specific document.

REPORT DOCUMENTATION PAGE

Form Approved
OMB No. 0704-0188

1. AGENCY USE ONLY *(Leave blank)*	2. REPORT DATE February 1992	3. REPORT TYPE AND DATES COVERED Final for 1 Jan 1987 to 31 Oct 1990

4. TITLE AND SUBTITLE Composite Failure Analysis Handbook Volume I: Program Overview	5. FUNDING NUMBERS Contract Number F33615-87-C-5212
6. AUTHOR(S) R.J. Kar	

7. PERFORMING ORGANIZATION NAME(S) AND ADDRESS(ES) Northrop Corporation Aircraft Division One Northrop Avenue Hawthorne, California 90250-3277	8. PERFORMING ORGANIZATION REPORT NUMBER

9. SPONSORING / MONITORING AGENCY NAME(S) AND ADDRESS(ES) Wright Laboratory (WL/MLSA) Materials Directorate Wright-Patterson AFB, Ohio 45433-6533	10. SPONSORING / MONITORING AGENCY REPORT NUMBER WL-TR-91-4032 DOT/FAA/CT-91/23 Volume I

11. SUPPLEMENTARY NOTES Additional Funding/Sponsorship Provided By:	FEDERAL AVIATION ADMINISTRATION TECHNICAL CENTER U. S. DEPARTMENT OF TRANSPORTATION ATLANTIC CITY, NEW JERSEY 08405

12a. DISTRIBUTION / AVAILABILITY STATEMENT Approved for public release; distribution is unlimited	12b. DISTRIBUTION CODE

13. ABSTRACT *(Maximum 200 words)*

The objective of this program was to create a comprehensive handbook for use in conducting failure analysis investigations on failed composite structure. This program builds upon previous efforts as documented in the "Compendium of Post-Failure Analysis Techniques for Composite Materials," AFWAL-TR-86-4137. The purpose of creating this handbook was to document the techniques, the fractographic and material property data and case history studies currently being utilized in the analysis of failed composite structure. The major tasks on this program included: (1) procedural guidelines for field investigation techniques; (2) an expanded fractographic data base for carbon/epoxy materials tested under known conditions, (3) a fractographic data base for resin based composite materials other than carbon/epoxy; (4) fractographic documentation of composite material and processing defects; (5) documentation of fracture characteristics in adhesive and mechanical joint failures; (6) compilation of material property data for composite materals; and (7) documentation of case histories recently conducted on failed composite structure.

14. SUBJECT TERMS Composites; Composite Structures; Failure Analysis; Fractography Adhesive Joints; Mechanical Joints; Case History Studies	15. NUMBER OF PAGES 178
	16. PRICE CODE

17. SECURITY CLASSIFICATION OF REPORT UNCLASSIFIED	18. SECURITY CLASSIFICATION OF THIS PAGE UNCLASSIFIED	19. SECURITY CLASSIFICATION OF ABSTRACT UNCLASSIFIED	20. LIMITATION OF ABSTRACT

NSN 7540-01-280-5500

Standard Form 298 (Rev 2-89)
Prescribed by ANSI Std Z39-18
298-102

SUMMARY

The objective of this program was to develop a comprehensive handbook for failure analyses of fiber-reinforced composites. The program objectives were accomplished through technical tasks that resulted in the compilation of a reference manual for evaluating failed composite structures.

A field handling logic network was prepared for on-site handling of composites during accident investigations. Procedural guidelines were developed from inputs provided by key field personnel from several government agencies, and from the results of tests performed in-house at Northrop. Several current and new fractographic techniques were evaluated to identify methods for initiation site determination and failure sequence identification in failed composite specimens. Macrophotography, ply-sectioning, and photographic methods were determined to be valuable supplemental techniques but could not directly provide initiation site/fracture propagation direction when used alone. The microchemical analysis technique of Fourier Transform Infrared Spectroscopy was determined to be useful in contaminant failure investigations but will require development of a database of chemical "signatures."

Northrop expanded the fractographic database originally developed by the Boeing Company for AS4/3501-6 graphite/epoxy (Gr/Ep) under Air Force Contract No. F33615-84-C-5010 to include the effects of load, manufacturing, processing, and environmental variables on simple interlaminar and translaminar test coupons. It was determined that applied load was the principal parameter that altered the fracture surface characteristics in Gr/Ep. Material form and processing variables indirectly affected the fracture characteristics in that these caused localized variations in applied load, thereby altering fractographic features. No significant effects of environment on fracture surface features were determined. The fractographic database also included documentation of manufacturing and processing defects that occur in Gr/Ep. The flaws were characterized using optical microscopy, and macrophotography techniques.

Failure modes in adhesively bonded Gr/Ep and graphite/bismaleimide (Gr/BMI) specimens were also characterized. Variations in ply thickness, orientation, and loading were carried out to develop mixed cohesive-adhesive, and singular cohesive or adhesive failures. It was determined that specimen geometry, lap/strap ratios, and test load played roles in controlling fracture surface characteristics. Fracture characteristics in the failed adherends served as indicators of fracture direction in mixed and total adhesive failure modes. The crack directions could not be readily determined in pure cohesive joint failures.

A test matrix was developed for characterizing the six different failure modes in mechanically joined composite structures. A computer code entitled SAMCJ (Strength Analysis of Multifastened Composite Joints), previously developed by Northrop for the USAF was run to develop the matrix for quasi-isotropic AS4/3501-6 Gr/Ep joined with titanium "Hi-Lok" tension or

shear-type flush head fasteners. Failure tests and fractographic evaluation were carried out on the specimens. It was determined that the failure modes were a function of applied load, specimen, and fastener geometries.

Detailed in-plane shear tests were also carried out for Gr/Ep. This failure mode was characterized by the occurrence of hackles on fractured resin and tension fracture characteristics on fractured fiber ends. Processing variables did not significantly alter the fracture surface characteristics for Gr/Ep tested under in-plane shear. The information gained from the Northrop and Boeing Gr/Ep studies was used in initiating a fractographic database for other material systems. The material systems chosen were kevlar 49/3501-6 epoxy (K/Ep), AS4 graphite/5250-3 bismaleimide (Gr/BMI), and AS4 graphite/APC-2 PEEK thermoplastic (Gr/PEEK). Testing and fractographic evaluation were carried out for baseline and several variable conditions. The results for these systems indicated that the type of resin and fiber played strong roles in controlling the resulting fracture surface characteristics. As for Gr/Ep, environment and processing variables did not significantly alter fracture characteristics.

Northrop reviewed formats previously used for reporting metallic and composite fractography and failure analysis data. Based on an assessment of existing report schemes, Northrop proposed three data formats for 1) reporting fractographic data, 2) failure analysis information, and 3) organization of the Composite Failure Analysis Handbook. These were subsequently approved by the Air Force with minor modifications.

Northrop compiled material properties on current and near-term composite structural materials. Literature searches were carried out on government and commercial databases for product information and properties. Properties obtained were incorporated into database files using a personal computer. The data were organized into tabular formats for reporting in the Handbook. The properties for several classes of fiber, prepreg, and laminates were compiled and organized into the Handbook.

Under an engineering services agreement between Northrop and the University of Utah, Professor Willard Bascom of the University of Utah performed a literature search and made on-site visits to several government agencies to gather information on composite fractography and failure analysis that may have been performed at these agencies. No other information was found other than that previously reported by Boeing. Dr. Bascom also reviewed stress analysis methods and failure micromechanisms for use in failure analysis investigations. A new failure criterion developed by Dr. Richard Christensen of Lawrence Livermore Laboratories was determined to be of utility in composite failure investigations.

Verification of the composite failure analysis logic system was performed through evaluation of several failed structural items provided by the Air Force. The structural items represented "real-world" configurations and included 1) a vertical stabilizer, 2) a horizontal torque box assembly, 3) a canopy support fitting, and 4) two simple components. All the results are presented as case histories in the Handbook.

As part of the verification process, two simple Gr/Ep structures containing intentional defects were fabricated and tested to failure under controlled laboratory conditions. The failed

iv

specimens and related test documentation were shipped to the Air Force for subsequent evaluation by the Boeing Company.

The Composite Failure Analysis Handbook is divided into two volumes. Volume I is the Program Overview. Volume II comprises the Technical Handbook, and is divided into three parts. Part 1 describes all the techniques and procedures for performing composite failure analysis. Part 2 represents an atlas of fractographs. Part 3 is a compilation of case histories of investigations performed by Northrop, Boeing, and General Electric.

In summary, Northrop has achieved the objective of producing a Handbook containing all the known techniques, procedures, sample data, and reference supporting data for performing post-failure analysis of fiber-reinforced composite structures.

Accession For	
NTIS GRA&I	☑
DTIC TAB	☐
Unannounced	☐
Justification	
By	
Distribution/	
Availability Codes	
Dist	Avail and/or Special
A-1	

FOREWORD

TABLE OF CONTENTS

TABLE OF CONTENTS (Continued)

TABLE OF CONTENTS (Continued)

TABLE OF CONTENTS (Continued)

TABLE OF CONTENTS (Concluded)

Appendix   **Page**

LIST OF FIGURES

LIST OF FIGURES (Continued)

LIST OF FIGURES (Continued)

LIST OF FIGURES (Concluded)

LIST OF TABLES

SECTION 1

INTRODUCTION AND PURPOSE

Significant accomplishments in the development of composite materials have been made over the past decade. During the 1970s composites were established as credible structural materials through extensive testing and service experience. In the 1980s and 1990s attention has been focused on solving problems associated with the use of these materials. One of the areas that needs to be developed is composite failure analysis technology. Establishing a set of systematic procedures for performing analyses is best facilitated through compilation of a Composite Failure Analysis Handbook to be used as an investigation guide.

This program was aimed at achieving the overall Air Force and Federal Aviation Administration objectives of creating a comprehensive Composite Failure Analysis Handbook as a guide for conducting post-failure analysis of fiber-reinforced composite structures. The specific goals achieved in this program were the creation of the following:

1. A comprehensive Handbook containing all procedures, techniques, and data necessary to successfully conduct analyses of failed composite structures

2. Composite specimen handling and data gathering techniques for field representatives

3. Fully developed fractographic techniques for failure analyses of composite structures

4. A complete comprehensive fractographic database on the model AS4/3501-6 graphite/epoxy (Gr/Ep) system as well as several other material systems being evaluated at the Northrop Corporation and the Boeing Company under Air Force sponsorship (References 1-3)

5. Well established data reporting formats for Handbook inputs

6. A database of chemical and mechanical properties of current and next-generation composite materials

7. Comprehensive information on failure micromechanisms and stress analysis techniques

8. A proven post-failure analysis logic network with numerous case histories of failures performed by Northrop, Boeing, and General Electric

9. An integrated compilation of all useful information from Contracts F33615-84-C-5010, Failure Analysis for Composite Structure Materials (Reference 3), F33615-86-C-5071, Composite Failure Analysis Handbook (Reference 4), and F33615-87-C-5212, Composite Failure Analysis Handbook (Reference 5).

The following sections of Volume I present an overview of the program. Detailed results of the specific tasks - a natural outcome of this program - are presented in the Technical Handbook, which is Volume II, Parts 1, 2 and 3. Part 1 describes the techniques and procedures for failure analysis of composites. Fracture data, useful as a reference source, are presented in Part 2. Part 3 consists of a compilation of case histories of failure investigations performed on test specimens and real-world components by Northrop, Boeing, and General Electric.

SECTION 2

TECHNICAL APPROACH

Northrop's approach to meet the goal of the program consisted of seven technical tasks (Tasks 1 through 6, and Task 9), and two administrative tasks (Tasks 7, and 8). Figure 2-1 presents a schematic overview of the overall program. The technical tasks and subtasks were as follows:

1. Task 1 – Handling and Data Gathering Techniques for Field Representatives

2. Task 2 – Expansion of Fractographic Techniques in Composite Failure Analysis

    a. Subtask 2.1 – Study, Use and Documentation of Fractographic Techniques Developed By David Purslow

3. Task 3 – Expansion of the Fractographic Database

    a. Subtask 3.1 – Expansion of the AS4/3501-6 Gr/Ep Fractographic Database

    b. Subtask 3.2 – Expansion of the Fractographic Database to Other Material Systems

    c. Subtask 3.3 – Fractography of Composite Defects and Flaws

    d. Subtask 3.4 – Fractography of Adhesively and Mechanically Bonded Composites

    e. Subtask 3.5 – Fractography of In-Plane Shear Tested Gr/Ep

    f. Subtask 3.6 – Fractography of Impact and Post-Impact-Compression (PIC) Specimens

4. Task 4 – Development of Data Formats

5. Task 5 – Documentation of Material Properties

6. Task 6 – Verification of the Composite Failure Analysis System

    a. Subtask 6.1 – Fabrication of Two Simple Composite Structures

    b. Subtasks 6.2 and 6.3 – Failure Analyses of Two Air Force Supplied Structures, and Additional Investigations

    c. Subtask 6.4 – Documentation of DOD/NASA/FAA Composite Post-Failure Analysis Case History Studies

7. Task 9 – Documentation

    a. Subtask 9.1 – Documentation of Failure Micromechanisms and Stress Analysis Methods

Field Representative Input
- Compile Procedures
- Verify Procedures

Literary Review of Material Properties
- Chemical/Mechanical Property Database Compilation

Identify/Evaluate Current and New Techniques
- Contact Other Experts
- Assimilate/Verify Techniques
- Technical Interchange With David Purslow

Failure Analysis of Failed "Real-World" Specimens
- Fabrication of Test Specimens
- Review/Compilation of DOD/NASA/FAA Case Studies

Expanded Gr/Ep Data Base
- Fractography of Other Materials
- Fractography of Defects/Flaws
- Fractography of Adhesively-Bonded Composites
- Bolted Joint Fractography
- In-Plane Shear Fractography
- Impact/PIC Fractography

Program Progress/Cost Scheduling
- Meetings/Presentations

Fractographic Data Format
- Failure Analysis Report Format
- Handbook Format

Additional Stress Analysis Methods
- Analysis of Boeing/Northrop Fractographic Data
- Organization of Handbook

COMPOSITE FAILURE ANALYSIS HANDBOOK

Vol I - Program Overview

Vol II - Technical Handbook
1 - Procedures & Techniques
2 - Atlas of Fractographs
3 - Case Histories

Figure 2-1. Schematic Overview of Composite Failure Analysis Program

b.   Subtask 9.2 – Analysis of Fractographic Results From Northrop and Boeing Programs

c.   Subtask 9.3 – Organization of the Composite Failure Analysis Handbook.

Details of the technical approach taken in each of the tasks and subtasks are discussed below.

2.1 TASK 1 – HANDLING AND DATA GATHERING TECHNIQUES FOR FIELD REPRESENTATIVES

In this task, Northrop was required to generate guidelines for field personnel for handling failed composite specimens and for data in the field. Task 1 consisted of the following activities:

1. Interaction with selected government field representatives (AFLC, NARF, DOT/NTSB, FAA) for input into field handling procedural guidelines

2. Compilation of these guidelines based on Northrop's own extensive failure analysis experience and input obtained from government field personnel in accordance with MIL-STD-847B, containing information on:

   a. Analytical and safety equipment for field investigators

   b. Wreckage analysis

   c. Collection of background data and selection of samples

   d. Preliminary examinations

   e. Effect of environment on failed parts

   f. Field tests to determine failure locations

   g. Selection of fracture surfaces for laboratory examination

   h. Sectioning, packaging, and shipping procedures

   i. Safety and health issues

3. Draft copies of guidelines (Air Force Project Engineer-approved) sent to field personnel for review/comments prior to handbook incorporation

4. Final Handbook input provided in an Air Force-approved format.

2.2 TASK 2 – EXPANSION OF FRACTOGRAPHIC TECHNIQUES IN COMPOSITE FAILURE ANALYSIS

In this task, Northrop was required to examine current and new fractographic techniques and identify methods required in composite failure analysis for initiation site determination and failure sequence identification. This activity included the following:

1. Detailed technical review of current and new visual, optical, and scanning electron microscopy techniques (including photographic collaging, cross sectioning, and ply-removal coupled with mechanical behavior theories for initiation site/failure sequence)

2. Identification/contact with other technical investigators working in related fractographic technologies

3. Evaluation of the most promising techniques for applicability on up to 12 specimens (singular-failure and multiple-failure modes)

4. Assimilation of valid techniques into systematic procedures for use in composite failure analysis

5. Use of these techniques in the failure analysis of failed semi-structural items in Task 6 and incorporation of these procedures into the Handbook, following Air Force approval.

As part of this Task, Northrop was also required to perform a separate subtask, Subtask 2.1 – Study, Use and Documentation of Fractographic Techniques Developed by David Purslow. This activity included the following:

1. Visit to the Royal Aerospace Establishment by a fractographic expert for technical exchange

2. Joint evaluation of failed specimens by a Northrop expert and Dr. Purslow.

2.3 TASK 3 – EXPANSION OF THE FRACTOGRAPHIC DATABASE

This task was performed as several subtasks (Subtasks 3.1 through 3.6) which are discussed below.

2.3.1 Subtask 3.1 – Expansion of the AS4/3501-6 Gr/Ep Fractographic Database

In this subtask, Northrop performed the following activities:

1. Initial review of the specimen test matrix and AS4/3501-6 fractographic data generated under the Air Force/Boeing program

2. Design of an updated specimen test matrix for AS4/3501-6 Gr/Ep with a minimum of 125 additional test variables, which included:

    a. Tape versus filament winding versus 3-D weave

    b. Effect of loading rate (variable-amplitude fatigue versus constant load versus impact loading)

    c. Effect of environment (moisture, temperature, moisture plus temperature) before, during, and after failure

    d. Water immersion versus humidity

    e. Effect of impact damage on post-impact material behavior

    f. Effect of processing defects (undercure, overcure, low fiber content)

3. Following Air Force approval of the test matrix and variables, acquisition of materials, and fabrication and testing of specimens under controlled laboratory conditions; performance of fractographic examination with documentation of fracture surfaces using the scanning electron microscope (SEM)

4. Input of approved fractographic data into the Handbook using an approved data format (established in Task 4).

2.3.2 Subtask 3.2 – Expansion of the Fractographic Database to Other Material Systems

In this subtask, Northrop performed the following activities:

1. Verification of the applicability of materials characterization, nondestructive evaluation (NDE), fractography, and stress analysis techniques to the other composite materials with identification of alternate methods (if required)

2. Statistical analysis of the test matrix and fractographic data obtained on the previous Air Force/Boeing program and current program (in Task 3, Subtask 3.1)

3. Selection of three material systems for expansion of the fractographic database

4. Development of test matrices for the three selected material systems; each matrix to contain multiple study variables and to include those with the most significant effects on the fracture features; most tests to be under singular failure mode conditions

5. Upon Air Force Project Engineer approval of the test matrices, implementation of the test program by:

   a. Acquiring materials

   b. Designing and fabricating test specimens

   c. Performing mechanical testing to produce controlled failures

6. Fractographic examination and documentation of the failed specimens; fractographs organized and correlated to dominant failure modes predicted by stress analysis

7. Upon Air Force Project Engineer approval, input of the fractographic data into the handbook using the same data format as in Task 3, Subtask 3.1.

2.3.3 Subtask 3.3 – Fractography of Composite Defects and Flaws

Northrop documented defects and flaws that occasionally occur during manufacture or fabrication of Gr/Ep components, and which could affect their service life. Laminates were fabricated containing one or more defects identified in the Rockwell Flaw Criticality Study (Reference 6). These defects were characterized using conventional macro-photography, SEM, or sectioning and optical microscopy.

2.3.4 Subtask 3.4 – Fractography of Adhesively and Mechanically Bonded Composites

In this subtask, Northrop documented the failure modes in adhesively-bonded and mechanically-joined composite structures. Failures in adhesively-bonded structures would be studied for AS4/3501-6 Gr/Ep and AS4/5250-3 Gr/bismaleimide (BMI) adherends using FM300 and EA9673 adhesives. Variations in loading and lap/strap ply orientations were used to achieve cohesive, adhesive, and mixed-mode failures.

For mechanically-fastened joints, Northrop characterized the six different failure modes associated with bolted-joints in quasi-isotropic Gr/Ep composite structures. Different failure

modes were achieved through variations in the composite thicknesses, specimen widths, and fastener-to-edge distances.

2.3.5 Subtask 3.5 – Fractography of In-Plane Shear Tested Gr/Ep

Northrop expanded the fractographic database to include AS4/3501-6 Gr/Ep tested to failure under in-plane shear. Tests were conducted on baseline Gr/Ep (defect-free) and Gr/Ep containing manufacturing/processing defects. Failure testing was performed using rail-shear specimens.

2.3.6 Subtask 3.6 – Fractography of Impact and Post-Impact-Compression Specimens

Northrop documented the failure modes of AS4/3501-6 Gr/Ep and AS4/APC-2 Gr/thermoplastic (TP) tested under impact loads, or impact plus post-impact-compression (PIC) testing. Testing was performed as recommended in NASA specification RP 1092 (Reference 7) and included the use of impact loads to induce through-hole damage, composite buckling, and matrix-cracking/delaminations. Documentation of the failure modes was accomplished as in Subtask 3.1.

2.4 TASK 4 – DEVELOPMENT OF DATA FORMATS

In this task, Northrop compiled several data format schemes for reporting data generated in this program. These data format schemes were in accordance with MIL-STD-847B and resulted in recommendations for final data reporting. Specifically, Northrop generated the following:

1. Data format schemes for reporting fractographic information generated in Task 3, Subtasks 3.1 and 3.2, of the program, and similar data generated under the Air Force/Boeing program

2. Formats for reporting failure analysis investigations

3. A suitable format for compilation of the Composite Failure Analysis Handbook.

2.5 TASK 5 – DOCUMENTATION OF MATERIAL PROPERTIES

Northrop gathered and compiled material properties on current and near-term composite structural materials used in military aircraft via the following activities:

1. Detailed literary review of chemical and mechanical property data for composite materials; information sources investigated included:

   a. Texts and journals

   b. Manufacturers' material specifications

   c. Published reports on government contractual activities and independent research and development (IR&D) programs

   d. Established databases

2. Compilation of chemical/mechanical data, including properties of:

    a. Fibers and resins

    b. Prepregs

    c. Laminates

3. Compilation of chemical/mechanical property data including:

    a. Glass transition temperature

    b. Normal fiber volume fraction

    c. Transverse/longitudinal ultimate tensile and compressive strengths

    d. Shear strength

    e. Failure strain

    f. Tensile moduli

4. Compilation of material information in an approved data format as per MIL-STD-847B; following Air Force approval, incorporation of data into the Composite Failure Analysis Handbook.

2.6 TASK 6 – VERIFICATION OF THE COMPOSITE FAILURE ANALYSIS SYSTEM

Northrop demonstrated and verified the composite failure analysis system. Failure analysis was performed on semi-structural failed component demonstration items provided by the Air Force Project Engineer to establish failure origin, failure sequence, and failure mode. Northrop used the assimilated set of failure analysis procedures established in Task 2 to perform these examinations. All procedures, techniques, and data developed were analyzed and documented in accordance with the formats developed in Task 4.

2.6.1 Subtask 6.1 – Fabrication of Two Simple Composite Structures

Northrop fabricated two simple Gr/Ep composite structures containing intentional defects. Northrop tested the structures to failure under controlled laboratory test conditions. Northrop subsequently shipped the failed specimens to the Air Force Project Engineer for verification of the logic network by Boeing.

2.6.2 Subtasks 6.2 and 6.3 – Failure Analyses of Two Air Force Supplied Structures, and Additional Investigations

In these subtasks Northrop was required to perform failure analyses of additional "real-world" structural components provided by the Air Force Project Engineer.

2.6.3 Subtask 6.4 – Documentation of DOD/NASA/FAA Composite Post-Failure Analysis Case History Studies

Under an engineering services agreement with Northrop, Professor W. Bascom of the University of Utah reviewed and compiled existing case history studies of composite failure analysis investigations performed by DOD, NASA, and the FAA. The compilation was included in the Handbook.

2.7 TASK 9 – DOCUMENTATION

This task consisted of actual compilation of the Handbook. The work was performed in the following three subtasks.

2.7.1 Subtask 9.1 – Documentation of Failure Micromechanisms and Stress Analysis Methods

Under a technical services agreement with Northrop, Professor W. Bascom of the University of Utah compiled information on composite failure micromechanisms and stress analysis methods that were useful in a composite failure investigation. This information was incorporated with the stress analysis techniques previously compiled by Boeing (Reference 3) and included in the Handbook.

2.7.2 Subtask 9.2 – Analysis of Fractographic Results From Northrop and Boeing Programs

Northrop was required to analyze the fractographic results of work performed in the current program and the Air Force/Boeing programs (References 3 and 4) to determine correlations that existed between the fracture characteristics of resin-based composites and the experimental variables used in their study. The results of this study were reported in the Handbook.

2.7.3 Subtask 9.3 – Organization of the Composite Failure Analysis Handbook

In this subtask Northrop organized results from the current program and the Air Force/Boeing programs into a Handbook in a form that could be used as a guide for conducting post-failure investigations of composite structures. The Handbook was organized in a manner to permit easy incorporation of any composite failure analysis data available in the future from other sources.

SECTION 3

RESULTS

3.1 HANDLING AND DATA GATHERING TECHNIQUES FOR FIELD REPRESENTATIVES

In Task 1, Northrop developed guidelines that field representatives could use for handling failed composite specimens on-site, for gathering background data to aid in failure analysis investigations, and for selection of specimens for detailed laboratory failure analysis examination.

Seven key field personnel from AFLC, NARF, DOT, NTSB, and FAA were identified for providing, in consultation with the Air Force Project Engineer, technical input into the field procedural guidelines. All of these representatives were formally contacted by Northrop and agreed to participate. The names and addresses of these individuals and associated WRDC representatives participating in this activity are as follows:

1. Lt. Andrew Kenny
    Ogden ALC/MAQCM
    Hill Air Force Base, Utah 84056-5149
    (801) 777-2826

2. Mr. John Meininger
    Sacramento ALC/MAQCC
    McClellan Air Force Base, California 95652
    (916) 643-6832

3. Mr. Warren M. Wandel
    National Transportation Safety Board
    Federal Building, Room 7A07
    819 Taylor Street
    Fort Worth, Texas 76102
    (817) 334-2616

4. Mr. Joseph R. Soderquist
    Federal Aviation Administration
    800 Independence Avenue, AIR-103
    Washington, DC 20591
    (202) 267-9585

5. Ms. Patricia Stumpff
   WRDC/MLSA
   Wright-Patterson AFB, Ohio 45433-6533
   (513) 255-2623

6. Mr. Joseph F. Tilson
   USAF Inspection and Safety Center
   Norton Air Force Base
   San Bernadino, California 92409
   (714) 382-6844

7. Mr. James M. Dobson
   NAVAIR/NESO Code 341
   North Island
   San Diego, California 92135
   (619) 437-6711

8. Mr. Burton P. Chesterfield
   Transportation Safety Institute
   6500 S. MacArthur
   TSI/DMA-603
   Oklahoma City, Oklahoma 72135
   (405) 686-2614

9. Mr. Frank J. Fechek
   WRDC/MLSE
   Wright-Patterson AFB, Ohio 45433-6533
   (513) 255-7483.

All of the representatives were requested for inputs in the following areas:

1. Prior experience in the area of composite materials failure analysis

2. Availability of established field procedures for metallic materials

3. Prior experience in performing wreckage analysis of metallic airframe structures

4. Recommendations for topics that needed to be addressed in the guidelines.

Based on the inputs received, Northrop summarized information on topics of interest to field investigators, including safety and health issues, protective or corrective measures, handling of failed parts/fractured surfaces, and packaging. Additionally, a cleaning study for field/laboratory cleaning of Gr/Ep fracture surfaces was performed. Based on all the data received and generated in-house, Northrop compiled a Field Handling Logic Network (FHLN) for handling fire and non-fire damaged composite components at crash sites. Figure 3-1 shows the FHLN which logically defines the recommended safety steps and associated handling, packaging, and shipping procedures that are being suggested to field investigators. A discussion of critical issues that were established in this task follows.
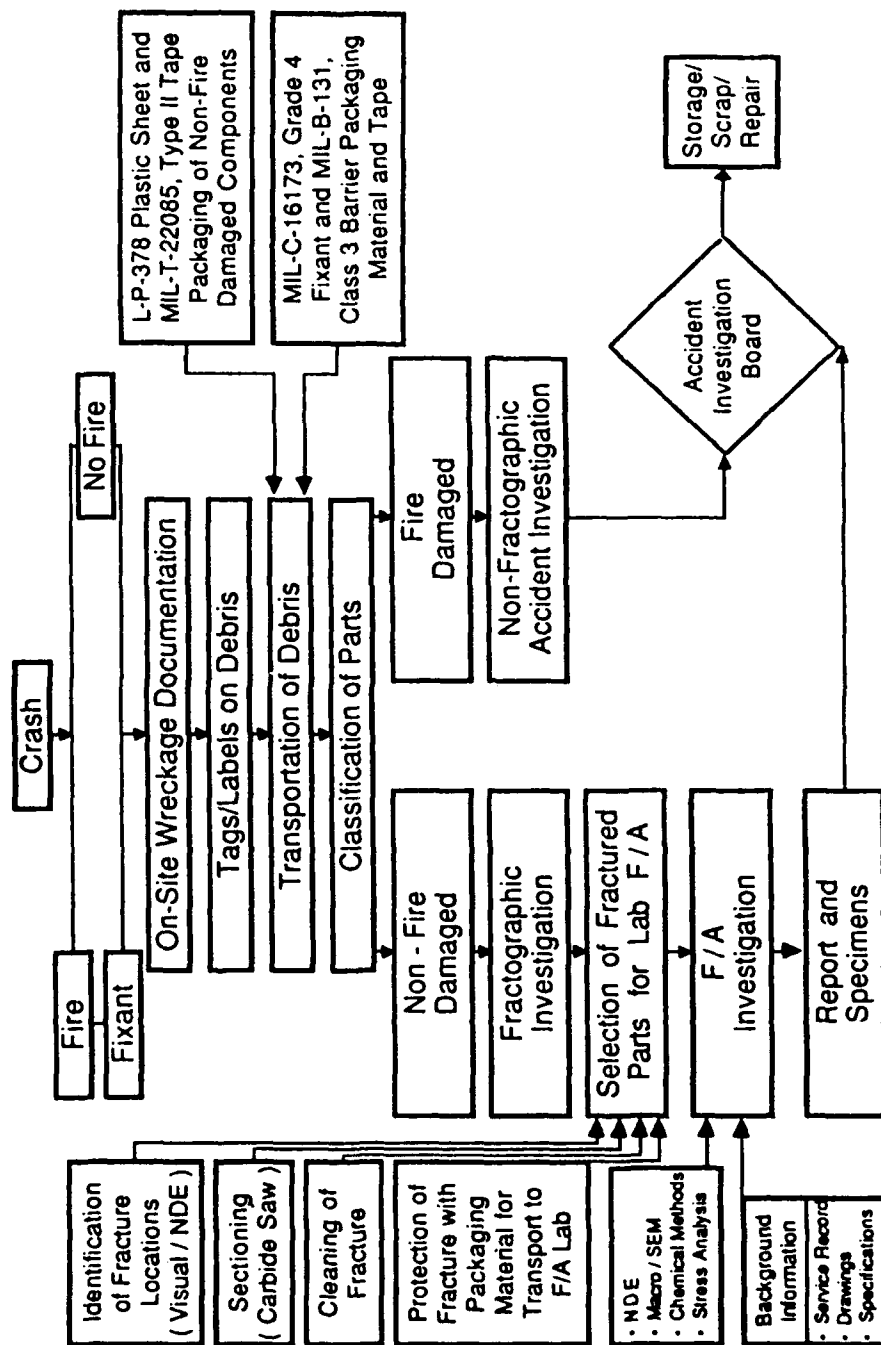
Figure 3-1. Field Handling Logic Network for Composite Parts

3.1.1 Avionics Hazards

Fibers released in aircraft crashes or from machining/handling of fire damaged composite materials can cause damage in electrical or avionics equipment. Released fibers settling on or across electrodes or circuits can short out low power electrical systems or cause severe electrical arcs in high power systems.

3.1.2 Health Issues

Fibers may be released during airplane accidents which can be a health hazard. Primary release occurs during post-crash aircraft fires, although some release may occur during transportation of components to a safe-area, during on-site crash investigation, or during scrap disposal. Graphite fibers act as skin, eye, and lung irritants in a manner similar to moderate/heavy amounts of glass fiber exposure. Except for skin irritation, no evidence was found that any serious effects resulted from graphite fibers being imbedded in human skin.

With regard to other health threats associated with carbon fibers, the National Institution for Occupational Safety and Health (NIOSH) has determined that fiber particles, including carbon fibers, fiberglass, and asbestos, will not cause malignant disease if they exceed 3.5 microns. The average size of carbon fibers currently in use in composite structures ranges between 4 and 7 microns. Based on these observations, it is generally believed that carbon fiber-based composite panels fractured in aircraft crashes but not subjected to fire, are biologically benign and would constitute no more hazard than fractured aluminum aircraft pieces.

3.1.3 Safety Guidelines

The following guidelines are recommended as minimum safety precautions in the handling of carbon fiber-based composites in crash/fire incidents:

1. Base/squadron safety officers should:

    a. Determine if aircraft contains carbon fiber materials

    b. Identify specific carbon fiber components/panels

2. Pre-mishap training should include:

    a. Identifying locations of carbon fiber

    b. Proper handling of components with regard to accidents without post-crash fires and those involving a post-crash fire

3. For aircraft mishaps where carbon fibers are released by fire:

    a. Firefighters and rescue personnel should be the only personnel in the immediate vicinity of the burning/smoking wreckage

    b. Personnel should be prevented from approaching the crash site and restricted from assembling down-wind of the fire at the crash site

c. Once the fire is completely out and the wreckage has cooled, all carbon fiber should be sprayed down with a fixant to contain the release of carbon fibers

d. The area should be roped off as soon as possible and a single entry/exit point should be established to the mishap site

4. For aircraft mishaps where no carbon fibers are released by fire:

a. Leather palmed gloves should be worn

b. Carbon fiber panels can be handled similar to aluminum panels

5. All personnel involved with crash/fire-damaged composite parts should be provided with a suitable shower facility before going off duty to preclude injury from loose fibers.

3.1.4 Safety Equipment

The following safety equipment should be used:

1. In a crash involving fire-damaged wreckage, personnel required to enter wreckage should wear adequate protection to minimize irritation, including:

a. NIOSH approved industrial dust masks

b. Disposable paper coveralls with hoods

c. Goggles or visors

d. Leather palmed gloves

2. For aircraft mishaps where no carbon fibers are released by fire, leather palmed gloves should be worn

3. If breaking or ripping apart of carbon fiber components with carbide saws is to be performed, mono-goggles or face shield protection should be used

4. Safety officers should ensure that the following items are readily available at all operating sites or included in premishap kits:

a. An adequate supply of industrial fixant, preferably commercially procured polyacrylic acid (PAA) such as BF Goodrich "Carboset" XL-11 (if not available, acrylic floorwax or light oil is an acceptable fixant)

b. Industrial dust masks (NIOSH approved), disposable coveralls or equivalent, leather palmed gloves, and mono-goggle eye protection for use if fire has occurred.

3.1.5 On-Site Crash/Wreckage Reconstruction and Handling

1. Once fixant has contained carbon fiber material, the use of industrial dust masks and gloves is considered sufficient for work around the crash site if large amounts of carbon fiber material are not being stirred up.

2. Complete documentation of all debris at the crash site should be carried out using conventional photographic equipment. Aerial photography of the crash site to include a "global" perspective of the crash investigation is also useful.

3. Inspection of the crash-damaged aircraft to identify crash/fire-damaged composite parts should be carried out. Classification of all composite components into fire damaged and non-fire-damaged is also useful. Tagging and labeling of all debris should be carried out, preferably at the crash site or prior to transport to an accident reconstruction area.

4. Sectioning of crash/fire-damaged components for further engineering investigation should be performed using carbide saws and mono-goggle protection. Sectioning should be performed in areas well away from visible fracture and areas that contain internal damage as determined by nondestructive tests (coin-tap, portable ultrasonic, X-ray, etc.).

5. Crash/fire-damaged parts which require laboratory evaluation and/or repair should have fibers contained by wrapping of the affected area with 0.006 inch thick plastic sheet (MIL Specification L-P-378) and by taping in place with aircraft preservation tape (MIL-T-22085, Type II tape).

6. Crash/fire-damaged parts which do not require evaluation as part of the accident investigation and/or that are to be scrapped should have fibers contained (to ensure fibers are immobilized) by using Corrosion Preventative Compound, MIL-C-16173, Grade 4 spray applied as a fixant material.

7. Transport of the wreckage to a "safe-area" for accident/wreckage reconstruction should be carried out as soon as possible. During the accident investigation/repair disposition operations, the crash-damaged aircraft should be in an enclosed area not subject to the elements of weather. This precaution prevents degradation of the tape/plastic sheet fiber containment system and precludes the spread of loose fibers.

8. Crash/fire-damaged aircraft to be stored locally awaiting repairs should have crash/fire-damaged parts wrapped or preserved as previously described. All sharp projections from damaged composite parts should be covered and padded to prevent accidental injuries. Damage or abrasion to the cover assembly can be minimized by applying foam with tape.

9. Those crash/fire-damaged hulks to be scrapped should have fibers contained as stated previously and should be wrapped in barrier material and taped. The hulk thus preserved is suitable for outside storage.

10. Those operations performed on crash/fire-damaged parts which generate loose fibers (such as sectioning of parts using carbide saws) require that personnel be protected from fiber exposure. Control of loose fibers is provided by vacuuming with a vacuum system containing a high efficiency particulate air filter (HEPA) designed to provide filtration levels down to 0.3 microns in particle size. Respiratory protection is

provided by portable respirators containing HEPA filters with the same filtration levels as the vacuum system.

11. Composite material that is not required for investigation should be disposed of at an approved hazardous material waste site.

3.1.6 Cleaning of Gr/Ep Fracture Surfaces

A cleaning study of Gr/Ep fracture surfaces was performed on an overloaded area of an impact damaged Gr/Ep multi-spar panel. The objectives of this study were (1) to determine if conventional cleaning methods used in metal fractography could be successfully used for fiber/resin composite material without damaging fracture details, and (2) to investigate whether fracture surface contaminants, such as JP-4 jet fuel or hydraulic fluid, normally found in a crash site environment, could be successfully removed from composite fracture surfaces.

For this study, nine 1/2 inch x 1/2 inch specimens were excised from the fractured panel and cleaned using the various methods listed as follows:

1. As cut, with heavy air blow

2. Acetone/ultrasonically cleaned for one minute, light air blow

3. Methanol/ultrasonically cleaned for one minute, light air blow

4. Purified water rinse, light air blow

5. Purified water/ultrasonically cleaned for one minute, light air blow

6. Five percent NOX soap (NOX = trade name) in purified water, ultrasonically cleaned for one minute, ultrasonically cleaned again in purified water for one minute (to remove soap residue), light air blow

7. Methyl ethyl ketone (MEK) solvent for three hours, rinsed in acetone for a few seconds

8. JP-4 jet fuel, immersed for four hours, rinsed in acetone

9. MIL-H-83282 hydraulic fluid, immersed for two hours, rinsed in acetone.

Figure 3-2 shows the effect of cleaning with 5 percent NOX soap as indicated in Method 6 above. Figure 3-3 shows the effects of cleaning jet fuel off the fracture surface with acetone. Figure 3-4 shows the effects of cleaning hydraulic fluid with acetone. All the cleaning methods worked well on Gr/Ep composite fracture surfaces and to the same extent on all specimens. Contaminants such as hydraulic fluid or jet fuel could be successfully removed from the fracture surfaces without damage to the fracture detail. No fracture surface artifacts were caused either by jet fuel, hydraulic fluid or the cleansers.

Based on these results, Northrop concluded that conventional cleaning techniques used for metallic fractures can also be used for Gr/Ep fractures.
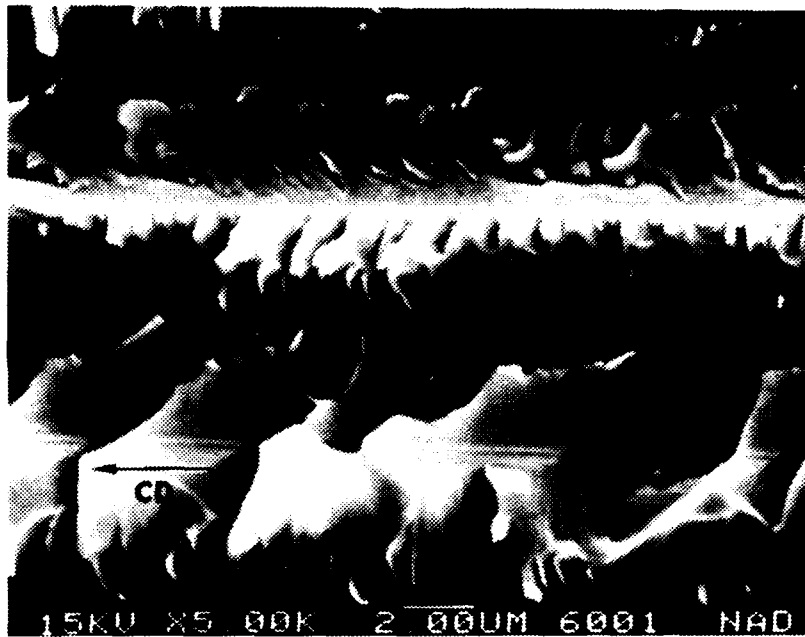
Figure 3-2. SEM Photograph of Gr/Ep Fracture (Cleaned With Soap)
CD = Crack-propagation direction

Figure 3-3. SEM Photograph of Gr/Ep Fracture (Jet Fuel Immersed and Acetone Cleaned)
CD = Crack-propagation direction
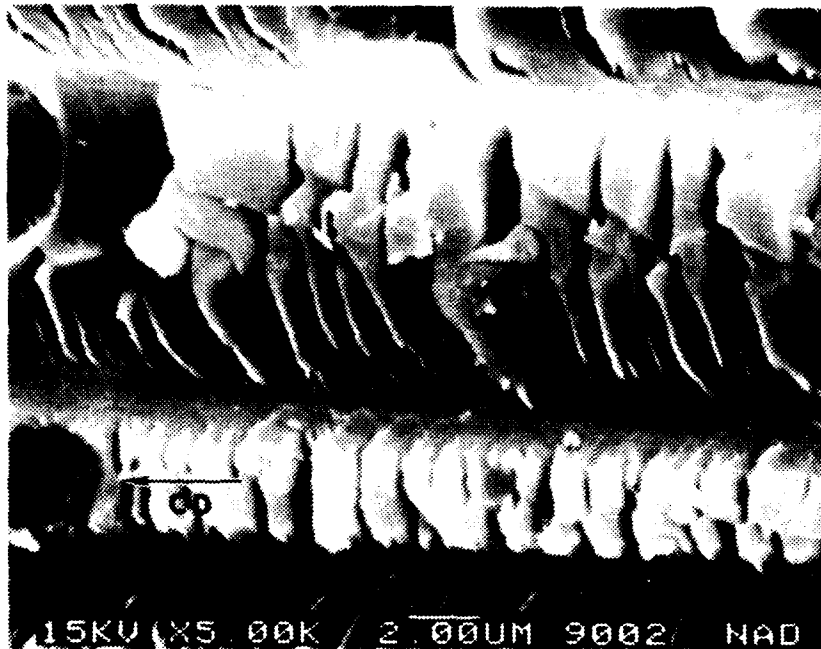
Figure 3-4. SEM Photograph of Gr/Ep Fracture (Hydraulic Fluid Immersed and Acetone Cleaned)
CD = Crack-propagation direction

3.2 EVALUATION OF ADDITIONAL FRACTOGRAPHIC TECHNIQUES

In Task 2, Northrop evaluated several current and new fractographic techniques. The objective was to identify methods required in composite failure analysis for initiation site determination and failure sequence identification. The techniques investigated were:

1. Advanced ultrasonic imaging NDE

2. Fourier transform infrared (FTIR) spectroscopy

3. Photographic collaging, cross sectioning, and ply removal.

3.2.1 NDE Techniques

Three failed Gr/Ep specimens were supplied by the Air Force for use in Task 2. Northrop used these specimens for evaluation of ultrasonic NDE and materialographic techniques for their potential in failure analysis investigations, as a supplement to conventional SEM fractography. The specimen details and test techniques investigated are listed in Table 3-1. Northrop also used sections of a multispar Gr/Ep panel for testing in this task. Information on the tests performed on these sections (NAD Specimen No.2 and NAD Specimen No. 3) is also given in Table 3-1. The results obtained are discussed below.

Figure 3-5 shows a 2-D ultrasonic B-scan of USAF Specimen RJ24984-1, No. 4. Figure 3-6 shows a 3-D ultrasonic B-scan image of the impacted area in this specimen. Damaged areas in impacted specimens or compression-after-impact specimens could be identified and isolated using ultrasonic B-scan techniques. Based on grey-level intensity differences in the images, the

3-9

SPECIMEN ID	FAILURE CONDITION/DESCRIPTION	TEST METHODS
USAF RJ24984-1, No. 2	Impacted With Force of 10 ft lbs and 1-in dia Indenter	NDE and SEM fractography
USAF RJ24984-1, No. 4	Impacted With Force of 4.75 lbs and 0.5-in dia Indenter	NDE and Materialographic Sectioning
USAF No. 6	Compression After Impact, No Other Information Available	NDE and Materialographic Sectioning
NAD No. 3	Impacted Section of Gr/Ep Multispar Panel – 100 in-lb Impact Energy	NDE and SEM Fractography
NAD No. 2	Compression After Impact, Section Panel – 100 in-lb Impact Energy	NDE and Materialographic Sectioning

planes of maximum delamination could be located and generally could be determined to be at t/3 (t = laminate thickness) from the back face of the panel.

Analysis of the data established that the ultrasonic B-scan method was very useful in determining failure locations in impacted and compression-after-impact specimens. However the technique did not directly indicate failure initiation site(s) or failure propagation direction.

3.2.2 Microchemical FTIR/IR Microscope Technique

Northrop used failed Gr/Ep Mode II end-notched flexure (ENF) specimens (0/90, ±45 orientations) from the Air Force/Boeing program to investigate the FTIR/IR method. Details of the specimens are shown in Table 3-2. These had been intentionally contaminated with either Frekote or Teflon, and interlaminar fracture had been initiated at the contaminants.

Figure 3-5. 2-D Ultrasonic B-Scan Image of Impact Damaged Gr/Ep Panel, USAF Specimen No. 4
Note: Labels P and I indicate porosity and impact damage, respectively.
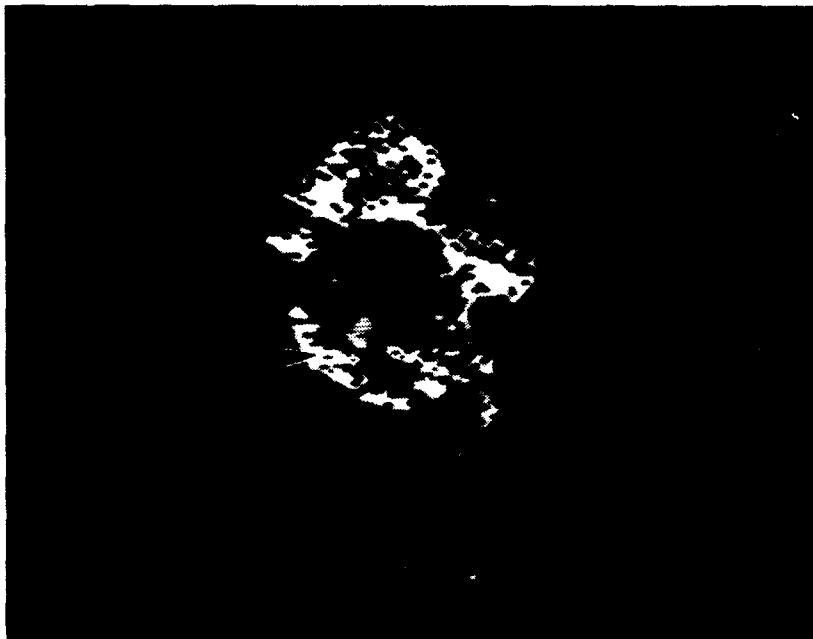
Figure 3-6. 3-D Ultrasonic B-Scan Image of Impact Delamination in USAF Specimen No. 4
Note: The plane of maximum delamination (arrow) is approximately 2.8 mm below the impacted surface.

3-11

Table 3-2. Description of Failed Gr/Ep Specimens

SPECIMEN NO.	TYPE	DESCRIPTION
1	0/90, Mode II ENF	Frekote at Initiation Site
2	0/90, Mode I ENF	Teflon at Initiation Site
3	±45, Mode II ENF	Frekote at Initiation Site
4	±45, Mode II ENF	Teflon at Initiation Site

FTIR characterization was performed on the specimens using diffuse reflectance methods in conjunction with the infrared (IR) microscope. The objective was to determine FTIR profiles/differences between the precrack (Teflon or Frekote contaminated) region and the crack-growth locations.

Figures 3-7 and 3-8 show FTIR spectra (diffuse reflectance method) taken from the precrack (contaminated) and crack-growth (noncontaminated) regions of a Teflon contaminated specimen. Both spectra show strong N-H stretch absorption, as well as strong C-H absorption. At wavenumbers around 1200 cm^{-1}, strong absorption is observed in both spectra, characteristic of the C-O bonds, with unspecified absorption at 1600 cm^{-1}, believed to be C-O stretch. However, a comparison of the spectra showed that the precrack region was associated with a higher overall reflectance than the crack-growth region. In addition there was greater differentiation below 1750 cm^{-1}. This increased differentiation is believed to be due to the absorption by the Teflon.

Figure 3-9 shows FTIR spectra (diffuse reflectance method) taken from virgin Frekote and Frekote from a 90/0 ENF specimen. Figure 3-10 is a comparison of spectra from the contaminated and noncontaminated regions of the Frekote specimen. As shown by the results, substantial differences existed in the characteristic stretches of all three spectra. The differences between virgin Frekote and Frekote on the fracture were believed to be due to the cure and post-cure treatment carried out on the Gr/Ep laminate from which the ENF specimen was fabricated. These results also indicated that direct comparisons of spectra from contaminants, such as Frekote, with those from virgin material would not be sufficient for a chemical failure analysis investigation.

Based on the work performed, it was concluded that the FTIR/IR microscope technique does have promise for use in failure analysis investigations for chemical contaminant identification. However, further developmental work, which is beyond the scope of this program, would be

```
SAMPLE 1: TEST REGION.   LOC: 126.0.17.5
0.'90, MODE II, TEFLON.   M. D. ENSMINGER
05/27/87  16:15:39
      87.40 SEC. MEAS. TIME
DFN =        115      NSK =         0
NSD =        200
NDP =       6144
NTP =       4096
```
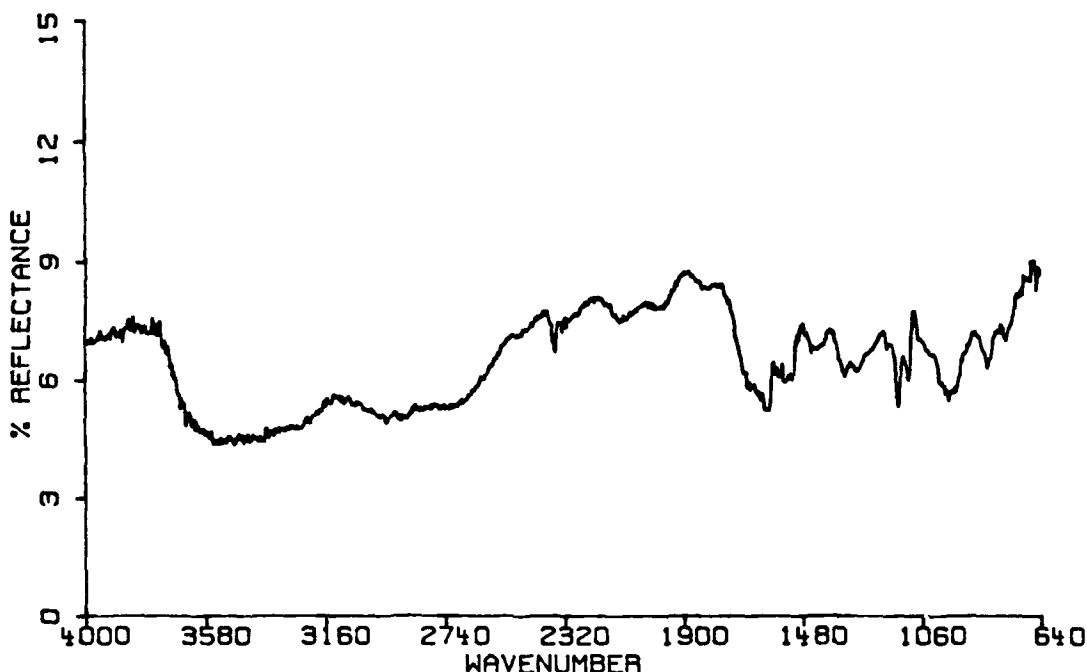
Figure 3-7.   FTIR Spectrum (Diffuse-Reflectance Method) of Contaminated Precrack
Region in Mode II ENF Specimen (Teflon Contaminated Specimen)

necessary to fully document characteristic signatures of contaminants, including the effects of
thermal processing and environments. Availability of such library spectra would then enable use
of the FTIR/IR instrument in chemical failure analysis investigations.

3.2.3   Ply Sectioning and Materialographic Techniques

Northrop investigated ply sectioning and materialographic techniques for failure
analysis investigations. The specimen details, techniques investigated, and background
information are listed in Table 3-1.

3.2.3.1   Ply Sectioning

Figure 3-11 shows a macrophotograph of the impacted area in USAF Specimen No. 2 (refer
to Table 3-1). The region illustrated is the plane of maximum delamination caused by impact,
and identified by 2-D ultrasonic B-scanning of the panel. The damaged area was isolated and
exposed by subjecting nondamaged peripheral regions to Mode I tension overload, with subsequent
ply-by-ply removal of the overload fracture fragments. As shown in Figure 3-11, the impact-

SAMPLE 1: REFERENCE.   LOC: 126.0, 21.0

05/27/87 15:27:38
        87.40 SEC. MEAS. TIME
DFN =   80   NSK =   0
NSD =   200
NDP =   6144
NTP =   4096
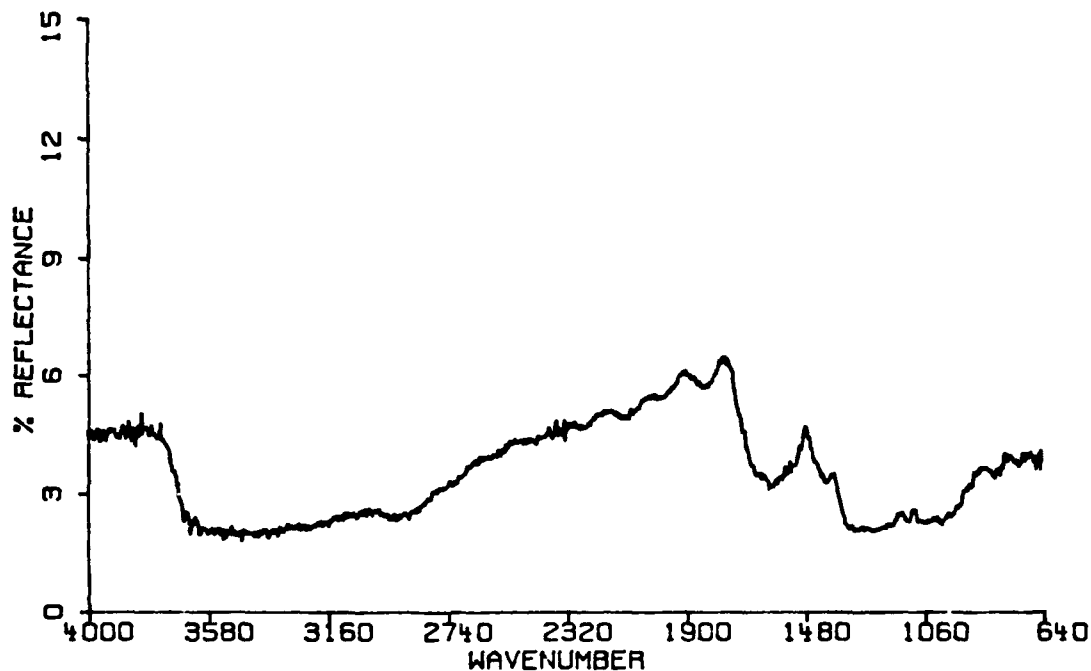
*Figure 3-8. FTIR Spectrum (Diffuse-Reflectance Method) of Noncontaminated Precrack
Region in Mode II ENF Specimen (Teflon Contaminated Specimen)*

damaged region had a unique visual fracture signature that was noticeably different from the nonimpact fracture regions. The specimen was examined using SEM techniques to determine the fracture propagation directions from the site of impact.

SEM examination of the impacted region indicated that the fracture surface was characterized by delamination fracture at a 0/90 interface. The fractured resin was decorated with river-patterns that extended radially outwards, as shown in Figure 3-12. The specimen was examined using this technique and the fracture propagation directions were mapped from the site of impact. Figure 3-13 illustrates the mapped crack-propagation directions observed by SEM analysis. It was determined through examination of the fracture features that crack-propagation occurred radially in the delamination caused by impact.

Figure 3-14 shows a macrophotograph of the impacted area in NAD Specimen No. 3, part of a multispar Gr/Ep panel. The region illustrated is the plane of maximum delamination caused by impact, and was identified by 2-D ultrasonic B-scanning of the panel. The damaged area was isolated and exposed by ply-by-ply removal of the overload fracture fragments. As shown in
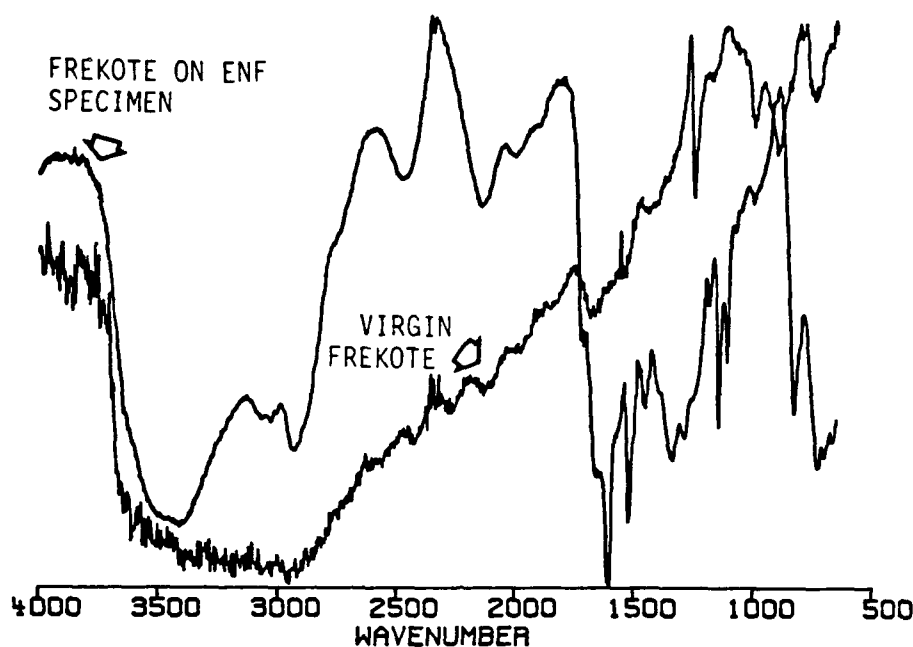
Figure 3-9. *FTIR Spectra of Virgin Frekote and Frekote Contaminated Fracture*

Figure 3-14, the impact-damaged region again had a unique visual fracture signature that noticeably differed from that of nonimpacted fracture regions. SEM examination could again be used to determine crack-propagation directions in the delamination caused by impact. A mapping of the observed crack-propagation directions in the delamination is shown in Figure 3-15. Note that the spar had a considerable effect on the delamination fracture features caused by impact in that deviations from general radial propagation were observed.

In summary, it can be concluded that the technique of ply removal enables the fractographic characterization/documentation of failures not immediately visible from the exterior, such as delamination fractures caused by impact. However, the technique must be used in conjunction with the conventional optical and SEM techniques for determination of the crack-propagation directions and fracture origins.

3.2.3.2 Materialographic Evaluation

Figure 3-16 shows a photographic collage of USAF Specimen No. 4 which was impacted with a 1/2 inch diameter indenter creating a force of 4.75 ft.-lbs. The metallographic sections were taken normal to the impact damage fracture in the directions of the 0, 45, and 90 plies, and oriented so that the fractures were in profile. As can be seen in Figure 3-16, impact resulted in delaminations and matrix cracking, with no through-hole damage.

Figure 3-17 shows a photographic collage of the impacted/PIC area in USAF Specimen No. 6. The materialographic sections were taken normal to the impact damage fracture in the directions of the 0, 45, and 90 degree plies, and oriented so that the fractures were in profile. Matrix cracks and fiber breakage that occur in impact/PIC failures were readily detected.

SAMPLE 2: FREKOTE. LOC: C.00,0.00
0/90, MODE II, FREKOTE. PRECRACK REGION. LOC IS LOWER RIGHT COR
06/11/87 10:42:56
     872.59 SEC. MEAS. TIME
DFN =   50   NSK =   0   COR = LO
NSD =   2000   GAN =   1   VEL =   40
NDP =   6144   AFN = HG   DET =   2
NTP =   4096   APT = FL

contaminated

WAVENUMBER
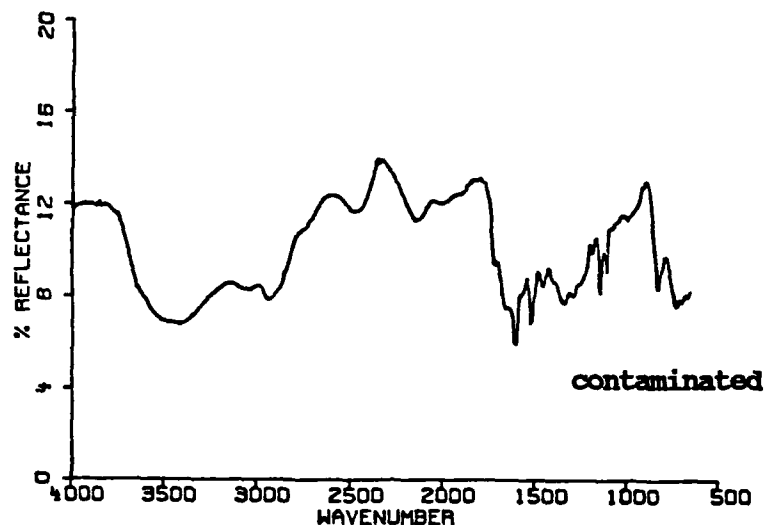
SAMPLE 2: FREKOTE. LOC: -10.48,-0.04
0/90, MODE II, FREKOTE. PROPAGATION REGION. LOC: UPPER RIGHT COR
06/11/87 14:39:58
     872.51 SEC. MEAS. TIME
DFN =   85   NSK =   0   COR = LO
NSD =   2000   GAN =   1   VEL =   40
NDP =   6144   AFN = HG   DET =   2
NTP =   4096   APT = FL

non-contaminated

WAVENUMBER
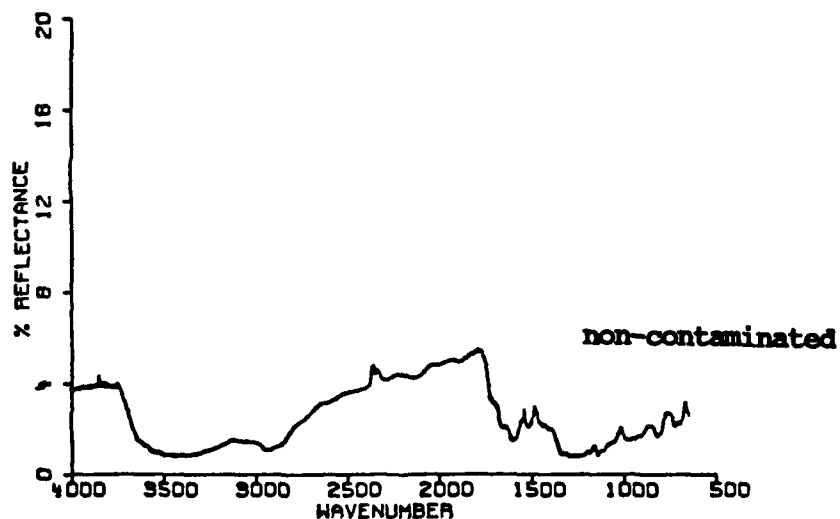
Figure 3-10. FTIR Spectra of Frekote Contaminated and Noncontaminated
             Regions in ENF Specimens

3-16
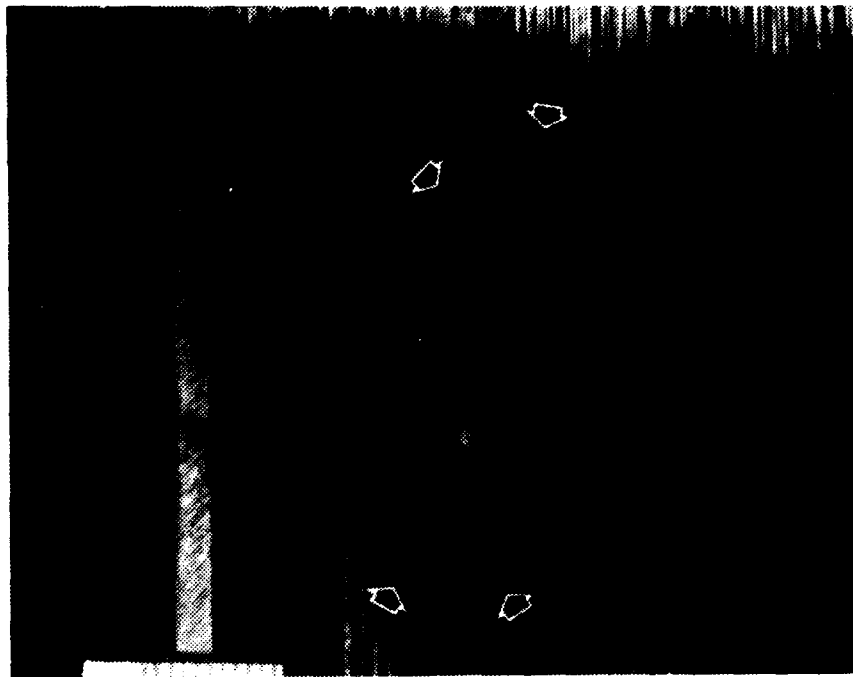
Figure 3-11. Macrophotograph of Delamination Fracture Area (Arrows) in Impacted USAF Specimen No. 2

Figure 3-18 shows a similar photographic collage of NAD Specimen No. 2, part of a multi-spar Gr/Ep panel that had been impacted and PIC tested. The materialographic sections were prepared as before, normal to the fracture in the direction of the 0, 45, and 90 degree plies, and oriented so that the fractures were in profile. The effect of the bolted joint on the fracture characteristics could be determined by this technique. As shown in Figure 3-18, mechanical joining of the composite to a spar had resulted in the plane of maximum delamination (caused by impact) being shifted closer to the top face of the panel rather than the bottom face, as is normally observed in impact failures.

Analysis of these results indicates that the technique of materialographic sectioning provides useful failure analysis information that would not be readily detected by conventional SEM/macroscopic techniques. However, the technique must be used as a supplement to conventional macrophotography/SEM fractography, since if used alone it would not provide information on the fracture initiation site(s) or crack-propagation direction(s).

3.3   STUDY, USE, AND DOCUMENTATION OF DAVID PURSLOW'S FRACTOGRAPHIC TECHNIQUES

As part of Subtask 2.1, the Northrop Program Manager, Dr. Ramesh Kar, visited Dr. David Purslow in Farnham, United Kingdom, from 22 June through 24 June 1988, for technical exchange on fractographic techniques for failed composites. The Air Force was unable to send a failed specimen for use during the exchange, as originally planned and therefore, only small test coupons that Dr. Purslow had available were used.
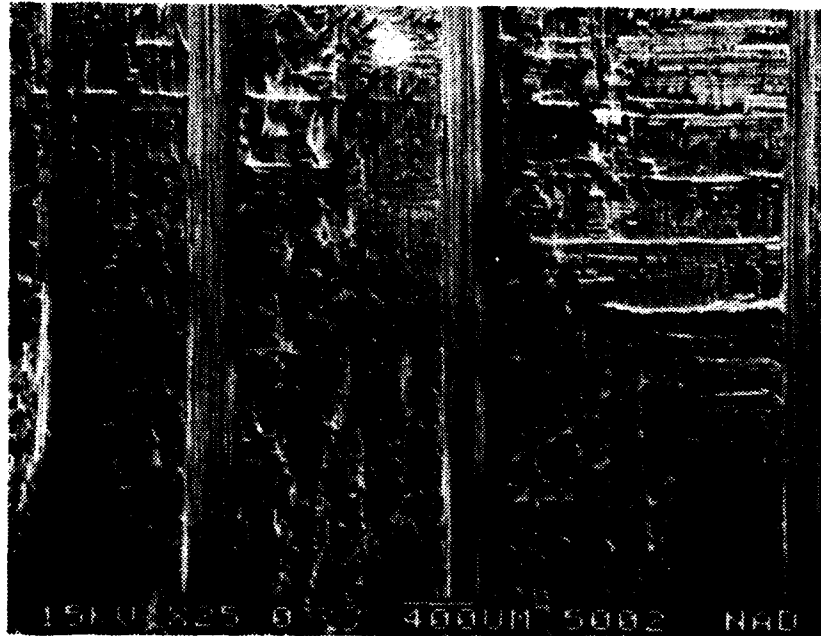
(a)

(b)

Figure 3-12.   SEM Photographs of Delamination Fracture in Impacted Specimen
Note river patterns shown by arrows

3-18
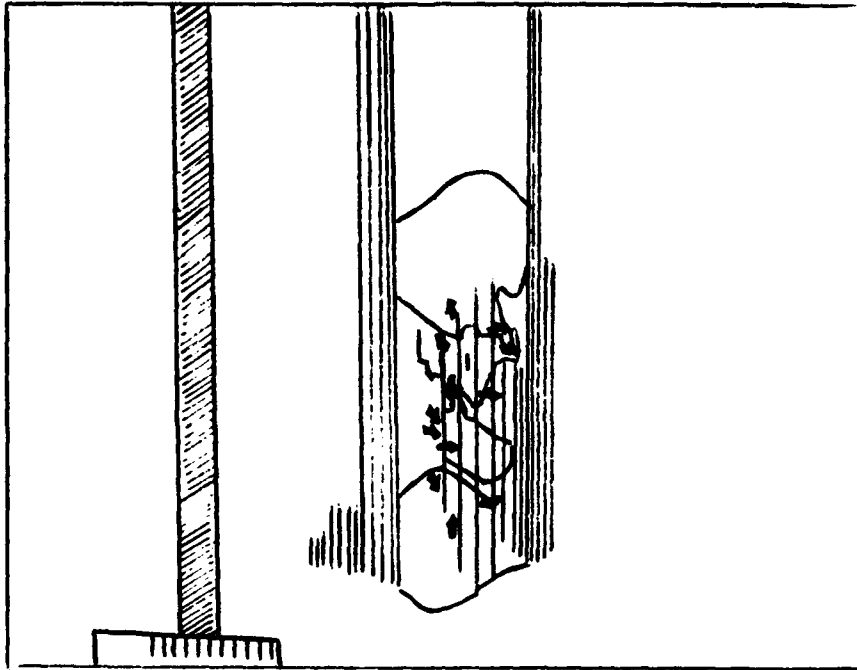
Figure 3-13. Mapping of Crack-Propagation (Arrows) in the Delamination Region of the Impacted Specimen (I = Impact Point)

The techniques that Dr. Purslow uses for failure investigations are similar to those used by other investigators, namely optical microscopy and SEM. Dr. Purslow occasionally uses NDE and chemical methods, but primarily relies on the technique of optical microscopy with SEM as backup. Dr. Purslow's experience has been in the areas of thermoset (epoxy) and thermoplastic (primarily polyetherketone, PEEK) systems. He indicated that over the past decade he had examined a large number of test coupons both optically and using the SEM. As a result, he could now establish, with a high degree of confidence, the failure mode(s) in specimens through optical examination alone. The following paragraphs summarize significant fractographic observations made during the visit.

3.3.1 Macroscopic Fracture Features

In thermosets and thermoplastics, Dr. Purslow characterizes "real-world" interlaminar fractures into two types — shear and peel (mixed-mode). On a macroscopic scale, peel fractures can be distinguished from shear fractures through differences in specular reflectance. Pure interlaminar shear fractures are whitish and dull, whereas peel fractures appear darker and reflect more light. Peel failures can be confirmed through additional examination of broken fibers in the fractured areas. Fiber ends will exhibit no evidence of compression in this failure mode.

Dr. Purslow also uses the concept of gross chevrons for tracking fractures in translaminar tension failures. These are particularly prominent in 90/0 translaminar fractures and radiate from 90° plies toward 0° plies. Additionally, real-world in-plane shear fractures in +45/-45 plies can be treated as translaminar tension fractures in 90/0 plies.

3-19
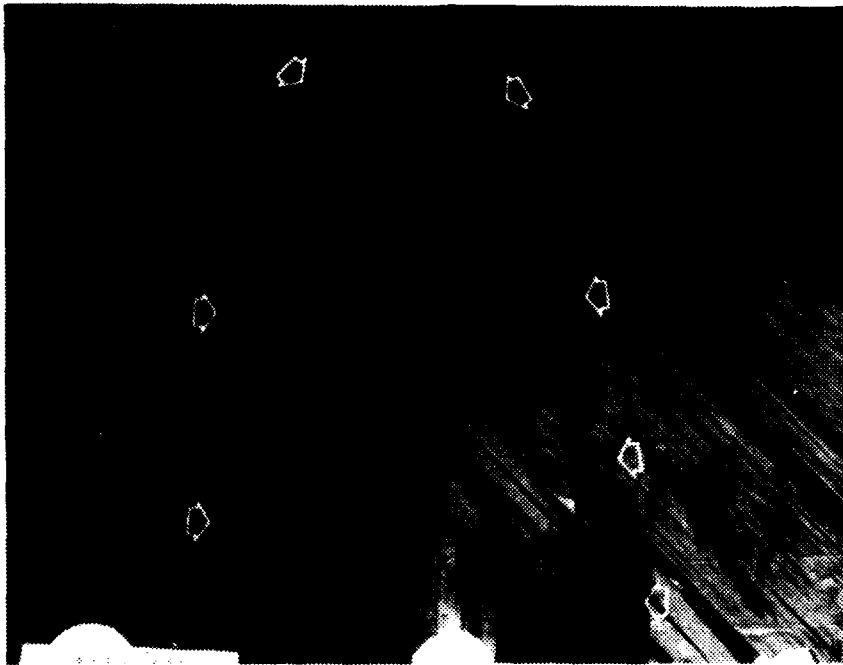
Figure 3-14. Macrophotograph of Delamination Fracture Area (Arrows) in
NAD Specimen No. 3 (Multispar Panel)
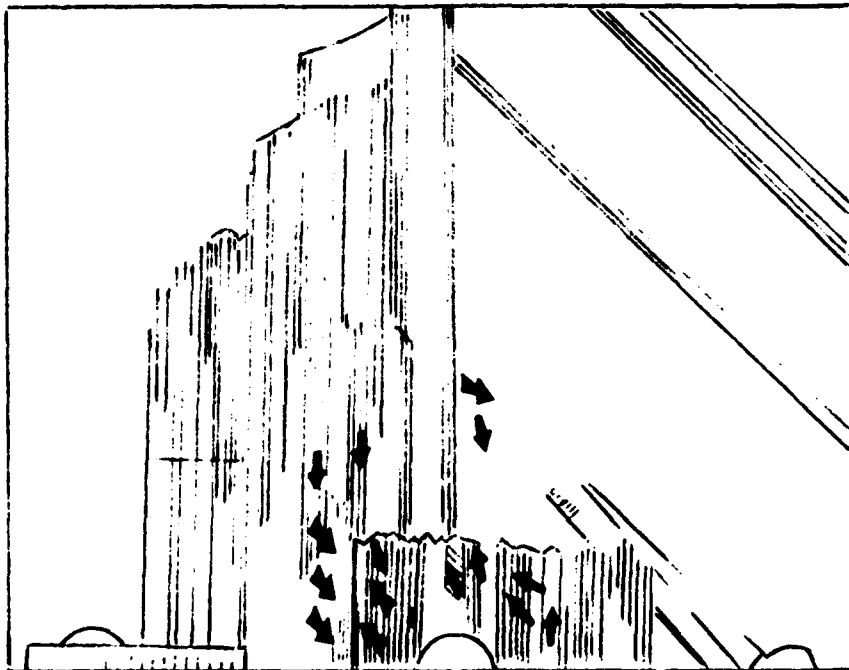
Figure 3-15. Mapping of Crack-Propagation Direction (Arrows) in Delamination
Region of Multispar Panel

Figure 3-16. Photographic Collage of Impacted Gr/Ep (USAF Specimen No.4)

3-21

Figure 3-17. Photographic Collage of Impact and PIC Gr/Ep (USAF Specimen No.6)

IMPACT ZONE

POINT OF IMPACT

0

5mm

45

5mm

60
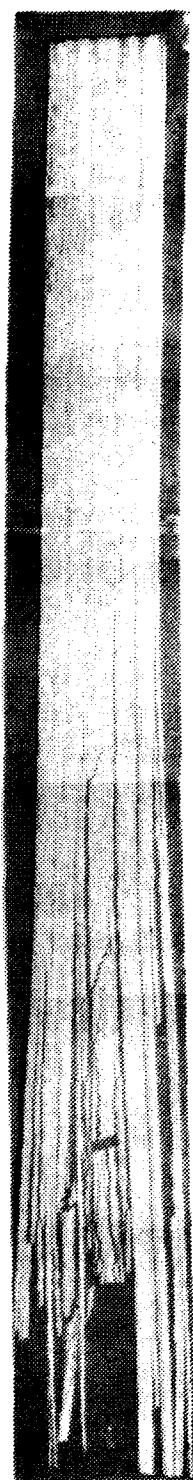
POINT OF IMPACT
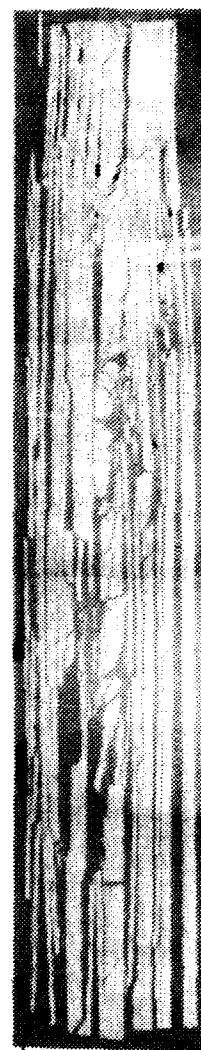
Figure 3-18. Photographic Collage of Impact and PIC Multispar Panel (NAD Specimen No. 2)

3-23

3.3.2 Microscopic Fracture Features

In epoxy-based systems, river patterns can be used successfully to determine the crack-growth direction in pure Mode I interlaminar tension and peel (mixed mode) fractures. In pure shear, cusps (hackles) form in an orientation normal to the plane of shear, but these cusps cannot be used to determine crack-growth direction. In real-world situations, however, pure shear is often associated with local interlaminar tension, giving rise to local rivers, which can then be used to establish fracture direction.

In thermoplastic-based systems, especially Gr/PEEK, the fracture surface morphology is a function of crack-growth rate. In peel fractures, transverse tensile forces cause "slow-ductile," "intermediate-brittle," and "fast-brittle" fracture modes. Slow-ductile peel is characterized by drawing of matrix craze filaments, similar to those observed in shear, whereas intermediate-brittle and fast-brittle fractures are characterized by the formation of cusps and rivers. The rivers can then be used to determine crack-growth direction. Slow-ductile peel can be distinguished from pure shear through examination of mating fracture surfaces. In peel, the filaments will be oriented in the same direction on mating halves, whereas in shear, these will be oriented in opposite directions. Additionally, peel fractures are characterized by the formation of "ribs" that do not form in shear.

Dr. Purslow also cautioned that fractographic features in toughened thermosets were not as simple as epoxies or thermoplastics, and developmental work would be required for these materials.

3.3.3 Real-World Failures

Dr. Purslow very briefly discussed several real-world components that he had analyzed while working at the RAE. These included a wind-tunnel component, a Jaguar CFC (carbon fiber component) wing, spar webs, and a helically wound tube. He indicated that it was important that the laboratory failure analyst work with accident investigators in failure analysis of real components. Accident investigators possess the skills/expertise in isolating post-accident damage from actual mishap damage, and their experience/knowledge should be used for selection of components for primary fracture evaluation.

The techniques that Dr. Purslow used to analyze these components were optical microscopy and SEM, with fracture origin(s), propagation direction(s) and failure mode(s) being established through the background knowledge he had obtained through evaluation of test coupons.

Dr. Kar also visited Emile Greenhalgh and Matthew Hiley at the RAE in Farnborough on 27 June 1988. Mr. Greenhalgh and Mr. Hiley have taken over Dr. Purslow's activities at RAE, following his retirement. Discussions with Mr. Greenhalgh and Mr. Hiley established that their experience was limited to compression failures in I-beams, using microscopic techniques shown to them by Dr. Purslow just prior to his retirement from the RAE.

3.4 EXPANSION OF THE FRACTOGRAPHIC DATABASE

The objective of this task was to make the fractographic database started under the Air Force/Boeing program on the model Gr/Ep system (AS4/3501-6) as complete as possible, and then to extend the database to include information on other material systems. Northrop performed this activity as several subtasks.

3.4.1 Subtask 3.1 – Expansion of the AS4/3501-6 Gr/Ep Fractographic Database

In this subtask, Northrop expanded the test data developed under the Air Force/Boeing program for AS4/3501-6 Gr/Ep to include the effect of additional variables. Northrop performed the following activities:

1. Analysis of all test data developed under the Air Force/Boeing program

2. Development of a new test matrix to include additional variables (a minimum of 125 new varied conditions)

3. Design and fabrication of laminates, and testing of specimens

4. Examination and documentation of fracture surfaces using the SEM.

3.4.1.1 Gr/Ep Specimen Test Matrices

Northrop reviewed the final report prepared by Boeing under a previous Air Force contract (Reference 3). Based on the results of the fractographic study reported by Boeing, Northrop designed updated test matrices to examine and document the effects of variables not previously addressed on the interlaminar and translaminar fracture characteristics of Gr/Ep. The tests for interlaminar and translaminar fractures are shown in Tables 3-3 and 3-4. These test conditions built upon the previous Air Force/Boeing program and did not duplicate any of the previous conditions. The testing and variables were designed as follows.

Interlaminar Fractures. A total of 76 varied interlaminar fracture tests (two to three replicates) were proposed. The test conditions included singular and multiple failure modes.

Translaminar Fractures. Thirty-six varied translaminar fracture tests (two to three replicates each) were proposed. These tests would result primarily in singular failure modes.

Material Forms. Test specimens fabricated from unidirectional and quasi-isotropic tape, filament wound, and 3-D woven laminates were to be tested under controlled tension, shear, and tension plus shear to compare the effects of material form on fracture characteristics. The fracture data could also be compared with fractures produced in tape specimens from the Air Force/Boeing program.

Effect of Loading Rate. The test matrices included variable-amplitude (spectrum) fatigue and impact-tested coupons. The variable-amplitude spectrum would be the generic FALSTAFF tension-tension spectrum.

Effect of Impact. Impact-damaged unidirectional and multi-ply orientation specimens were to be tested under singular and multiple failure conditions to assess the effect of impact before failure loading on the subsequent fracture characteristics.

Table 3-3. AS4/3501-6 Gr/Ep Interlaminar Fracture Test Specimens

Specimen Loading	Variable Condition	No of Plies/Orientation			
		24/0	24/±45	24/0.45	24/0.90
Mode I DCB, Tension Mode II ENF/CLS, Shear Mode I + II MMF, Tension + Shear	Filament Wound	3 3 3	3 - -	3 3 3	3 3 -
Mode I DCB, Tension Mode II ENF/CLS, Shear Mode I + II MMF, Tension	3-D Weave	3 3 3	3 - -	3 3 3	3 - -
Mode I DCB, Fatigue Mode II ENF/CLS, Fatigue Mode I + II MMF, Fatigue	Spectrum-Fatigue (T-C Spectrum)	3 3 3	- - -	3 3 3	3 - -
Mode I DCB, Tension Mode II ENF/CLS, Shear Mode I + II MMF, Tension + Shear	Impact-Damaged Before Test	3 3 3	3 - -	3 - 3	- 3 -
Mode I DCB, Tension Mode II ENF/CLS, Shear Mode I + II MMF, Tension + Shear	Water Immersion Before Test	3 3 3	- - -	- - -	- 3 -

Specimen Loading	Variable Condition	No of Plies/Orientation			
		24/0	24/±45	24/0.45	24/0.90
Mode I DCB, Tension Mode II ENF/CLS, Shear Mode I + II MMF, Tension + Shear	Water Immersion After Test	2[a] 2[a] 2[a]	2[a] - -	2[a] 2[a] 2[a]	2[a] 2[a] -
Mode I DCB, Tension Mode II ENF/CLS, Shear Mode I + II MMF, Tension + Shear	Undercure (Processing Defect)	3 3 3	- - -	3 3 3	3 - -
Mode I DCB, Tension Mode II ENF/CLS, Shear Mode I + II MMF, Tension + Shear	Overcure (Processing Defect)	3 3 3	- - -	3 3 3	- - -
Mode I DCB, Tension Mode II ENF/CLS, Shear Mode I + II MMF, Tension + Shear	High Resin Content (Improper Bleedout + Pressure)	3 3 3	3 - -	3 - -	- 3 -
Mode I DCB, Tension Mode II ENF/CLS, Shear Mode I + II MMF, Tension + Shear	Conditioned 2 Weeks @ 180 F After Failure	2[b] 2[b] 2[b]	- - -	2[b] 2[b] 2[b]	2[b] - -
Mode I DCB, Tension Mode II ENF/CLS, Shear Mode I + II MMF, Tension + Shear	Conditioned 2 Weeks @ 180 F + Moisture After Failure	2[c] 2[c] 2[c]	- - -	2[c] 2[c] 2[c]	- - -

DCB = Double Cantilever Beam, ENF = End-Notched Flexure, a = Filament Wound Specimens Tested to Failure, CLS = Cracked Lap Shear
MMF = Mixed Mode Flexure, b = High Resin Content Specimens to be Conditioned, c = Overcured Specimens to be Conditioned

3-26

Table 3-4. AS4/3501-6 Gr/Ep Translaminar Fracture Test Specimens

Specimen Loading	Variable Condition	No of Plies/Orientation		Specimen Loading	Variable Condition	No of Plies/Orientation	
		32/0	32/Quasi			32/0	32/Quasi
Mode I Tension (Four Point Load)	Filament Wound	3	3	Mode I Compression (Four Point Load)		2*	–
Mode I Compression (Four Point Load)		3	–	Mode II Shear (Side – Notched Rail)		–	2*
Mode II Shear (Side – Notched Rail)		–	3	Mode I Tension (Four Point Load)	Conditioned 2 weeks @180F After Test	2**	–
Mode I Tension (Four Point Load)	3 – D Weave	3	–	Mode I Compression (Four Point Load)		2**	2**
Mode I Compression (Four Point Load)		3	3	Mode II Shear (Side – Notched Rail)		2**	–
Mode II Shear (Side – Notched Rail)		3	–	Mode I Tension (Four Point Load)	Low Fiber Content	–	3
Mode I Tension (Four Point Load)	Spectrum Fatigue (T – C Spectrum)	3	3	Mode I Compression (Four Point Load)		3	–
Mode I Compression (Four Point Load)		–	3	Mode II Shear (Side – Notched Rail)		–	–
Mode I Tension (Four Point Load)	Impact Damaged Before Test	3	3	Mode I Tension (Four Point Load)	Undercure (Processing Defect)	–	3
Mode I Compression (Four Point Load)		3	3	Mode I Compression (Four Point Load)		3	–
Mode II Shear (Side – Notched Rail)		3	–	Mode II Shear (Side – Notched Rail)		–	3
Mode I Tension (Four Point Load)	Water Immersion Before Test	3	3	Mode I Tension (Four Point Load)	Overcure (Processing Defect)	3	–
Mode I Compression (Four Point Load)		3	3	Mode I Compression (Four Point Load)		–	3
Mode I Tension (Four Point Load)	Water Immersion After Test	2*	2*	Mode II Shear (Side – Notched Rail)		3	–

* Filament Wound   ** 3 – D Weave

Water Immersion. Tape and filament-wound specimens were to be immersed in water before and after testing to evaluate the effect of water immersion on the fracture surface features.

Processing Defects. The test matrices included undercured, overcured and high resin-content specimens (due to improper pressure plus bleedout) to assess the effect of processing variables on the fracture characteristics.

Combined Variables. The test matrices included the effects of combined experimental variables such as moisture plus temperature or overcuring plus post-failure conditioning.

3.4.1.2 Gr/Ep Laminates

Based upon the number of test specimens outlined in Tables 3-3 and 3-4, a total of 42 laminates were required. The dimensions, layups and test conditions of the laminates are shown in Tables 3-5 and 3-6. The laminates included six filament-wound, six 3-D woven, and thirty-six panels fabricated from tape.

3.4.1.3 Test Specimens

Northrop fabricated double-cantilever beam (DCB), mixed-mode flexure (MMF), and crack lap-shear (CLS) specimen configurations for interlaminar fracture tests. The dimensions of these specimens are shown in Figures 3-19 and 3-20. The starter cracks were to be obtained through use of Armalon film in the specimens. For translaminar tests Northrop proposed use of four-point load tension, compression, and side-notched rail shear specimens. These are shown in Figure 3-21. Impact tests were to be performed with a blunt one-inch diameter hemispherical impacter.

3.4.1.4 Mechanical Tests

All mechanical tests were performed in accordance with established ASTM or Northrop specifications/laboratory standards. The inter- and translaminar tension and compression tests were performed under displacement-controlled conditions, whereas the interlaminar shear tests were under strain-controlled conditions.

3.4.1.5 Fractographic Examination and Documentation

All relevant fracture features in the failed test specimens were examined and documented using SEM in conjunction with visual methods. SEM documentation consisted of detailed characterization of all macroscopic and microscopic fracture features. The fractographs were organized to illustrate the initiation sites, directions of crack-growth, and macroscopic/microscopic fracture features that were of significance.

Detailed fractographic results for the various test conditions described in Tables 3-3 and 3-4 are presented in Part 2 – Atlas of Fractographs. The results for some of the variable conditions and their analyses are presented below.

Mode I DCB Interlaminar Fractography. Figures 3-22 and 3-23 are photographs of fracture in unidirectional Gr/Ep that was undercured. On a macroscopic scale, the fracture could be

Table 3-5. *Dimensions, Layups and Test Conditions for Interlaminar Fracture Gr/Ep Laminates*

LAYUP	SIZE (in.)	CONDITION	# OF LAMINATES
24/0	23X20	Filament	1 ea
24/±45	8X13	Wound	
24/0,±45	23X20		
24/0,90	14X13		
24/0	23X20	3-D Weave	1 ea
24/±45	8X13		
24/0,±45	23X20		
24/0,90	8X13		
24/0	23X20	Spectrum	1 ea
24/0,±45	23X20	Fatigue	
24/0,90	8X13		
24/0	23X20	Impact	1 ea
24/±45	8X13	Damage	
24/0,±45	24X17		
24/0,90	8X13		
24/0	23X20	Water	1 ea
24/0,90	8X13	Immersion	
24/0	23X20	Undercure	1 ea
24/0,±45	23X20		
24/0,90	8X13		
24/0	23X20	Overcure	1 ea
24/0,±45	23X20		
24/0	23X20	High Resin	1 ea
24/±45	8X13	Content	
24/0,±45	8X13		
24/0,90	8X13		

characterized into three regions labeled I, II, and III. Region I was the precrack region (Mode I tension) and Region II was the crack-growth area where compliance changes were measured. Region III was the laboratory overload to expose the fracture surface for fractographic work.

Mode I interlaminar fracture initiated in the precrack region at resin-rich areas adjacent to the Armalon insert (Figure 3-22b). The fracture surface in all three regions was characterized

3-29

Table 3-6. *Dimensions, Layups and Test Conditions for Translaminar Fracture Gr/Ep Laminates*

LAYUP	SIZE (in.)	CONDITION	# OF LAMINATES
32/0	9X11	Filament	1 ea
32/Quasi	11X17	Wound	
32/0	17X12	3-D Weave	1 ea
32/Quasi	9X7		
32/0	9X7	Spectrum	1 ea
32/Quasi	9X11	Fatigue	
32/0	17X12	Impact	1 ea
32/Quasi	9X11	Damage	
32/0	9X11	Water	1 ea
32/Quasi	9X11	Immersion	
32/0	9X7	Undercure	1 ea
32/Quasi	11X17		
32/0	11X17	Overcure	1 ea
32/Quasi	9X7		
32/0	9X7	High Resin	1 ea
32/Quasi	9X7	Content	

by river patterns. These were initially oriented at an angle to the crack-propagation direction and at long crack lengths aligned themselves in the direction of crack-propagation (Figure 3-22c). The effect of undercure was manifested in the form of stray porosity (Figure 3-22d) that randomly decorated the entire fracture surface.

Figure 3-23 presents photographs illustrating macroscopic and microscopic fracture features in unidirectional impact damaged Gr/Ep, using a one inch diameter hemispherical indenter with a force of 60 inch-pounds. On a macroscopic scale, Regions I, II, III, and IV (precrack, crack-growth, laboratory overload, and impact delamination) were not as distinct as for the other variable conditions.
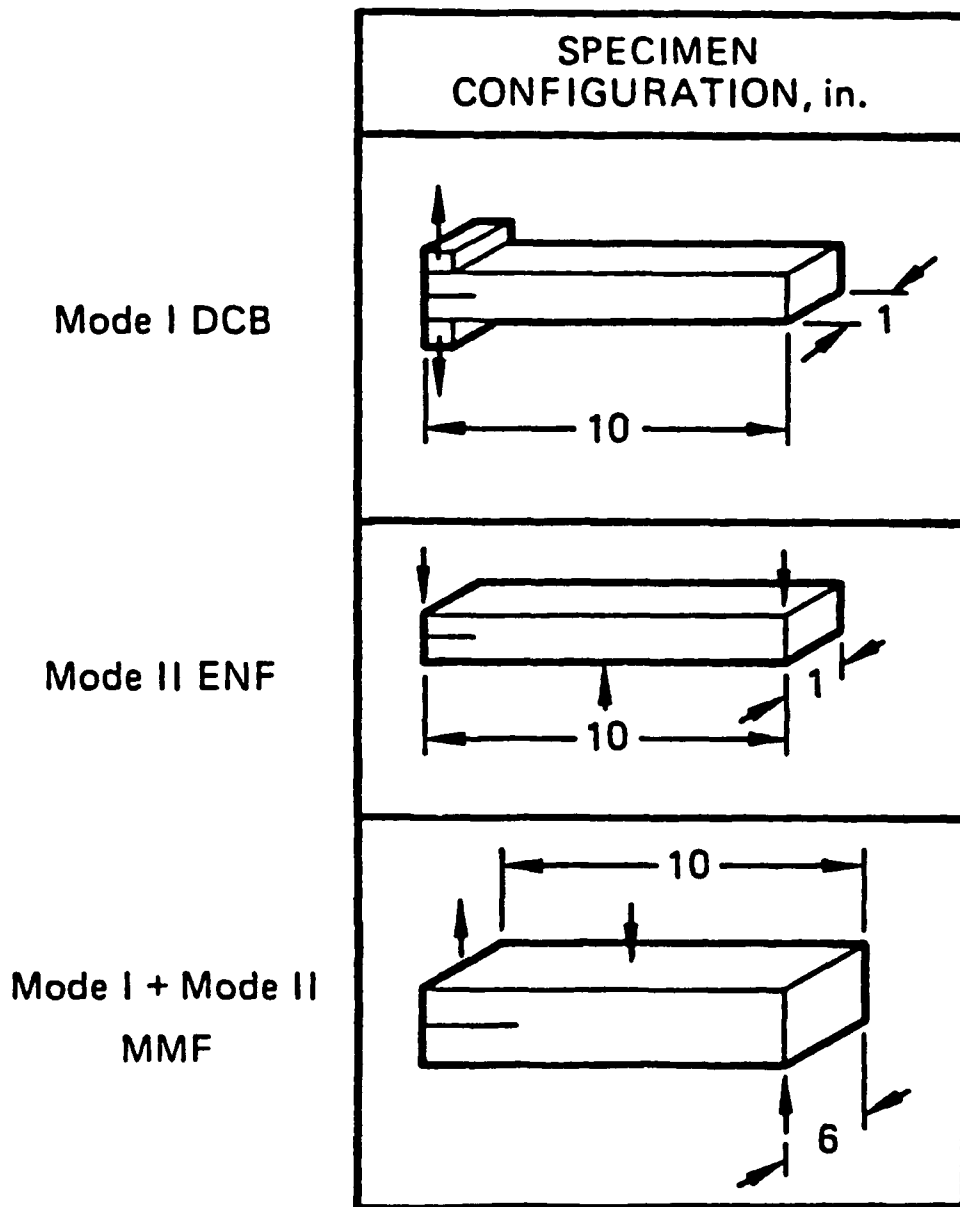
SPECIMEN CONFIGURATION, in.

Mode I DCB

Mode II ENF

Mode I + Mode II MMF

Figure 3-19. Interlaminar Fracture Test Specimens

Microscopic examination of Mode I fracture features in the precrack region revealed that initiation occurred in the resin-rich areas (Figure 3-23b). The crack-propagation direction could be mapped, as for the other variable conditions, by the orientation of the river patterns. These were initially inclined at an angle to the crack-growth direction (Figure 3-23c), and at larger crack lengths, aligned themselves along the direction of crack-growth. Figures 3-23d and 3-23e illustrate the impact area. The region was characterized by coarse hackles and rivers on the fractured epoxy (Figure 3-23d) and extensive fiber breakage (Figure 3-23e). The crack-propagation direction could not be clearly mapped in this region; however, regions beyond the impact area exhibited river patterns as before.
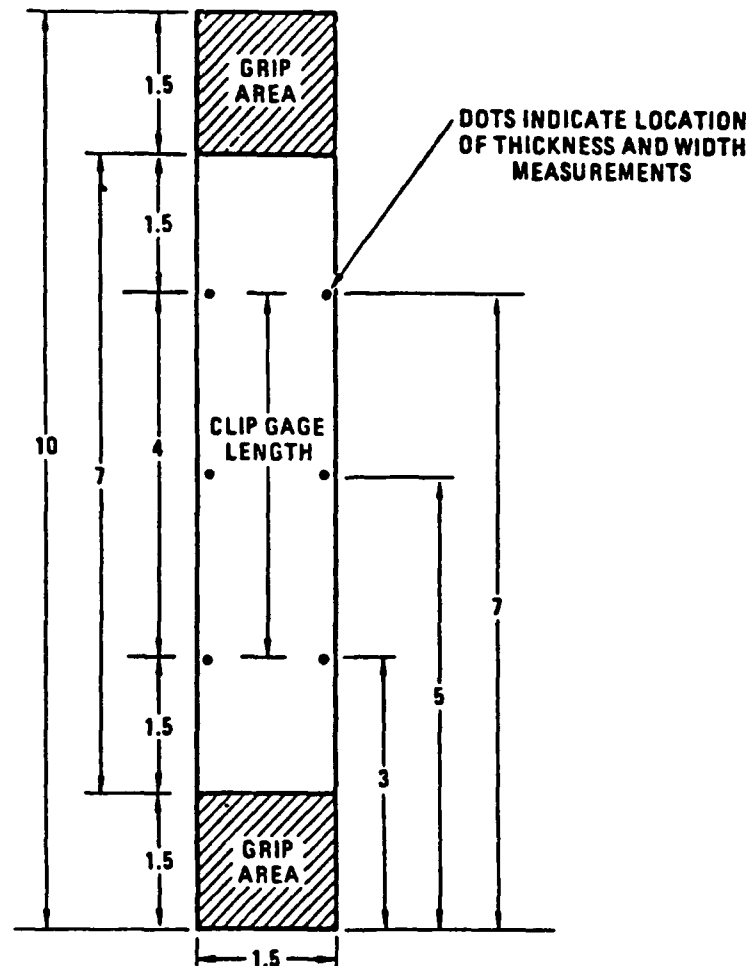
Figure 3-20. Crack-Lap Shear Specimen (All Dimensions in Inches)

Mode II ENF Interlaminar Fractography. Figure 3-24a represents the macroscopic fracture observed in unidirectional $[0]_{24T}$ ENF test coupons, that were undercured. The undercured condition was achieved by eliminating the four hour post-cure treatment cured out at 350°F for 3501-6 Gr/Ep. Interlaminar fracture occurred at 0/0 interface and consisted of three distinct regions, as for the Mode I DCB specimen. Region I was the precrack area (Mode I tension); Region II was the crack-growth region, where interlaminar fracture had occurred under Mode II shear; and Region III was the overload fracture area formed under Mode I tension. The fracture surface in Region II was characterized by bands oriented perpendicular to the direction of crack-growth.

SEM examination of Region I indicated that interlaminar fracture in the precrack region initiated at the resin-rich areas adjacent to the Armalon insert. The fractured resin was decorated with river patterns oriented radially outwards and extending into the fractured resin in between fibers, as shown in Figures 3-24b and 3-24c. Analyses of the river patterns in between fibers indicated that these were generally oriented at angles of ±30 - 45 degrees to the crack-growth direction. The macroscopic crack-propagation direction could be mapped through simple addition of the directions of the river patterns on either side of individual fibers.
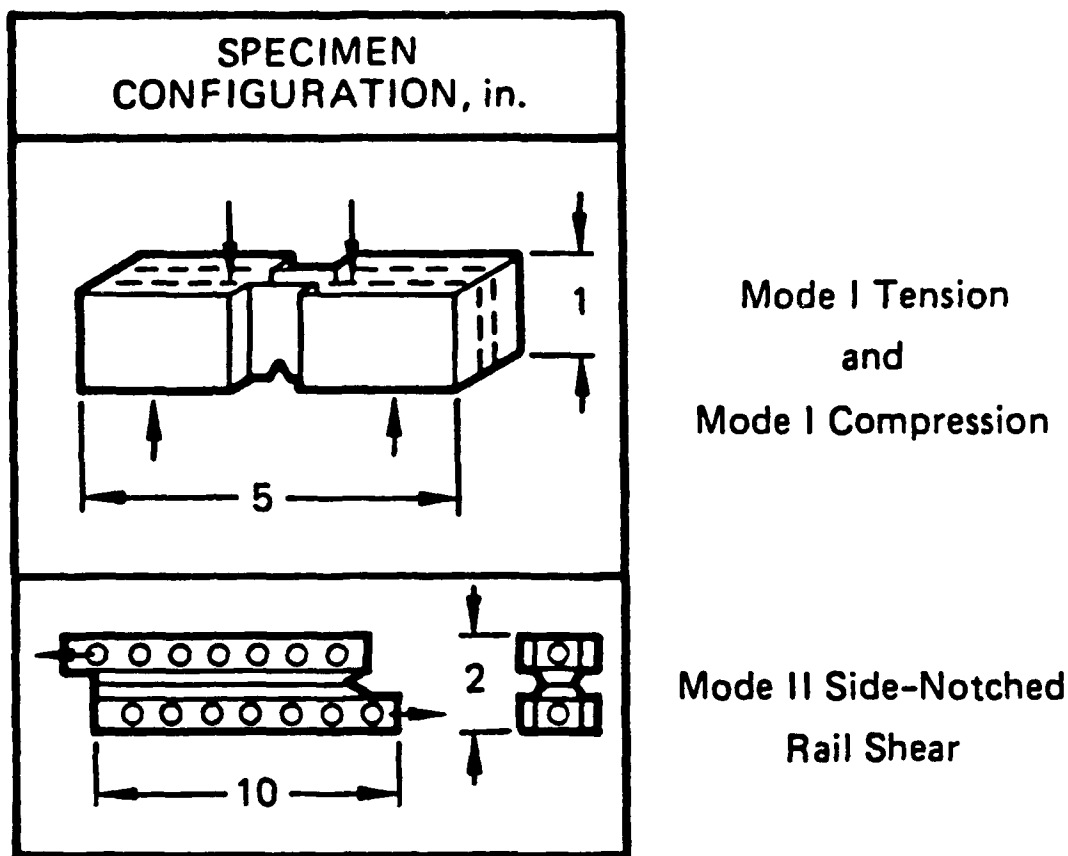
SPECIMEN CONFIGURATION, in.

Mode I Tension
and
Mode I Compression

Mode II Side-Notched
Rail Shear

*Figure 3-21. Translaminar Fracture Test Specimens*

Figure 3-24d presents a SEM photograph of the Region I/Region II boundary. Pronounced differences in fracture surface morphology were observed, as illustrated, on transition from Mode I tension to Mode II shear. There were no unique features at the boundary, such as chevrons or radial lines indicative of Mode II shear fracture initiation. The features observed in Region II consisted of hackles and scallops of various shapes and sizes (Figure 3-24e). The crack-propagation direction could not be established based upon the inclination(s) of the hackles. As illustrated in Figure 3-24f, a few fractured resin troughs (where fibers had pulled out) and fractured resin on individual fibers had V-shaped tears oriented in the macroscopic crack-propagation direction. However, these features were not frequent enough to unequivocally map the crack-propagation direction.

Mixed Mode Interlaminar Fractography. Figure 3-25 presents photographs illustrating macroscopic and microscopic fracture features observed in [+45/0/-45]$_{4S}$ Gr/Ep that was impact damaged using a one inch diameter hemispherical indenter with a force of 60 inch-pounds. The specimen had been impacted to assess the effect of impact on mixed-mode crack-growth.

As shown in Figure 3-25a, delamination fracture caused by impact had a characteristic macroscopic fracture signature which is easily distinguishable. Regions labeled I and III were Mode I tension interlaminar fractures (precrack and laboratory overload, respectively) whereas Region II was the crack-growth region under Mode I tension and Mode II shear. Region IV was the impact damaged region.

I   II   III

(a)

15KV X50.0 200UM 0017 NAD

(b)

→
CD
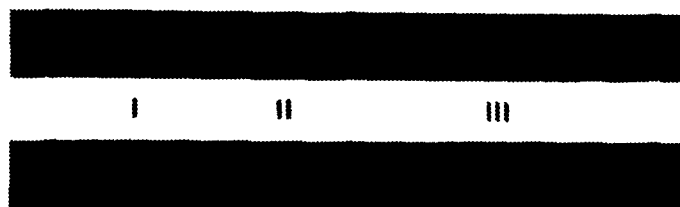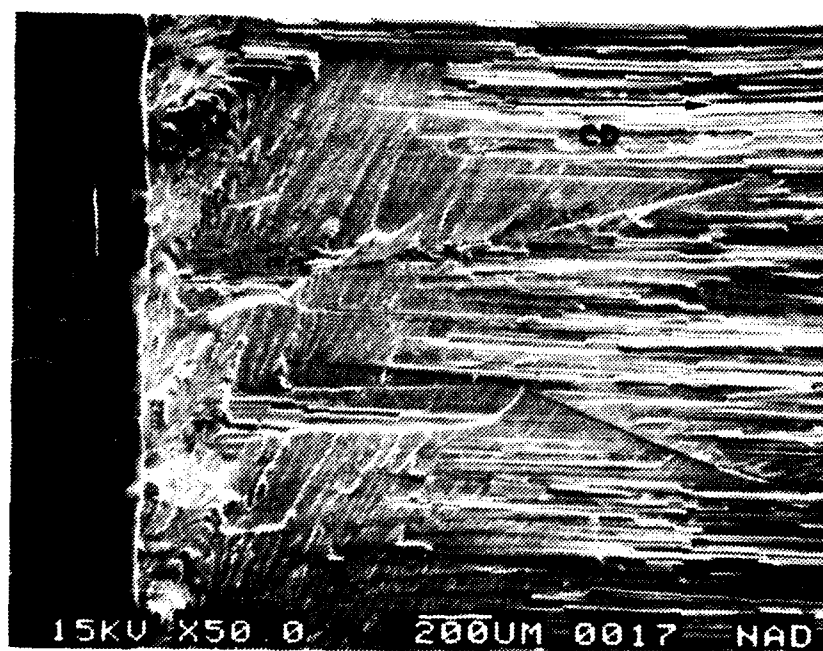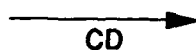
Figure 3-22. *Optical and SEM Photographs of Mode I DCB Interlaminar Fracture in Undercured Gr/Ep - $[0]_{24T}$ (a) Macrophotograph Showing Regions I, II, and III (b) Initiation in Region I Adjacent to Armalon (A)*

CD = Crack-propagation direction

3-34

(c)

(d)

Figure 3-22. (Continued)
(c) River Patterns Indicating Crack-Propagation Direction
(d) Porosity (Arrows)

(b)

(c)

(a)

CD
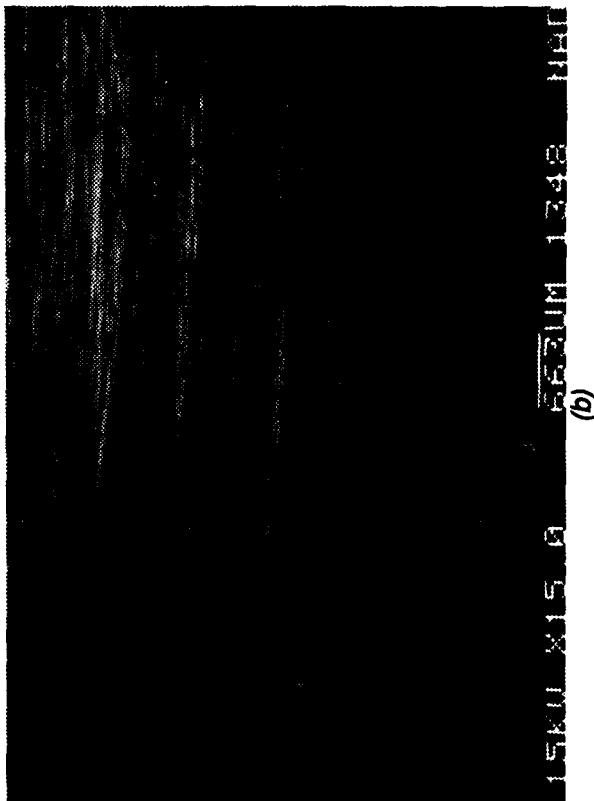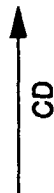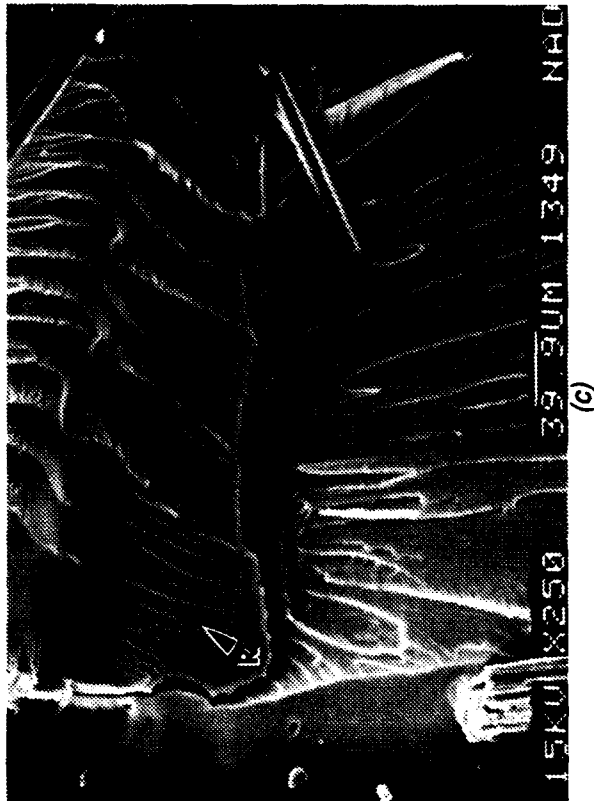
Figure 3-23. *Optical and SEM Photographs of Mode I DCB*
Impact Damaged Gr/Ep - [0]₂₄T
(a) Macrophotograph
(b) Initiation in Precrack
(c) River Patterns (R) in Mode I Region

CD = Crack-propagation direction

(e)

(d)
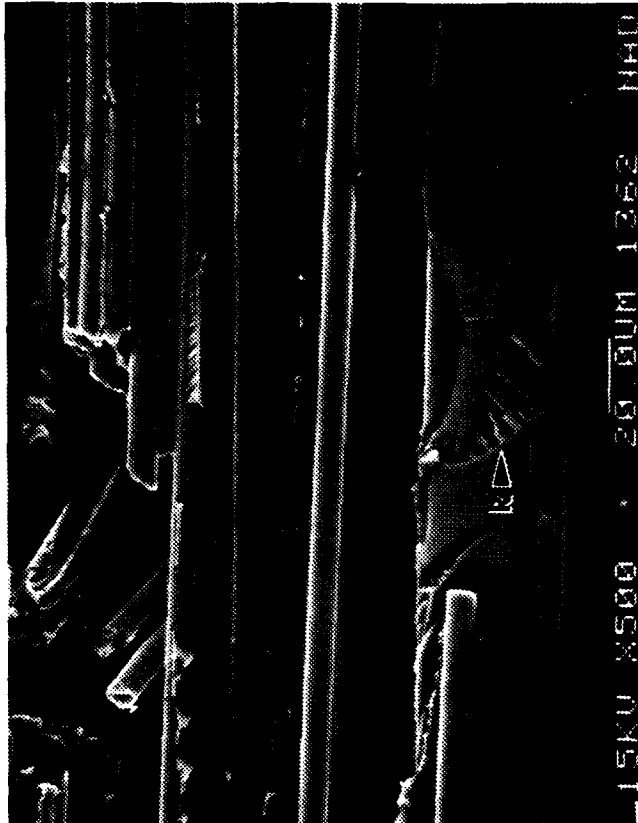
Figure 3-23. (Continued)
(d) Impact Center
(e) Broken Fibers in Impact Area
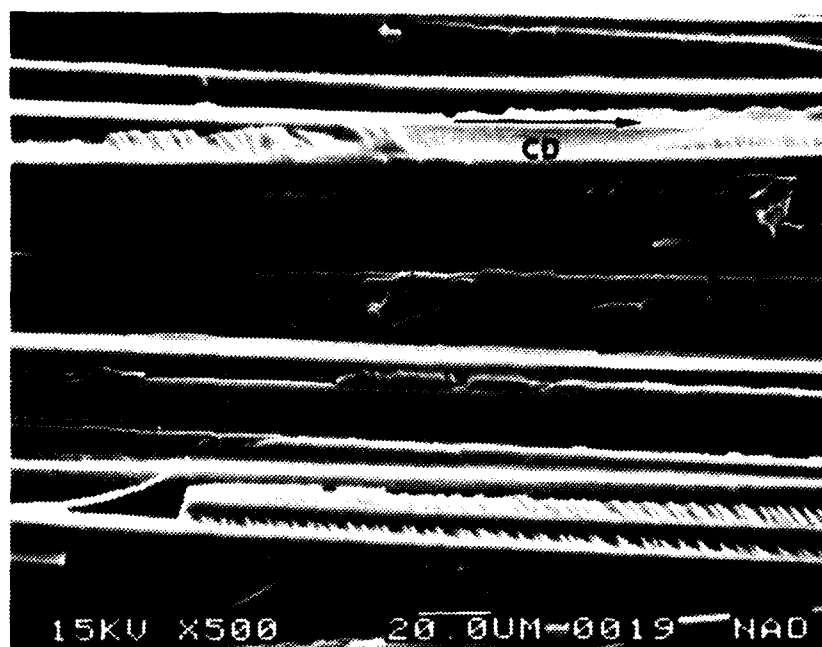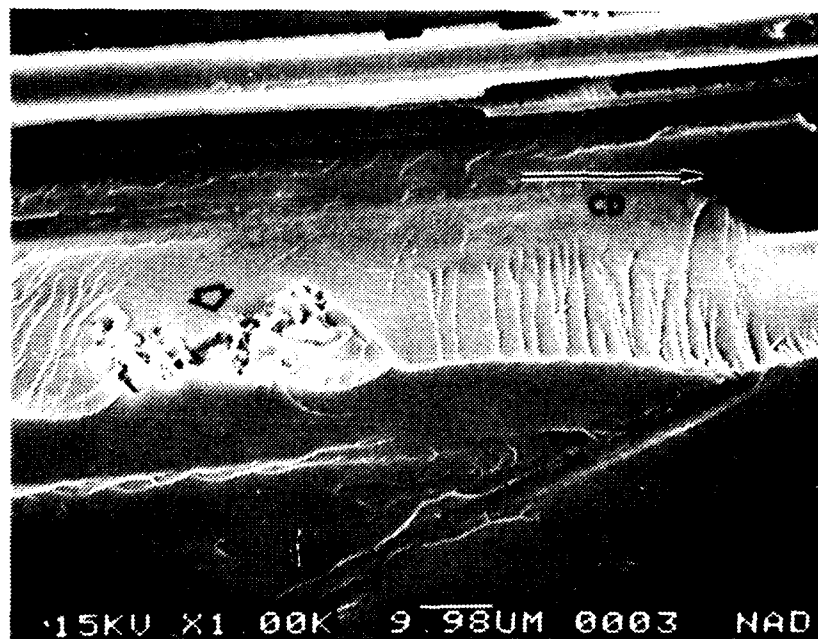Note river patterns in resin

H = Hackles (cusps)
R = River patterns
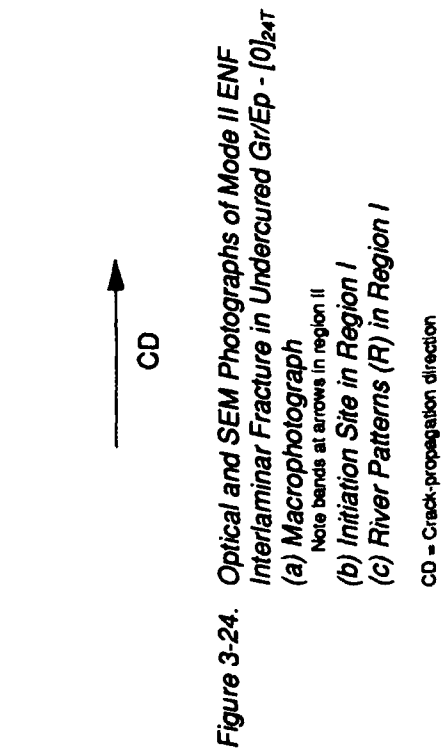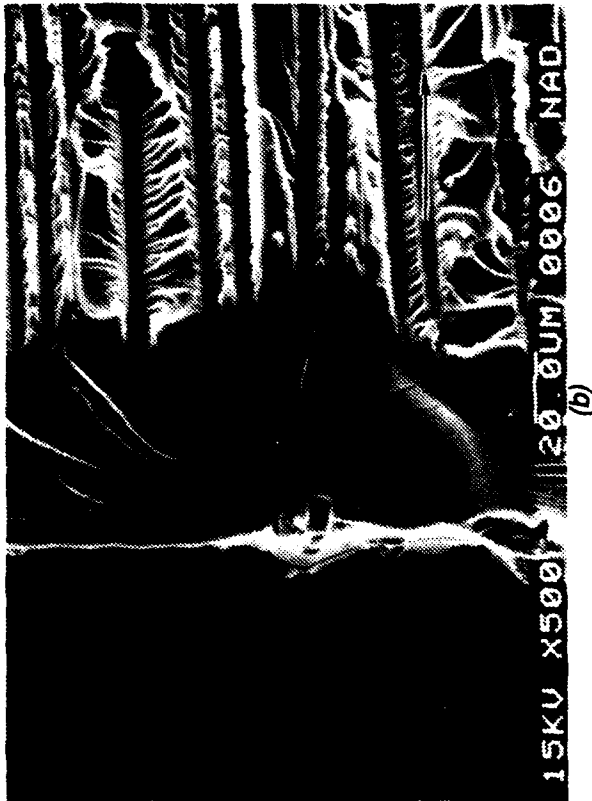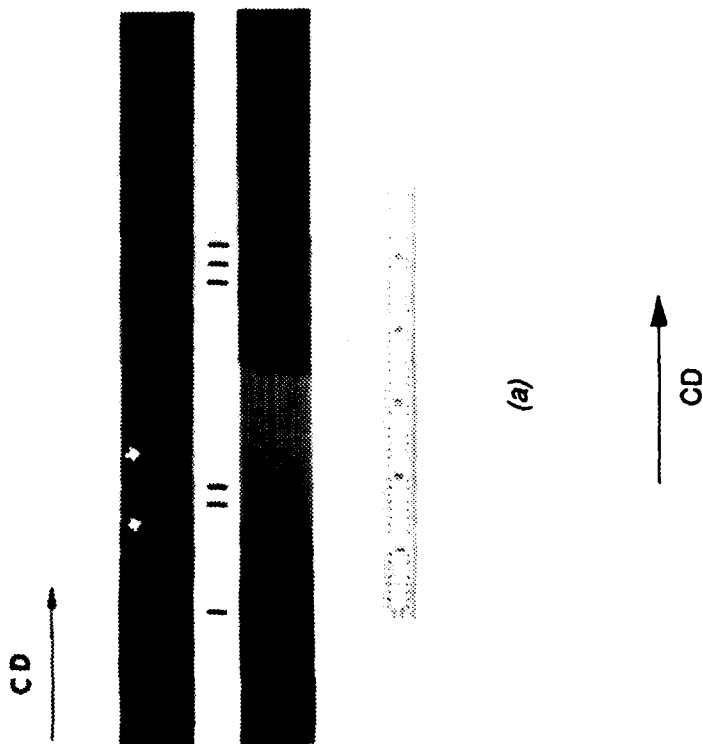
Figure 3-24. *Optical and SEM Photographs of Mode II ENF Interlaminar Fracture in Undercured Gr/Ep - [0]$_{24T}$*

(a) Macrophotograph
   Note bands at arrows in region II
(b) Initiation Site in Region I
(c) River Patterns (R) in Region I

CD = Crack-propagation direction
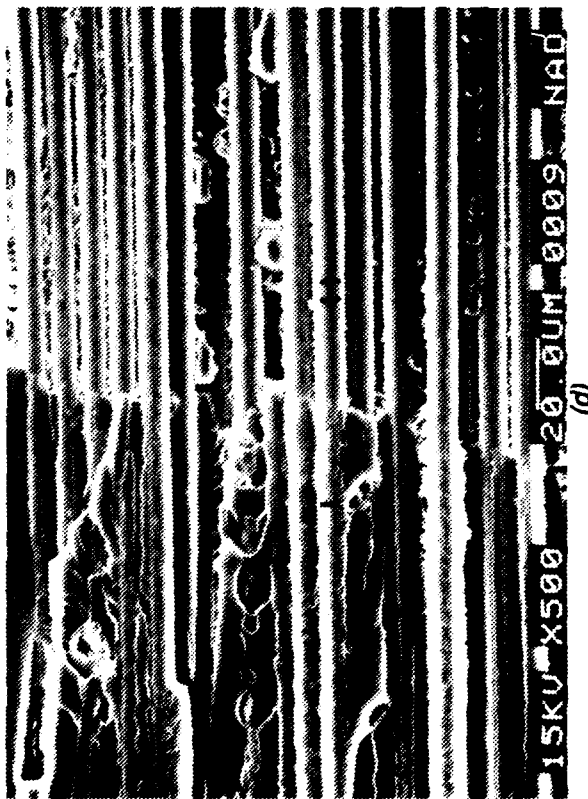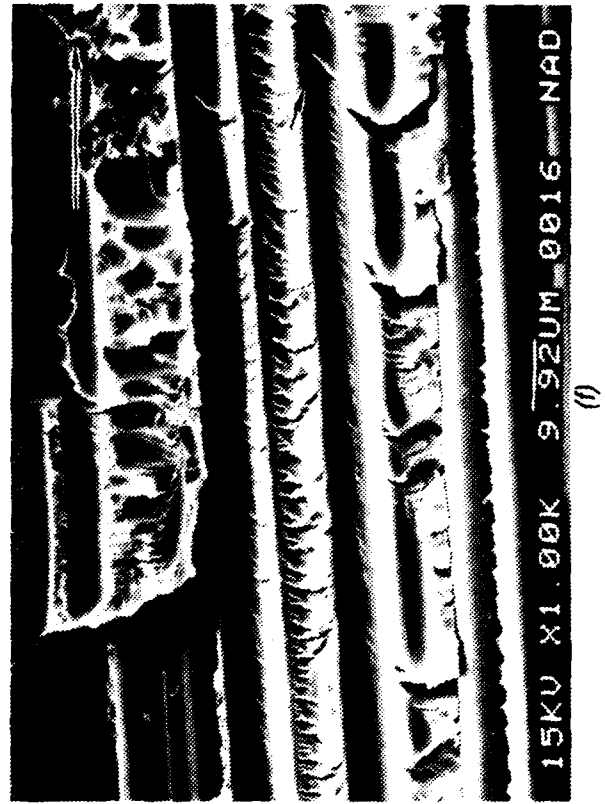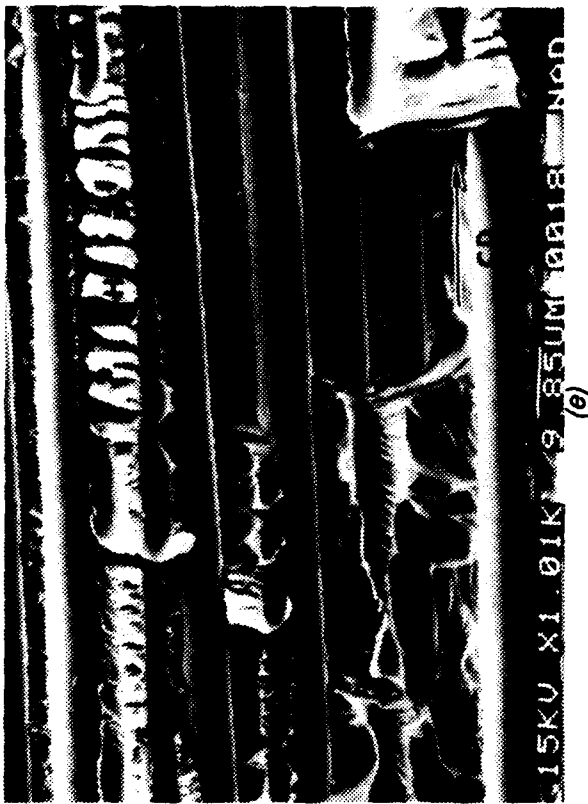
Figure 3-24. *(Continued)*
(d) Region I/II Interface
(e) Hackles (H) and Scallops (S) in Region II
(f) V-Shaped Tears in Region II

CD = Crack-propagation direction
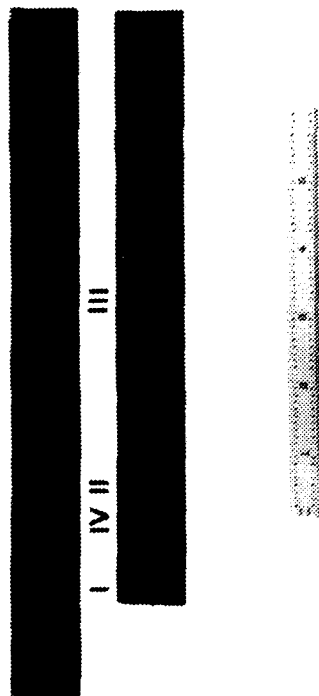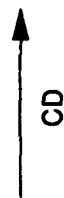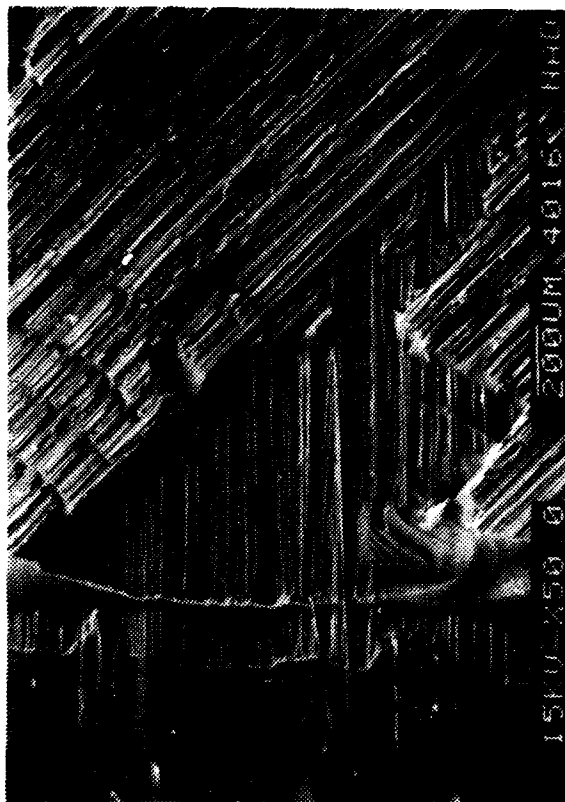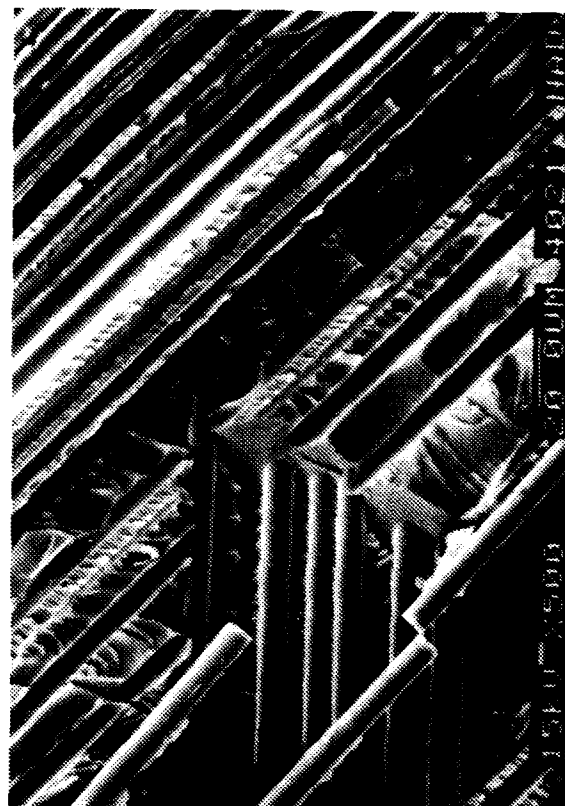
Figure 3-25. Optical and SEM Photographs of Mode I and II MMF Impact Damaged Gr/Ep - [+45/0/-45]₄s

(a) Macrophotograph Showing Regions I, II, III and IV (Precrack, Crack Growth Under Mode I Tension and Mode II Shear, Laboratory Overload, Impact Damage)
(b) Initiation in Resin-Rich Areas
(c) River Patterns in the Mode I Fracture Region

CD = Crack-propagation direction

CD

CD
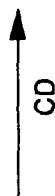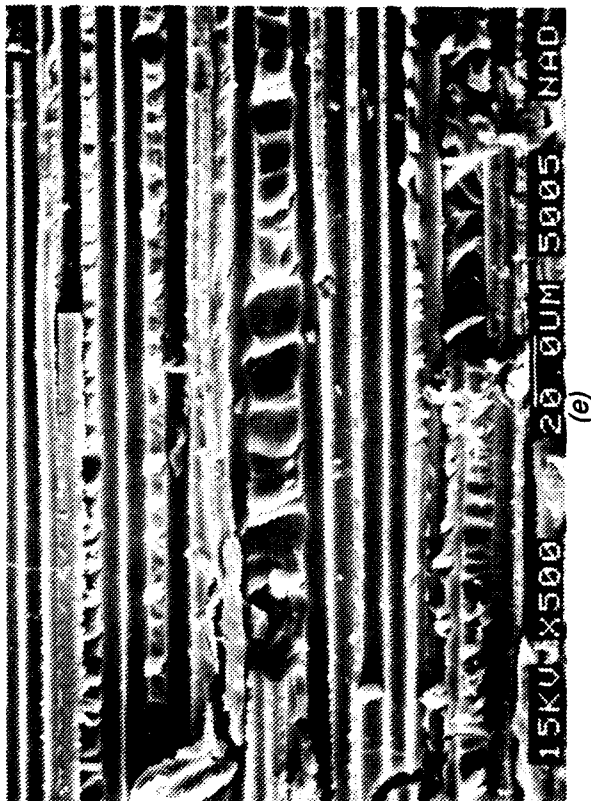
Figure 3-25. (Continued)
(d) Interface Between the Mixed-Mode Region II and the Impact Region IV
(e) Crushed Resin and Debris in the Impact Damaged Area
(f) Mode I Tension and Mode II Shear Fracture Region
Note the presence of river patterns (R), hackles (H), scallops (S) and localized cracks

CD = Crack propagation direction

3-41
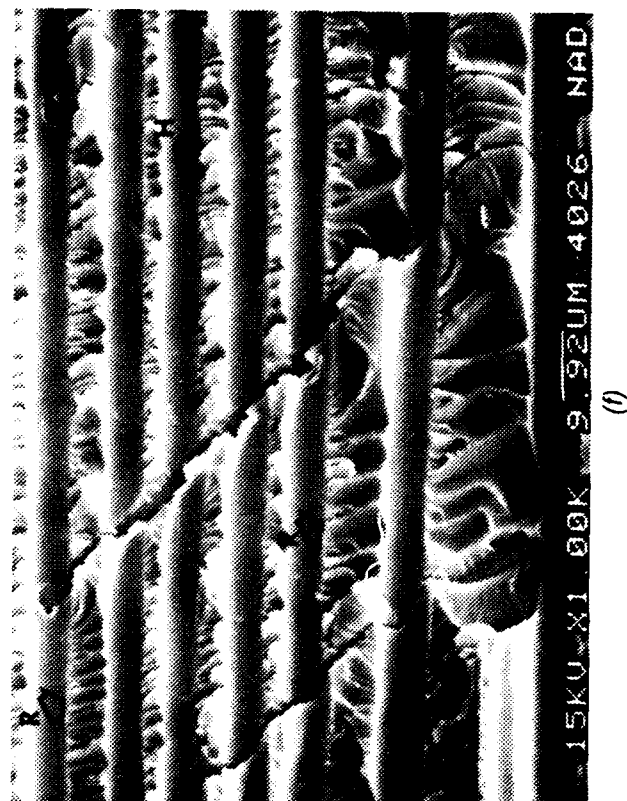
Microscopic examination of Mode I fracture features revealed that initiation occurred in the resin-rich areas between the 0 and 90 degree plies (Figure 3-25b). The crack-propagation direction could be mapped by the orientation of the river patterns, which were initially inclined at an angle to the crack-growth direction (Figure 3-25c), and at larger crack lengths tended to align themselves along the direction of crack-growth. The Mode I area (shown in Figure 3-25c) appeared to show localized hackles and scallops.

Figure 3-25d shows a low magnification photo of the mixed-mode and impact damaged regions. Impact (Region IV) could easily be distinguished and differentiated from Region II (crack-growth area). Figure 3-25e shows microscopic fracture details in the impact damaged region. Crushed resin and debris were present among the hackles, scallops and river patterns within the impact damage zone. Mapping of the river patterns, which would indicate delamination due to impact, was complicated by the river patterns present in the Mode I tension and Mode II shear fracture.

Examination of Region II (crack-growth areas under Mode I tension and Mode II shear) revealed river patterns interspersed between subdued hackles and scallops as previously reported for other mixed-mode variable conditions. The macroscopic crack-growth direction could be mapped in these areas from the orientation of the river patterns (Figure 3-25f). Examination of the fracture surface propagated under Mode I tension and Mode II shear revealed the presence of localized parallel cracks which were at a 45 degree angle to the crack-propagation direction (Figure 3-25f) which were extremely similar to those reported by Boeing for mixed-mode fracture in Gr/Ep.

Translaminar Fractography. Fractographic analysis was carried out on High Resin Content Gr/Ep specimens tested to failure under Mode I Tension or Mode I Compression loading. The results for all the variable conditions are described in Part 2 of Volume II – Atlas of Fractographs. The results for two of the conditions examined were as follows.

Mode I Tension High Resin Content Gr/Ep - 32/Quasi. Figure 3-26 presents photographs illustrating macroscopic and microscopic translaminar tension fracture features observed in 32 ply/quasi-isotropic Gr/Ep that was processed with a high resin content.

Figure 3-26a shows the fracture surface and the apex of the notch machined to initiate crack-propagation under translaminar Mode I tension. Translaminar tension fracture was characterized by fiber end fracture, fiber pullout, and matrix fracture.

Evaluation of the fractured fiber ends in plies oriented normal to the direction of macroscopic fracture revealed the occurrence of radial lines that fanned outward and away from local fracture origins. These indicators could be used to map the overall direction of crack-propagation (Figures 3-26b and 3-26c) in individual fiber bundles. The radial lines were believed to be 'DAF radials' (DAF = directly attributable failure) reported by Dr. Purslow that form during translaminar fracture.

Examination of plies that were oriented either parallel or at an angle to the direction of macroscopic fracture revealed primary fracture in the epoxy, decorated with mixtures of
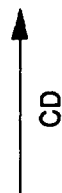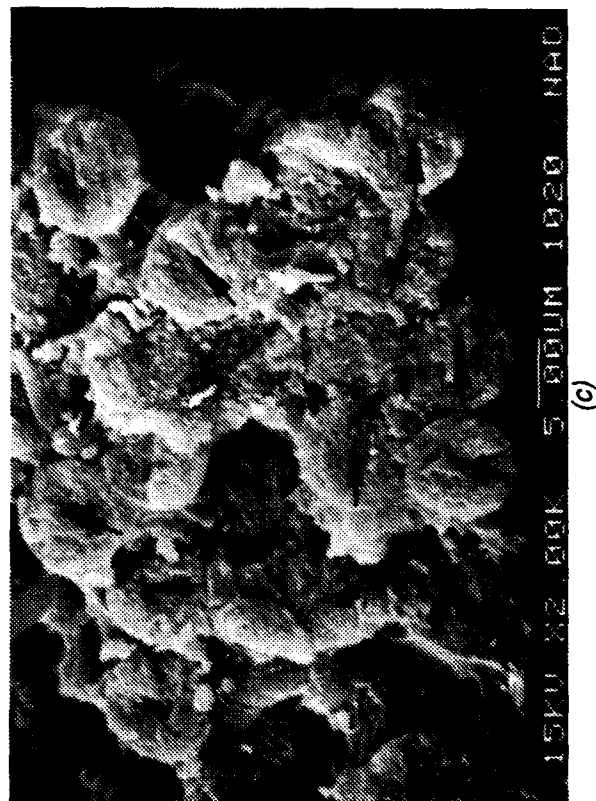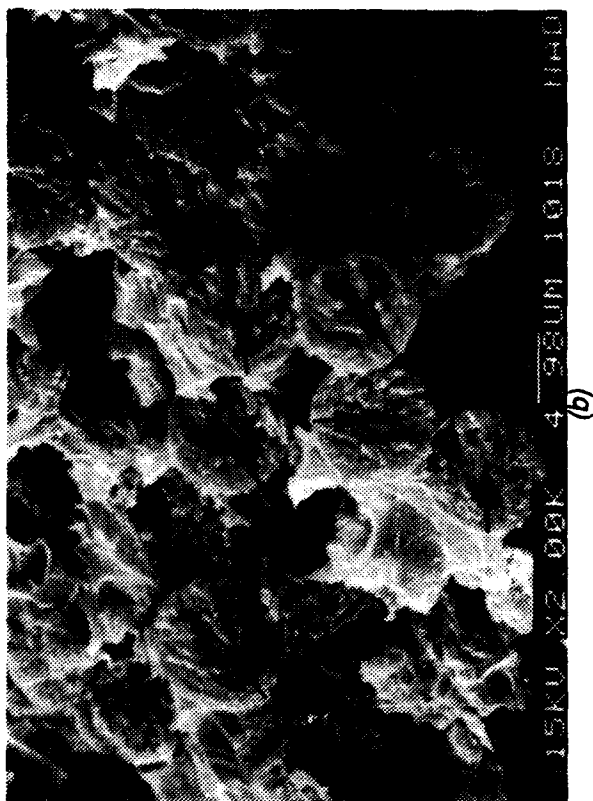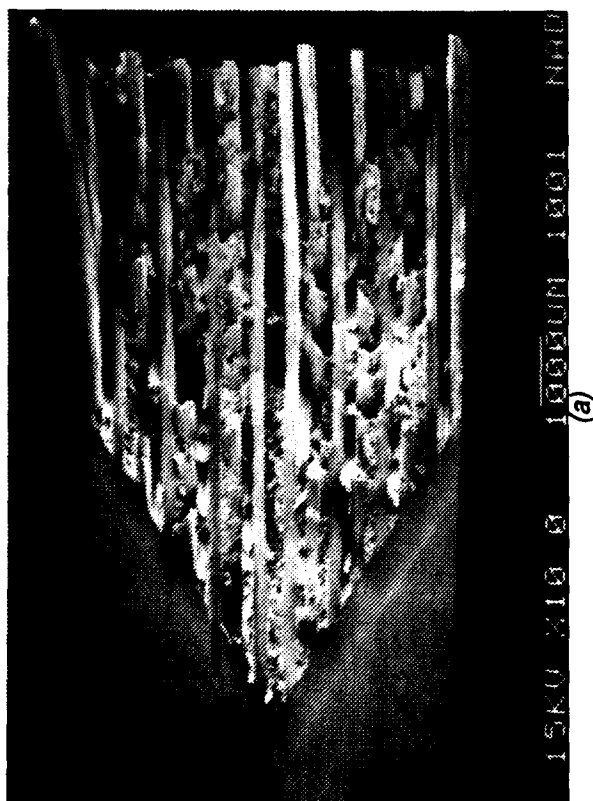
Figure 3-26. SEM Photographs of Mode I Translaminar Tension
Fracture in High Resin Content Gr/Ep - 32 Ply
Quasi-Isotropic
(a) Macrophotograph of the Fracture and Apex
(b) Fracture Near the Apex
Note: Radial lines on fractured fiber ends indicate local fracture path
(shown by arrows).
(c) Fracture Features Present in Ply Oriented
Normal to Fracture and in the Center of the Test
Specimen
Note: Fracture path indicated by arrows.

CD = Crack-propagation direction
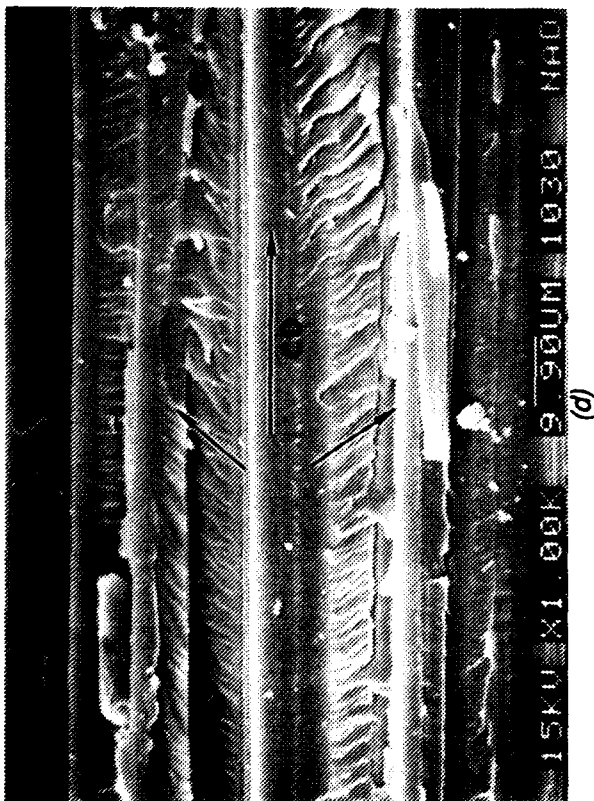
Figure 3-26. (Continued)
(d), (e) River Patterns (Arrows) Present in the
Fractured Epoxy Regions of a 90 Degree Ply
(f) Hackles (H), Scallops (S) and Broken Fibers
in a 45 Degree Ply

CD = Crack-propagation direction
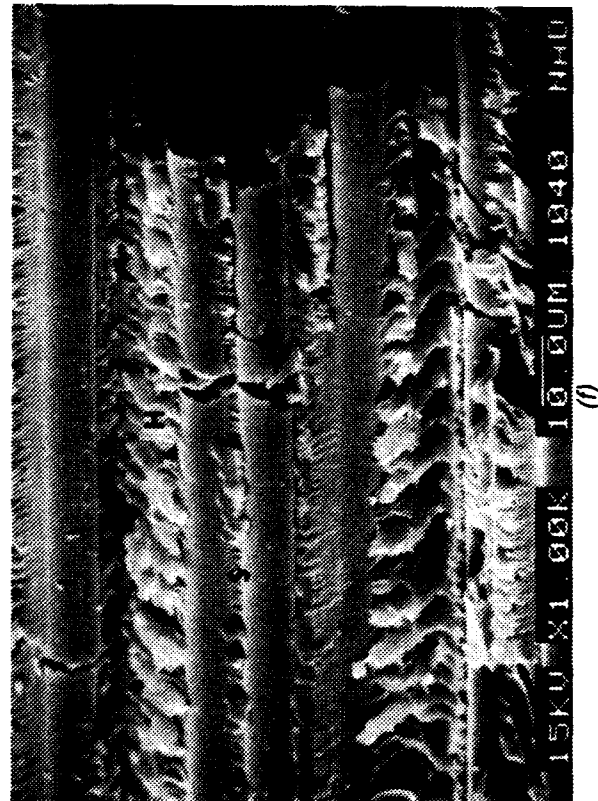
river patterns, hackles, and scallops (Figure 3-26d, e, and f), similar to those previously observed in interlaminar failures. Plies oriented parallel to the macroscopic crack growth direction exhibited more pronounced river pattern formation that coalesced and pointed in the direction of crack-growth. The plies oriented at 45 degrees to the macroscopic crack growth direction showed more pronounced scallop and hackle formation and broken fibers (Figure 3-26f). The river patterns could again be used to map the direction of crack-growth in these plies.

Mode I Compression High Resin Content Gr/Ep - 32/Quasi. Figure 3-27 presents photographs illustrating macroscopic and microscopic translaminar compression fracture features in 32 ply/quasi-isotropic Gr/Ep processed with high resin content.

Figure 3-27a shows the fracture surface and the apex of the notch machined to initiate crack-propagation under translaminar Mode I compression. Translaminar compression fracture was typified by fiber buckling, fiber-end fracture, resin shear fracture, and post-fracture damage.

Evaluation of the fractured surface revealed a flat topography and post-fracture damage (Figures 3-27b and 3-27c). As shown in Figure 3-27d, flexural fracture was observed as a result of translaminar compression. Fractured fiber ends were decorated with "chop" marks that are typical of failure due to compression microbuckling. The crack-propagation direction could not be determined through observation of these fracture features.

Hackles and scallops were observed in the fractured epoxy in plies oriented parallel to the crack-propagation direction (Figure 3-27e). Multiple fiber breaks were also observed in all the plies, as illustrated in Figure 3-27f, and this is typical of failure due to compression microbuckling.

3.4.1.6 Analysis of Fractographic Results for Gr/Ep

An analysis of the fracture results for the specimens evaluated indicates that processing variations (overcure or undercure), material form (filament winding versus tape), or post-processing variables (thermal conditioning, or water immersion) do not significantly alter the fracture characteristics in interlaminar or translaminar failures in Gr/Ep.

Mode I tension interlaminar fracture is characterized by fracture surface river patterns that are oriented at an angle or parallel to the direction of macroscopic fracture. The river patterns can be used to determine local fracture origins since these patterns would be oriented away from the initiation site, and toward propagating fracture.

For pure Mode II shear interlaminar fracture, the characteristic fracture features consist of hackles and scallops that are of different shapes and sizes. These may be oriented toward and/or away from the local fracture initiation site(s) and therefore cannot be used to determine initiation site(s) or crack-propagation directions in Mode II shear interlaminar fracture failures.
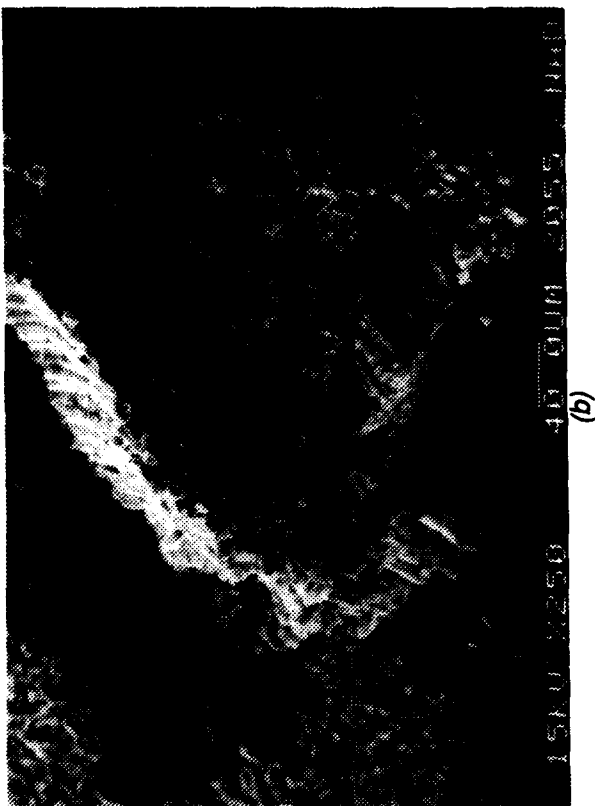
(a)
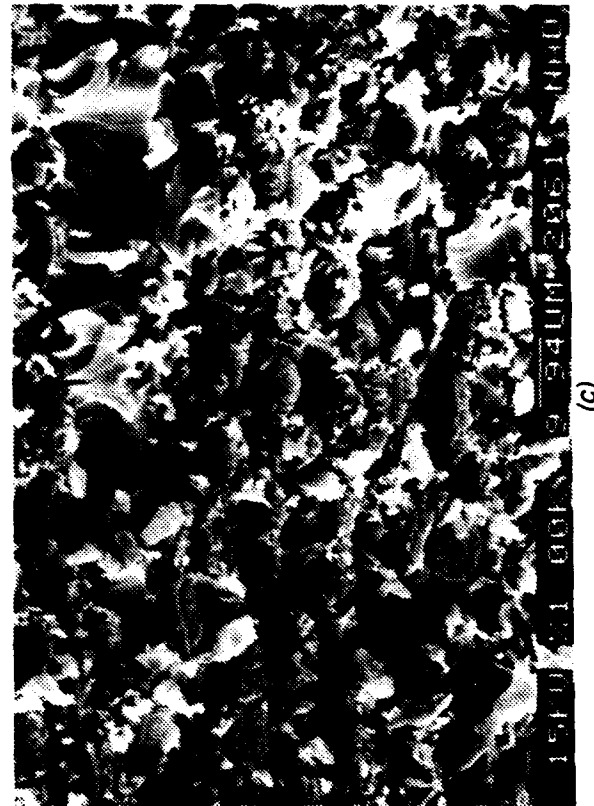
(b)
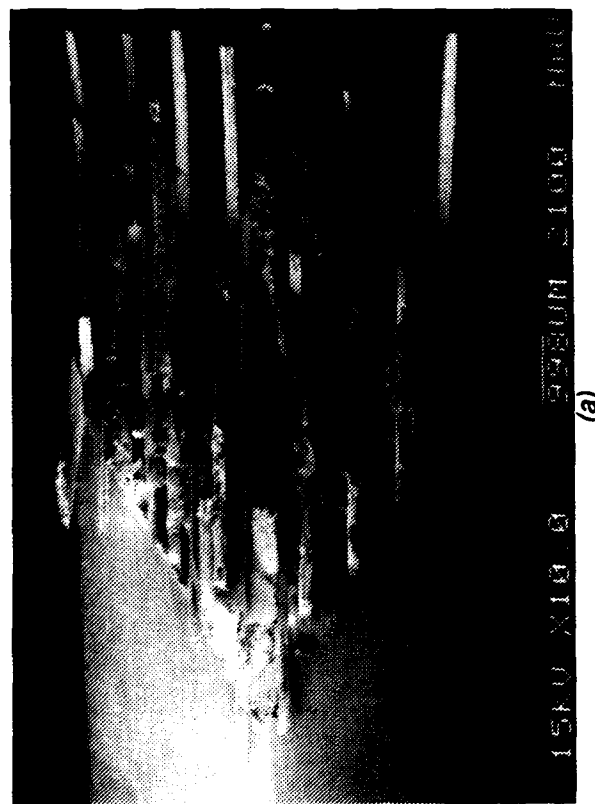
(c)
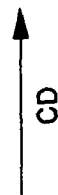
CD

Figure 3-27. SEM Photographs of Mode I Translaminar
Compression Fracture in High Resin Content
Gr/Ep - 32 Ply Quasi-Isotropic
(a) Macrophotograph of the Fracture and Apex
(b) Fracture Near the Apex
Note the flat fracture surface and the post fracture damage
(c) High Magnification of (b) Showing Crushed
Fibers

CD = Crack-propagation direction
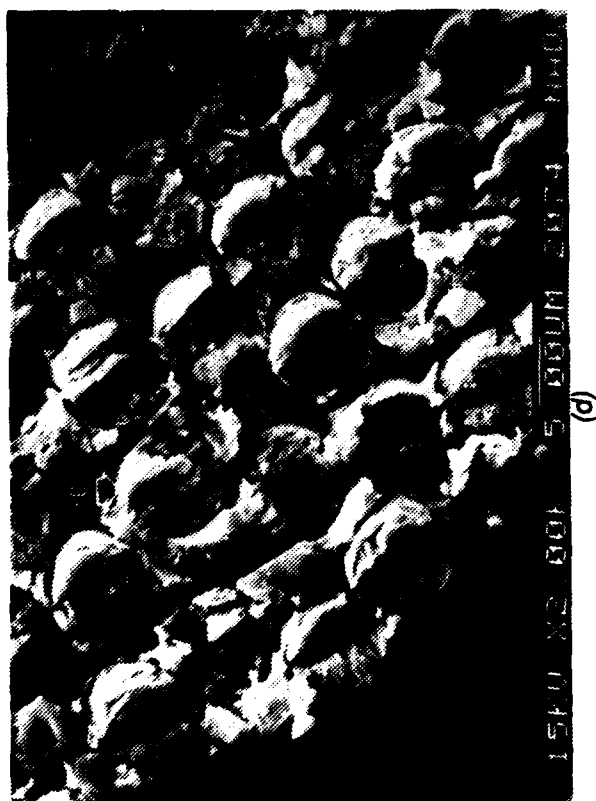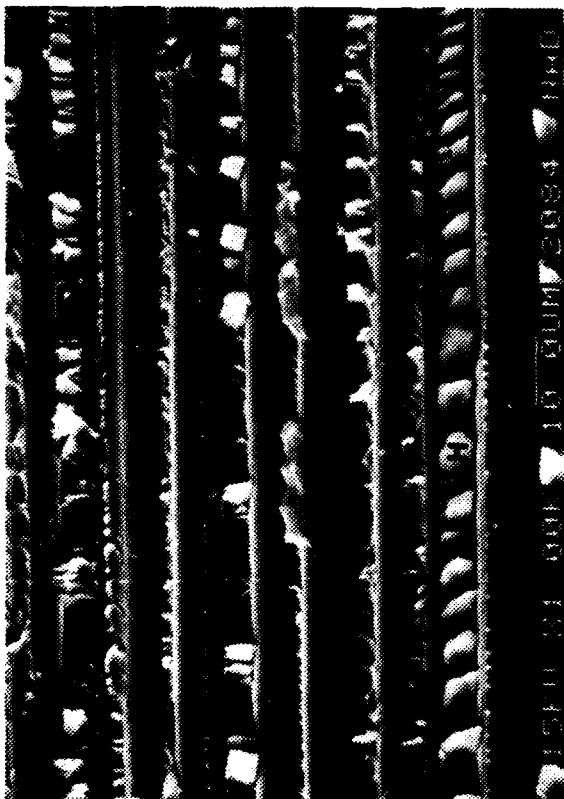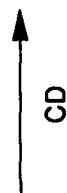
Figure 3-27. (Continued)
(d) Flexural Fracture Features
Note chop marks (C) on individual fiber ends typical of flexural fracture in compression
(e) Hackles (H) and Scallops (S) in a 90 Degree Ply
(f) Multiple Fiber Breaks Due to Microbuckling

CD = Crack-propagation direction

3-47

Mixed-mode interlaminar failures are characterized by mixtures of hackles or scallops and river patterns that are generally interspersed between the hackles. The river patterns can be used to map local fracture origins and direction as for pure Mode I tension.

Evaluation of the translaminar fracture results indicate that variations do not affect fracture characteristics in Mode I tension or Mode I compression failures. Translaminar tension failures can be mapped by the DAF radials on fiber ends, or river patterns on fractured epoxy. In compression failures, there are no indicators of crack-origin or crack-propagation direction in the compression regions; however, these can be determined in tensile failure regions that also form during Mode I compression testing.

3.4.2   Expansion of the Fractographic Database to Other Materials

Northrop prepared a General Test Plan/Procedural Document for expansion of the fractographic database to other materials. This technical activity was part of Task 3, Subtask 3.2. Northrop selected three material systems for expansion of the fractographic database as follows:

1.   Kevlar/Epoxy (Kevlar 49/3501-6)

2.   Graphite/Bismaleimide (AS4/5250-3)

3.   Graphite/PEEK (AS4/APC-2)

The test plan was submitted to the Air Force and subsequently approved.

3.4.2.1   Material Systems

The choice of these three material systems for expansion of the fractographic database was based on the following rationale:

Fleet Applicability. Kevlar/epoxy components are currently used on several military aircraft including the B-1B bomber and the F/A-18 fighter. Graphite/PEEK and graphite/bismaleimide (Gr/BMI) systems are being used in several near-term military aircraft that will form part of the Air Force fleet.

Comparison of Fiber Variation. Choice of the Kevlar 49/3501-6 system would permit a one-on-one comparison of the effect of organic (Kevlar) fibers versus carbon (AS4) fibers on the resulting fracture characteristics in an epoxy system.

Comparison of Matrix Variation. Selection of AS4/5250-3 and AS4/APC-2 would provide information on the effects of 1) toughening the matrix, and 2) thermoset versus thermoplastic resin on the resultant fracture characteristics.

3.4.2.2   Test Details

The tests performed for interlaminar and translaminar fracture are shown in Tables 3-7 through 3-12. These were based on the results of the fractographic study performed by Northrop in Task 3, Subtask 3.1, and the work performed by Boeing under Air Force Contract F33615-84-C-5010.

A total of 21 varied interlaminar fracture tests (two to three replicates) were carried out for Kevlar 49/3501-6, AS4/5250-3 and AS4/APC-2. The test conditions primarily consisted of singular failure modes. For translaminar characterization, a total of 15 varied tests were performed that would result in singular failure modes. The tests included the effects of impact damage, water immersion, and combined experimental variables such as moisture plus temperature.

For the tests, a total of 13 laminates were required. The dimensions and layups for the laminates are shown in Tables 3-7 through 3-12. All laminates were from tape prepreg.

3.4.2.3 Test Specimens

Northrop used interlaminar and translaminar fracture test specimens ((Mode I DCB, Mode II ENF/CLS, Mode I and Mode II MMF, Mode I Tension (four point load), Mode I Compression (four point load) and Mode II side-notched rail shear specimens)) similar to those used in Subtask 3.1 of this program.

Mechanical tests of the specimens were performed in accordance with ASTM specifications or standard Northrop laboratory practice. The objective was to achieve fractures under controlled laboratory conditions.

Table 3-7. 49/3501-6 Kevlar/Epoxy Interlaminar Fracture Test Matrix

SPECIMEN, LOADING	VARIABLE CONDITION	LAYUP	LAMINATE DIMENSIONS	NO. OF LAMINATES
Mode I DCB, Tension	RTA			
Mode II ENF, Shear	RTA	24/0	22 X 11	1
Mode I+II MMF, Tension+Shear	RTA			
Mode I DCB, Tension	Cond. 180 F 2 weeks before test	24/0	13 X 13	1
Mode II ENF, Shear				
Mode I DCB, Tension	RTA			
Mode II ENF, Shear	RTA	24/0,45	22 X 11	1
Mode I DCB, Tension	Water Immer. before test			

RTA = Room Temperature Ambient
Laminate dimensions in inches

Table 3-8. 49/3501-6 Kevlar/Epoxy Translaminar Fracture Test Matrix

SPECIMEN, LOADING	VARIABLE CONDITION	LAYUP	LAMINATE DIMENSIONS	NO. OF LAMINATES
Mode I Tension, 4 pt. load	RTA			
Mode I Compression, 4 pt. load	Water Immer. before test	32/90,0	14 x 7	1
Mode I Compression, 4 pt. load	RTA			
Mode I Compression, 4 pt. load	RTA			
Mode I Compression, 4 pt. load	Water Immer. before test	32/quasi	14 X 7	1
Mode I Compression, 4 pt. load	Cond. 180 F 2 weeks before test			

RTA = Room Temperature Ambient
Laminate dimensions in Inches

3.4.2.4 Fractographic Examination and Documentation

Northrop performed fracture examination of test coupons from all three material systems using visual and SEM techniques. The fractographs have been organized in a logical manner in Volume II , Part 2 – Atlas of Fractographs in sections classified according to the type of material. For the purpose of information, selected data for all three material systems and general fracture observations made on these materials is presented below.

Kevlar/Epoxy. Evaluation of the test coupons for this material system established that the type of fiber present in the system plays a strong role in controlling resultant fracture surface characteristics. In general, the fracture surfaces were associated with dense tangles of fractured fibrils, as illustrated in Figures 3-28 and 3-29. These generally precluded meaningful determination of fracture origins and crack-growth directions. Representative samples of interlaminar and translaminar fractures for baseline and some of the variable conditions are discussed below. Detailed information is available in Volume II, Part 2 – Atlas of Fractographs.

Table 3-9. AS4/5250-3 Gr/BMI Interlaminar Fracture Test Matrix

SPECIMEN, LOADING	VARIABLE CONDITION	LAYUP	LAMINATE DIMENSIONS	NO. OF LAMINATES
Mode I DCB, Tension	RTA			
Mode I DCB, Tension	Water immer. before test			
Mode II ENF, Shear	RTA	24/0	22 X 16.5	1
Mode II ENF, Shear	Water immer. before test			
Mode I + II MMF, Tension + Shear	RTA			

RTA = Room Temperature Ambient
Laminate dimensions in Inches

Table 3-10. AS4/5250-3 Gr/BMI Translaminar Fracture Test Matrix

SPECIMEN, LOADING	VARIABLE CONDITION	LAYUP	LAMINATE DIMENSIONS	NO. OF LAMINATES
Mode I Tension, 4 pt. load	RTA			
Mode I Compression, 4 pt. load	RTA	32/90,0	14 X 7	1
Mode I Compression, 4 pt. load	Water immer. before test			
Mode I Tension, 4 pt. load	RTA	32/quasi	8 X 6	1

RTA = Room Temperature Ambient
Laminate dimensions in Inches

Table 3-11. AS4/APC-2 Gr/PEEK Interlaminar Fracture Test Matrix

SPECIMEN, LOADING	VARIABLE CONDITION	LAYUP	LAMINATE DIMENSIONS	NO. OF LAMINATES
Mode I DCB, Tension	RTA			
Mode II ENF, Shear	RTA			
Mode I DCB, Tension	Cond. 180 F 2 weeks before test	24/0	22 X 16.5	1
Mode I DCB, Tension	Water immer. before test			
Mode I+II MMF, Tension + Shear	RTA			
Mode I DCB, Tension	RTA			
Mode I DCB, Tension	Cond. 180 F 2 weeks before test	24/0,45	13 X 13	1
Mode I DCB, Tension	Cond. 180 F 2 weeks before test	24/90,0	13 X 8	1

RTA = Room Temperature Ambient
Laminate dimensions in inches

Interlaminar Fractography. Figures 3-28 and 3-29 present photographs for the 24/0 and 24/0, ±45 baseline K/Ep specimens tested to failure under Mode I interlaminar tension. On a macroscopic scale, the precrack, crack-growth, and laboratory overload areas could not be distinguished as in baseline Gr/Ep. Interlaminar fracture was characterized by fibers being "pulled out" from the matrix (Figure 3-28b). In the 24/0, ±45 variant fracture initiated at a 0/45 interface and "skipped" from one ply to the adjacent ply.

SEM examination revealed that fracture could be mapped by stray river patterns present in resin-rich areas (Figures 3-28c, and 3-29b). Fractured resin associated with pulled fibers exhibited occasional hackles (Figure 3-29c) indicating that locally the applied loads were mixed (tension and shear) in nature.

Table 3-12. AS4/APC-2 Gr/PEEK Translaminar Fracture Test Matrix

| SPECIMEN, LOADING	VARIABLE CONDITION	LAYUP	LAMINATE DIMENSIONS	NO. OF LAMINATES
Mode I Tension, 4 pt. load	RTA			
Mode I Compression, 4 pt. load	RTA			
Mode I Compression, 4 pt. load	Water Immer. before test	32/90,0	15 X 8	1
Mode I Compression, 4 pt. load	Impact damage before test			
Mode I Tension, 4 pt. load	Cond. 180 F 2 weeks before	32/quasi	8 X 6	1

RTA = Room Temperature Ambient

Laminate dimensions in inches

Figure 3-30 shows photographs for thermally-conditioned K/Ep. Fractographic examination of this condition revealed no differences in comparison with the room temperature ambient (RTA) condition. Fracture was associated with stray rivers, pulled fibers, and stray hackles.
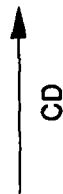
Translaminar Fractography. SEM photographs illustrating translaminar tensile fracture in 32/90,0 K/Ep are shown in Figure 3-31. On a macroscopic scale, the fracture surfaces consisted of dense tangles of fibrils (Figure 3-31a) with no indicators of the tension and compression zones that are normally observed in Gr/Ep. Careful examination of the 90 and 0 degree plies revealed stray hackles (Figure 3-31b); however, there were no features that could be unequivocally used to map the crack-growth direction.

Figure 3-32 shows SEM photographs of quasi-isotropic K/Ep that was thermally conditioned prior to testing to failure under Mode I translaminar tension loads. The macroscopic fracture features were similar to the nonconditioned K/Ep specimen. Again there were no features that could be used to predict the crack-propagation direction.

Graphite/Bismaleimide. In general, the fracture surface characteristics associated with this type of material were similar to that for AS4/3501-6. Fracture features in the resin such as river patterns or hackles were not as abundant as in Gr/Ep. However, careful evaluation of large areas generally permitted determination of fracture origins and crack-growth directions.

(a)

CD
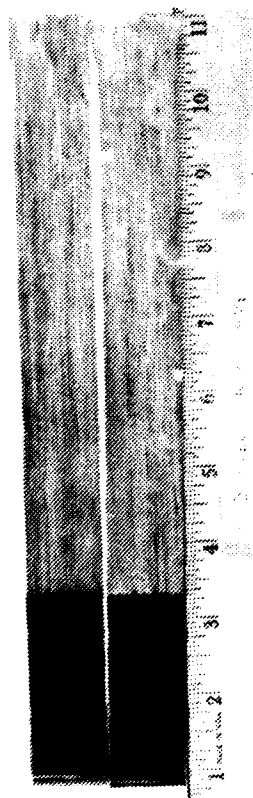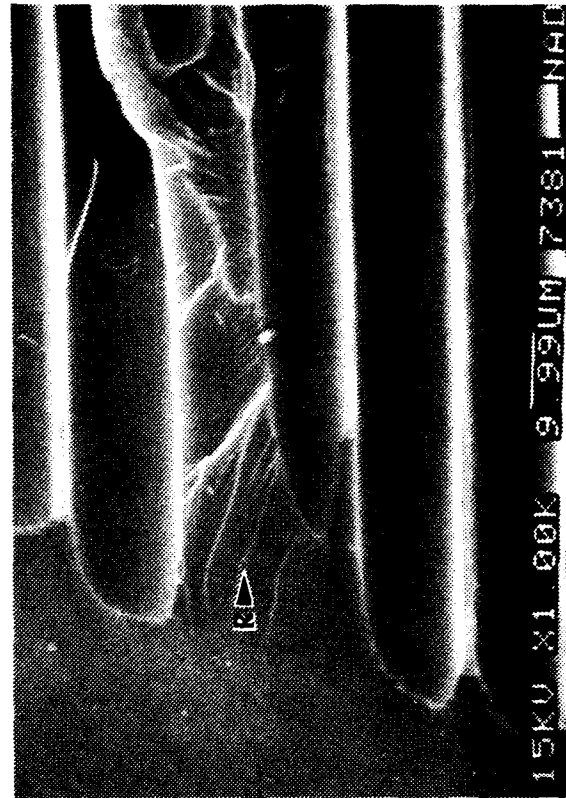
Figure 3-28. Optical and SEM Photographs of Mode I DCB Interlaminar Fracture in 49/3501-6 Kevlar/Ep - [0]$_{24T}$, Room Temprature Ambient
(a) Macrophotograph
(b) Fiber Pull-Out
(c) River Patterns (R) in Fractured Resin

CD = Crack-propagation direction
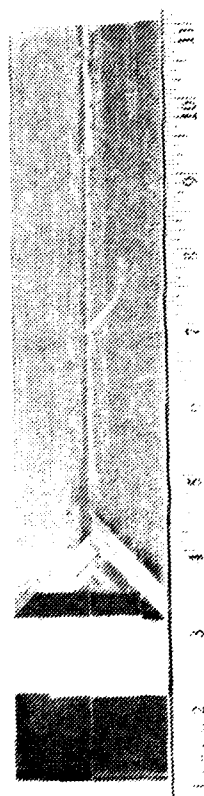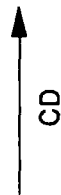
Figure 3-29. Optical and SEM Photographs of Mode I DCB
Interlaminar Fracture in 49/3501-6 Kevlar/Ep -
[+45/0/-45]₄s , Room Temperature Ambient
(a) Macrophotograph
(b) River Patterns (R) at Initiation Site
(c) Hackles (H) in Fractured Resin

CD = Crack-propagation direction
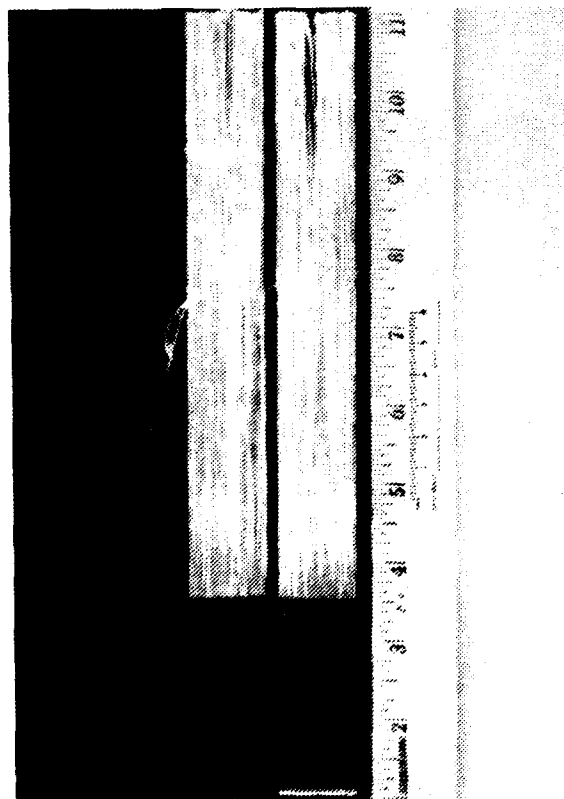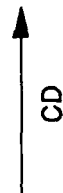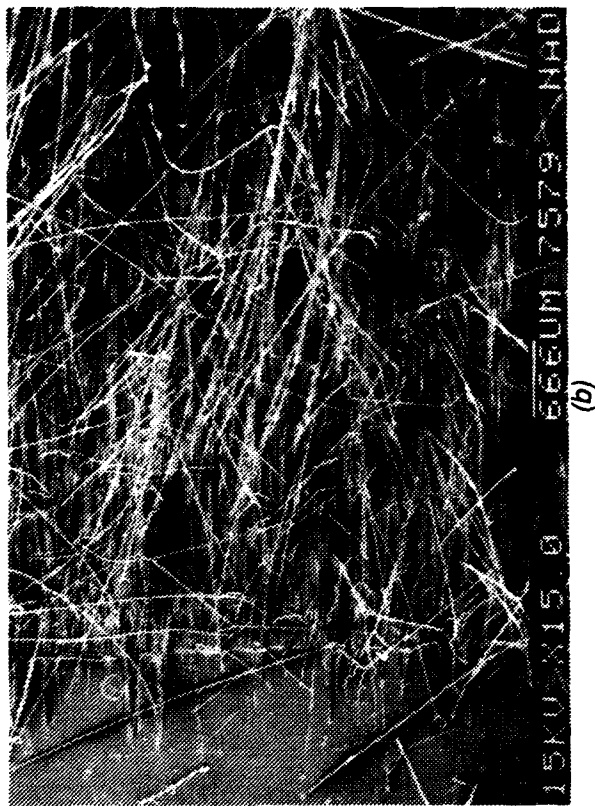
Figure 3-30. *Optical and SEM Photographs of Mode I DCB Interlaminar Fracture in 49/3501-6 Kevlar/Ep - [0]$_{24T}$, Conditioned 180 Degrees F, Dry, 2 Weeks Before Test*
(a) Macrophotograph
(b) Fiber Pull-Out
(c) River (R) and Hackles (H) in Pre-Crack Region

CD = Crack propagation direction

(b)

(a)

CD
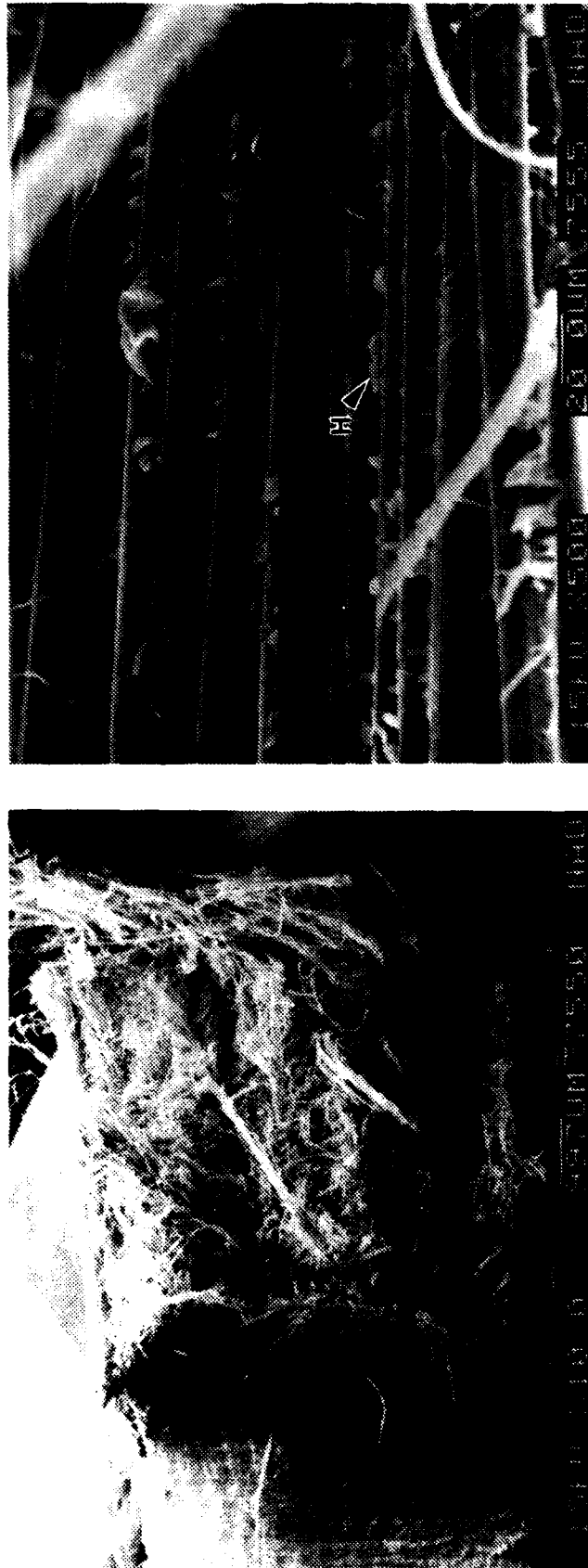
Figure 3-31. SEM Photographs of Mode I Translaminar Tension Fracture in 49/3501-6 Kevlar/Ep - $[90/0]_{8s}$, Room Temperature Ambient
(a) Dense Tangles of Fibrils
(b) Hackles (H)

CD = Crack-propagation direction
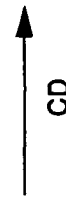
Figure 3-32. *SEM Photographs of Mode I Translaminar Tension Fracture in 49/3501-6 Kevlar/Ep - [90/0]$_{8s}$, Conditioned 180 Degrees F, Dry, 2 Weeks Before Test*
(a) Dense Tangles of Fibrils
(b) Buckling of Plies

CD = Crack-propagation direction

Representative samples of interlaminar and translaminar fractures for baseline and some of the variable conditions are discussed below. Detailed information is available in Volume II, Part 2 – Atlas of Fractographs.

Interlaminar Fractography. Figure 3-33 presents fracture features in unidirectional Gr/BMI tested to failure under mixed Mode I tension and Mode II shear interlaminar loads. The fracture could be categorized on a macroscopic level into three regions as for baseline Gr/Ep (Figure 3-33a). Fracture initiated at resin rich regions adjacent to the Armalon film, and could be mapped by the river patterns in the fractured BMI resin. Peel fracture in Region II was characterized by a mixture of hackles, cusps, and river patterns, with the rivers being oriented at an angle to the crack-growth direction (Figure 3-33c).

Translaminar Fractography. Figure 3-34 provides photographs of fracture in AS4/5250-3 Gr/BMI tested under translaminar tension. Fractured zero degree fibers in the tensile regions resembled coarse chevrons oriented toward the fracture origin (Figure 3-34a). These features were similar to those reported by David Purslow for 90/0 translaminar fractures in Gr/Ep (Reference 8). These served as indicators of the fracture origins in a manner similar to chevrons in metallic materials.

Unlike Gr/Ep, translaminar failure in Gr/BMI was characterized by extensive fiber pull-out, with local fiber bundles in the tensile regions exhibiting bending caused by flexural loads (Figure 3-34b).

Figures 3-34c and 3-34d show microscopic fracture characteristics in the tensile regions. Unlike Gr/Ep, fracture in local plies oriented normal to the applied load exhibited extensive pull-out and ductile separation of fibers from the adjoining resin (Figure 3-34c). In addition, fractured fibers in the tensile regions exhibited a mix of DAF radials (indicative of tension failure), and chop marks (indicative of compression failure), as shown in Figure 3-34d. The compression characteristics are believed to be caused by localized flexural loading of fiber bundles in the tensile regions.

Figure 3-34e illustrates characteristics in plies oriented normal to the applied load (tensile fracture areas). As for Gr/Ep, fracture in Gr/BMI was characterized by a mix of rivers and hackles. However not enough river patterns were present to establish local crack direction. Local fracture in compression regions was characterized by chop marks (Figure 3-34f).

Graphite/Thermoplastic. Detailed results for all the variable conditions examined for this material system are presented in Volume II, Part 2 – Atlas of Fractographs. In general, interlaminar peel fractures could be mapped through macroscopic evaluation of light and dark bands that were present on the fractures. These features were generally oriented in the direction of crack-propagation, and were not observed in shear failures.

On a microscopic scale interlaminar shear fracture could be distinguished and differentiated from peel fracture through examination of mating fracture surfaces, as will be discussed in the next few paragraphs.

An evaluation of the translaminar fracture characteristics for this system indicated that the fracture features on broken fiber ends were similar to that in Gr/Ep; namely, DAF radials in

(a)

(b)

(c)

CD

CD = Crack-propagation direction
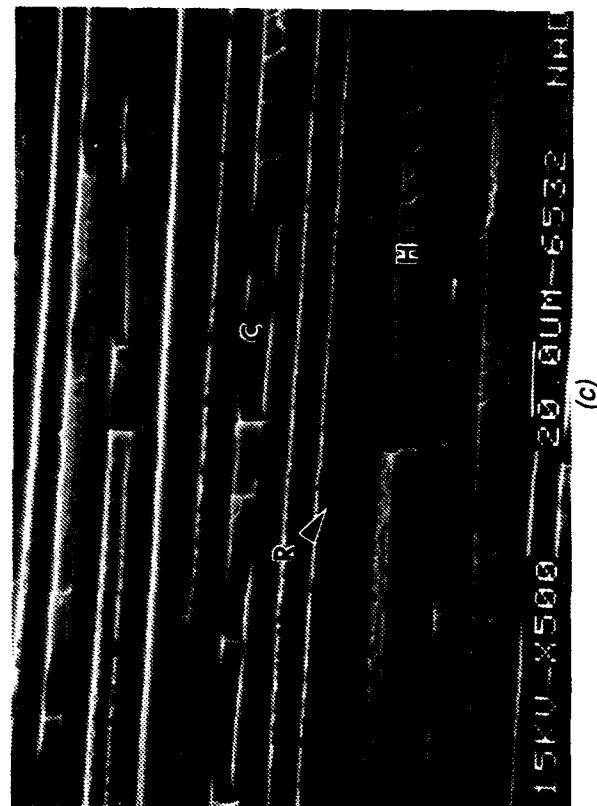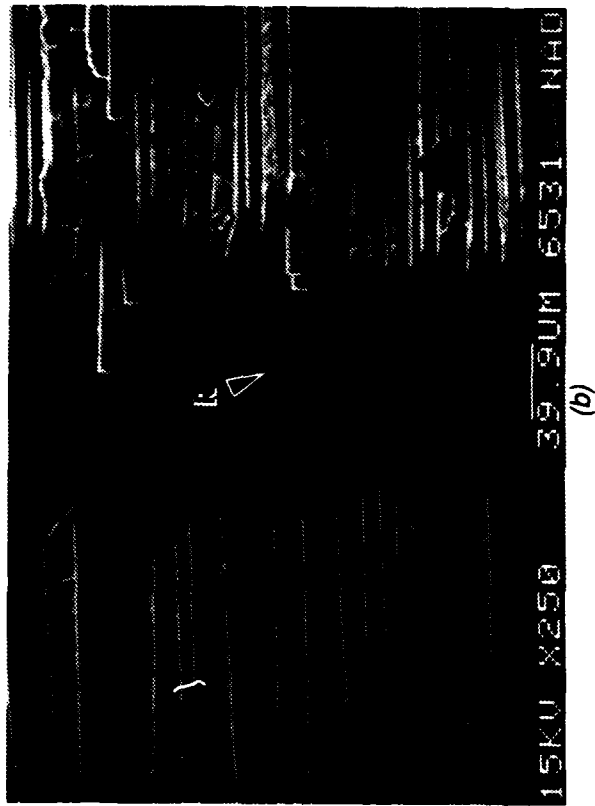
Figure 3-33. Optical and SEM Photographs of Mode I and II MMF Interlaminar Fracture in AS4/5250-3 Gr/BMI - [0]$_{24T}$, Room Temperature Ambient
(a) Macrophotograph of Regions I, II, III (Precrack, Crack-Growth, and Laboratory Overload Fracture Areas)
(b) River Patterns (R) in Initiation Region in Precrack
(c) Rivers (R), Hackles (H), and Cusps (C) in Crack-Growth Region
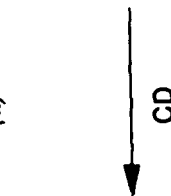
Figure 3-34. SEM Photographs of Mode I Translaminar Tension Fracture in AS4/5250-3 Gr/BMI - [90/0]8s
(a) Normal Views of Fracture
Note: Arrows indicate chevrons.
(b) Oblique View of Fracture
Note extensive fiber pull-out and local bending of fiber bundles (arrow)
(c) Fiber Pull-Out and Separation From Resin in Tension Region of Fracture

C = Compression region
CD = Crack-propagation direction
T = Tension region
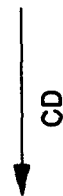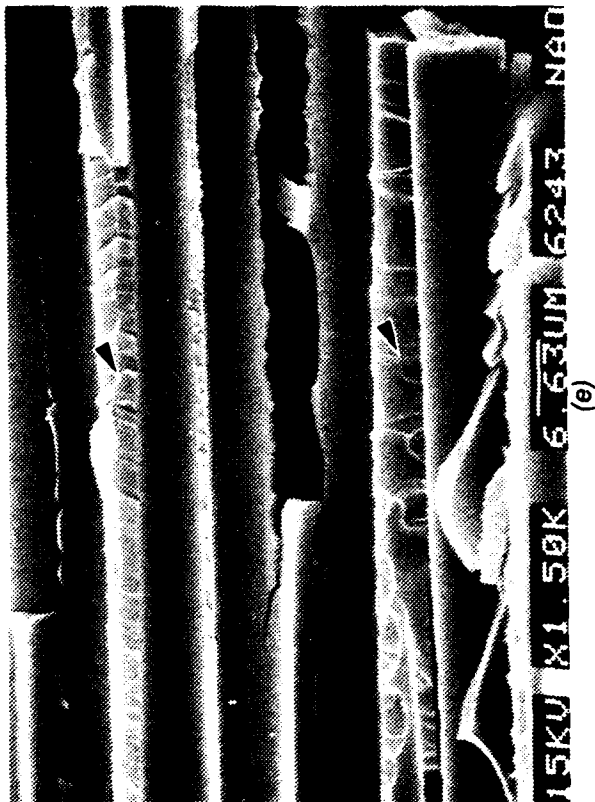
Figure 3-34. (Continued)
(d) Chop Marks (Solid Arrows) and DAF Radials
(Hollow Arrows) on Fiber Ends
(e) Resin Fracture in 90 Degree Ply (Tension)
Note river patterns (arrows)
(f) Chop Marks on Fiber Ends in Compression
Region

CD = Crack-propagation direction

tension failures, and chop marks in compression failures.

No differences were observed between the baseline condition and variable conditions examined for this system.

Interlaminar Fractography. Figure 3-35a shows a macrophotograph of fracture in a unidirectional AS4/APC-2 ENF specimen tested to failure. On a macroscopic scale, the fracture could be categorized into Regions I, II and III. Regions I and III were areas of peel fracture. Region II was the shear fracture.

Figures 3-35b and 3-35c are low magnification photographs of the fracture. Regions I and III were characterized by ribs (Figure 3-35b) that were concentric about the initiation area. In contrast, Region II was devoid of ribs (Figure 3-35c). These observations confirm Purslow's findings that ribs did not form in pure shear.

Figures 3-35d, 3-35e and 3-35f present high magnification SEM photographs of fracture in Region I. This precrack region did not exhibit indicators of crack-growth direction; however, examination of mating halves of the fracture in Region II (interlaminar shear region) revealed the occurrence of drawn fibrils that were oriented <u>toward</u> the crack-growth direction in one half, and <u>away</u> from the crack-growth direction in the mating half (Figure 3-35g and 3-35h).

Figure 3-36 presents fracture features in unidirectional Gr/PEEK tested to failure under mixed Mode I tension and Mode II shear interlaminar loads. The fracture could be categorized on a macroscopic level into three regions as before (Figure 3-36a). Examination at low magnifications (Figure 3-36b) revealed the presence of rib formation all over the fracture that could be used to map crack-propagation direction, since these were oriented radially outward and emanating from the initiation regions. The presence of ribs all over the fracture surface would be expected since the precrack, crack-growth and laboratory overload fracture regions (Regions I, II, and III, respectively), had all formed under peel loads.

SEM examination of the microscopic fracture features in mating fracture halves (Figures 3-36c and 3-36d) revealed drawn fibrils that were oriented either <u>away</u> from the crack-growth direction or <u>toward</u> the crack-growth direction in both halves. Pure shear fracture was characterized by fibrils drawn toward the crack-growth direction in one half, and away from the crack-growth direction in the mating half. It was determined that the drawn fibrils could not be used to establish crack-growth direction in mixed mode fractures; however, examination of these features on mating halves permitted identification of peel failure regions from regions of shear.

Translaminar Fractography. Figure 3-37 presents macroscopic and microscopic fracture features in AS4/APC-2 Gr/PEEK tested under Mode I translaminar tension loading. There were no macroscopic differences between the tension and compression fracture regions that normally occur during translaminar testing. However, as shown in Figure 3-37a, fractured fibers in the 0 degree plies resembled gross chevrons that radiated toward the machined notch.

Figures 3-37b and 3-37c show microscopic fracture features in local tensile fracture
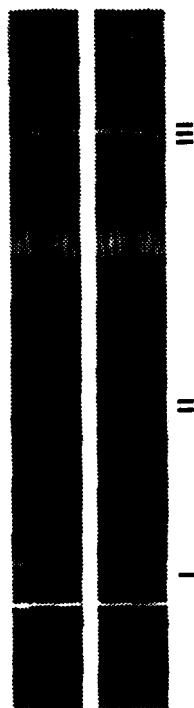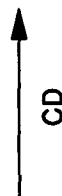
Figure 3-35. Optical and SEM Photographs of Mode II ENF Interlaminar Fracture in AS4/APC-2 Gr/PEEK - [0]$_{24T}$, Room Temperature Ambient

(a) Macrophotograph of Regions I, II, III (Pre-Crack, Crack-Growth, and Laboratory Overload)
Note banded appearance in region III

(b) Ribs in Region I Oriented Along CD

(c) Region I/II Transition
Note absence of ribs in region II

CD = Crack-propagation direction
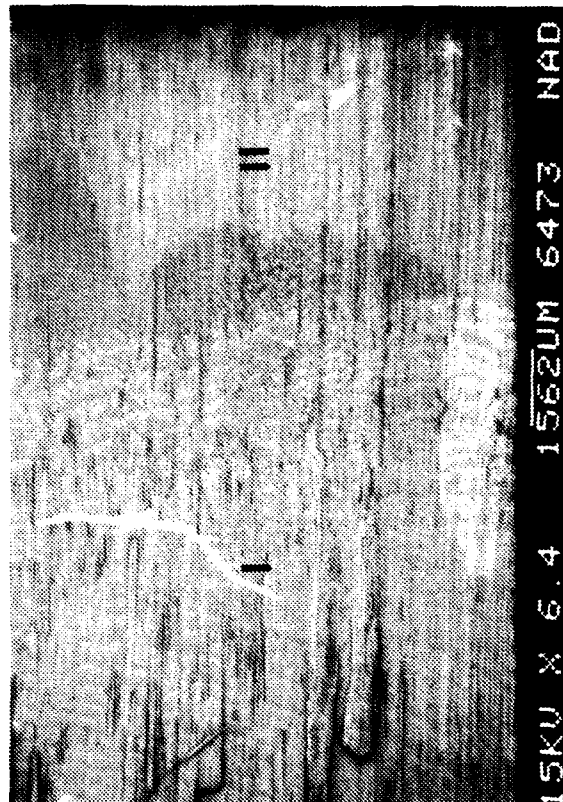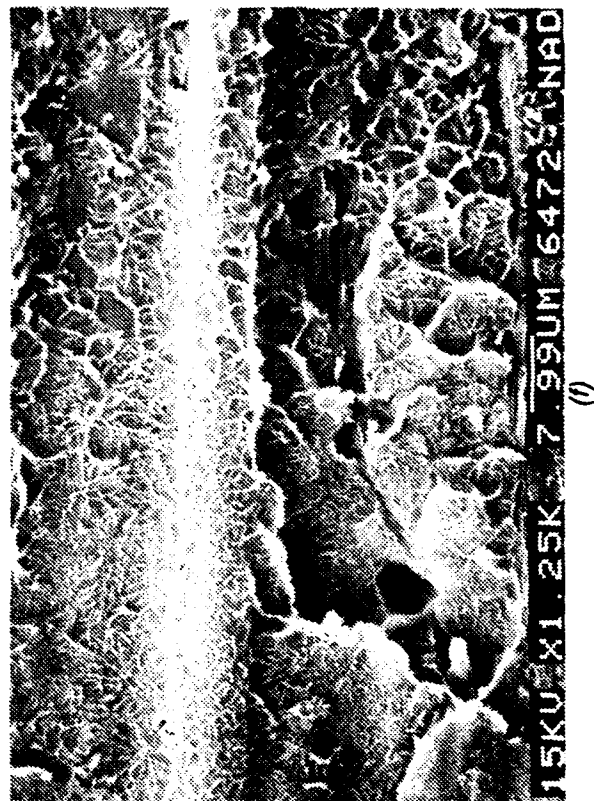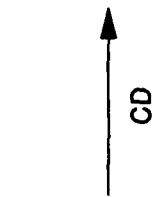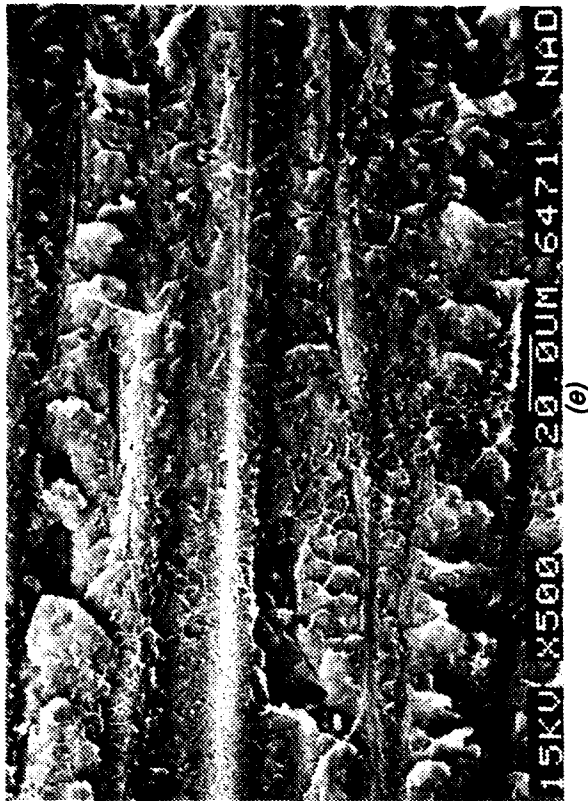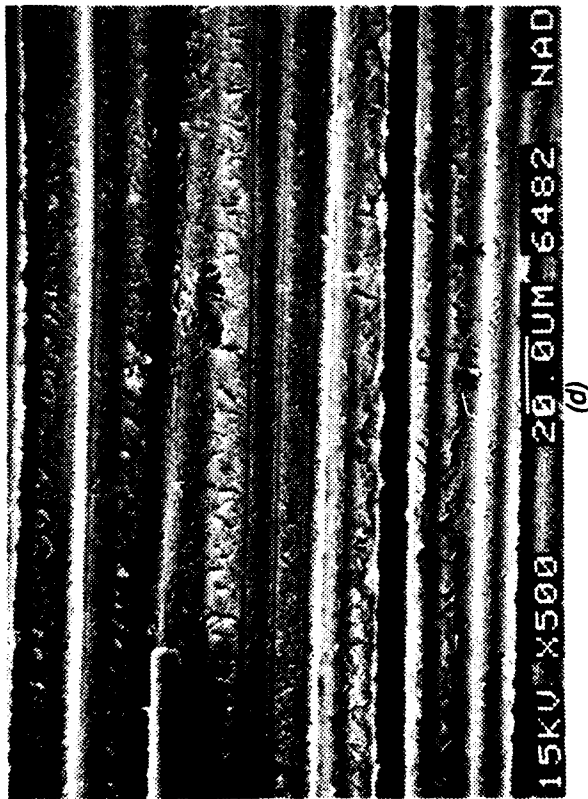
Figure 3-35. (Continued)
(d), (e) Region I Fracture
(f) Peel Fracture in Region I

CD = Crack-propagation direction
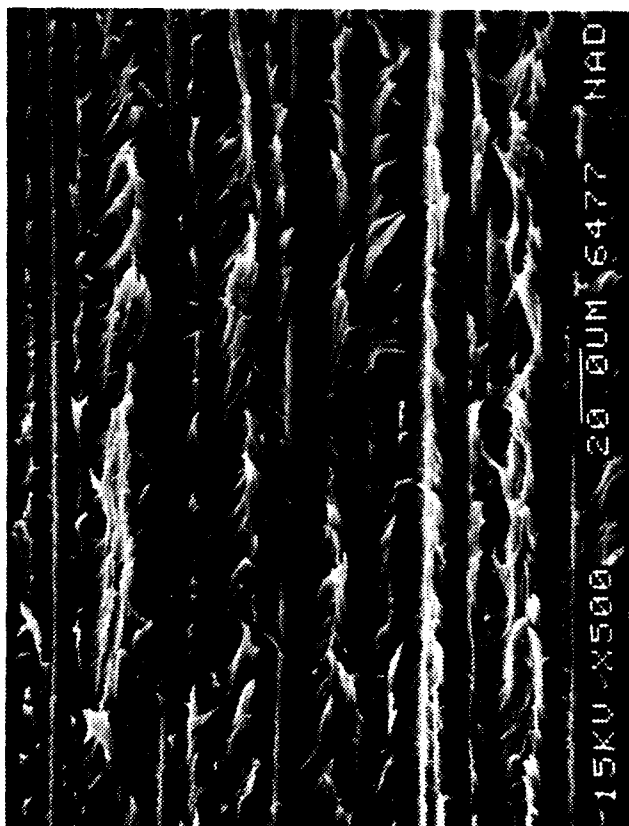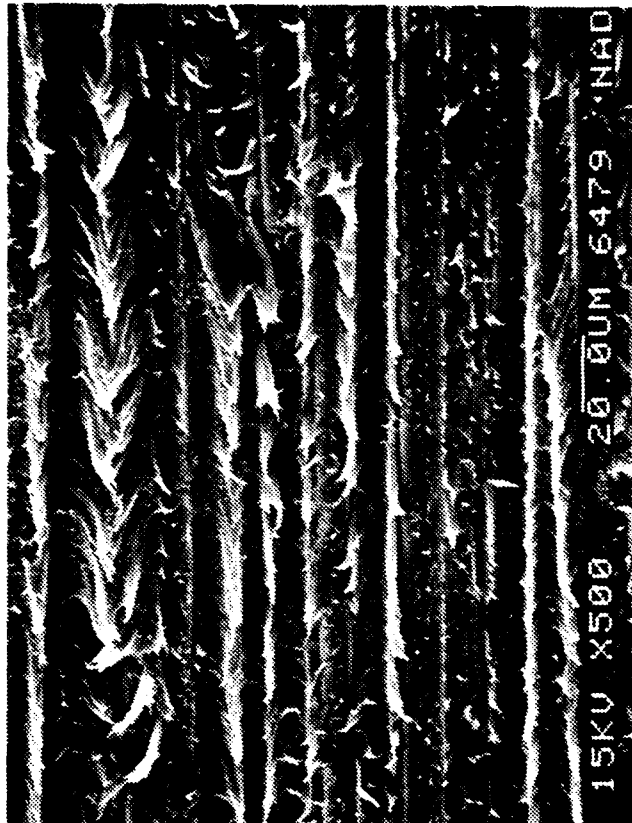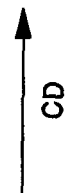
Figure 3-35. *(Continued)*
(g), (h) Shear Fracture Regions in Mating Fracture Halves
Note orientation of drawn fibrils (arrows) in relation to CD

CD = Crack-propagation direction

(b)

CD
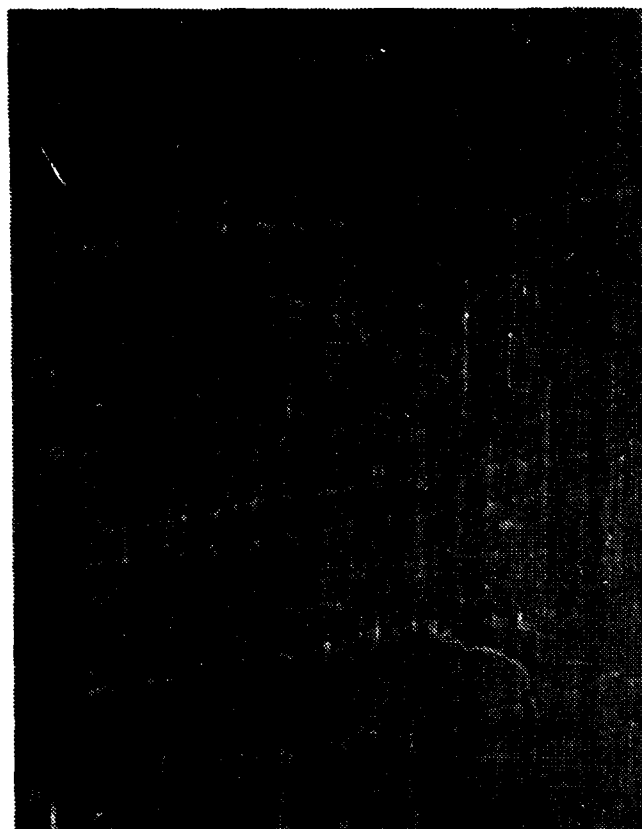
(a)
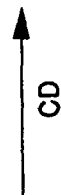
Figure 3-36. Optical and SEM Photographs of Mode I and Mode II MMF Interlaminar Fracture in AS4/APC-2 Gr/PEEK - [0]$_{24T}$, Room Temperature Ambient
(a) Macrophotograph
Note: I, II, III are pre-crack, crack-growth, and laboratory overload regions and arrows indicate ribs in region III.
(b) Ribs in Region II

CD = Crack-propagation direction

(d)
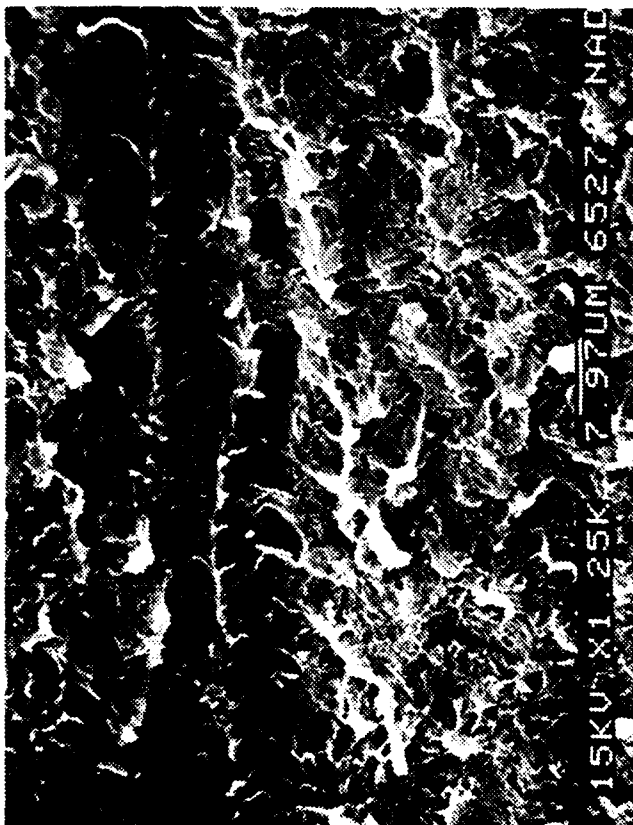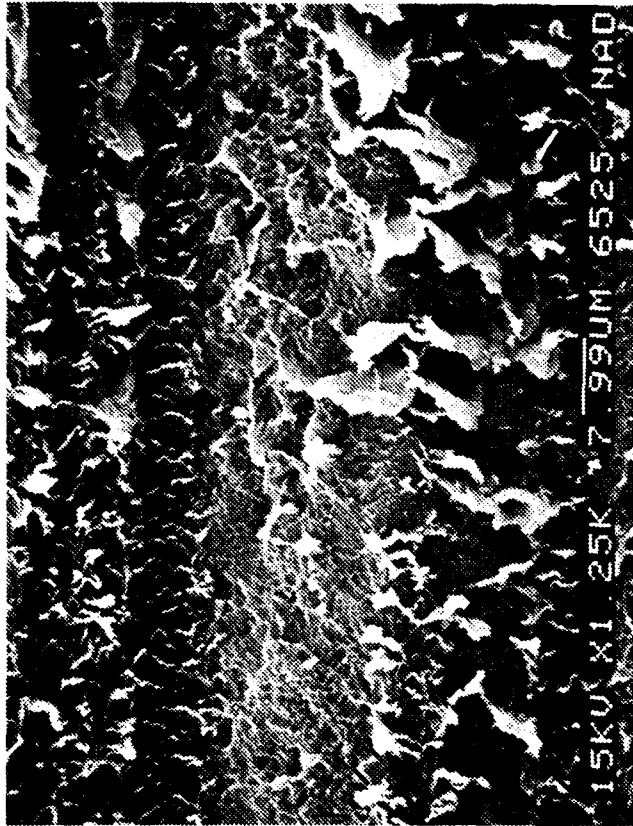
CD
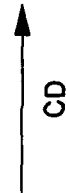
Figure 3-36. (Continued)
(c), (d) Shear Fracture Region in Mating Fracture Halves
Note orientation of drawn fibrils (arrows) in relation to CD

CD = Crack-propagation direction

(c)
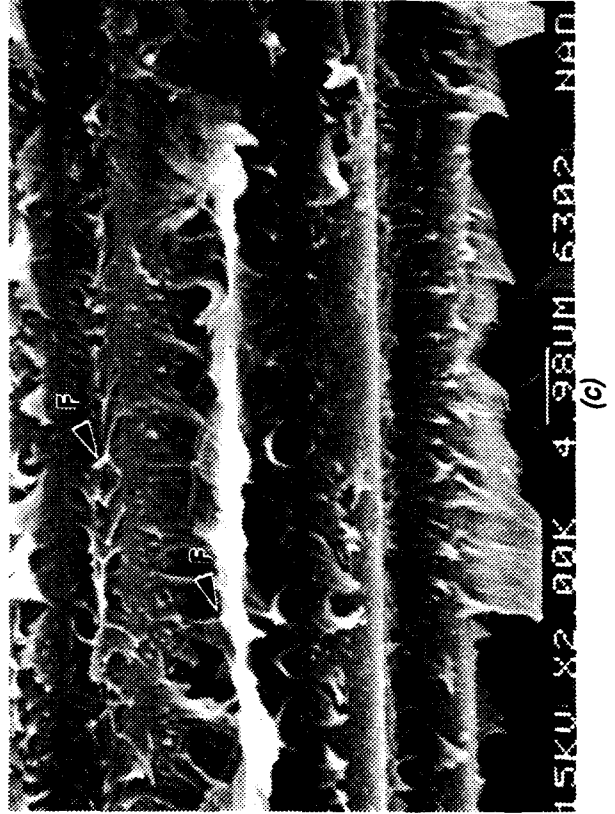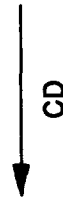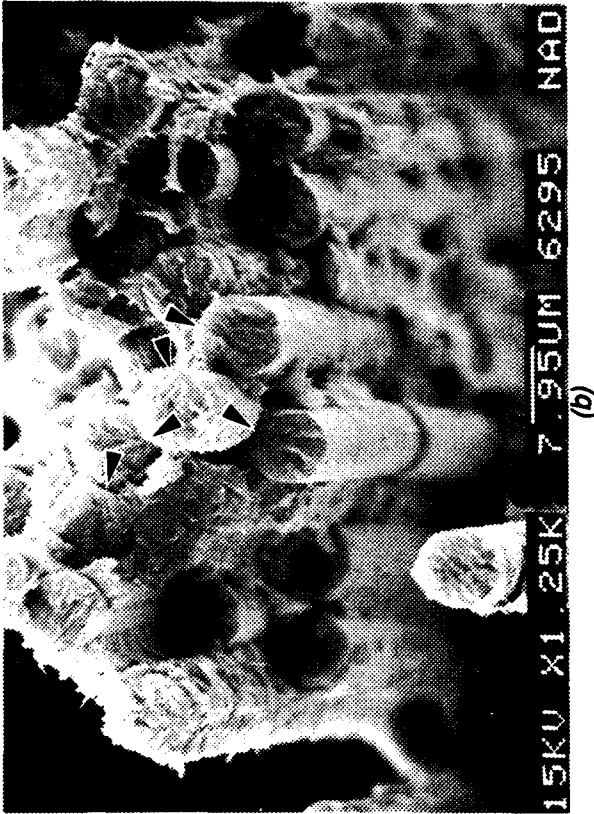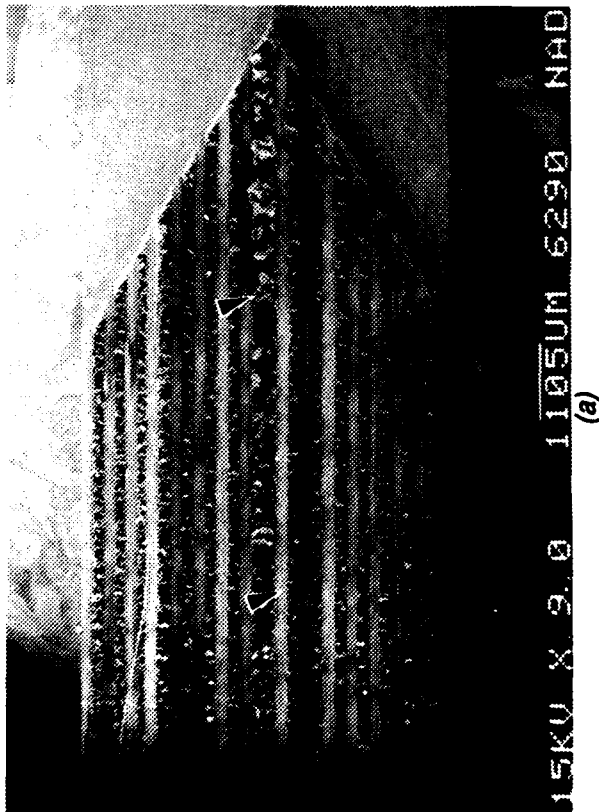
Figure 3-37. SEM Photographs of Mode I Translaminar Tension
Fracture in AS4/APC-2 Gr/PEEK - [90/0]₈ₛ
(a) Macrophotograph Showing Chevrons (Arrows)
(b) Fracture in 0 Degree Fibers (Tension Region)
Note: Arrows indicate DAF radials.
(c) Resin Fracture in 90 Degree Plies, Fractured
Fibrils (F) Oriented Along CD

CD = Crack-propagation direction

CD

regions. Fractured fibers in 0 degree plies (oriented normal to the applied load) were decorated with DAF radials, as previously reported for Gr/Ep. The fractured resin in 90 degree plies (oriented parallel to the applied load) exhibited fractured fibrils that closely resembled river patterns (Figure 3-37c). These could be used to map local crack-propagation direction. The compression fracture regions (away from the machined notch) were characterized by "chop" marks as for Gr/Ep.

3.4.3 Rockwell Flaw Criticality Study Defects

As part of Task 3, Subtask 3.3, Northrop documented manufacturing and processing defects that occur in Gr/Ep. These have been identified in the Rockwell Flaw Criticality Study (Reference 6) as defects that could affect the service life of composite structural components. The defects were characterized using optical microscopy, and macro-photography techniques.

Photographs illustrating all the defects documented are shown in Volume II, Part 1 – Procedures and Techniques (Section 2.4). A list of these defects is given in Table 3-13. The corresponding Rockwell study defect number and the stage at which each defect occurs, as defined in the Rockwell study, are also given. Figure 3-38 shows some of the defects documented.

Table 3-13. Rockwell Criticality Study Defects

| Defect No.	Defect	Manufacturing Stage
1	External Delamination	Layup
2	Blister, Internal Delamination	Layup
3	Oversized Hole	Attachment
4	Hole Exist Side Broken Fibers Breakout	Attachment
5	Tearout in Countersink	Attachment
8	Resin-Rich Areas	Fiber/Prepreg Generation
9	Excessive Porosity	Fiber/Prepreg Generation
10	Scratch, Fiber Breakage	Handling
11	Dent	Handling
12	Fiber Breakaway from Impact Surface	Handling
13	Edge Delamination, Splintering	Handling
14	Overtorqued Fastener	Attachment
16	Edge Notch, Crack	Handling
17	Corner Notch	Handling
18	Mislocated Hole, Not Repaired	Attachment
27	Misoriented Ply	Layup
28	Ply Overlap	Layup
29	Ply Underlap, Gap	Layup
31	Improper Fastener Seating	Attachment
33	Figure 8 Hole	Attachment
35	Off-Axis Drilled Hole	Attachment
36	Countersink on Wrong Side of Laminate	Attachment
39	Burned Drilled Hole	Attachment
41	Undersize Fastener	Attachment
42	Dent, Fiber Breakage From Production Mishandling	Handling
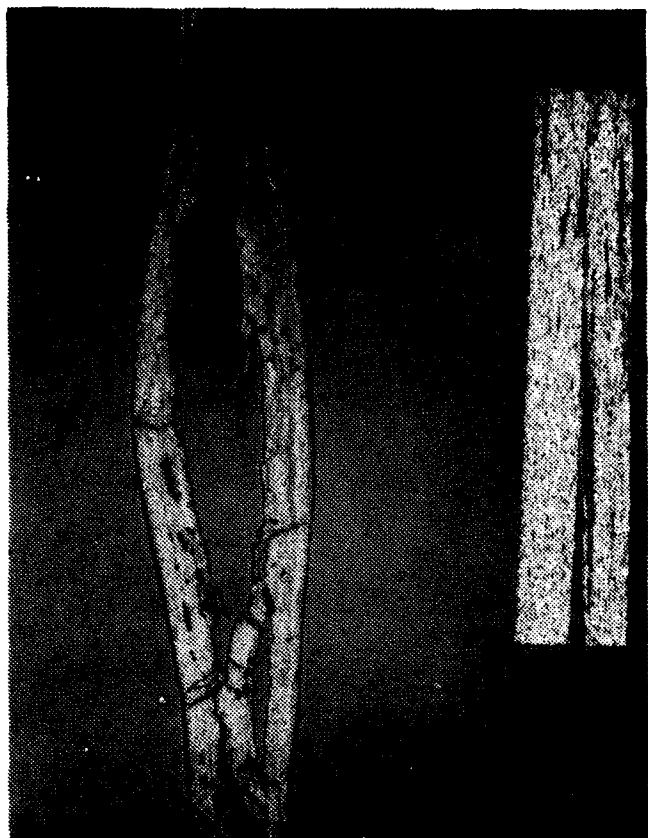
Figure 3-38. Rockwell Flaw Criticality Study Defects
(a) Defect 1: External Delamination (8.3X)
(b) Defect 2: Blister, Internal Delamination (6.5X)

(a)

(b)

CRACKS

(d)

(e)

(c)
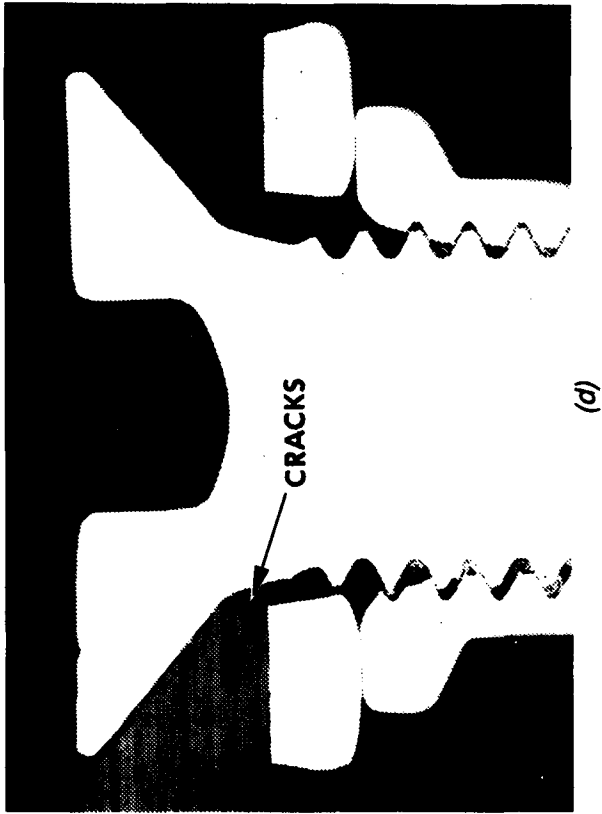
Figure 3-38. (Continued)
(c) Defect 13: Splintering, Edge Delamination (2X)
(d) Defect 14: Overtorqued Fastener (7X)
(e) Defect 16: Edge Notch, Crack (5X)

3.4.4 Fractography of Bolted Joint Structures

Northrop ran the SAMCJ (Strength Analysis of Multifastened Composite Joints) computer program to develop the specimen test matrix for characterizing the six different failure modes in mechanically joined composite structures. This computer program, developed by Northrop for the USAF (Reference 1), enabled prediction of the failure mode(s) in single and multi-fastened bolted composite joints. Predictions were made through summation of the critical stresses at stress concentration points in the laminates, using known constitutive equations. The program also took into account the effects of the specimen geometries and bolt positions in prediction(s) of the failure mode(s).

A test matrix (Table 3-14) was developed for quasi-isotropic AS4/3501-6 Gr/Ep joined with titanium "Hi-Lok" tension or shear-type flush head fasteners, using single lap-shear test specimens. Different failure modes were achieved through variations in the composite thicknesses (8 ply, 32 ply, 56 ply), specimen widths (w), and fastener to edge distances (e). In all cases, except for bolt pull through failure, a tension head type fastener was used with fastener diameter (d) being 0.25 in. The SAMCJ code also enabled the determination of the w/d and e/d ratios needed to create the required failure modes in the single-lap shear specimens, and these are shown in Table 3-15.

The results of the fractography are discussed below.

Table 3-14. Test Matrix for Mechanically Joined Composites

Failure Mode	No. of Specimens		
	32/Quasi	56/Quasi	8/Quasi
Tension	3	–	–
Tension Cleavage	3	–	–
Shear-Out	3	–	–
Bearing	3	–	–
Bolt Failure	–	3	–
Bolt Pull Through	–	–	3

Table 3-15. Specimen Width/Fastener Diameter (w/d) and Fastener Edge Distance/Fastener Diameter (e/d) Ratios

Failure Mode	w/d	e/d
Tension	3	3
Tension Cleavage	3	1.5
Shear-Out	3	1
Bearing	5	3
Bolt Failure	6	3
Bolt Pull Through	6	3

3.4.4.1 Tension Failure

Figure 3-39 illustrates fracture characteristics for tension failure. Net-section tension failures occur in mechanically-joined composite specimens with small w/d and large e/d ratios (w = composite width, d = fastener diameter, and e = distance of fastener from edge). This failure mode was achieved using w/d and e/d ratios of 3 and 3, respectively, using 32-ply quasi-isotropic AS4/3501-6 Gr/Ep adherends, and a tension head "Hi-Lok" titanium fastener with a head diameter of 0.25 inches. In this type of failure, fracture occurs due to insufficient specimen width.

Figures 3-39b and 3-39c show macrographs of mating halves of the adherends in the vicinity of the machined hole. Examination of peripheral regions of the bolt-hole revealed compression characteristics indicating that failure in the joint region was a compression dominated event.

Figures 3-39d, 3-39e and 3-39f illustrate microscopic fracture characteristics in 90, 45, and 0 degree plies. The 90 and 45 degree plies were characterized by hackles (Figures 3-39d and 3-39e), and "chop" marks on fiber ends indicating that these plies had failed in shear. The 0 degree plies were associated with translaminar tension features, namely DAF radials (Figure 3-39f), that appeared to originate from adjacent 45 degree plies rather than the bolt-hole.

It is believed that during loading of the joint, the 90 and 45 degree plies initially failed in shear as a consequence of the compression load applied by the fastener on peripheral regions of the bolt-hole. Subsequent catastrophic fracture occurred due to interlaminar tension fracture of the 0 degree plies.

3.4.4.2 Tension-Cleavage Failure

Figure 3-40 illustrates macroscopic fracture characteristics for tension-cleavage failure. It is believed that the bolted joint failed in this manner due to the shear-out and net-section failure strengths of the joint being similar. The failure was achieved using w/d and e/d ratios of 3 and 2 respectively (w = specimen width, e = fastener to edge distance, d = fastener diameter).

Figure 3-40b and 3-40c show macrographs of mating halves of the adherends in the vicinity of the machined hole. The chamfered region failed in compression with non-chamfered peripheral regions of the bolt-hole exhibiting tensile failure characteristics.

Figures 3-40d, 3-40e, and 3-40f illustrate microscopic fracture characteristics in 90, 45, and 0 degree plies. Catastrophic translaminar fracture initiated in 90 degree plies in tensile regions of the bolt hole and propagated radially outward, as determined by mapping of the rivers in the fractured resin (Figure 3-40d). This was followed by combined inter/translaminar fracture in the ±45 plies (Figure 3-40e), and translaminar fracture in the 0 degree plies. Mapping of the DAF radials in 0 degree plies (Figure 3-40f) indicated that fracture in these regions had originated at adjacent 45 degree plies, rather than at the periphery of the hole.

3.4.4.3 Shear-out Failure

Figure 3-41 shows photographs illustrating shear-out failure. This failure mode occurred due to small edge distances, i.e. small e/d ratios with concomitant large w/d values (e/d = 1.5, w/d = 3).
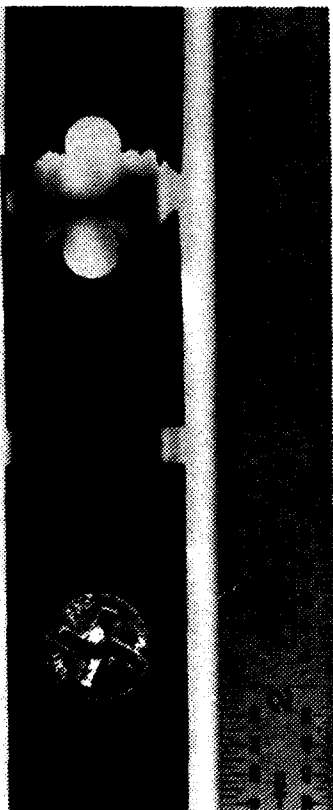
(a)
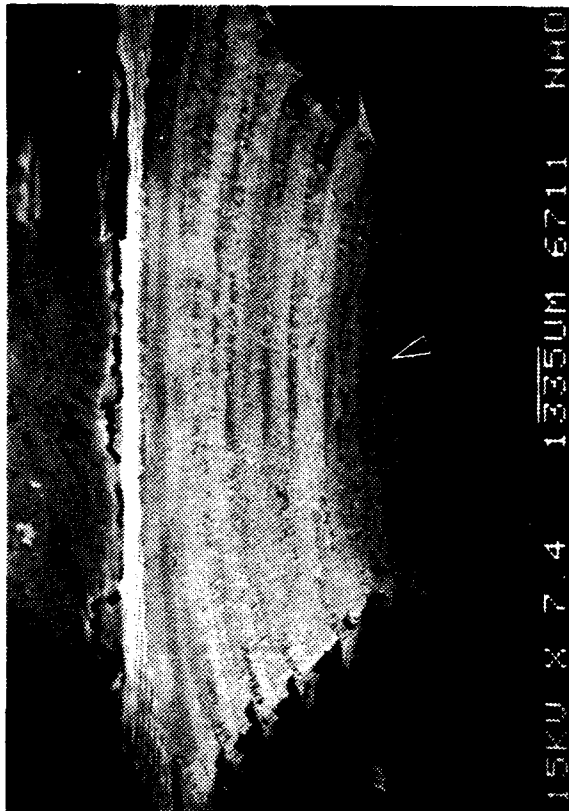
(b)
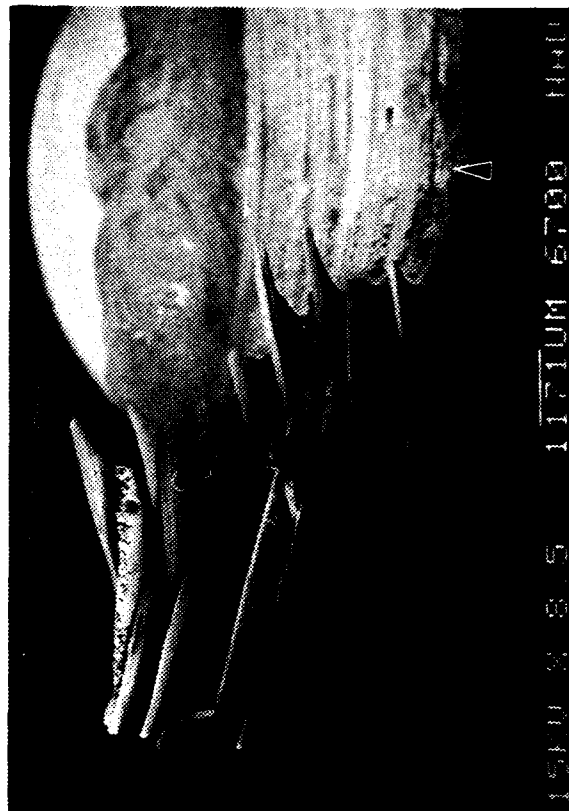
(c)

Figure 3-39. *Optical and SEM Photographs of Tension Failure*
in AS4/3501-6 Gr/Ep Bolted Joint
(a) Macrophotograph of Failed Joint
(b), (c) Macrophotographs of Failed Adherends
Note compression damage (arrows)

(e)

(f)

(d)
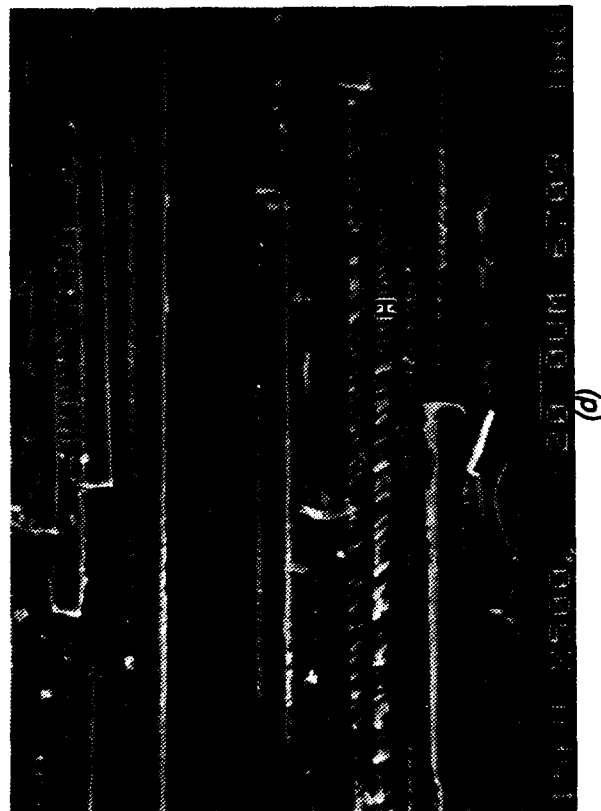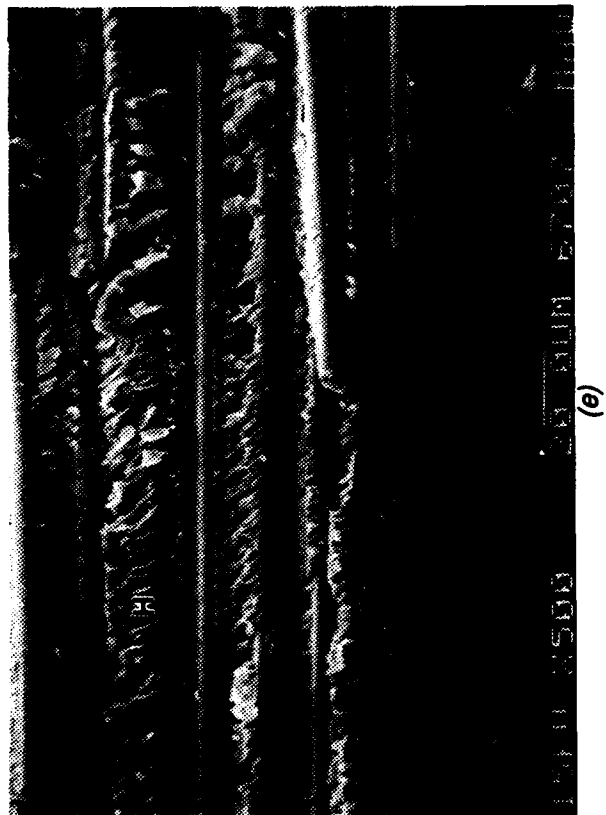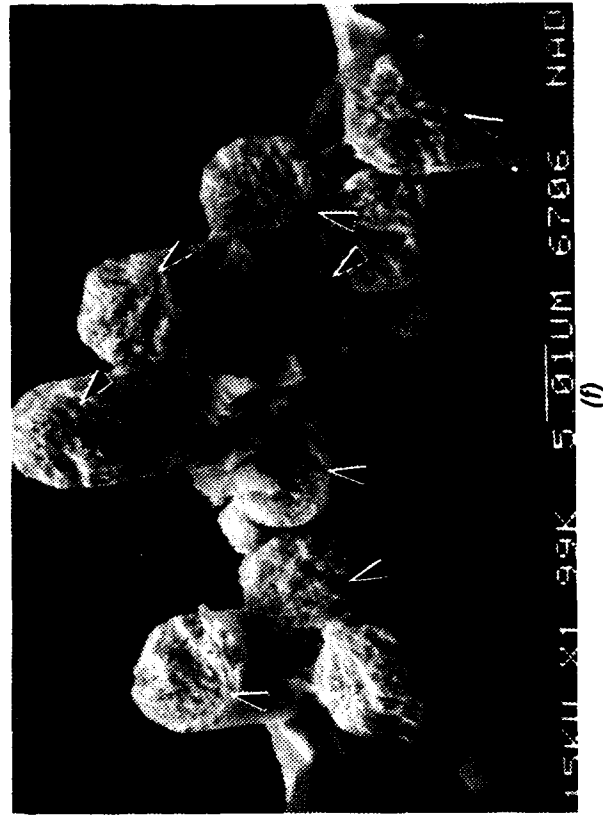
Figure 3-39. (Continued)
(d), (e) Hackles (H) in 90 and 45 Degree Plies
(f) DAF Radials on 0 Degree Fibers
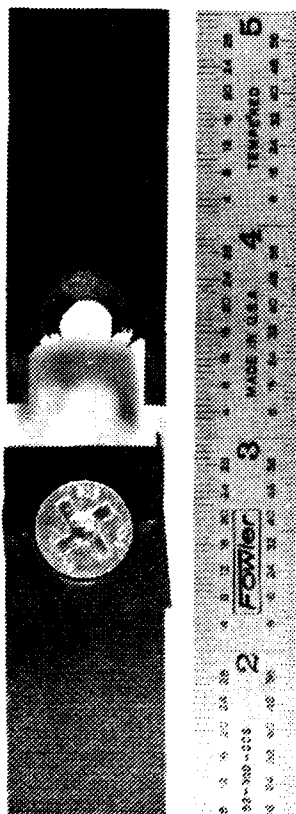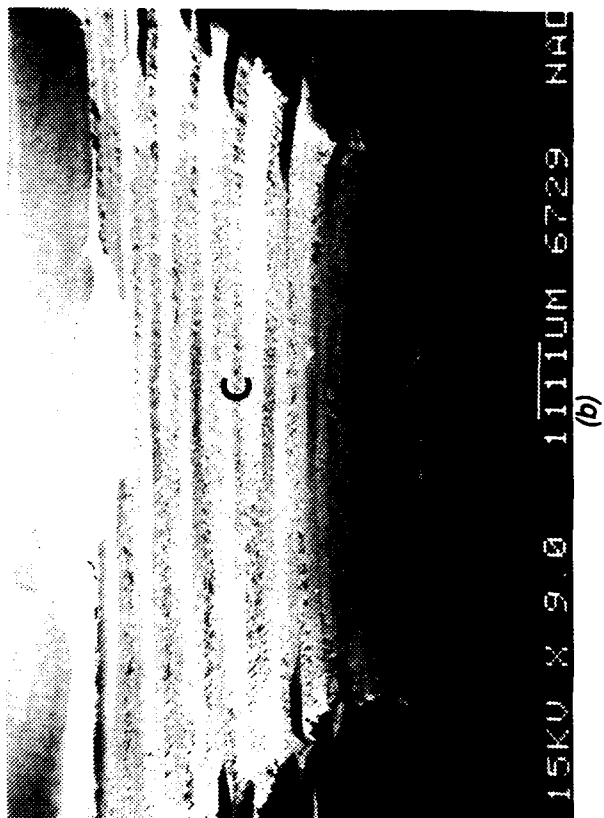
(b)

(c)

Figure 3-40. Optical and SEM Photographs of Tension-Cleavage
Failure in AS4/3501-6 Gr/Ep Bolted Joint
(a) Macrophotograph of Joint
(b), (c) Macrophotographs of Peripheral Regions of
Bolt-Hole in Mating Halves

C – Compression failure
T – Tension failure

(a)

3-77
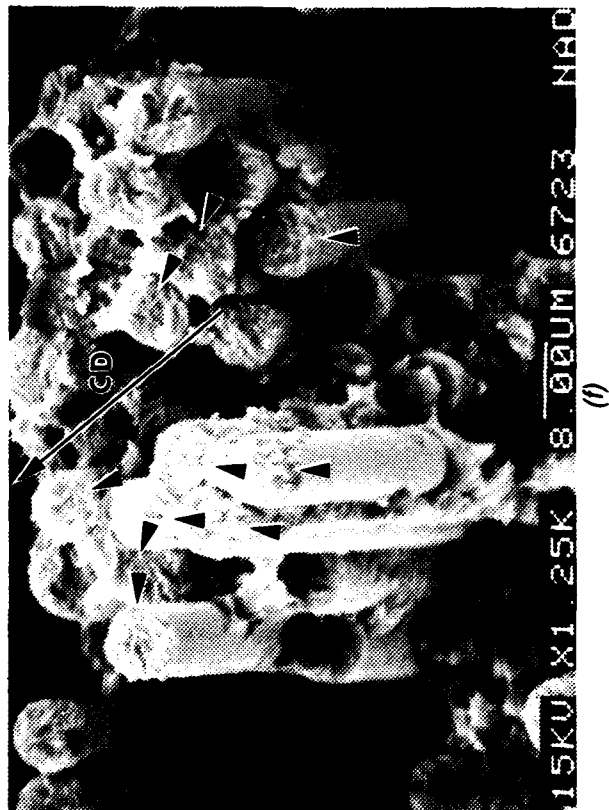
Figure 3-40. (Continued)
(d) Translaminar Fracture in 90 Degree Ply in Tensile
Fracture Region
(e) Fracture in 45 Degree Ply
(f) Tensile Fracture in 0 Degree Ply
Note DAF radials (Arrows)

CD = Crack-propagation direction

Figure 3-41. Optical and SEM Photographs of Shear-Out Failure
in AS4/3501-6 Gr/Ep Bolted Joint
(a) Macrophotograph of Failed Joint
(b), (c) Macrophotographs of Failed Adherends
Note compression (C) and tension (T) regions
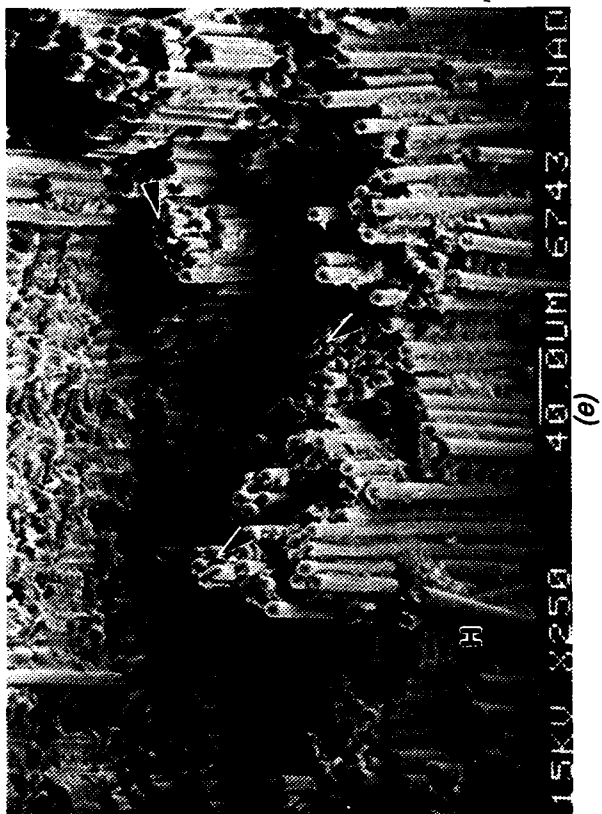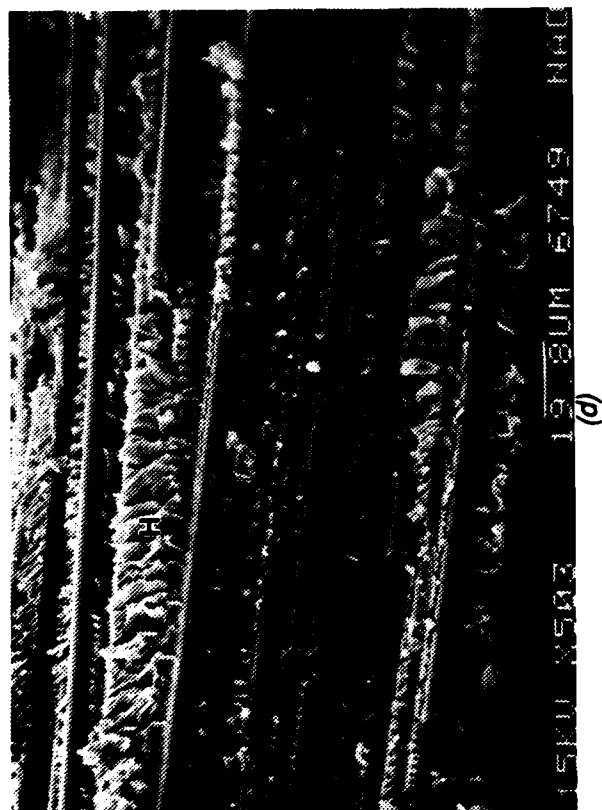
Figure 3-41. (Continued)
(d) Hackles (H) in 45 Degree Plies
(e) DAF Radials (Arrows) and Hackles (H) in 0 Degree Plies
(f) Peel Characteristics in 90 Degree Plies
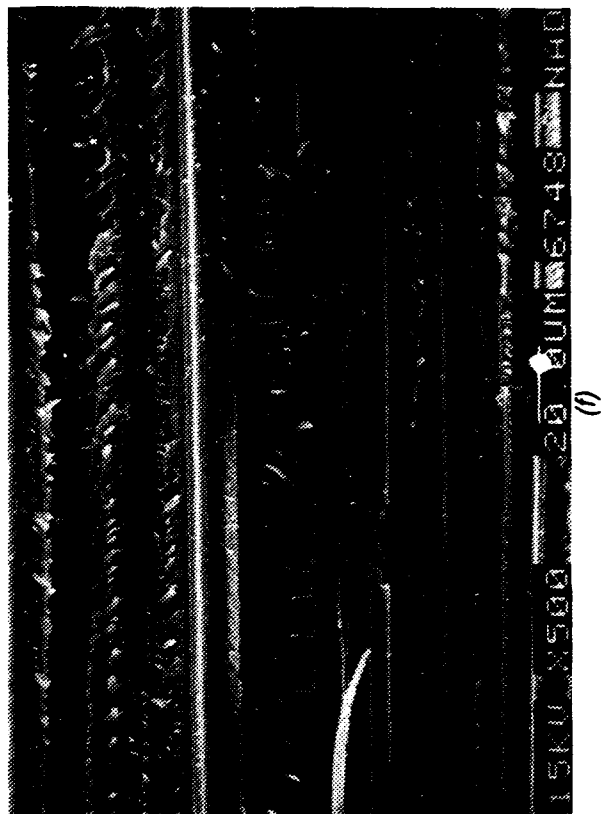
Macroscopic examination of the peripheral regions of the hole revealed that the non-chamfered regions were associated with compression damage. The 45 degree plies were characterized by hackles on fractured resin (Figure 3-41d) and chop marks on fiber ends, indicating failure due to shear loads. The 0 degree plies exhibited DAF radials and hackles on fractured resin (Figure 3-41e) as would occur under "in-plane" shear. The 90 degree plies had failed in peel originating away from the bolted joint rather than at the joint (Figure 3-41f).

Based on these observations it appears that on loading of the joint, failure initiated due to compression loads in non-chamfered regions of the hole. The 45 degree plies failed under shear with subsequent in-plane shear failure of the 0 degree plies, and final failure of the 90 degree plies in peel.

3.4.4.4 Bearing Failure

Bearing failures are the preferred failure mode for most joint applications since "local" yielding of the material occurs in this mode, with the surrounding material remaining intact. Figures 3-42a through 3-42f illustrate this failure mode which occurred in specimens with e/d and w/d ratios of 5 and 3.5. In quasi-isotropic Gr/Ep, this failure mode has been reported to occur for w/d ratios greater than 5 and e/d ratios greater than 3 (Reference 1).

Macroscopic examination of the bolt-hole revealed that peripheral regions not subjected to the local bearing load had failed under in-plane shear, as indicated by the fiber splits and DAF radials on broken fiber ends (Figure 3-42c). Examination of the 45, 90, and 0 degree plies revealed pronounced hackle formation in the fractured resin as would occur under shear loading (Figure 3-42d through 3-42f). These observations indicate that during loading of the joint, local regions in the bolt-hole failed under compression, with subsequent fiber-splitting and delaminations across the adherends under shear loads.

3.4.4.5 Bolt Failure

Figure 3-43 provides photographs illustrating bolt failure. This failure mode occurred due to excessive bending of the joint, and was achieved by using w/d and e/d ratios of 6 and 3, respectively. Macroscopic failure consisted of 1) bolt fracture, 2) crushing of fiber bundles due to bearing loads, and 3) delaminations along 45 degree plies. SEM examination of the crushed regions revealed compression failure characteristics. The delaminations exhibited shear characteristics (Figure 3-43d).

3.4.4.6 Bolt Pull Through

Figure 3-44 provides photographs of this failure mode. Fastener pull through occurred because the depth of countersinking exceeded 70 percent of the bolted joint thickness (w/d = 6, e/d = 3, 8 ply quasi-isotropic adherends).

Macroscopic failure consisted of delaminations in the outer plies that initiated at the machined bolt hole. The microscopic fracture features for this failure mode are shown in Figures 3-44b, 3-44c, and 3-44d. Delamination occurred by peel (Mode I tension and Mode II shear). Mapping of the rivers indicated fracture initiation at the periphery of the hole with radial propagation in an interlaminar manner.
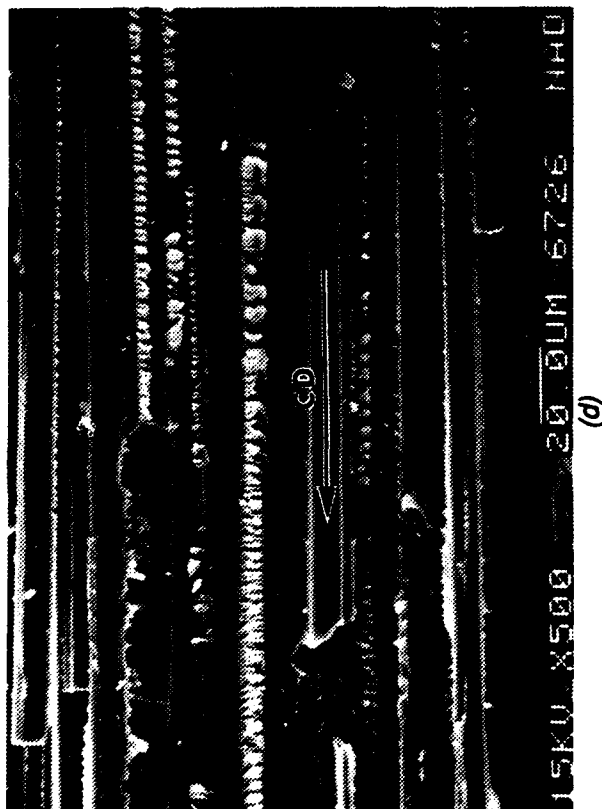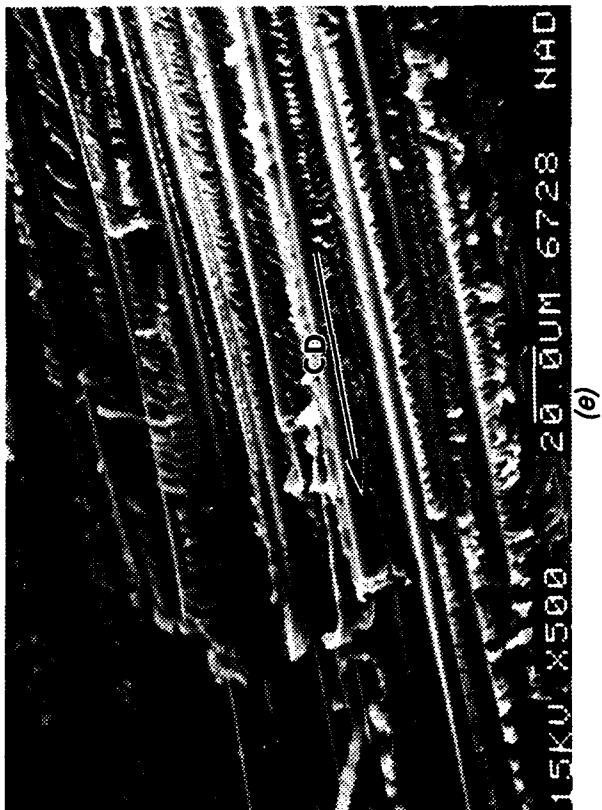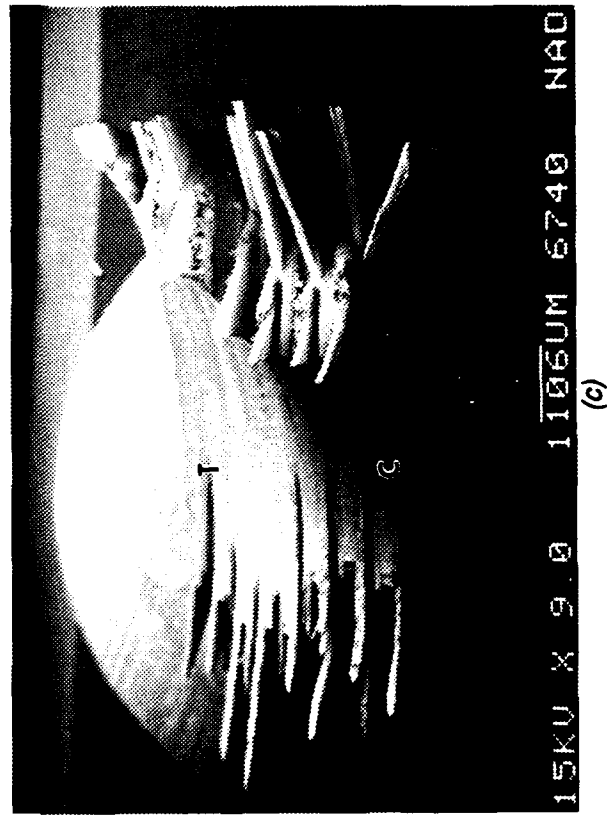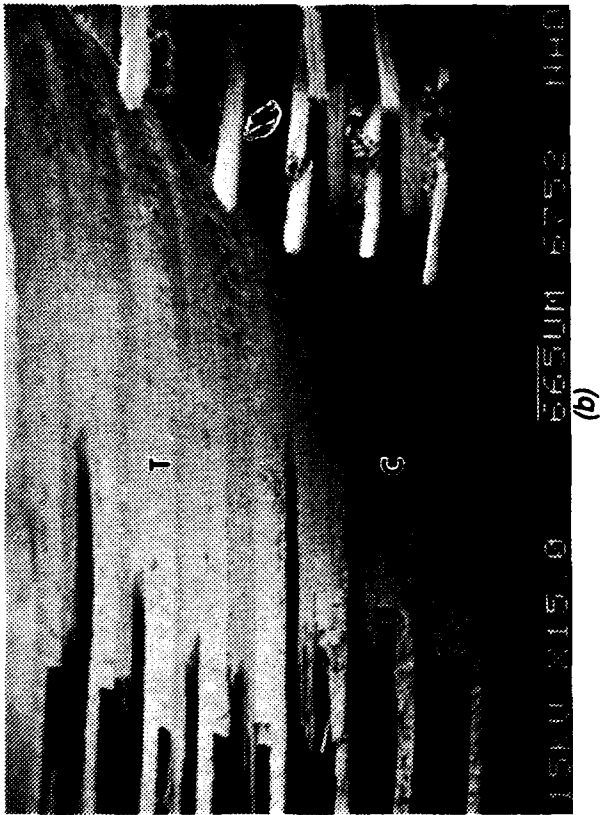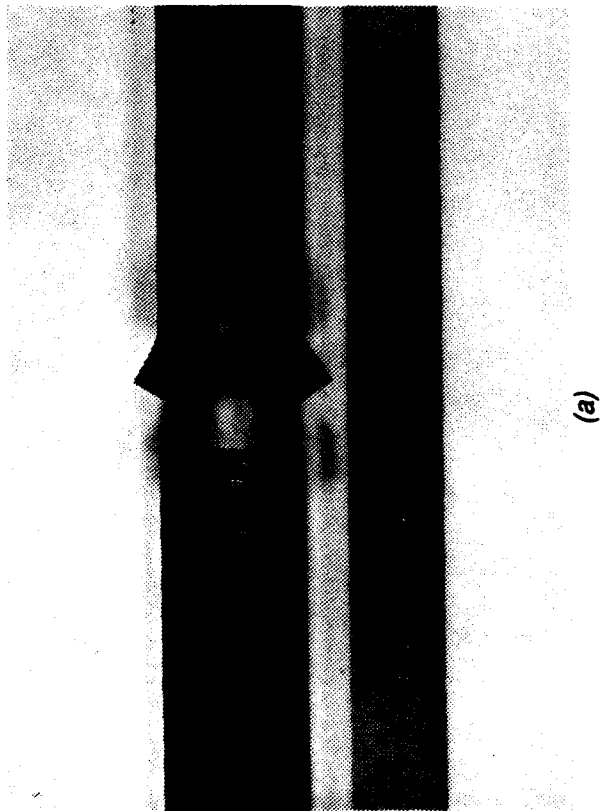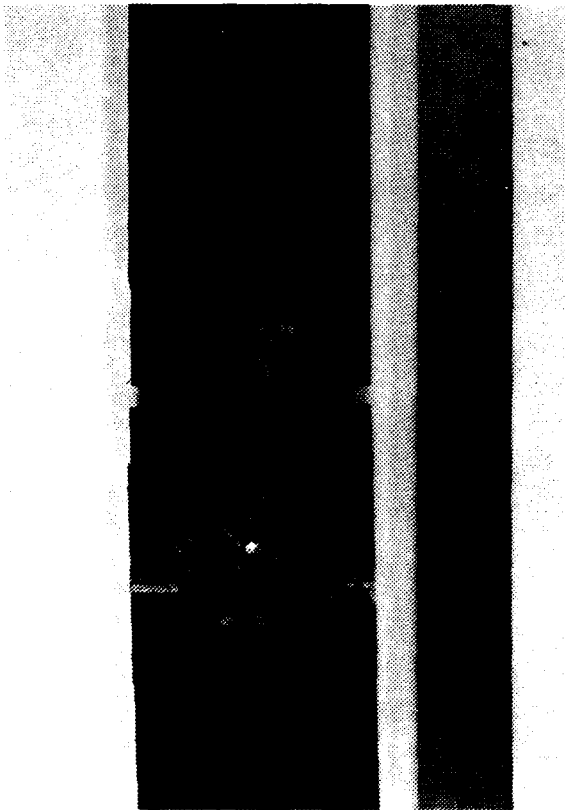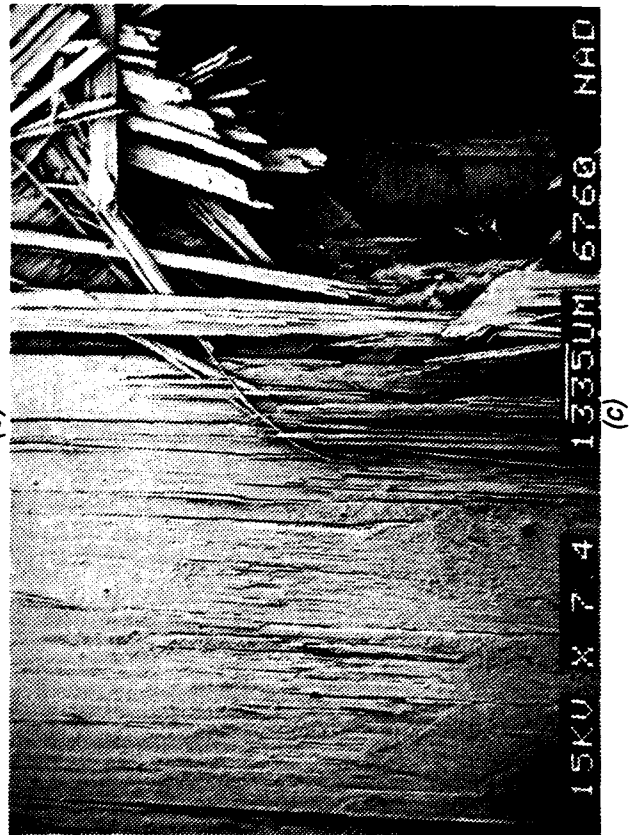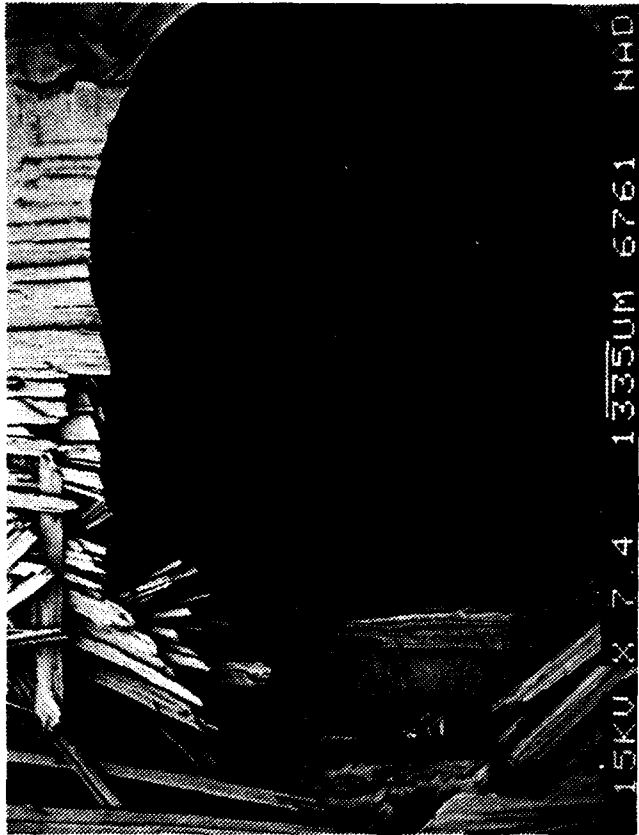
Figure 3-42. Optical and SEM Photographs of Bearing Failure in
AS4/3501-6 Gr/Ep Bolted Joint
(a) Macrophotograph of Failed Joint
(b) Detail Near Bolt-Hole
(c) Fractured Adherends
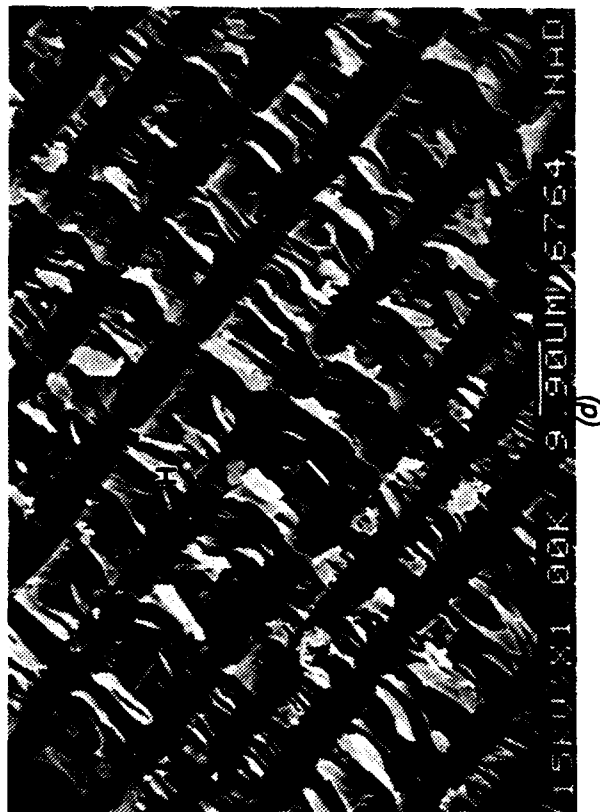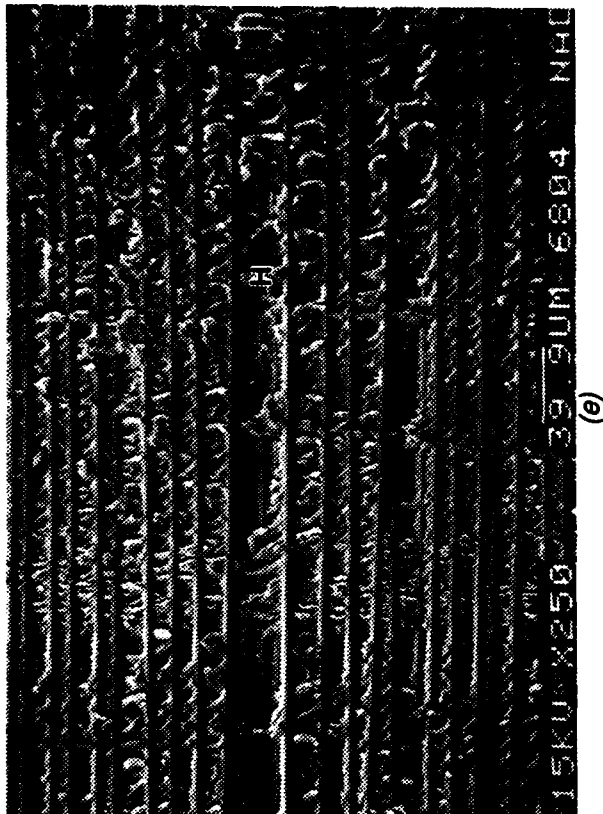
Figure 3-42. (Continued)
(d), (e). (f) Hackles (H) in 45, 90, and 0 Degree Plies

3-83
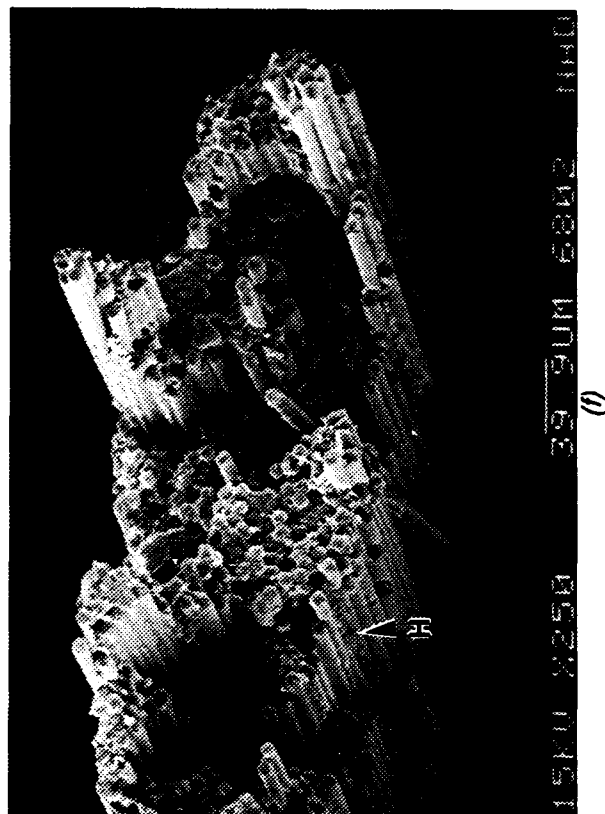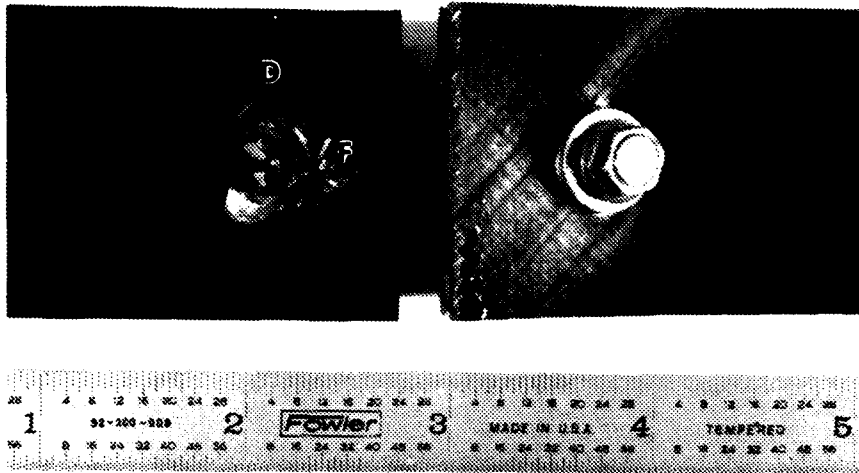
(a)
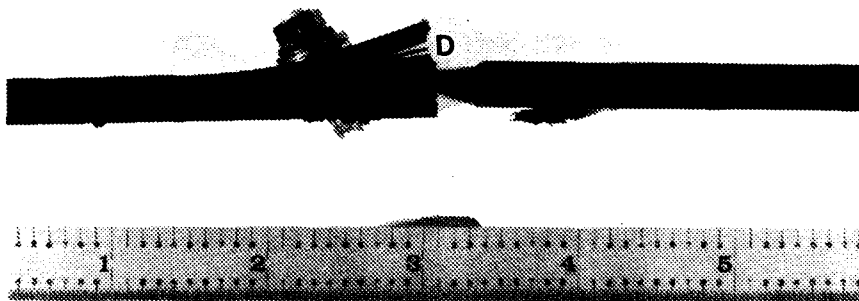
(b)

Figure 3-43. Optical and SEM Photographs of Bolt Failure in
AS4/3501-6 Gr/Ep Bolted Joint
(a), (b) Macrophotographs of Fracture
Note fiber crush (F) and delamination (D)

(c)
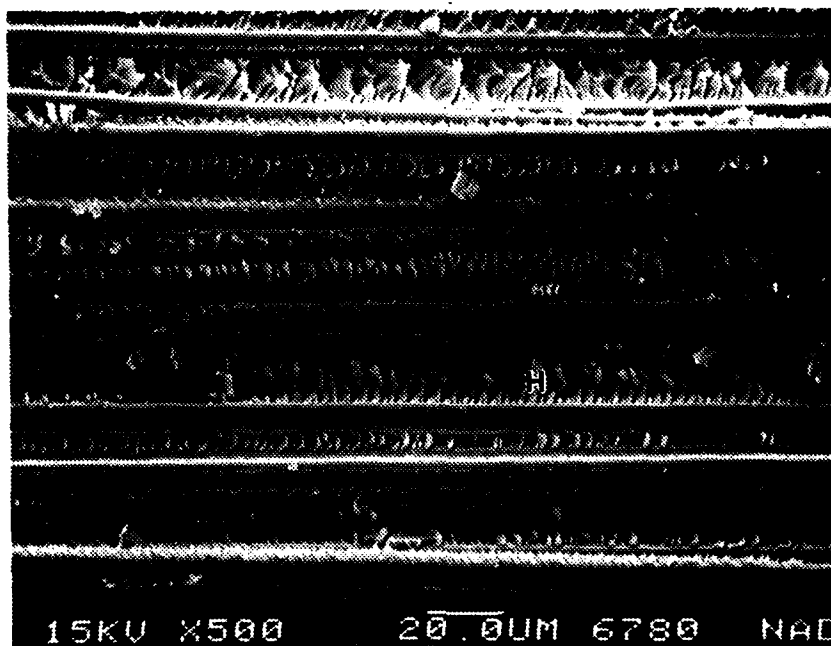
(d)

Figure 3-43. (Continued)
(c) Fracture Detail in Fiber Crush Region
(d) Shear Fracture in Delamination Region
Note hackles (H)

(a)

15KV X25.0 399UM 6791 NaC
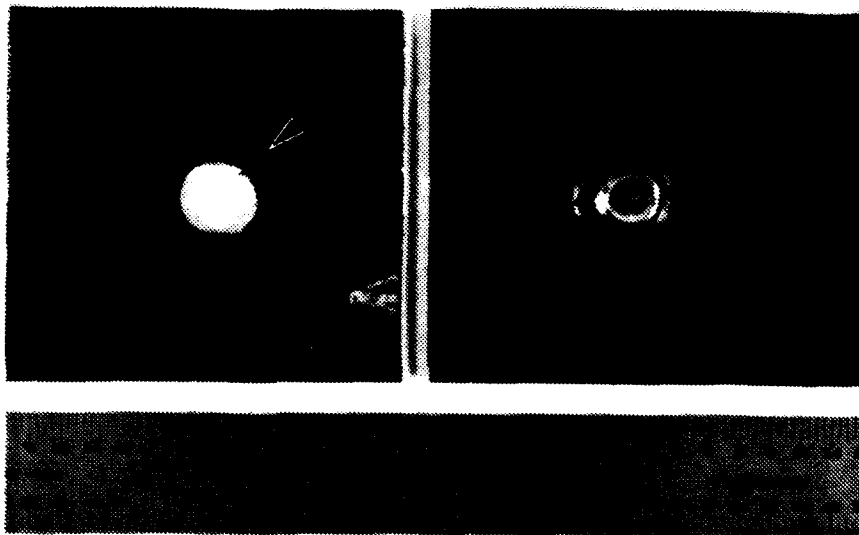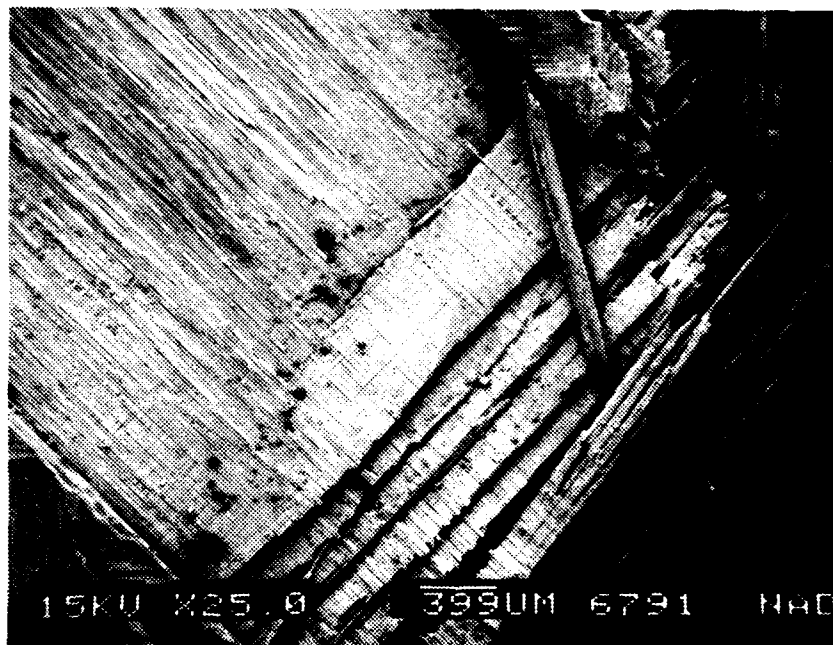
(b)

Figure 3-44. *Optical and SEM Photographs of Bolt Hole Pull Through in an AS4/3501-6 Gr/Ep Bolted Joint*
(a) Macrophotograph
Note delamination in adherends (arrow)
(b) Low Magnification of Peel Fracture in Surface Delamination
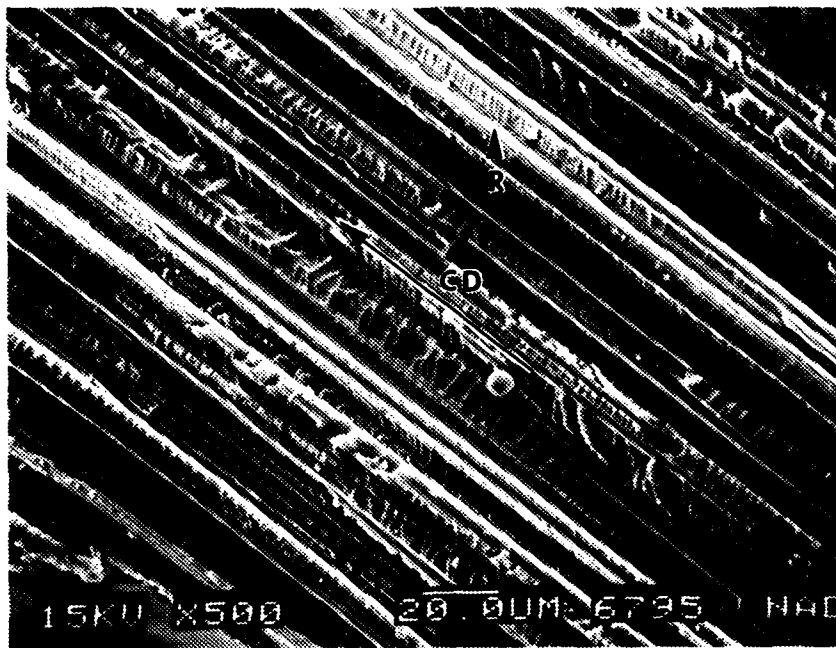
(c)
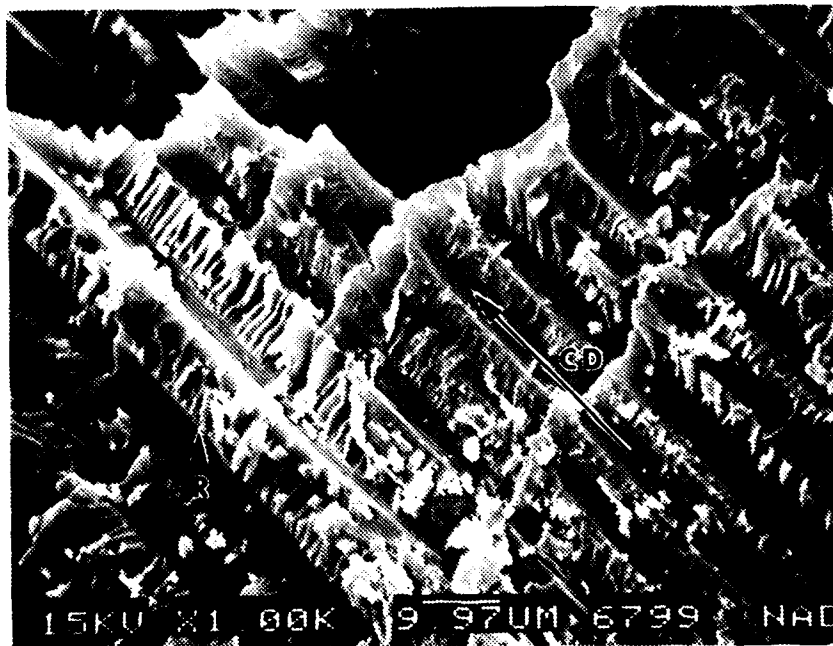
(d)

Figure 3-44. (Continued)
(c) Intermediate Magnification of Peel Fracture in Surface Delamination
(d) Peel Fracture in an Internal Delamination
Note arrays of rivers (R) oriented along CD

CD = Crack-propagation direction

3.4.4.7 Analysis of Results

An analysis of the results indicates that all the bolt-failure conditions were associated with varying microscopic failure characteristics. For tension-cleavage, transverse fracture in 90 degree plies was the principal cause for catastrophic failure. In bolt failure, fiber crushing and delamination due to shear were the principal fracture characteristics. In bolt pull through, delamination due to peel was the principal cause for failure in the adherends. Bearing failure was due to in-plane shear whereas shear-out was caused by compression dominated events.

3.4.5 Fractography of Adhesively Bonded Composites

The objective of this activity was to document the failure modes associated with joining of composite structures, when joined by adhesive bonding methods. Northrop chose two material systems, Gr/Ep and Gr/BMI, that have current or near-term Air Force fleet applicability for evaluation. Table 3-16 shows the test matrix that Northrop used for characterizing the failure modes. FM-300 adhesive was used for adhesive bonding of AS4/3501-6 Gr/Ep. The AS4/5250-3 Gr/BMI adherends were joined using EA 9673 adhesive.

The adhesively joined structures were tested under simple Mode I tension, Mode II shear, or mixed-Mode I tension plus Mode II shear loading. Northrop used double-cantilever beam, and unconstrained and constrained cracked-lap shear specimens, shown in Figures 3-45 through 3-47.

Testing of the specimens resulted in cohesive, adhesive, and mixed cohesive-adhesive failure modes. The detailed fractographic results for all the variable conditions are presented in Volume II, Part 2 - Atlas of Fractographs. Sample results for the three failure modes are presented

Table 3-16. Test Matrix for Adhesively Bonded Composite Fractography

MATERIAL: AS4/3501-6 GR/EP   ADHESIVE: FM-300

LOADING/SPECIMEN	LAP/STRAP PLY ORIENTATIONS	
	0°/0°	0°/32 QUASI
MODE I TENSION, DCB	3	3
MODE II SHEAR, CONSTRAINED CLS		
OVERLAP 1	3	3
OVERLAP 2	3	--
MODE I TENSION + MODE II SHEAR, UNCONSTRAINED CLS		
OVERLAP 1	3	—
OVERLAP 2	3	3

MATERIAL: AS4/5250-3 GR/BMI   ADHESIVE: EA 9673

LOADING/SPECIMEN	LAP/STRAP PLY ORIENTATIONS	
	0°/0°	0°/32 QUASI
MODE I TENSION, DCB	3	3
MODE I TENSION + MODE II SHEAR, UNCONSTRAINED CLS		
OVERLAP 1	3	3

DCB = DOUBLE CANTILEVER BEAM   OVERLAP 1 = 7 INCHES
CLS = CRACKED LAP SHEAR   OVERLAP 2 = 5 INCHES
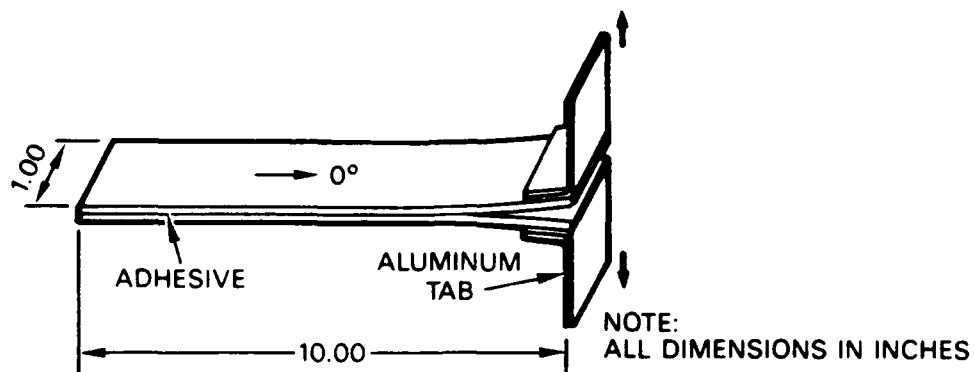
Figure 3-45. Double-Cantilever Beam Specimen

NOTE: ALL DIMENSIONS IN INCHES
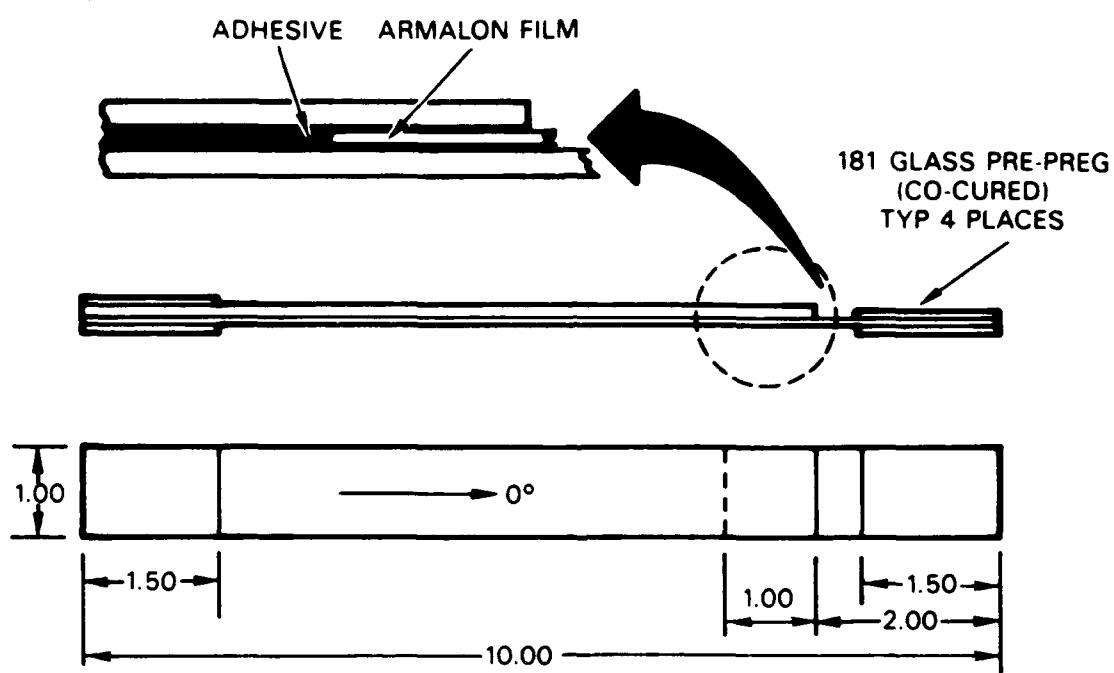
Figure 3-46. Cracked-Lap Shear Specimen

NOTE: ALL DIMENSIONS IN INCHES
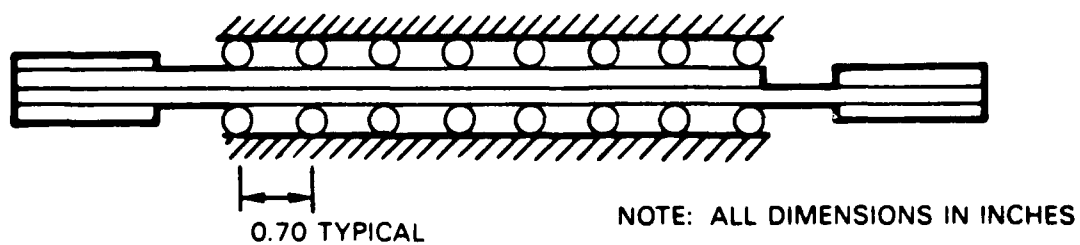
Figure 3-47. Constrained Cracked-Lap Shear Specimen

3-89

below. In general, it was determined that specimen geometry, lap/strap ratios, and test load played roles in controlling failure modes. Fractures could be mapped in adhesive- or mixed-mode conditions through evaluation of fracture features on the fractured adherends. Crack direction could not be readily mapped in pure cohesive joint failures, since there were no features that could be used as indicators of crack-growth direction in this type of failure.

3.4.5.1 Graphite/Epoxy

Figure 3-48 presents photographs of fracture for unidirectional Gr/Ep adherends bonded with FM-300 adhesive, and tested to failure under interlaminar Mode I tension. On a macroscopic scale, fracture initiated in a "cohesive" manner and then changed to an "adhesive" mode (Figures 3-48a, 3-48b, and 3-48c).

Figures 3-48d and 3-48e show SEM photographs of the cohesive and adhesive failure regions. The fractured adhesive in the cohesive failure region was characterized by stray river patterns (Figure 3-48d) oriented toward the direction of crack-propagation. Fracture could be mapped in the adhesive failure regions through mapping of the rivers in the fractured epoxy of the Gr/Ep adherend (Figure 3-48e).

Figure 3-49 presents photographs of unidirectional Gr/Ep adhesively-bonded to quasi-isotropic Gr/Ep with FM-300 adhesive, and tested to failure in Mode I tension. The effect of varying ply orientation in one of the adherends resulted in a change in type of failure. Catastrophic fracture initiated in a mixed cohesive-adhesive manner with adhesive failure being the predominant failure mode (Figure 3-49a). The fracture direction could be mapped as before through mapping of the rivers in the fractured epoxy at the adhesive-adherend interface (Figure 3-49c).

Figure 3-50 illustrates failure characteristics in unidirectional Gr/Ep adherends bonded with FM-300 adhesive, and tested under mixed loads (Mode I tension plus Mode II interlaminar shear). Application of peel resulted in a mixed cohesive-adhesive failure with no clear transition from one failure mode to the other. SEM examination of the fractured adhesive in the cohesive areas revealed no features indicative of crack-propagation direction. The fractured adherend in the adhesive failure areas exhibited peel characteristics (hackles plus river patterns).

3.4.5.2 Graphite/Bismaleimide

Figure 3-51 and 3-52 illustrate failure characteristics in unidirectional Gr/BMI adherends bonded with EA 9673 adhesive, and tested under interlaminar Mode I tension in a manner similar to the Gr/Ep coupons. On a macroscopic scale failure initiated in a mixed cohesive-adhesive mode (Figures 3-51a and 3-51b). With increasing crack length, there was a transition to a cohesive failure mode, and eventually to an adhesive failure mode. The fracture direction could be established as in the Gr/Ep specimens through mapping of the rivers in the adhesive or cohesive failure areas (Figure 3-52).

Figure 3-53 shows photographs of unidirectional Gr/BMI adhesively-bonded tc quasi-isotropic Gr/BMI with EA 9673 adhesive and tested to failure in Mode I tension. Fracture initiated due to adhesive failure. With increasing crack-length, there was a transition to cohesive failure
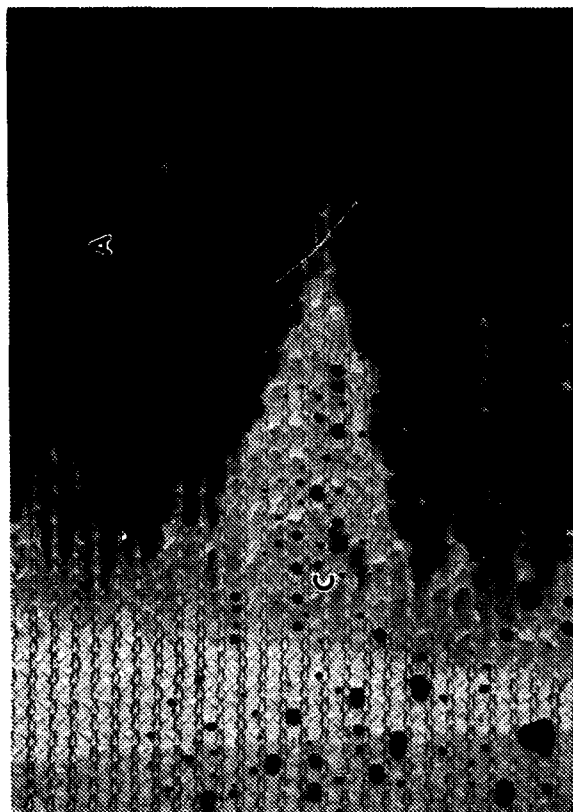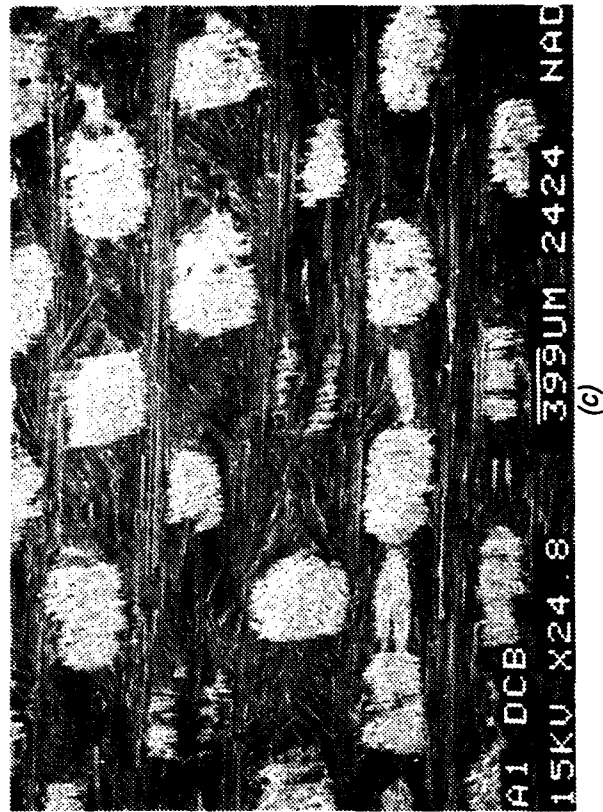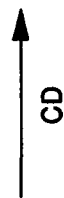
Figure 3-48. *Optical and SEM Photographs of Failure in
Unidirectional AS4/3501-6 Gr/Ep Adherends Bonded
With FM 300 Adhesive and Tested Under
Interlaminar Mode I Tension
(a) Macrophotograph
(b) Low Magnification (4X) Photograph Showing
      Failure Detail
(c) Adhesive Failure Region*

A = Adhesive failure
C = Cohesive failure
CD = Crack propagation-direction

(e)

(d)

CD

Figure 3-48. (Continued)
(d) River Patterns (R) in Fractured Adhesive in Cohesive Failure Area
(e) River Patterns (R) in Fractured Epoxy in Adhesive Failure Region

S = Scrim
CD = Crack-propagation direction
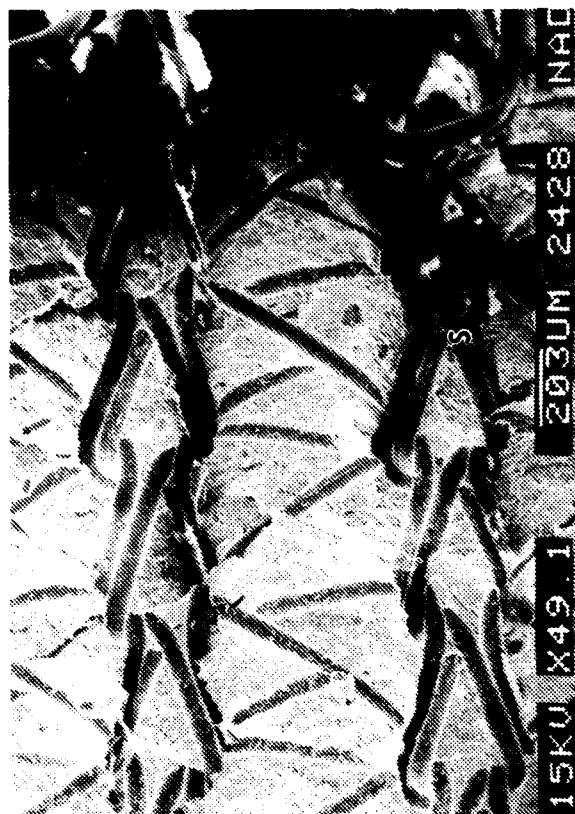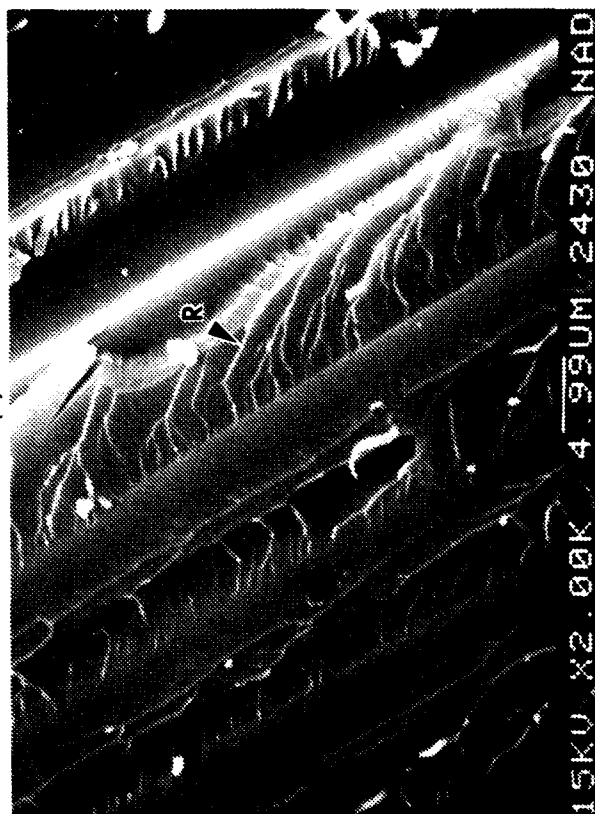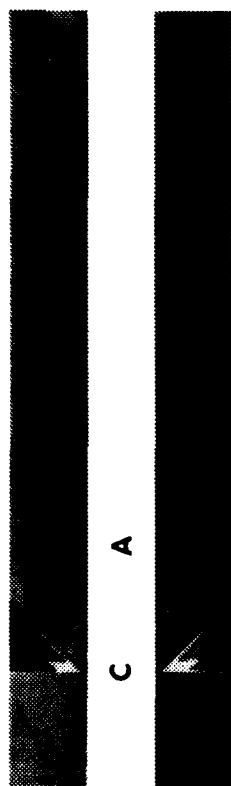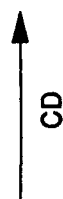
Figure 3-49. Optical and SEM Photographs of Failure in Unidirectional Gr/Ep Bonded to Quasi-Isotropic Gr/Ep With FM 300 Adhesive and Tested Under Mode I Tension
(a) Macrophotograph
(b) Rivers (R) in Adhesive Failure Region
(c) Cohesive Failure Area

A = Adhesive failure
C = Cohesive failure
CD = Crack-propagation direction
S = Scrim

(a)

CD →
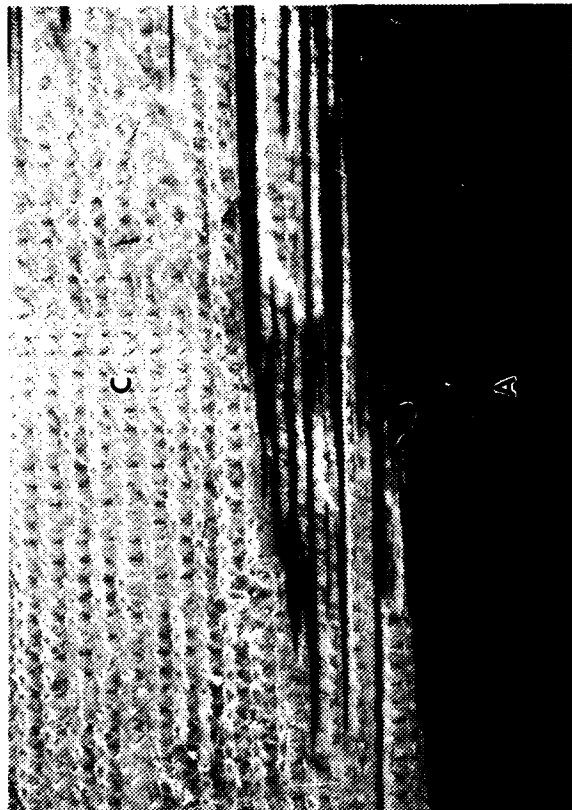
(b)

(c)

Figure 3-50. *Optical and SEM Photographs of Fracture in Unidirectional AS4/3501-6 Gr/Ep Adherends Bonded With FM 300 Adhesive and Tested Under Mode I Tension and Mode II Interlaminar Shear*
(a) Macrophotograph of Fracture
(b), (c) Low Magnification (4X) Photographs Showing Cohesive (C) and Adhesive (A) Failure Characteristics

A = Adhesive failure
C = Cohesive failure
CD = Crack-propagation direction

3-94

CD
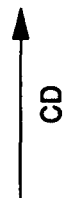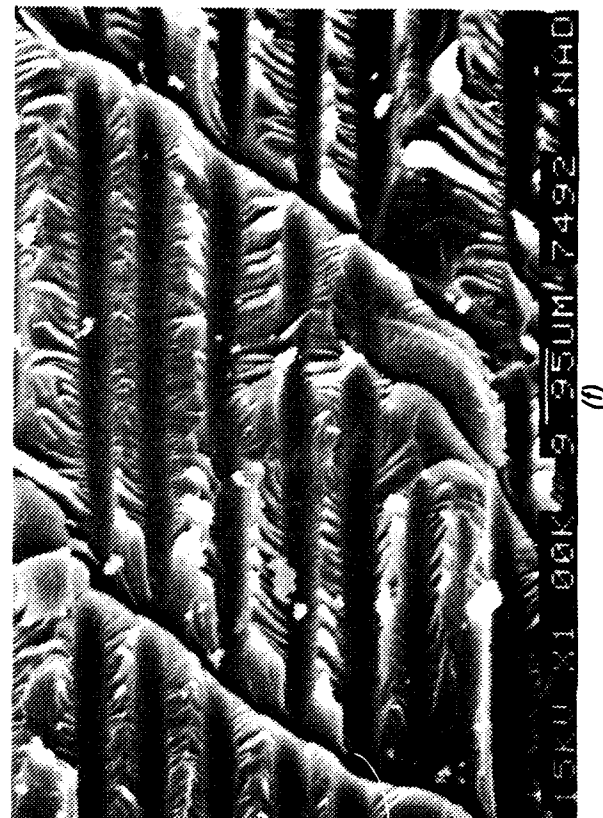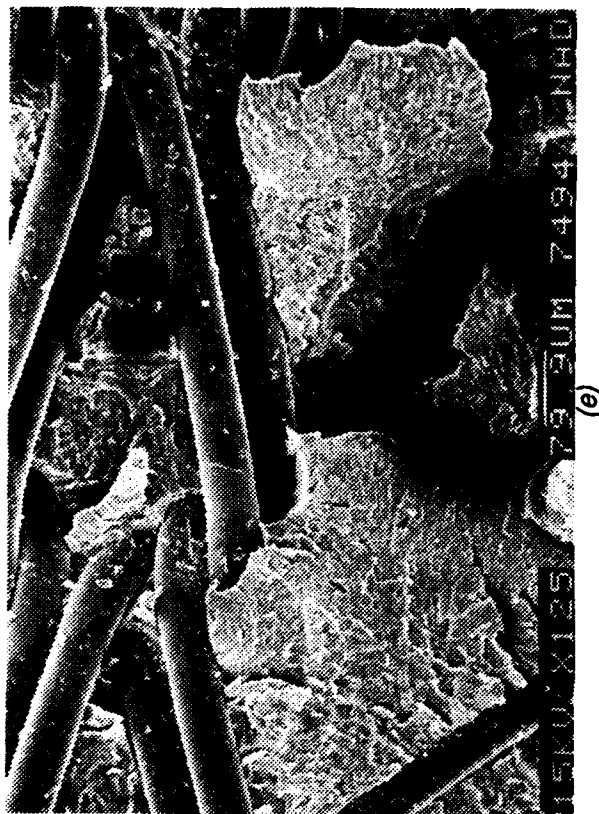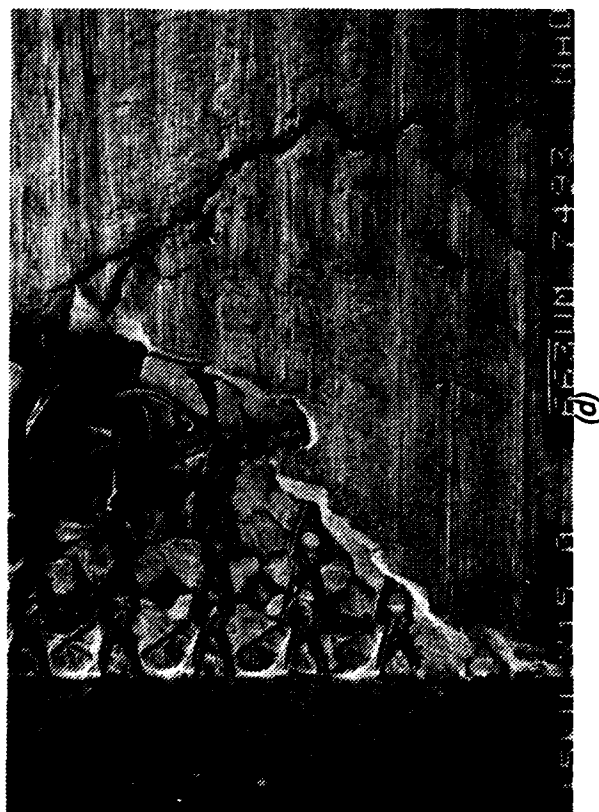
Figure 3-50. (Continued)
(d), (e) Cohesive Failure in FM 300 Adhesive
(f) Peel Characteristics in Fractured Adherends

CD = Crack-propagation direction

3-95
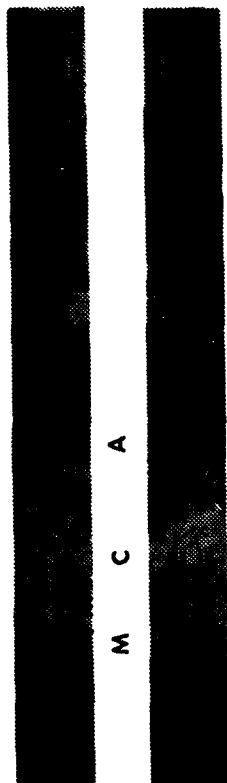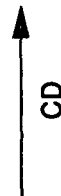
Figure 3-51. Optical Photographs of Failure in Unidirectional AS4/5250-3 Gr/BMI Adherends Bonded With EA 9673 Adhesive and Tested Under Interlaminar Mode I Tension

(a) Macrophotograph

(b), (c) Low Magnification (4X) Photographs Showing Details in Cohesive and Adhesive Failure Regions

A – Adhesive failure
C – Cohesive failure
CD – Crack-propagation direction
M – Mixed cohesive-adhesive failure
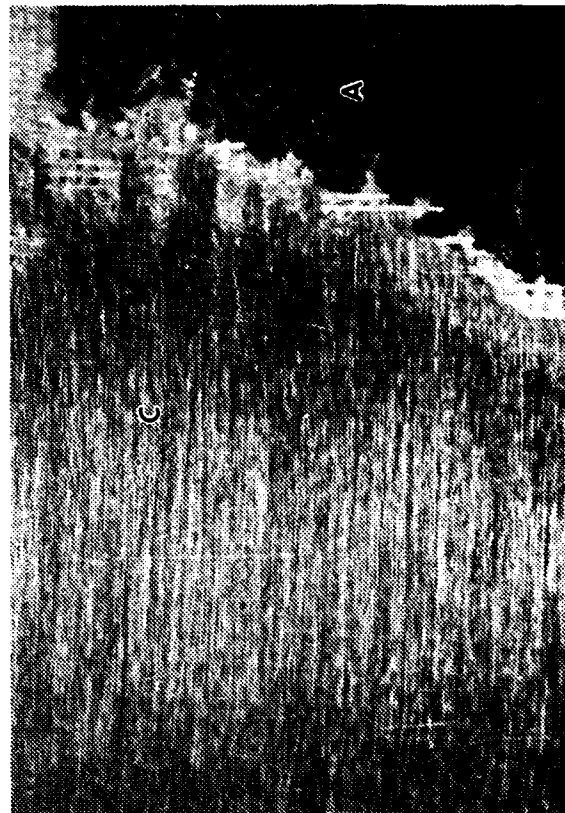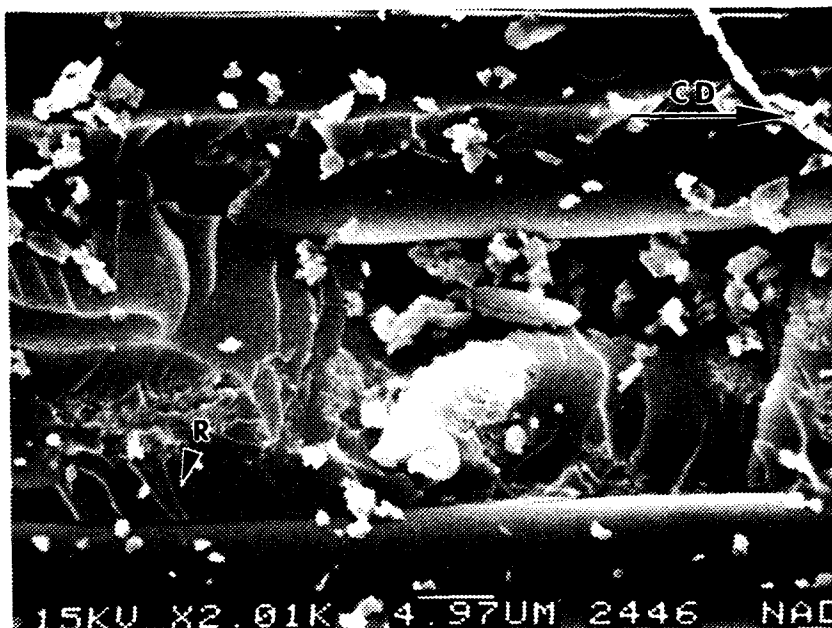
Figure 3-52. SEM Photograph of Failure in Unidirectional AS4/5250-3 Gr/BMI Adherends Bonded With EA 9673 Adhesive and Tested Under Interlaminar Mode I Tension Showing Rivers (R) in Adhesive Failure Region
CD = Crack-propagation direction

of the adhesive. The fracture direction could be mapped as before through mapping of the rivers oriented along the direction of crack-propagation (Figures 3-53c and 3-53d).

Figure 3-54 illustrates characteristics in unidirectional Gr/BMI adherends bonded with EA 9673 adhesive, and tested under mixed loads (Mode I tension plus Mode II interlaminar shear) in a manner similar to the Gr/Ep coupons. The fracture was characterized by total cohesive failure of the adhesive. There were no features on the adhesive surface that could be used to map crack-propagation direction.

3.4.6 Fractography of In-Plane Shear Tested Gr/Ep

As part of Task 3, Subtask 3.5, Northrop expanded the fractographic database developed by Boeing and Northrop to include AS4/3501-6 Gr/Ep specimens failed under in-plane shear. Table 3-17 shows the test matrix that Northrop developed for characterizing in-plane shear failures Northrop included some of the variable test conditions previously identified in Task 3, Subtask 3.1.

Northrop performed in-plane shear tests on rail-shear specimens tested per Northrop specification IT-58 (Reference 9). Figure 3-55 shows the configuration of the rail-shear specimen used. The rail-shear test set-up is shown in Figure 3-56.

Northrop evaluated failed rail-shear test specimens using visual and SEM methods. Impact testing of the $[+45/-45]_{6S}$ coupons, to achieve an impact-damaged condition prior to in-plane shear testing, was unsuccessful, since impact loads as low as 2 in-lbs resulted in catastrophic fracture. The results for the baseline and other variable conditions are reported below.

3-97

(b)

CD

(a)
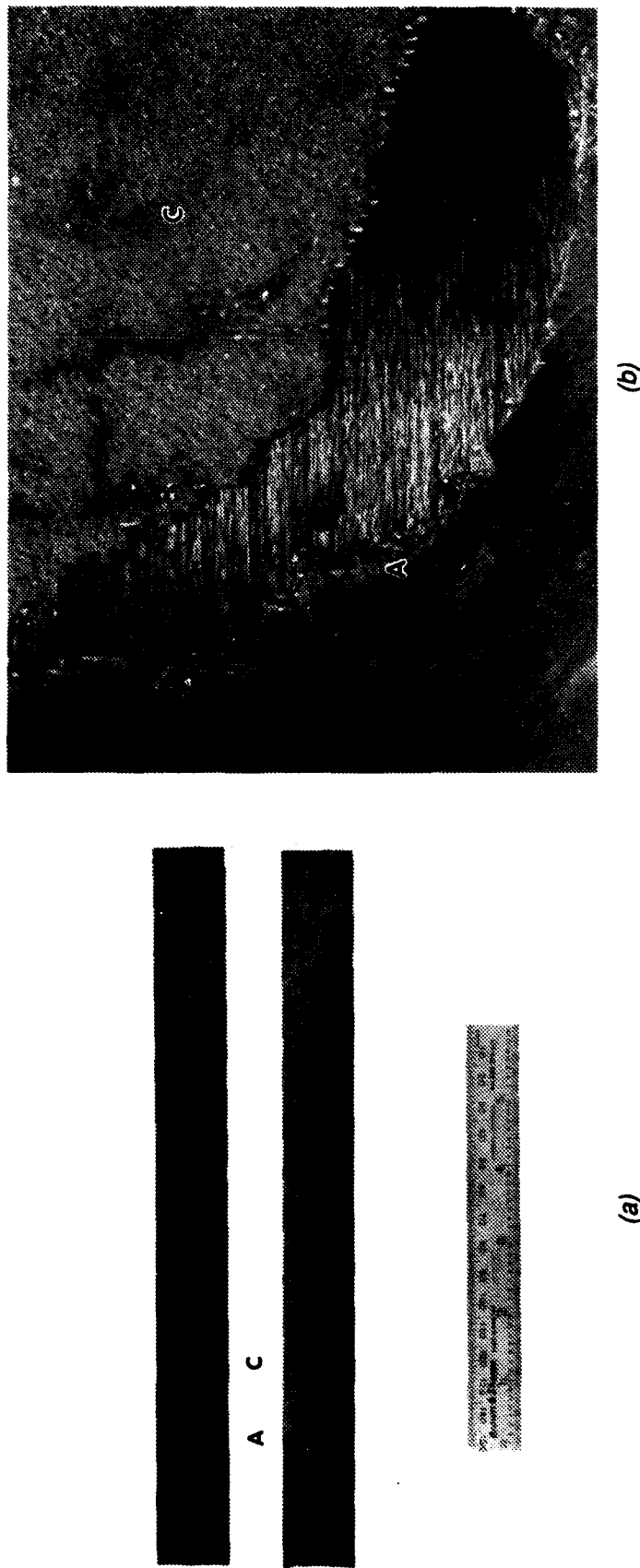
Figure 3-53. Optical and SEM Photographs of Failure in Unidirectional Gr/BMI Bonded to Quasi-Isotropic Gr/BMI With EA 9673 Adhesive and Tested Under Mode I Tension
(a) Macrophotograph
(b) Low Magnification (4X) Photograph Showing Transition From Adhesive to Cohesive Failure

A = Adhesive failure
C = Cohesive failure
CD = Crack-propagation direction
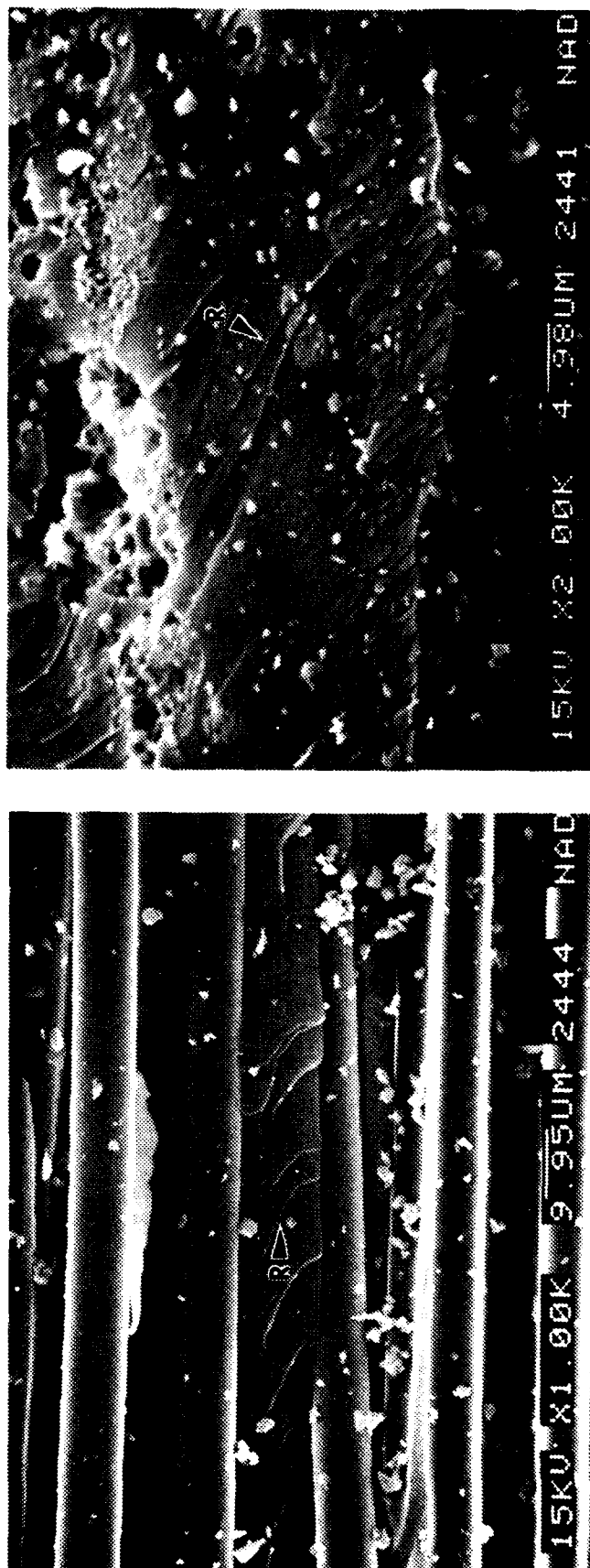
Figure 3-53. (Continued)
(c) Rivers (R) in Adhesive Failure Area
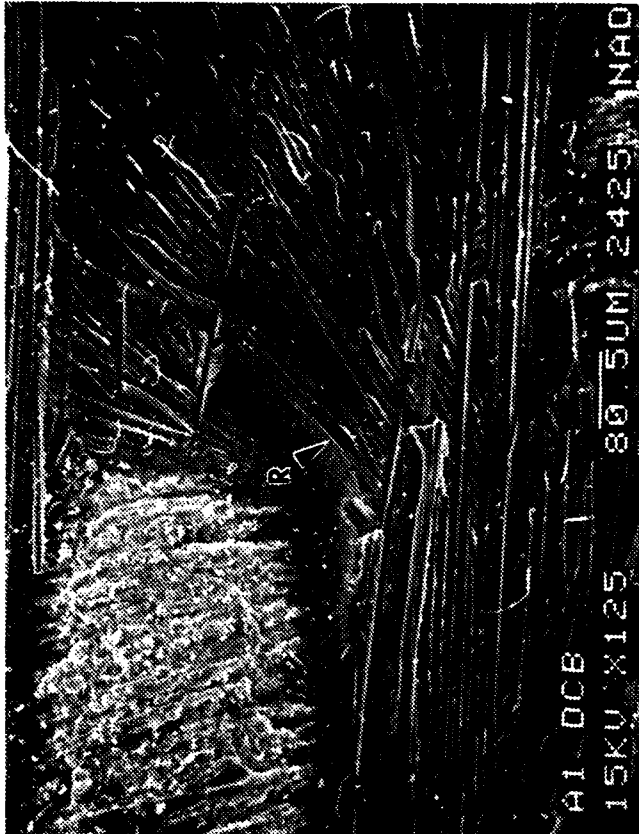(d) Rivers (R) in Cohesive Failure Area

CD = Crack-propagation direction

(a)

(b)

CD
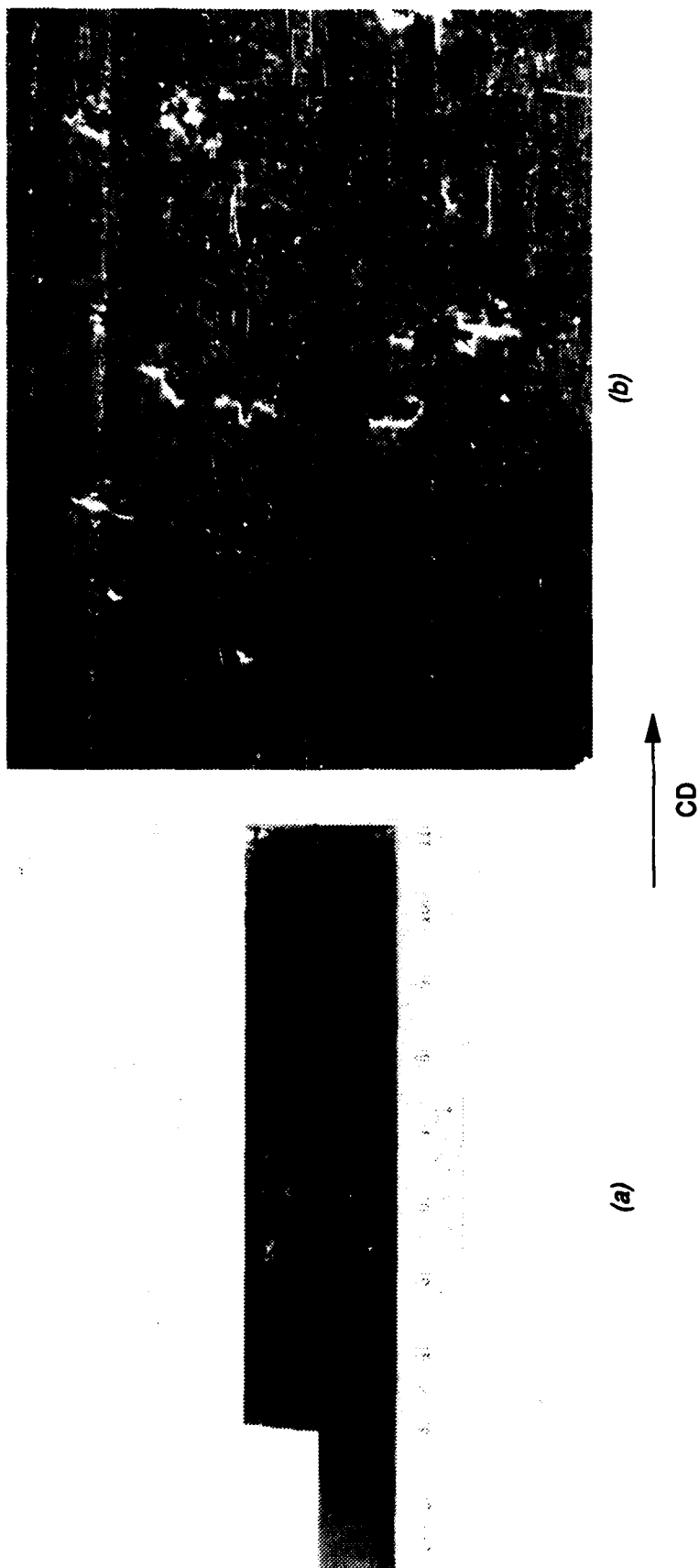
Figure 3-54. Optical Photographs of Fracture in Unidirectional AS4/5250-3 Gr/BMI Adherends Bonded With EA 9673 Adhesive and Tested Under Mode I Tension and Mode II Interlaminar Shear
(a) Macrophotograph of Fracture
(b) Low Magnification (4X) Photograph Showing Cohesive (C) Failure Characteristics

CD = Crack-propagation direction

Table 3-17. AS4/3501-6 Gr/Ep In-Plane Shear Test Specimens

VARIABLE CONDITION	NUMBER OF PLIES/ORIENTATION	
	24/ ±45	24/0, 90
BASELINE (DEFECT-FREE)	3	3
IMPACT DAMAGE	3	–
WATER IMMERSION BEFORE TEST	3	3
WATER IMMERSION AFTER TEST	3*	3*
UNDERCURE	3	–
OVERCURE	3	–

* NOTE: USE BASELINE SPECIMENS FOR WATER IMMERSION AFTER TEST.

3.4.6.1 Baseline AS4/3501-6 Gr/Ep – [90/0)]₆

Figures 3-57a and 3-57b present macrophotographs of a failed [90/0]$_{6S}$ Gr/Ep rail-shear specimen. Testing had resulted in in-plane shear failure in the central regions of the specimen. The 90-degree plies had been subjected to rotational bending loads, and this resulted in longitudinal splitting of the fibers, as illustrated in Figure 3-57b.

Figures 3-57c, 3-57d and 3-57e show SEM photographs of typical fracture characteristics. Testing had also resulted in delaminations between the 90 and 0 degree plies. Figure 3-57c shows a typical delaminated region (exposed by sectioning the outer plies). The fracture characteristics in the 90 and 0 degree plies were typical of shear, namely occurrence of hackles (Figures 3-57d and 3-57e). In addition resin debris were also observed indicating compression characteristics (Figure 3-57d). These observations suggest that the failure consisted of fiber splits, delamination due to shear, and compression of the fiber bundles.

3.4.6.2 Baseline AS4/3501-6 Gr/Ep – [+45/-45]₆

Figure 3-58a presents a macrophotograph of a failed [+45/-45]$_{6S}$ Gr/Ep rail-shear specimen. Testing had resulted in catastrophic fracture of the coupon. Figure 3-58b is a collage illustrating the through thickness fracture viewed end-on. The in-plane shear fracture regions could easily be distinguished from the secondary transverse tensile fracture that initiated at the bolt-hole. The in-plane shear fracture regions had a relatively smoother topography than the transverse tensile fracture regions, as shown in Figure 3-58b. The coarse chevrons indicate that the secondary fracture initiated at the bolt hole.
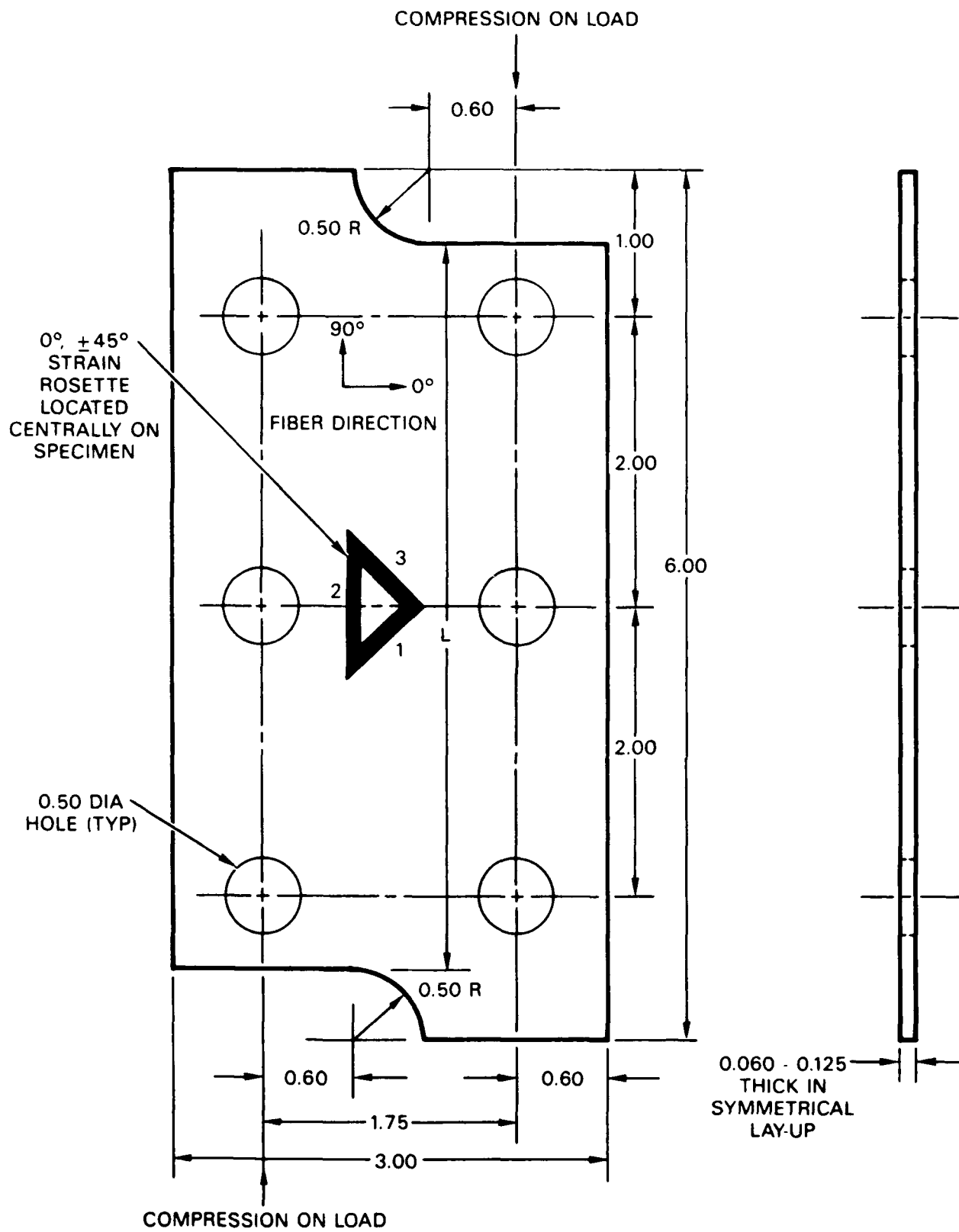
Figure 3-55. Rail-Shear Specimen
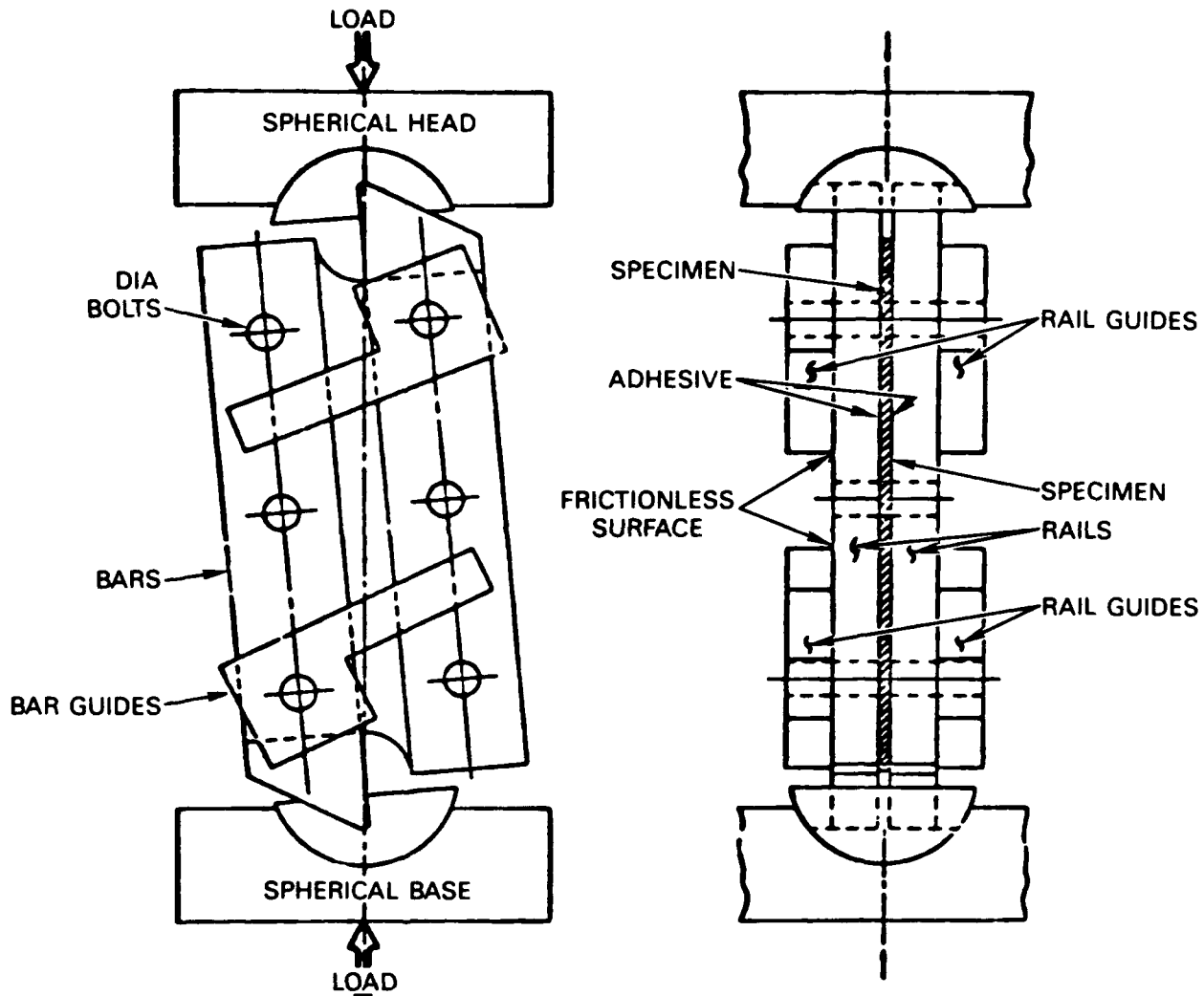
Figure 3-56. Rail-Shear Test Set-Up

Figures 3-58c through 3-58e illustrate microscopic fracture features in these regions. The +45-degree plies (oriented parallel to the applied shear loads) exhibited hackles and compression debris (Figure 3-58c) in the in-plane shear fracture region. The -45-degree plies (oriented normal to the applied shear loads) exhibited transverse tensile fracture characteristics, with individual fibers exhibiting DAF radials, oriented toward the direction of macroscopic fracture (Figure 3-58d).

Figure 3-58e shows the transverse tensile fracture characteristics observed in regions close to the bolt-hole. The fractured epoxy on the +45-degree plies was decorated with rivers and hackles, with the rivers oriented away from the bolt-hole, indicating that secondary failure had initiated at the bolt-hole.
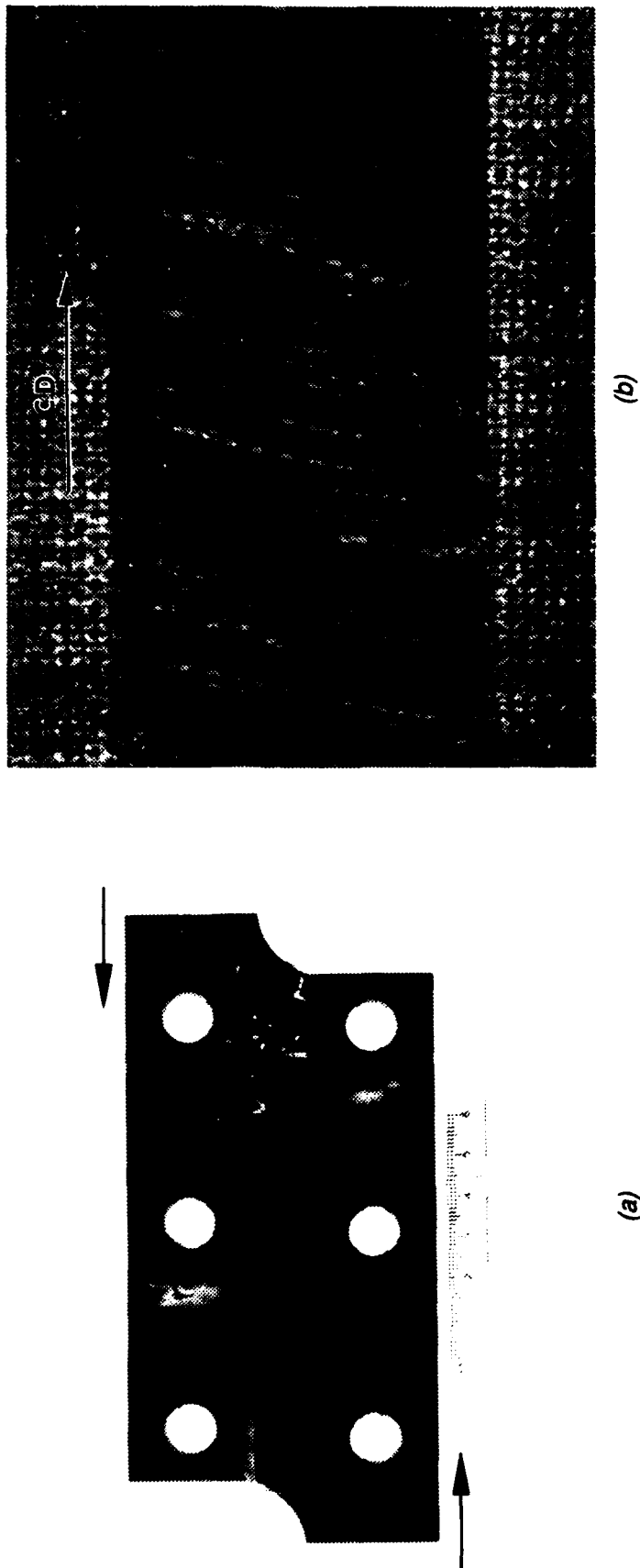
Figure 3-57. Optical and SEM Photographs of AS4/3501-6 Gr/Ep - $[0/90]_{6s}$, In-Plane Shear-Tested (Baseline)

(a) Macrophotograph of Rail Shear Specimen
Note: Arrows indicate loading direction.

(b) Close-Up View of In-Plane Shear Region

CD = Crack-propagation direction

CD →
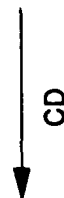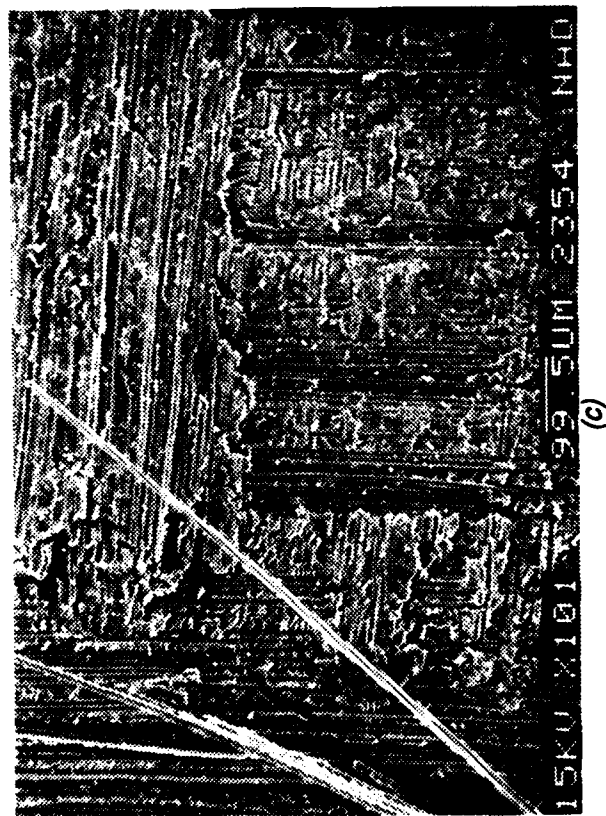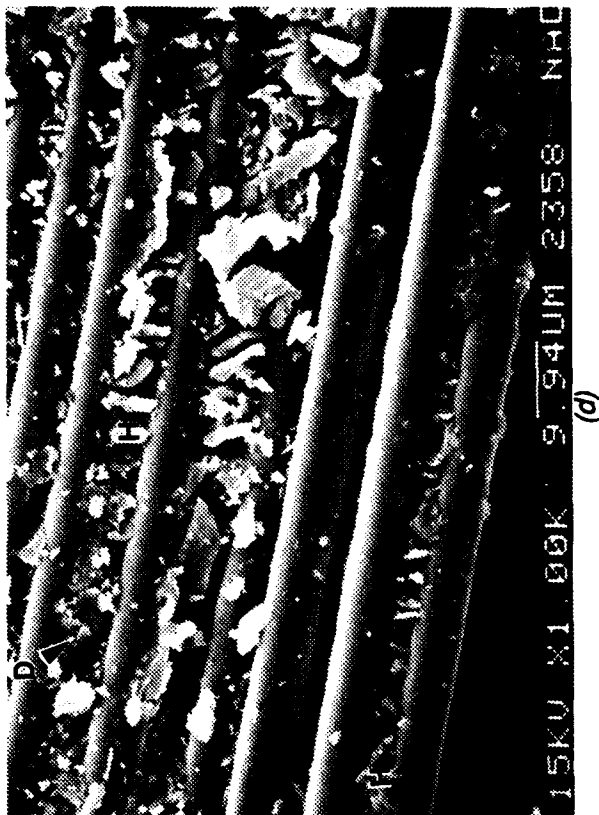
Figure 3-57. (Continued)
(c) Delaminated Fracture Surface of Region
Exposed by Sectioning Outer Plies
(d), (e) Fracture in 90 and 0 Degree Plies

CD = Crack-propagation direction
D = Compression debris
H = Hackles
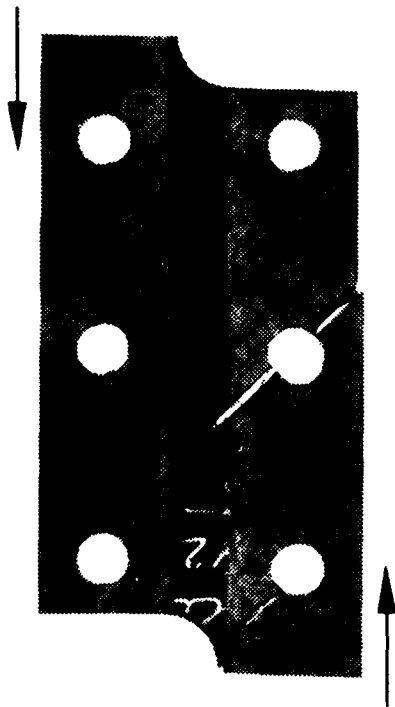
Figure 3-58. Optical and SEM Photographs of AS4/3501-6 Gr/Ep - [+45/-45]$_{6s}$, In-Plane Shear Tested (Baseline)

(a) Macrophotograph of Rail-Shear Specimen
Note: Arrows indicate loading directions.

(b) Close-up View of Fracture Viewed End-On
Note: Arrows indicate chevrons oriented toward bolt-hole.
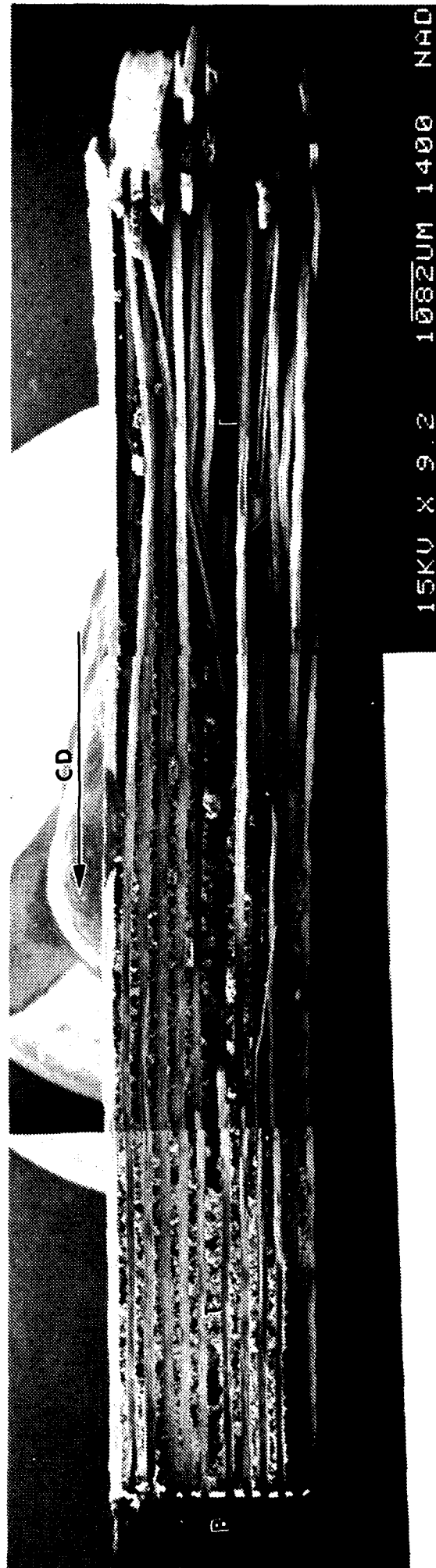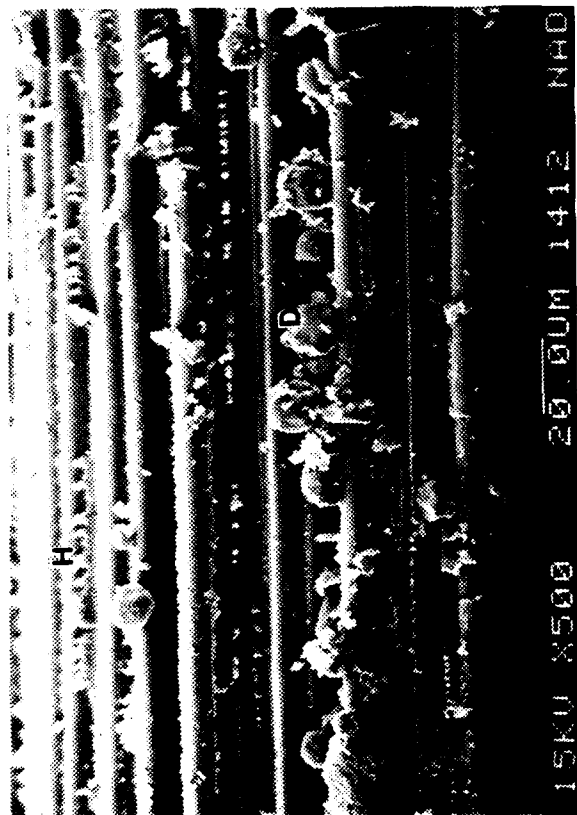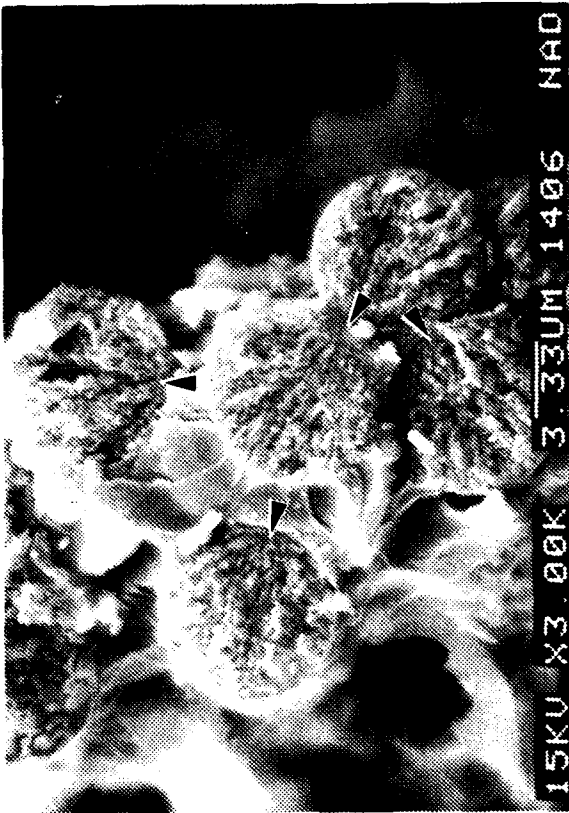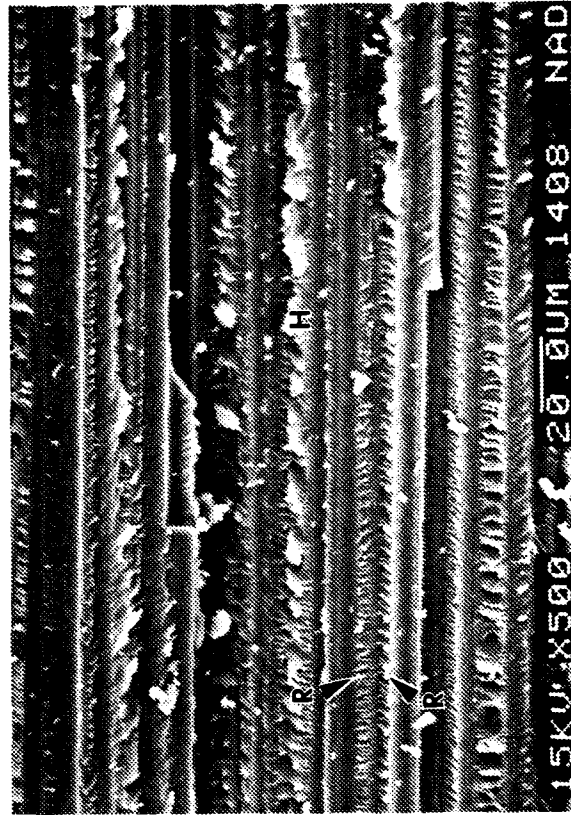
B = Bolt-hole
CD = Crack-propagation direction
I = In-plane shear region
T = Secondary transverse tensile fracture
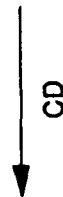
Figure 3-58. (Continued)
   (c) Fracture in +45 Degree Ply Showing Hackles (H)
       and Compression Debris (D)
   (d) Fracture in -45 Degree Ply Showing Tensile Fiber
       Breaks
       Note DAF radials (arrows)
   (e) Transverse Tensile Fracture in Secondary Failure
       Region Showing Rivers (R) and Hackles (H)
       Note rivers oriented away from bolt-hole

   CD = Crack-propagation direction
   D = Compression debris
   H = Hackles
   R = Rivers

3.4.6.3 Undercured AS4/3501-6 Gr/Ep – [+45/-44]$_{6S}$

Figure 3-59 shows macroscopic and microscopic fracture features in AS4/3501-6 Gr/Ep – [+45/-45]$_{6S}$, that was undercured (for undercure process details refer to Reference 5). The fracture characteristics were extremely similar to that of baseline Gr/Ep, described above. The in-plane shear fracture regions were characterized by either hackles (Figure 3-59b) or tensile fiber breaks (Figure 3-59c). Secondary fracture occurred, similar to the baseline, at the bolt holes.

3.4.6.4 Overcured AS4/3501-6 Gr/Ep – [+45/-45]$_{6S}$

Figure 3-60 shows macroscopic and microscopic fracture features in AS4/3501-6 Gr/Ep – [+45/-45]$_{6S}$, that was overcured (overcure process details are given in Reference 5). On a macroscopic scale, overcuring appeared to have resulted in more severe catastrophic fracture in the rail-shear specimen, than for the baseline. On a microscopic scale, the fracture characteristics were similar, as is illustrated in Figures 3-60b and 3-60c.

3.4.6.5 Water Immersed AS4/3501-6 Gr/Ep – [90/0]$_{6S}$, [+45/-45]$_{6S}$

Water immersion before or after testing had no effect on the fracture characteristics.

3.4.7 Fractography of Impact and Post-Impact-Compression (PIC) Specimens

In Subtask 3.6, Northrop characterized the failure modes of thin, medium and thick laminates that had been impact-tested, and tested in post-impact compression. The forces used for impact were sufficient to cause three failure modes: through-hole damage, composite buckling, and matrix cracking/delaminations.

Northrop performed the study for two material systems: AS4/3501-6 Gr/Ep, and AS4/APC-2 Gr/PEEK thermoplastic (Gr/TP). Selection of Gr/Ep was based upon the rationale for further expansion of the database for the baseline material. Gr/TP was chosen on the bases of its use in several near-term military aircraft that will form part of the Air Force fleet.

To assess the effects of thickness variations, Northrop performed impact and PIC tests on coupons fabricated from 16-, 32- and 48-ply quasi-isotropic panels. The three principal failure conditions (matrix cracking/delaminations, composite buckling, and through-hole damage) were established through trial tests on sample coupons. PIC testing was conducted in accordance with NASA specification RP 1092 (Reference 7).

Figures 3-61 through 3-63 show photographs of impact tested Gr/Ep in which the three principal failure conditions were developed. The damage zones for each of the three failure modes were mapped using A-scan techniques. In all cases, impact was characterized by a characteristic fracture signature, namely a zone of macroscopic delaminations. The plane of maximum delamination in each case was exposed using ply-removal techniques previously developed in Task 2.

Figures 3-64 through 3-66 illustrate the three failure modes in Gr/PEEK. A comparison of these results with the data for Gr/Ep shows that the damage zones in Gr/PEEK appear much
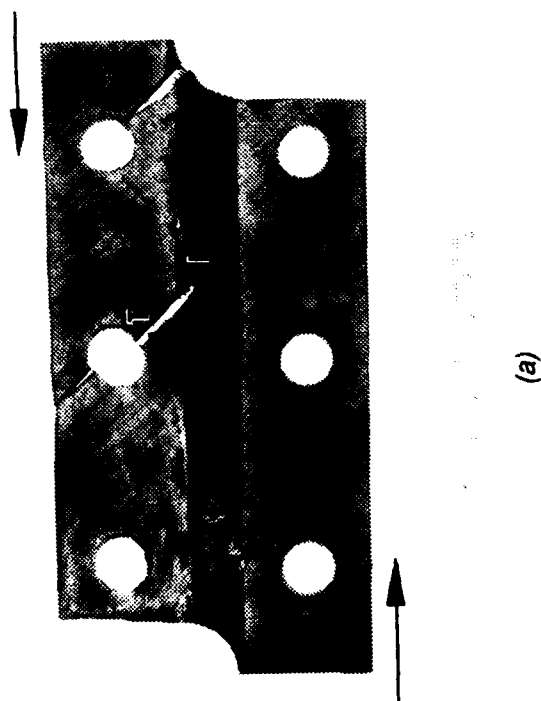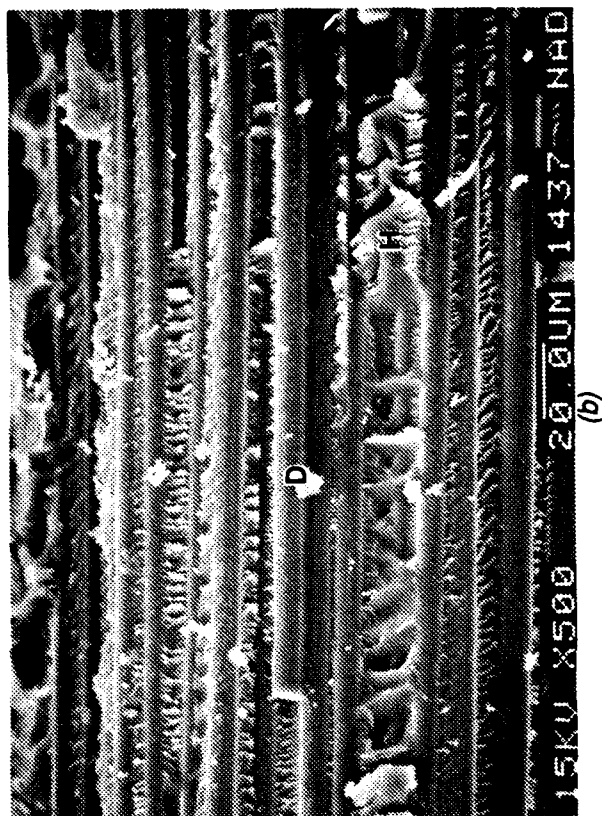
Figure 3-59. Optical and SEM Photographs of AS4/3501-6 Undercured Gr/Ep - [+45/-45]₆ₛ, In-Plane Shear Tested

(a) Macrophotograph of Rail Shear Specimen
  Note arrows indicating loading directions

(b) Fracture in +45 Degree Ply Showing Hackles (H) and Compression Debris (D)

(c) Fracture in -45 Degree Ply Showing Tensile Fiber Breaks
  Note DAF radials (arrows)

CD = Crack-propagation direction
I = In-plane shear region
T = Secondary transverse tensile fracture
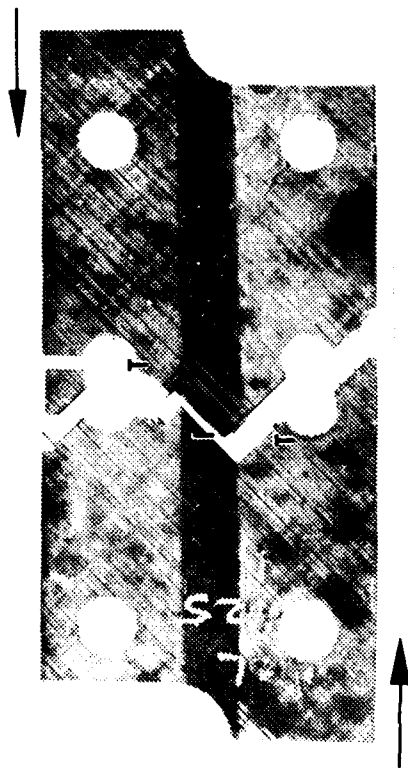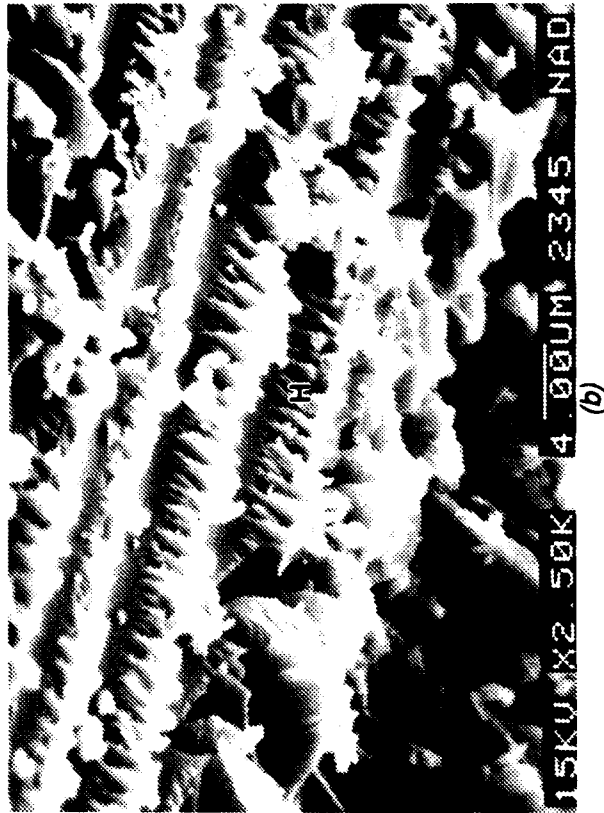
Figure 3-60. Optical and SEM Photographs of AS4/3501-6 Overcured Gr/Ep - [+45/-45]₆s, In-Plane Shear Tested

(a) Macrophotograph of Rail-Shear Specimen
Note arrows indicating loading direction

(b) Fracture in +45 Degree Ply Showing Hackles (H)

(c) Transverse Tensile Fracture in Secondary Failure Region

CD = Crack-propagation direction
I = In-plane shear region
T = Secondary transverse tensile fracture
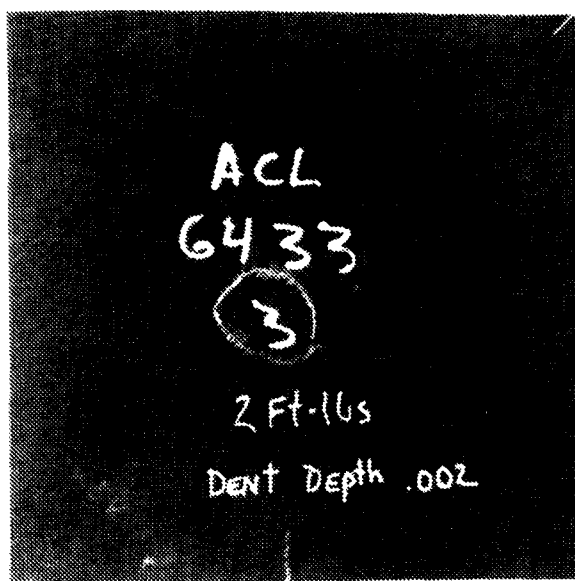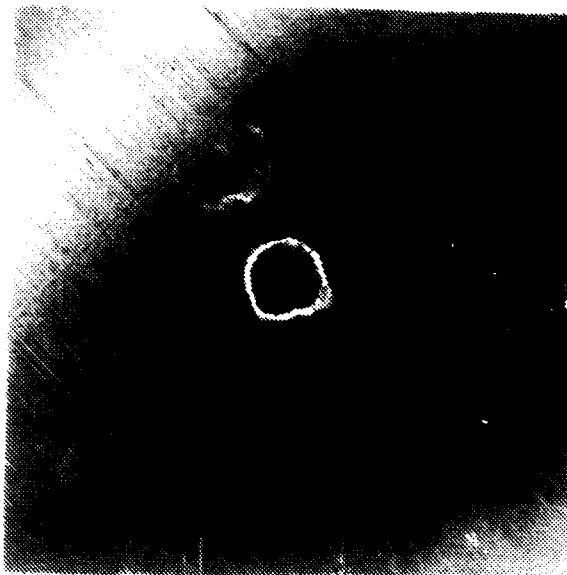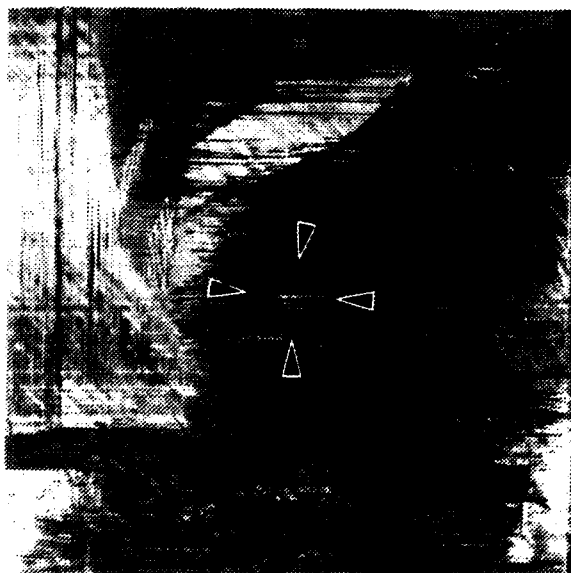
Figure 3-61. Photographs of 16-Ply AS4/3501-6 Gr/Ep Impacted With a Force of
2 ft-lbs to Achieve Matrix Cracking/Delamination
(a) As-Tested Specimen
(b) A-Scan of Impact Damage
(c) Mating Fracture Halves Showing Impact Signature (Arrows)

(a)

(b)

(c)
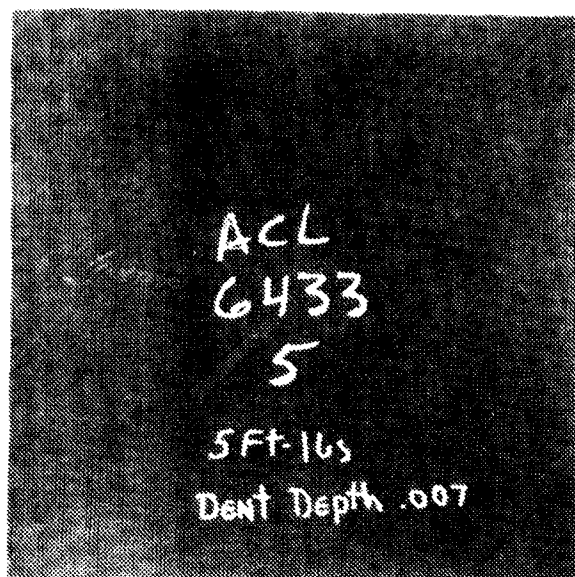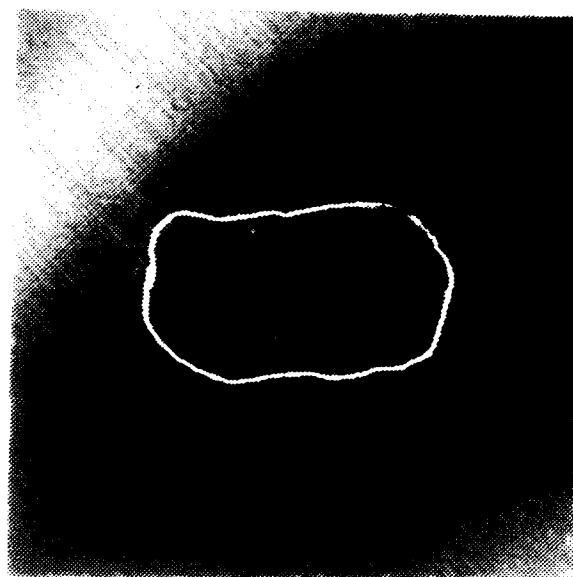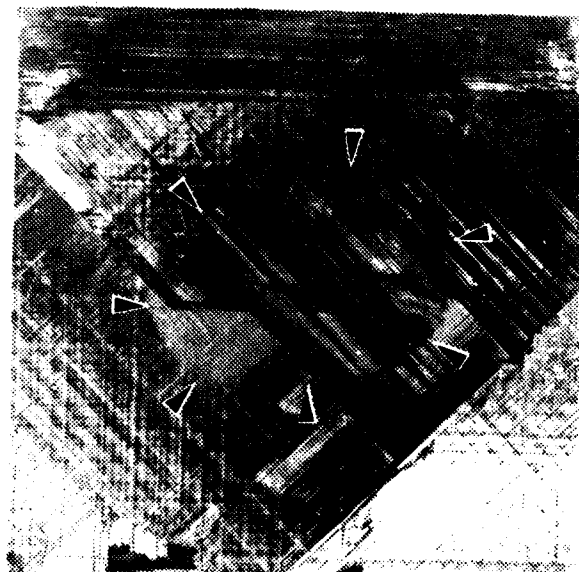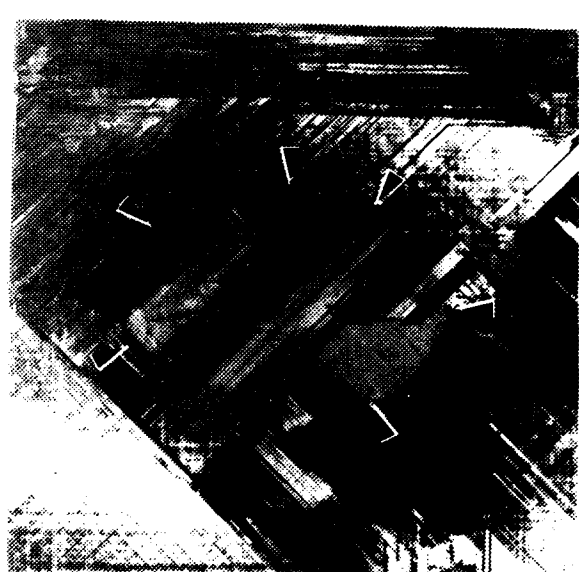
Figure 3-62. Photographs of 16-Ply AS4/3501-6 Gr/Ep Impacted With a Force of
5 ft-lbs to Achieve Composite Buckling
(a) As-Tested Specimen
(b) A-Scan of Impact Damage
(c) Mating Fracture Halves Showing Impact Signature (Arrows)

(a)

(b)
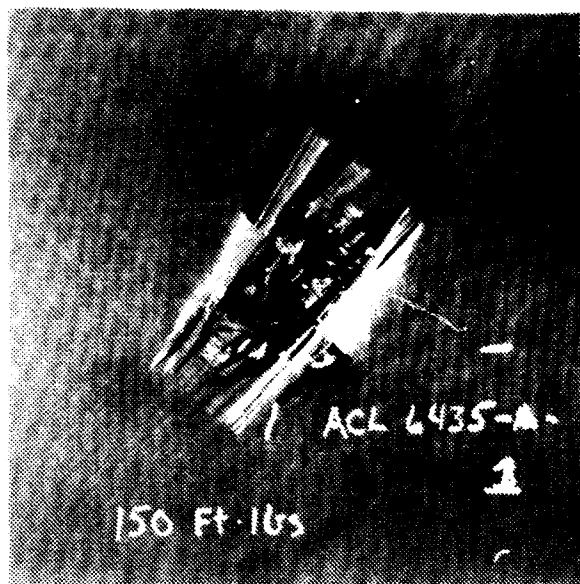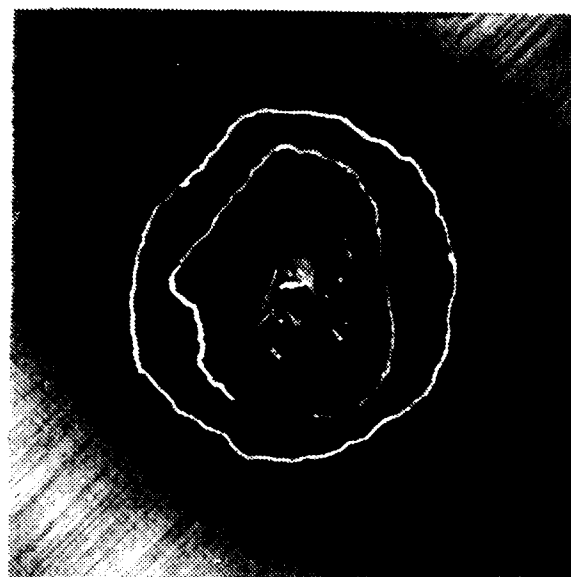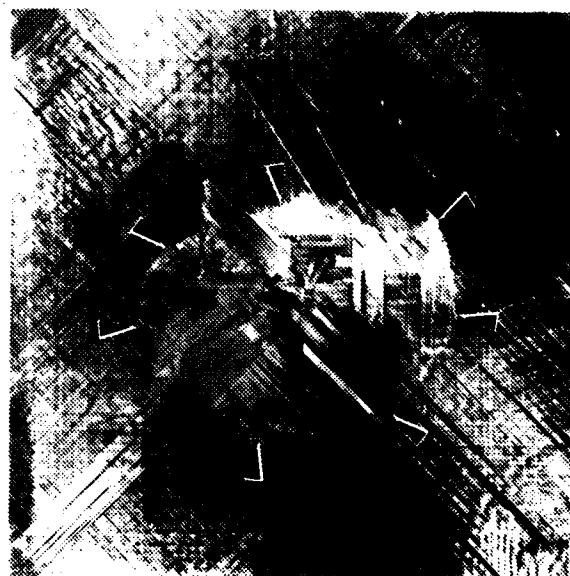
(c)

Figure 3-63.   Photographs of 48-Ply AS4/3501-6 Gr/Ep Impacted With a Force of
150 ft-lbs to Achieve Through-Hole Damage
(a) As-Tested Specimen
(b) A-Scan of Impact Damage
(c) Mating Fracture Halves Showing Impact Signature (Arrows)

3-113

(a)

(b)
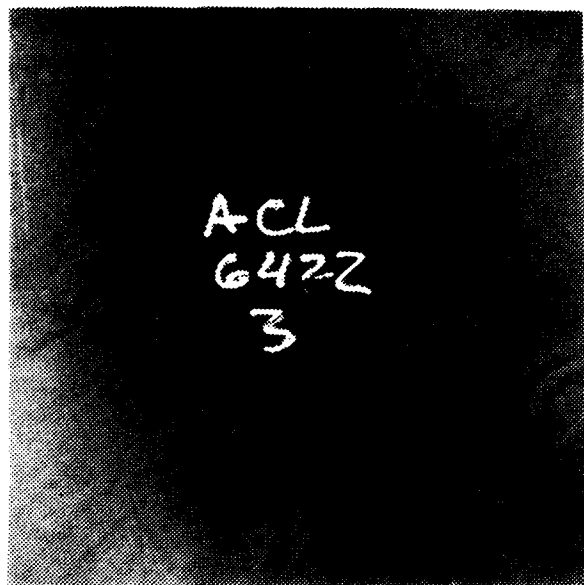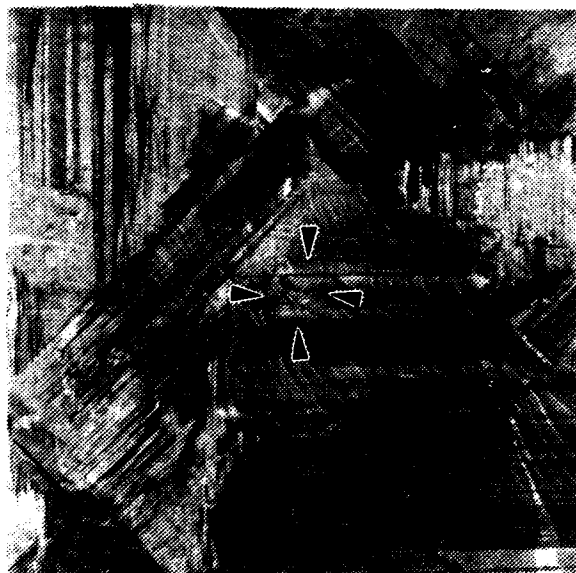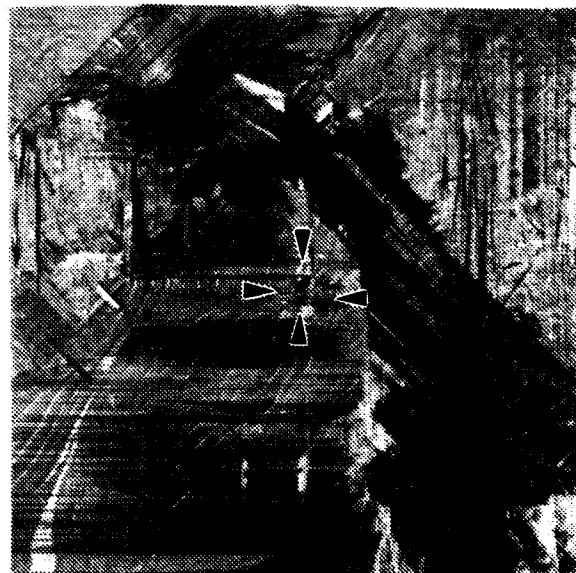
(c)

Figure 3-64. Photographs of 48-Ply AS4/APC-2 Gr/PEEK Impacted With a
Force of 40 ft-lbs to Achieve Matrix Cracking/Delamination
(a), (b) As-Tested Specimen (Top and Bottom Faces)
(c) Mating Fracture Halves Showing Impact Signature (Arrows)

(a)

(b)
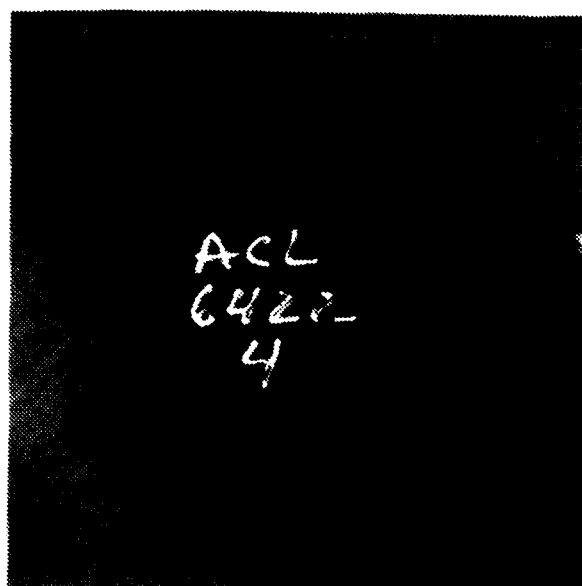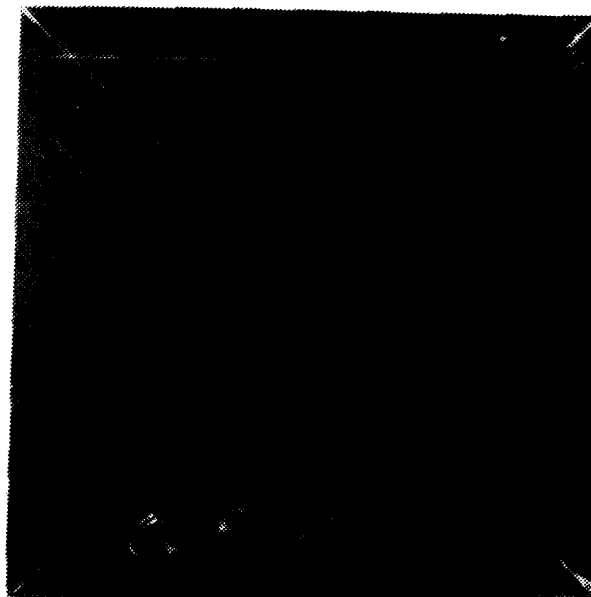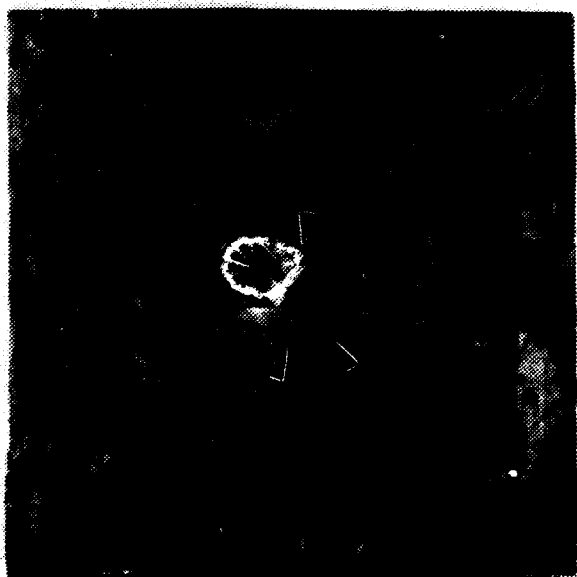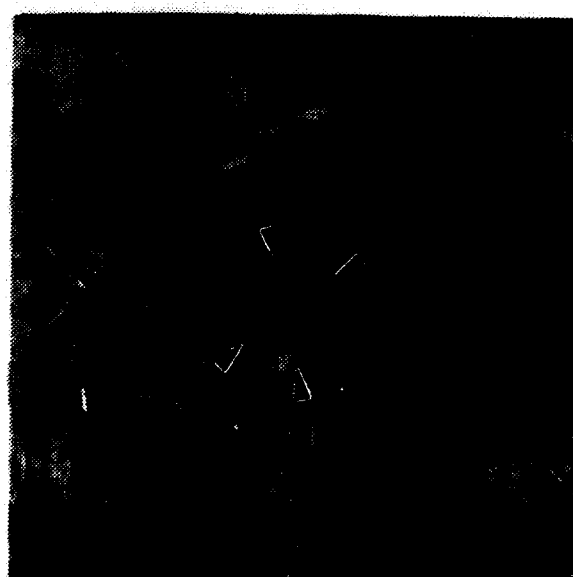
(c)

Figure 3-65. Photographs of 48-Ply AS4/APC-2 Gr/PEEK Impacted With a
Force of 60 ft-lbs to Achieve Composite Buckling
(a), (b) As-Tested Specimen (Top and Bottom Faces)
(c) Mating Fracture Halves Showing Impact Signature (Arrows)

(a)

(b)

(c)
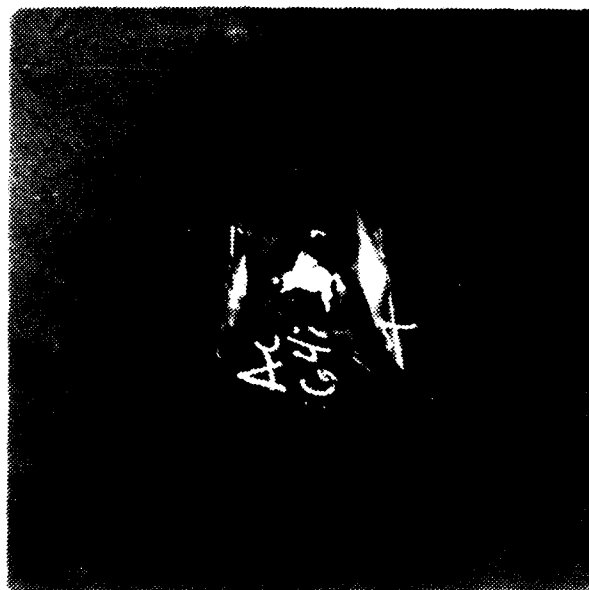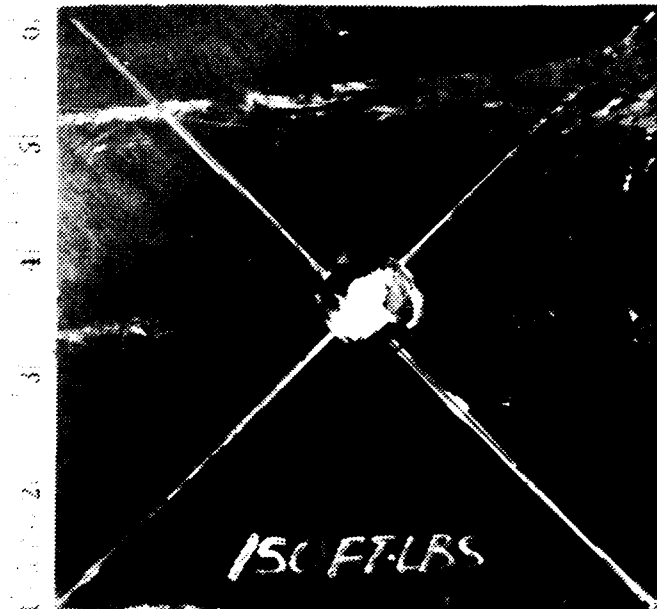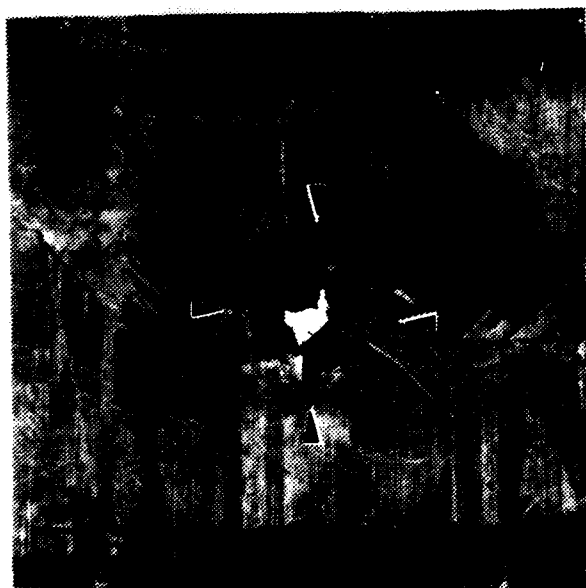
Figure 3-66. Photographs of 48-Ply AS4/APC-2 Gr/PEEK Impacted With a
Force of 150 ft-lbs to Achieve Through-Hole Damage
(a), (b) As-Tested Specimen (Top and Bottom Faces)
(c) Mating Fracture Halves Showing Impact Signature (Arrows)

smaller; and higher impact loads are required to create the desired failure modes. This is believed to be a consequence of the tougher thermoplastic matrix.

Figures 3-67 through 3-70 show photographs of fracture in Gr/Ep and Gr/PEEK that were impact damaged and subsequently PIC tested. Evaluation of the 16-ply Gr/Ep specimen indicated that the compression failure was unrelated to the impact damage (Figure 3-67). It is believed that this was a consequence of the PIC specimen being too thin (16-ply). In the thicker specimens, macroscopic compression failure initiated in the zones of delamination caused by impact (Figures 3-68 through 3-70).

3.5 DATA FORMATS FOR REPORTING RESULTS

Northrop reviewed formats that had been used in the past for reporting metallic and composite fractography and failure analysis data. The review included evaluation of formats used internally at Northrop, those reported in ASM's Metals Handbooks (References 10 and 11), and those used by The Boeing Company (References 3 and 4). In addition, Northrop reviewed the formats of handbooks previously produced by Northrop for the Air Force (Reference 1) and the Federal Aviation Administration (Reference 12).

Based on an assessment of existing report schemes, Northrop proposed data formats for: 1) reporting fractographic data, 2) failure analysis information, and 3) organization of the Composite Failure Analysis Handbook. These were subsequently approved by the Air Force with minor modifications.

3.5.1 Fractographic Data

Figure 3-71 shows the outline of the format that Northrop developed for reporting fractographic data on resin-based composite materials. The format contained information on the material type, prepreg type, laminate orientation, test type, test condition, test results, as well as the necessary fractographic information.

3.5.2 Failure Analysis Reports

Figure 3-72 shows the outline of the format that Northrop recommended for failure analysis investigations. The scheme was primarily based on the format used in ASM's Metals Handbook (Reference 11).

3.5.3 Composite Failure Analysis Handbook

The outline that Northrop proposed for the overall Handbook was reviewed by the Air Force. Based on discussions with the Air Force, the FAA, and Boeing, the outline was modified and forms the basis for Volume II of this report.

ACL 6403-3 16 PLY (GR/EP)
IMPACT 5 FT-LB

(a)
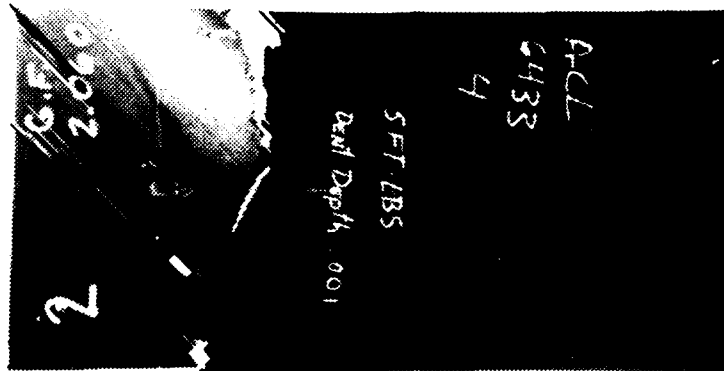
ACL 6403-4 16 PLY (GR/EP)
IMPACT 5 FT-LB

(b)

*Figure 3-67. Photographs of 16-Ply AS4/3501-6 Gr/Ep Impacted With a Force of
5 ft-lbs and PIC Tested
(a) As-Tested Specimen
(b) A-Scan of Impact Damage*

3-118
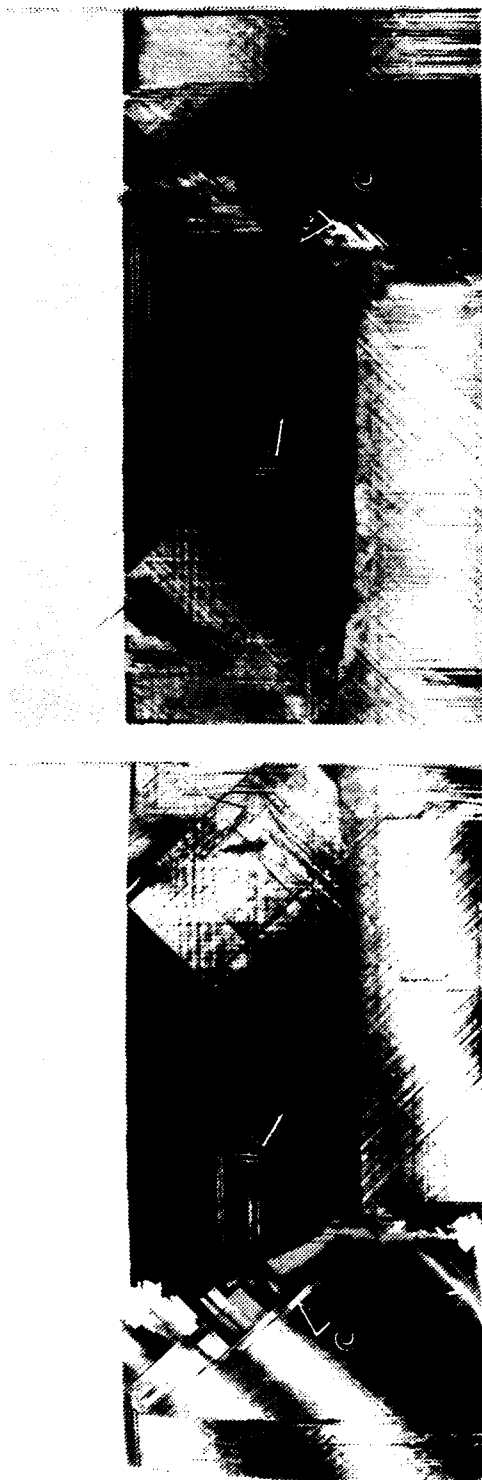
(c)

Figure 3-67. (Continued)
(c) Mating Fracture Halves Showing Impact (I) and Compression (C) Failure Regions
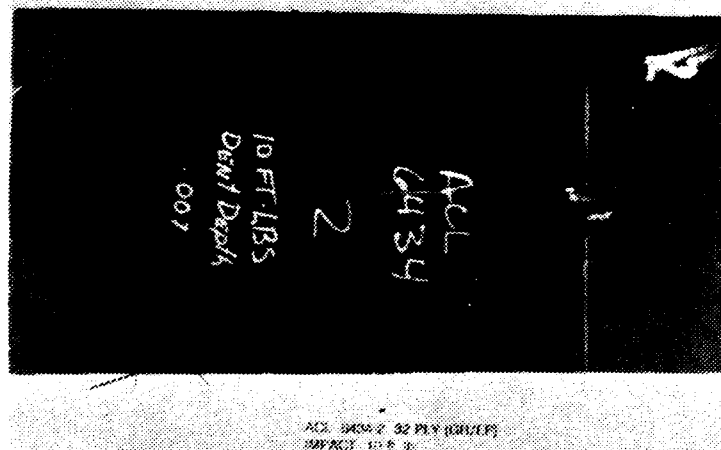
(a)
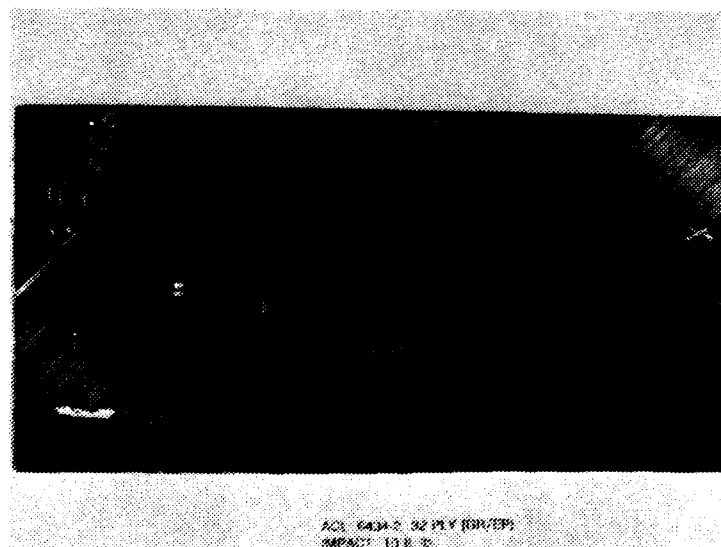
(b)

Figure 3-68.   Photographs of 32-Ply AS4/3501-6 Gr/Ep Impacted With a
Force of 10 ft-lbs and PIC Tested
(a), (b) As-Tested Specimen (Top and Bottom Faces)
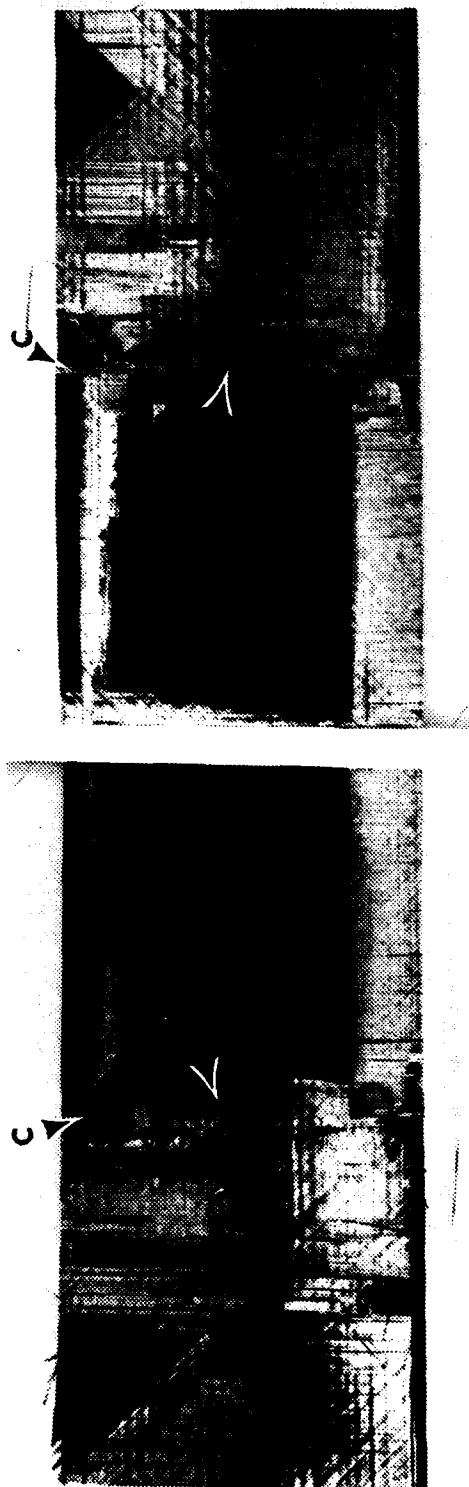
Figure 3-68. (Continued)
(c) Mating Fracture Halves Showing Impact (I) and Compression (C) Failure Regions
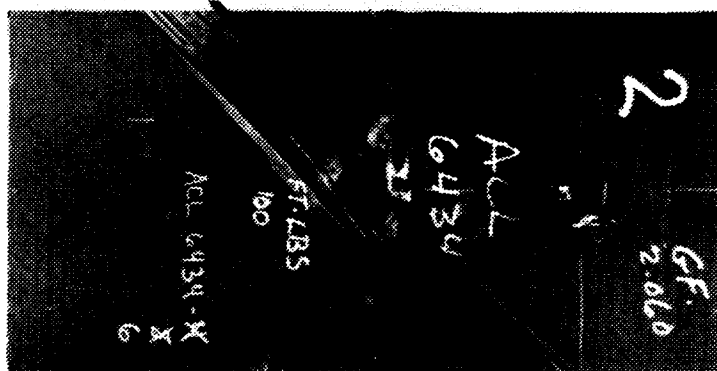
(a)
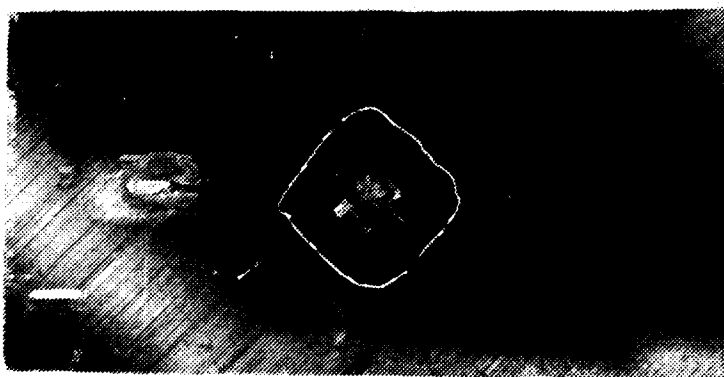
(b)

Figure 3-69. Photographs of 32-Ply AS4/3501-6 Gr/Ep Impacted
With a Force of 100 ft-lbs and PIC Tested
(a) As-Tested Specimen
(b) A-Scan Showing Impact Damage

ACL 6434-4 32 PLY (GR/EP)
IMPACT 100 ft. lb.

ACL 6434-4 32 PLY (GR/EP)
IMPACT 100 ft. lb.

(c)

Figure 3-69. (Continued)
(c) Mating Fracture Halves Showing Impact (I) and Compression (C) Failure Regions

(a)
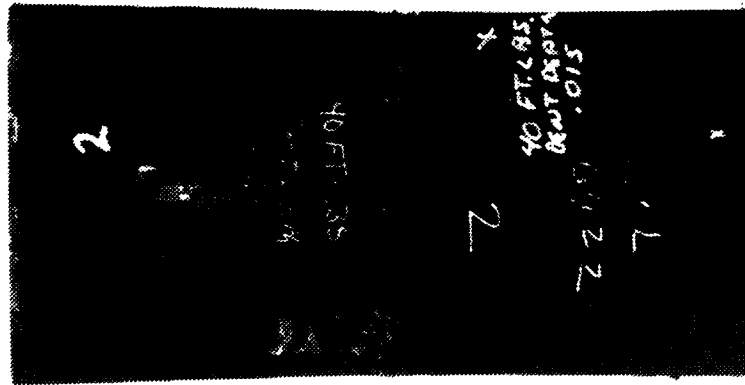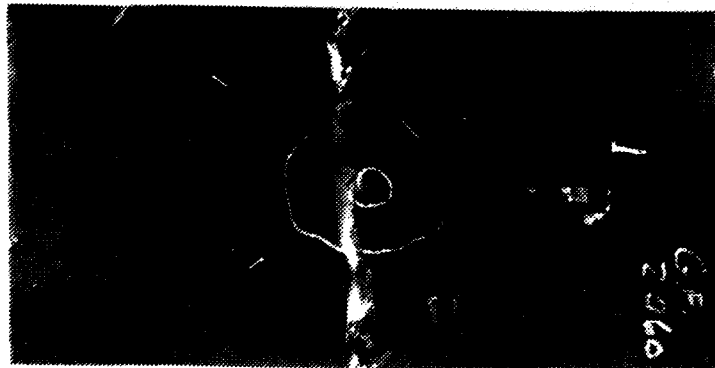
(b)

Figure 3-70. Photographs of 48-Ply AS4/3501-6 Gr/Ep Impacted With a Force of 40 ft-lbs and PIC Tested
(a) As-Tested Specimen
(b) A-Scan Showing Impact Damage

Figure 3-70. (Continued)
(c) Mating Fracture Halves Showing Impact (I) and Compression (C) Failure Regions

```
1.0     INTRODUCTION

2.0     MATERIAL

                - Prepreg Type (Fiber/Resin)
                - Laminate/Orientation
                - Processing Information

3.0     MECHANICAL TEST INFORMATION

                - Test Specimen Configuration
                - Loading Condition
                - Test Conditions
                - Mechanical Test Data

4.0     FRACTOGRAPHIC DATA

                - Visual /Microscopic Observations
                - SEM Macroscopic Observations
                - SEM Microscopic Observations
                - Analysis of Data - Initiation Site
                - Analysis of Data - Crack Propagation Direction

5.0     SUMMARY AND CONCLUSIONS
```

Figure 3-71. Fractographic Data Reporting Format

3.6 COMPILATION OF MATERIAL PROPERTIES

Northrop performed work in Task 5 on gathering and compiling material properties on current and near-term composite structural materials used in military aircraft. Literature searches were carried out on the Defense Technical Information Center (DTIC), the Plastics Center, and NASA databases. The keywords used and associated source(s) and abstracts that were found are shown in Table 3-18. Northrop requested copies for review and ordered the technical publications determined to be relevant.

In addition to the abstracts, Northrop reviewed product data sheets obtained from manufacturers. Northrop started compilation of properties obtained into database files using a personal computer. Totals of 317 mechanical and 227 uncured prepreg properties of commercial materials were entered into the database. The number of compiled data sets are shown in Table 3-19. The properties incorporated into the database for uncured prepregs include resin content, resin flow, resin volatile content, tack, drape, fiber areal weight, shelf life, out time, and gel time.

In the compilation of fiber properties, properties for 23 commercial fibers were entered into the database. The properties included filament diameter, shape, filaments per tow, density,

```
1.0    ABSTRACT

2.0    BACKGROUND

            - Part Identification
            - Manufacturing History
            - Service History
            - Field Information Relating To Fracture
            - Detection of Problem

3.0    ANALYSIS OF FAILURE

            - NDI Techniques Used and Results
            - Fractographic Techniques Used and Results
            - Chemical Properties
            - Mechanical Properties
            - Engineering Analysis

4.0    CONCLUSIONS

5.0    RECOMMENDATIONS
```

Figure 3-72. Failure Analysis Data Reporting Format

coefficient of thermal expansion (longitudinal and transverse), tensile strength, tensile modulus, and elongation to break.

Properties for 13 commercial resins have been entered into the database. The resin properties incorporated into the database include ultimate tensile strength, tensile modulus, elongation at break, compressive strength, compressive modulus, flexural strength, flexural modulus, density, glass transition temperature, viscosity, and gel time.

All the data were organized into tabular formats and are presented in Volume II, Part 1, Appendix A. Sample data illustrating properties compiled for carbon/epoxy prepreg are shown in Table 3-20.

3.7 VERIFICATION OF THE COMPOSITE FAILURE ANALYSIS SYSTEM

The goal of Task 6 was to demonstrate the applicability of the failure analysis logic networks (FALNs) and techniques developed. Northrop performed a total of five failure analysis investigations as part of this task. The components included 1) failed horizontal torque box assembly, 2) a failed rudder, 3) a section from an adhesively bonded joint, 4) a simple torsional

Table 3-18. Keywords, Sources, and Abstracts in Literature Search of DTIC, NASA, and Plastics Center Databases

Keyword(s)	Source(s)	No. of Abstracts

Chemical/Mechanical Properties -
    Thermosetting Resins
    Thermoplastic Resins
    Fibers
    Epoxy Resins
	DTIC	21

Chemical/Mechanical Properties -
    Fiber Reinforced
    Composites
	DTIC,
	 Plastics
	 Center Data Base
		103

Epoxy/Graphite	NASA	598
PEEK/Graphite	NASA	86
Bismaleimide/Graphite	NASA	28
Fiber Reinforced Composites - Multi-Ply Laminates	DTIC	3

test coupon, and 5) a composite arch reinforcement from a trainer aircraft. The work on the components labeled 3 through 5 was additional work that the Air Force requested in Subtasks 6.2 and 6.3 of Modification P0002 to the original contract. All the results on the components are presented as case studies in Volume II, Part 3 — Case Histories. Also included in this volume are case studies performed by Boeing and General Electric. The results obtained on Subtasks 6.1 and 6.4 are presented below.

Fiber/Resin System	Mechanical Properties	Uncured Prepreg Properties
Glass/Epoxy	87	59
Carbon/Epoxy	77	52
Kevlar/Epoxy	57	41
Glass/Polyimide	16	16
Carbon/Polyimide	16	9
Glass/Silicone	2	0
Glass/Phenolic	16	17
Carbon/Phenolic	4	4
Ablative/Phenolic	17	17
Kevlar/Phenolic	5	2
Glass/Polyester	15	10
Kevlar/Polyester	5	0

3.7.1 Fabrication and Testing of Two Simple Composite Structures

As part of Task 6, Subtask 6.1, Northrop fabricated two simple Gr/Ep composite structures containing intentional defects, and tested the structures to failure under controlled laboratory conditions. The specimens consisted of an L-shaped Gr/Ep stringer containing a delamination defect, and a simple Gr/Ep-Al honeycomb structure containing porosity in the skins. The geometries and failure tests are described below. Both parts were shipped to the USAF, as required by the contract, together with supporting test information.

3.7.1.1 Composite Stringer

Figure 3-73 shows a schematic diagram of the L-shaped stringer and a photograph of the fabricated part. The specimen (5 inches x 5 inches x 12 inches) was fabricated from AS4/3501-6 Gr/Ep (32-ply, quasi-isotropic 0-, 45-, and 90-degree ply orientations). As illustrated in Figure 3-73a, a defect in the form of Armalon film was introduced mid-plane in the radius of the stringer.

Figures 3-74a and 3-74b show a schematic of the test setup for failure testing of the stringer, and a photograph of the part being failure tested. The part was strain gaged on the inner and outer faces of one of the legs (labeled 1 through 6 in Figure 3-73b), and tested under interlaminar tensile loading. The load history, and measured strains are shown in Table 3-21.

Cracking initiated at an applied load of 163 lbs, with failure of the part at a load of 262 lbs. As expected, failure initiated in the bend section at the Armalon film in the form of delaminations and trans-ply cracks. After onset of failure, the load-carrying capacity of the part dropped to less than 25 of the maximum load. Strain measurements were discontinued after the onset of failure.

Table 3-20. Properties of Carbon/Epoxy Prepreg

Manufacturer	Product Number	Prepreg Type/ Orientation	Prepreg Cure	Resin Content (%)
AMERICAN CYANAMID	CYCOM 907/T-300	UNIDIRECTIONAL	-	40 ± 3
	CYCOM 919/T-300	F-134 WEAVE	-	45 ± 2
	CYCOM 985/CELION	UNIDIRECTIONAL TAPE 145	-	37 ± 2
	CYCOM 985/CELION	7 MIL PLAIN WEAVE	-	40 ± 2
	CYCOM 985/T-300	UNIDIRECTIONAL TAPE	-	37 ± 3
	CYCOM 985/T-300	F-134 WEAVE	-	42 ± 2
	CYCOM 980/T-300	YARN F-134 WEAVE	-	42 ± 2
	CYCOM 980/T-300	UNIDIRECTIONAL TAPE	-	37 ± 3
CIBA-GEIGY	R6268	-	-	40 ± 2
	RAC 6350	-	-	43 ± 3
	R6376	UNIDIRECTIONAL	-	35
FERRO CORPORATION	CE-9000-1/T-300	2424 8H SATIN WEAVE	-	40 ± 3
	CE-9000-2	2424	-	40 ± 3
	CE-9000-9/T-300	UNIDIRECTIONAL	-	39 ± 3
	CE-343/CELION 6000	UNIDIRECTIONAL	-	40
	CE-3201/T-300	UNIDIRECTIONAL	-	39 ± 4
	CE-9000-9/P-75S	-	-	40.3
	CE-339/HMS	UNIDIRECTIONAL	-	41.3
	CE-339/GY-70	-	-	36.6
	CE-339/T-300	UNIDIRECTIONAL	-	39 ± 4
	CE-324/T-300	UNIDIRECTIONAL	-	39 ± 4
	CE-324/T-300	2424	-	40 ± 3
HERCULES	A*370-5H/3501-5A	5H WEAVE	-	42 ± 3, 35 ± 3
	A*370-5H/3501-6	5H WEAVE	-	42 ± 3, 35 ± 3
	A*370-8H/3501-5A	8H WEAVE	-	42 ± 3, 35 ± 3
	A*370-8H/3501-6	8H WEAVE	-	42 ± 3, 35 ± 3
	A*193-P/3501-5A	PLAIN WEAVE	-	42 ± 3, 35 ± 3
	A*193-P/3501-6	PLAIN WEAVE	-	42 ± 3, 35 ± 3
	HMS/1908	UNIDIRECTIONAL	-	38 ± 3
	HMS/3501-6	UNIDIRECTIONAL	-	42 ± 3
	HMS/3501-5A	UNIDIRECTIONAL	-	42 ± 3
	AS4/1908	UNIDIRECTIONAL W/O GLASS SCRIM	-	38 ± 3
	AS4/1908	UNIDIRECTIONAL/108 GLASS SCRIM	-	38 ± 3
	AS4/3502	UNIDIRECTIONAL	-	42 ± 3, 35 ± 3
	AS4/3501-6	UNIDIRECTIONAL	-	42 ± 3, 35 ± 3
	AS/3501-6	UNIDIRECTIONAL	-	42 ± 3, 35 ± 3
	AS4/3501-5A	UNIDIRECTIONAL	-	42 ± 3, 35 ± 3
	AS/3501-5A	UNIDIRECTIONAL	-	42 ± 3, 35 ± 3
	IG360-5H/3501-6	5H SATIN WEAVE	-	32 - 42
	AS4 OR IM7X/8551-7	TAPE	-	32 - 42
	AS4/8551-7	TAPE & FABRIC	-	33 - 46
	AS4/2220-3	UNIDIRECTIONAL TAPE	-	37 ± 3
	AS4/4502	UNIDIRECTIONAL TAPE	-	42 ± 3, 35 ± 3
	AS4/1919	UNIDIRECTIONAL TAPE	-	38 ± 3
	HMS4/3501-5A	UNIDIRECTIONAL TAPE	-	42 ± 3, 35 ± 3
	HMS4/3501-6	UNIDIRECTIONAL TAPE	-	42 ± 3, 35 ± 3
	IM6/3501-6	UNIDIRECTIONAL TAPE	-	32 - 42
	A*185-CSW/3501-5A	CROW'S-FOOT SATIN WEAVE	-	42 ± 3, 35 ± 3
	A*185-CSW/3501-6	CROW'S-FOOT SATIN WEAVE	-	42 ± 3, 35 ± 3
	A*185-CSW/3502	CROW'S-FOOT SATIN WEAVE	-	42 ± 3, 35 ± 3
	A*370-5H/3502	5H WEAVE	-	42 ± 3, 35 ± 3
	A*370-8H/3502	8H WEAVE	-	42 ± 3, 35 ± 3
	A*193-P/3502	PLAIN WEAVE	-	42 ± 3, 35 ± 3
	A*280-5H/3501-5A	5H WEAVE	-	42 ± 3, 35 ± 3
	A*280-5H/3501-6	5H WEAVE	-	42 ± 3, 35 ± 3
	A*280-5H/3502	5H WEAVE	-	42 ± 3, 35 ± 3
HEXCEL	T-300/F263	UNIDIRECTIONAL 3000 TOW	-	42 ± 3
	T-300/F250	UNIDIRECTIONAL 3000 TOW	-	42 ± 3
	T-300/F263	BIDIRECTIONAL WOVEN 3000 TOW	-	43 ± 3
	T-300/F163	UNIDIRECTIONAL 3000 TOW	OVEN CURE	33 ± 3
	T-300/F163	UNIDIRECTIONAL 3000 TOW	AUTOCLAVE	42 ± 3
	T6T190/F584	T-300 6K	-	36 - 40
	T4A145/F584	AS6 12K	-	26 - 30
	T5A145/F584	IM6 12K	-	32 - 36
	T5A190/F584	IM6 12K	-	32 - 36
	T6U145/F584	T-700 6K	-	32 - 36
	T8A145/F584	AS4 12K	-	27 - 30
HITCO	EM-7125A	CHOPPED STRAND MOLDING CMPD	-	37 - 43
	E767HM	UNIDIRECTIONAL TAPE	-	36
	E767	3K PLAIN WEAVE	-	40

3-130

Table 3-20. (Continued)

Resin Flow (%)	Volatile Content (%)	Tack	Drape	Fiber Areal Weight (g/m²)	Shelf Life (months at 0 F)	Out Time (days at 77 F)	Gel Time (min)
15 ± 5 (50 PSI/350 F)	1	-	-	-	6 (70 F)	-	-
12 ± 5 (50 PSI/250 F)	1.5	-	-	-	6	-	-
24 ± 7 (50 PSI/500 F)	2.0	-	-	-	-	-	-
18 ± 7 (50 PSI/500 F)	2.0	-	-	-	-	-	-
18 ± 6 (50 PSI/350 F)	1.0	-	-	-	6	-	15 ± 3 (350 F)
18 ± 6 (50 PSI/350 F)	1.0	-	-	-	6	-	15 ± 3 (350 F)
15 ± 6 (50 PSI/350 F)	1.0	-	-	-	6	-	15 ± 3 (350 F)
15 ± 6 (50 PSI/350 F)	1.0	-	-	-	6	-	15 ± 3 (350 F)
5 - 19 (50 PSI/275 F)	2	-	-	-	-	14	3 - 14 (275 F)
15 ± 5 (50 PSI/350 F)	2	-	-	-	6 (40 F)	14	-
15 ± 5 (100 PSI/350 F)	1.5	-	-	-	6	21	18 ± 5 (350 F)
20 ± 4 (10 MIN/100 PSI/325 F)	2	-	-	-	-	-	4 - 13 (325 F)
17 ± 5 (15 PSI/325 F)	2 (10 MIN/325 F)	MEDIUM	MEDIUM	-	-	-	4 - 10 (350 F)
.	1 (10 MIN/350 F)	-	-	-	-	-	10 - 18 (350 F)
7 (15 PSI/250 F)	2 (250 F)	-	-	-	-	-	13 (250 F)
4 - 15 (15 PSI/324 F)	1.5 (10 MIN/325 F)	-	-	-	-	-	4 - 20 (325 F)
16.2 (15 PSI/350 F)	1.1 (15 MIN/275 F)	-	-	-	-	-	10.25 (350 F)
17.5 (10 MIN/15 PSI/250 F)	0.1 (10 MIN/250 F)	-	-	-	-	-	7.66 (250 F)
9.8 (10 MIN/15 PSI/250 F)	0.9 (10 MIN/250 F)	MEDIUM	-	-	-	-	12.9 (250 F)
5 - 20 (15 PSI/275 F)	1.5 (10 MIN/275 F)	-	-	-	-	-	4 - 20 (275 F)
4 - 15 (10 PSI/275 F)	1.5 (10 MIN/275 F)	-	-	-	-	-	4 - 20 (275 F)
10 (10 MIN/15 PSI/250 F)	2 (10 MIN/250 F)	-	-	-	-	-	8 (250 F)
-	1.5	-	-	370 ± 14	12	10	3 - 7 (350 F)
-	1.5	-	-	370 ± 14	12	10	6 - 12 (350 F)
-	1.5	-	-	370 ± 14	12	10	3 - 7 (350 F)
-	1.5	-	-	370 ± 14	12	10	6 - 12 (350 F)
-	1.5	-	-	193 ± 8	12	10	3 - 7 (350 F)
-	1.5	-	-	193 ± 8	12	10	6 - 12 (350 F)
-	1.5	-	-	146	12	14	7 - 14 (250 F)
-	1	-	-	146	12	10	6 - 12 (350 F)
-	1	-	-	146	12	10	3 - 7 (350 F)
-	1.5	-	-	146	12	14	7 - 14 (250 F)
-	1.5	-	-	146	12	14	7 - 14 (250 F)
-	1	-	-	164	12	10	12 - 32 (350 F)
-	1	-	-	150	12	10	6 - 12 (350 F)
-	1	-	-	150	12	10	6 - 12 (350 F)
-	1	-	-	150	12	10	3 - 7 (350 F)
-	1	-	-	150	12	10	3 - 7 (350 F)
-	1.5	-	-	.	12	10	6 - 12
-	1.5	-	-	75 - 200	12	7	8 - 20 (350 F)
-	1.5	-	-	355 - 385	12	7	8 - 20 (350 F)
-	1.0	-	-	150	12	14	2.5 (350 F)
-	1	-	-	150	12	17	19 (350 F)
-	1.5	-	-	145	12	14	5 - 12 (250 F)
-	1	-	-	150	12	10	3 - 7 (350 F)
-	1	-	-	146	12	10	6 - 12 (350 F)
-	1	-	-	150	12	10	6 - 12 (350 F)
-	1.5	-	-	185 ± 8	12	10	3 - 7 (350 F)
-	1.5	-	-	185 ± 8	12	10	6 - 12 (350 F)
-	1.5	-	-	185 ± 8	12	10	12 - 32 (350 F)
-	1.5	-	-	370 ± 14	12	10	12 - 32 (350 F)
-	1.5	-	-	370 ± 14	12	10	12 - 32 (350 F)
-	1.5	-	-	193 ± 8	12	10	12 - 32 (350 F)
-	1.5	-	-	280 ± 10	12	10	3 - 7 (350 F)
-	1.5	-	-	280 ± 10	12	10	6 - 12 (350 F)
-	1.5	-	-	280 ± 10	2	10	12 - 32 (350 F)
22 ± 4 (100 PSI/350 F)	2	GOOD	-	-	-	-	1 - 6 (350 F)
22 ± 4 (100 PSI/250 F)	2	GOOD	-	-	-	-	4 - 10 (250 F)
20 ± 4 (100 PSI/350 F)	2	GOOD	GOOD	-	-	-	1 - 6 (350 F)
10 ± 4 (15 PSI/350 F)	2	GOOD	GOOD	-	-	-	6 - 10 (350 F)
17 ± 4 (50 PSI/350 F)	2	GOOD	GOOD	-	-	-	6 - 10 (350 F)
5 - 15 (50 PSI/350 F)	1 - 4 (350 F)	-	-	190	-	-	-
5 - 15 (50 PSI/350 F)	1 - 4 (350 F)	-	-	145	-	-	-
5 - 15 (50 PSI/350 F)	1 - 4 (350 F)	-	-	145	-	-	-
5 - 15 (50 PSI/350 F)	1 - 4 (350 F)	-	-	190	-	-	-
5 - 15 (50 PSI/350 F)	1 - 4 (350 F)	-	-	145	-	-	-
5 - 15 (50 PSI/350 F)	1 - 4 (350 F)	-	-	145	-	-	-
-	0.5	-	-	-	12	90	-
-	2.0	-	-	145	-	-	-
-	-	-	-	193	-	-	-

32 PLIES QUASI-ISOTROPIC
AS4/3501-6

5.00

12.00

5.00

ARMALON FILM
CENTER IN RADIUS

NOTE: ALL DIMENSIONS
IN INCHES

(a)

(b)

Figure 3-73. Gr/Ep Composite Stringer
(a) Schematic Diagram
(b) Photograph of As-Fabricated Part
Note: Labels 1 through 6 indicate strain gages; 2, 4, 6
are on face shown; 1, 3, 5 are on rear side.

3-132

(a)

(b)

Figure 3-74. Failure Testing of Gr/Ep Composite Stringer
(a) Schematic of Test Configuration
(b) Photograph of Part Being Tested

3-133

Table 3-21. Interlaminar Tensile Test Data on L-Shaped Stringer

Load	Strain Gage 1	Strain Gage 2	Strain Gage 3	Strain Gage 4	Strain Gage 5	Strain Gage 6
lbs.	u-in/in	u-in/in	u-in/in	u-in/in	u/in/in	u-in/in
4	-11	+8	0	-4	-4	-4
9i	-1954	+3085	-2047	+2815	-993	+990
200	-3820	+6121	-3987	+5490	-1936	+1931
262**	-4978**	–	-4893**	+6742**	-2347**	+2358**
** – Catastrophic failure values						

3.7.1.2 Honeycomb Skin Structure

Figures 3-75a and 3-75b show a schematic diagram of the Gr/Ep-Al honeycomb structure, and a photograph of the fabricated part. The specimen (6 inches x 10 inches x 0.625 inches) consisted of two AS4/3501-6 Gr/Ep skins (16-ply, quasi-isotropic 0-, 45-, and 90-degree ply orientations), that contained porosity. Porosity was introduced in the skins by loss of cure pressure during processing. The skins were then secondarily bonded to 5052 Al honeycomb using FM-300 adhesive as per Northrop Process Specification MA 133 (Reference 13).

The part was impact-tested in accordance with NASA specification RP1092 (Reference 7) to introduce impact damage in the upper-skin. Impact testing was performed using a 1-inch diameter hemispherical indentor and 60 inch-lb load. Figure 3-76 is an AUSS scan of the part showing the impact damage in the part.

The honeycomb structure was subsequently failure tested under post-impact-compression loading. Figure 3-77 shows the part being failure tested. The part failed at a maximum load of 34,800 lbs, with catastrophic fracture initiating in the impact-damaged area. Subsequent loading resulted in significant drop in the load-carrying capacity of the part, with subsequent failure of the non-impacted bottom skin, and partial crushing of the core.

3.7.2 Investigation of DOD/NASA/FAA Post-Failure Analysis Case Histories

Under an engineering services agreement between Northrop and the University of Utah, Professor Willard Bascom of the University of Utah, performed work in Task 6, Subtask 6.4. Professor Bascom made on-site visits to several DOD and NASA facilities for the purposes of obtaining failure analysis case histories for inclusion in the Handbook. The agencies and contacts are listed in Table 3-22. Professor Bascom reported that the effort aimed at composite fractography for failure analysis at these agencies was extremely small. Most of these agencies indicated interest, but only at the Naval Research Laboratory in Washington, DC, was there ongoing activity which had just started.

16 PLIES
QUASI-ISOTROPIC
AS4/3501-6 WITH
POROSITY

10.00

6.00

0.625

ALUMINUM HONEYCOMB

NOTE: ALL DIMENSIONS IN INCHES
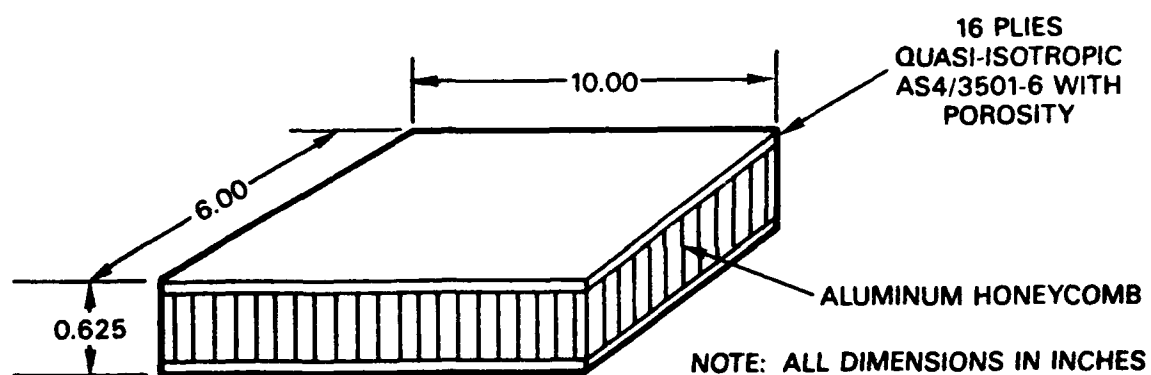
(a)
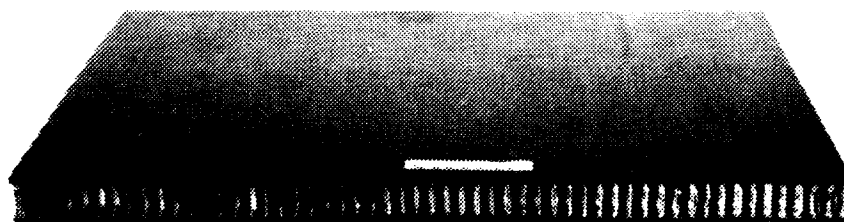
(b)

Figure 3-75.   Gr/Ep-Al Honeycomb Structure
(a) Schematic Diagram
(b) Photograph of As-Fabricated Part
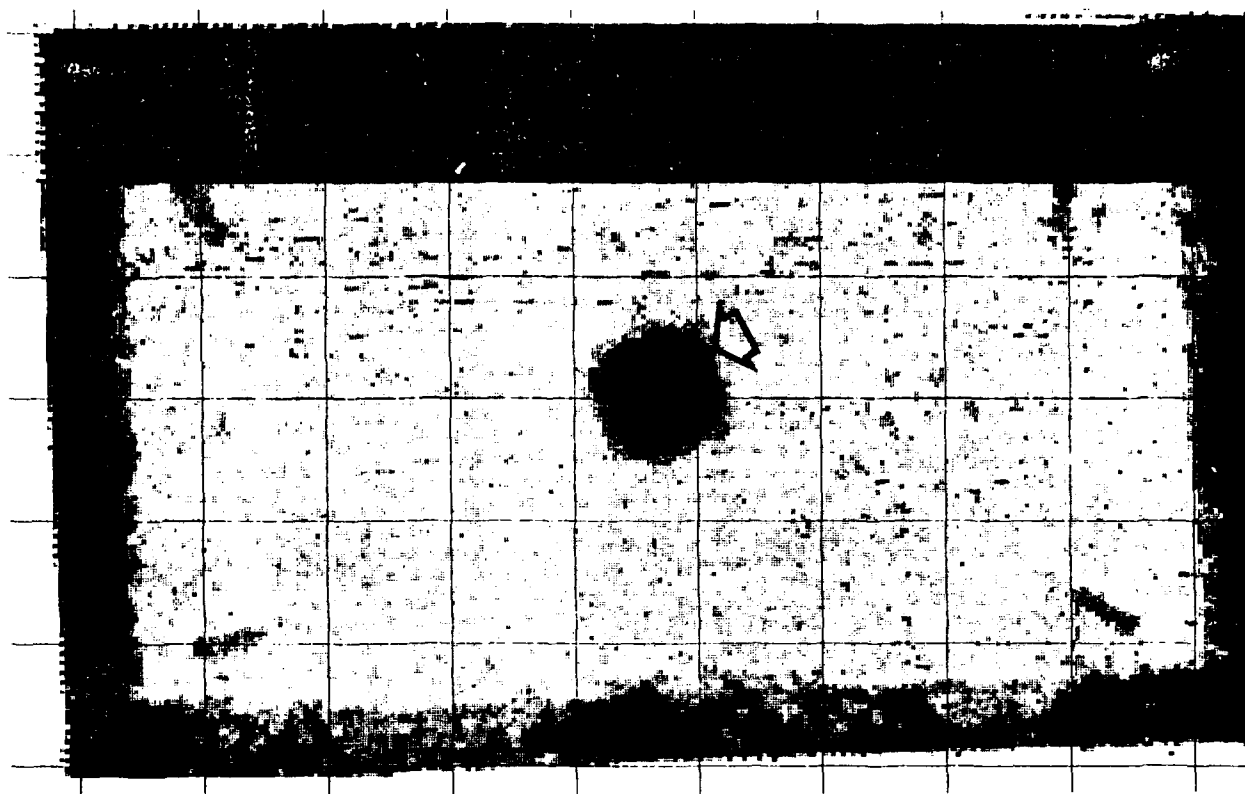
Figure 3-76.   C-Scan Showing Impact Damage (Arrow) in Skin
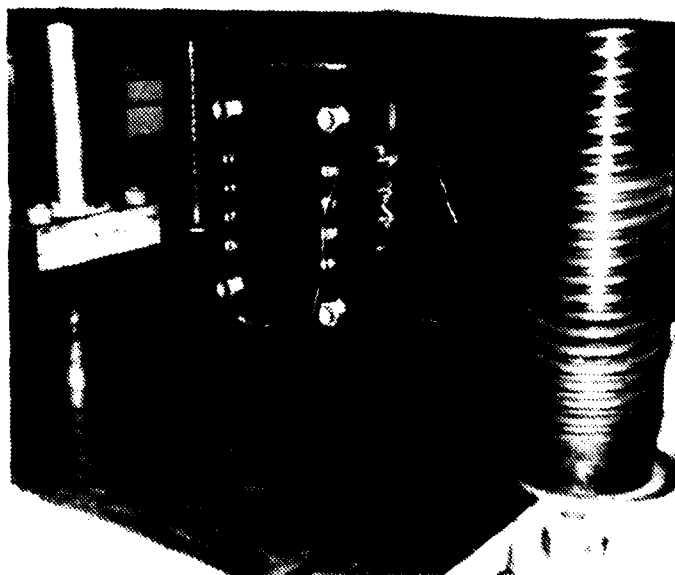
Figure 3-77.   Photograph of PIC Test on Gr/Ep-Al Honeycomb

Table 3-22. Agencies and Contacts

Agency	Contact	Phone
Hill AFB, Clearfield, UT	W. L. Peters	(801) 777-7378
Lawerence Livermore Labs, Livermore, CA	Dr. S. deTeresa	(415) 422-6466
NASA Langley Research Center Hampton, VA	Dr. C. Harris	(804) 865-3048
NADC, Warminster, PA	S. Toman	(215) 441-1235
NAD, North Island San Diego, Ca	R. Martinez	(619) 545-7812
NAD, Cherry Point, NC	R. Helms	(919) 466-7048
NAD, Jacksonville, FL	–	(904) 772-2164
Naval Research Lab, Washington, DC	D. Meyn	(202) 767-2380
Naval Ships R&D Center Annapolis, MD	Dr. T. Juska	(301) 267-3643
Naval Surface Weapons Center, Silver Spring, MD	Dr. W. Messick	(310) 394-2152

In addition to the on-site visits, a literature search was carried out at the University of Utah, as part of this subtask. Several databases including the NASA Scientific and Technical Information Facility, UPDATE and SCAN Notification, Chemical Abstract Services, CA Selects, and Fiber-Reinforced Plastics were searched for case histories. Professor Bascom reported finding a number of documents and research papers which contained fractographic data, usually in the form of SEM photographs. The results of the literature search were compiled and put into a computerized "card file" on a Macintosh computer. However, no documents were found that specifically related to composite fractography/failure analysis other than those previously reported in the USAF/Boeing study (References 3 and 4).

3.8 DOCUMENTATION

The overall objective of Task 9 was actual compilation of the Composite Failure Analysis Handbook that would be used as a reference for any composite failure analysis investigation. To compile the Handbook, Northrop used the results of Contracts F33615-86-5071 (Reference 4) and F33615-87-5212 (Reference 5) and the Compendium of Post-Failure Analysis Techniques for Composite Materials (Reference 14). Northrop supplemented information excerpted from the Compendium of Post-Failure Analysis Techniques on failure micromechanisms and stress analysis methods with additional information compiled by the University of Utah.

3.8.1 Failure Micromechanisms and Stress Analysis Methods

Professor Bascom performed work on Subtask 9.1 as part of the engineering services agreement between Northrop and the University of Utah. Professor Bascom reported that Dr. Richard Christensen of Lawrence Livermore Laboratories had developed a new failure criterion for continuous fiber composites that was a major departure from traditional analyses.

Dr. Christensen's theory was developed from an effort to extend conventional laminate theory to thick composite sections. In order to include out-of-plane stresses that are present in thick laminates, Christensen postulated a simplifying assumption, namely that the out-of-plane stresses in a laminate were independent of the orientation of the fibers. In doing so, Dr. Christensen reported that the failure criterion consisted of one in which fiber-dominated failure could be separated from matrix failure, and matrix-interface failure. Thus fiber failure and matrix failure could be treated as two separate events.

Professor Bascom submitted a summary of the criterion that he had obtained from Dr. Christensen. This summary is included in this report as Appendix A.

3.8.2 Analysis of Fractographic Results from Northrop and Boeing Programs

The objective of Task 9, Subtask 9.2 was to analyze the fractographic results obtained in the current program and the Air Force/Boeing programs. Based on this analysis the following correlations were determined.

1. Applied load was the principal parameter that affected the fracture surface characteristics in the model system, Gr/BMI, and Gr/PEEK.

2. For the systems studied, material form and processing variables (filament winding versus tape) indirectly affected the fracture characteristics, in that these may have caused localized variations in applied load, thereby altering fractographic features.

3. In fiber-dominated fracture events such as translaminar tension or compression, the type of fiber played a role in resultant fracture surface characteristics. In pitch base carbon fibers, fracture features such as DAF radials or chop marks occurred. These served as indicators of failure mode (tension, compression), and crack growth direction (DAF radials in tension failures). In organic fibers such as Kevlar 49, defibrillation of the fibers occurred, thereby resulting in loss of fracture feature information.

4. Work on Gr/BMI and Gr/PEEK indicated that the resin plays a strong role in controlling the resulting fracture surface characteristics. Fracture in AS4/5250-3 Gr/BMI could be mapped in a manner similar to baseline Gr/Ep. In Gr/PEEK, the fracture surface morphology included features not observed in baseline Gr/Ep or Gr/BMI.

5. Fractographic evaluation of bolted Gr/Ep joints indicated that varying failure modes occur in these specimens based on applied loads, specimen, and fastener geometries.

6. Evaluations of Gr/Ep and Gr/BMI bonded structures indicate that specimen geometry, lap/strap ratios, and test load play roles in controlling fracture surface characteristics. Failures under adhesive or mixed-mode conditions could be mapped through evaluation of fracture features on the fractured adherends.

7. In-plane shear failure in Gr/Ep was characterized by the occurrence of hackles on fractured resin, and tension fracture characteristics on fractured fiber ends. Processing variables did not significantly alter fracture surface characteristics for Gr/Ep tested under in-plane shear.

8. In-plane shear in Gr/Ep could be distinguished from out-of-plane shear failure in Gr/Ep through examination of fractured fiber ends. Out-of-plane shear resulted in compressive features on fiber ends, whereas in-plane shear resulted in tension fracture characteristics on fractured fiber ends.

9. Environmental variables such as moisture, temperature, or humidity did not significantly affect the fracture surface characteristics in thermoplastic or thermoset composites. The only exception was in elevated temperature failures for situations where pyrolysis of the resin occured (such as conditioning or testing above Tg). This led to loss of fracture information from the resin, thereby precluding unequivocal determination of crack-growth directions.

10. Processing variations such as fiber/prepreg variations, or post-consolidation treatments such as holes or impact, affected fracture surface characteristics only if they changed the local applied load state.

3.8.3 Organization of the Composite Failure Analysis Handbook

The objective of this subtask was actual organization of the Composite Failure Analysis Handbook from the results of the Northrop program, the Boeing program (Reference 4), and the Compendium of Post-Failure Analysis Techniques for Composite Materials (Reference 14), developed by Boeing under Contract F33615-84-C-5010 (Reference 3). Northrop has organized the Handbook so that it will be clear, concise, and easily usable as a reference by an investigator carrying out post-failure analysis of composite materials.

Northrop reviewed formats that had been used in the past for reporting metallic and composite fractography and failure analysis data. The review included evaluation of formats used internally at Northrop, those reported in ASM's Metals Handbooks (References 10 and 11), and those used by the Boeing Company under Air Force Contract F33615-84-C-5010 (Reference 3). In addition, Northrop has reviewed the formats of handbooks previously produced by Northrop for the Air Force, namely the DOD/NASA "Advanced Composites Repair Guide" (References 15 and 16) and Federal Aviation Administration Handbook "An Engineering Compendium for the Manufacture and Repair of Fiber-Reinforced Composites" (Reference 12).

Based on an assessment of exiting report schemes, and discussions with representatives from the FAA, Boeing, and the Air Force, Northrop has formulated and compiled the Handbook into three Parts. These are as follows:

- Volume II, Part 1 – Procedures and Techniques
- Volume II, Part 2 – Atlas of Fractographs
- Volume II, Part 3 – Case Histories

All these parts have been organized in a relatively open format so that data generated in future Air Force-sponsored programs can be readily integrated into the Handbook.

SECTION 4

SUMMARY AND CONCLUSIONS

The objective of this program was to develop a comprehensive Composite Failure Analysis Handbook for failure analyses of fiber-reinforced composites. The program objectives were accomplished through work performed on several technical tasks that resulted in the compilation of a reference manual that could serve as a guide.

A Field Handling Logic Network (FHLN) was prepared for on-site handling of composites during accident-investigations. Procedural guidelines were developed from inputs provided by key field personnel from several government agencies, and the results of tests performed in-house at Northrop. Several current and new fractographic techniques were evaluated to identify methods for initiation site determination and failure sequence identification in failed composite specimens.

Northrop expanded the fractographic database originally developed by the Boeing Company for AS4/3501-6 Gr/Ep under Air Force Contract F33615-84-C-5010 to include the effects of load, manufacturing, processing, and environmental variables. Also included was documentation of manufacturing and processing defects that occur in Gr/Ep.

The fractographic database was extended to other material systems including Kevlar/Epoxy, Graphite/PEEK, and Graphite/Bismaleimide. Also included was information on failure modes in adhesively bonded and mechanically joined composite structures.

Northrop compiled material properties on current and near-term composite structural materials. Literature searches were carried out on government and commercial databases for product information and properties. Properties obtained were incorporated into database files using a personal computer. The data were organized into a tabular formats for reporting in the Handbook. The properties for several classes of fiber, prepreg, and laminates were compiled and organized into the Handbook.

Verification of the composite failure analysis logic system was performed through evaluation of several failed structural items provided by the Air Force. The structural items represented "real-world" configurations and included: 1) a vertical stabilizer, 2) a horizontal torque box assembly, 3) a composite arch reinforcement, and 4) two simple components. All the results are presented as case histories in the Handbook.

Two simple Gr/Ep structures containing intentional defects were fabricated and tested to failure under controlled laboratory conditions. The failed specimens and related test documentation were shipped to the Air Force.

4-1

Northrop started organization of the Composite Failure Analysis Handbook into four major volumes. Volume I is the technical overview and is presented in this report. Volume II, which comprises the actual Handbook, is further divided into three parts. Part 1 describes the techniques and procedures for performing composite failure analysis. Part 2 represents an atlas of fractographs. Part 3 is a compilation of case histories of investigations performed by Northrop, Boeing, General Electric, and other contributors.

In summary, Northrop has achieved the Air Force objective of producing a Handbook containing all the techniques, procedures, sample data, and reference supporting data for performing post-failure analysis of fiber-reinforced composite structures.

Based on the work performed, the following conclusions were arrived at:

1. Applied load is the principal parameter that affects the fracture surface characteristics in the model system Gr/Ep, as well as other materials, such as K/Ep, Gr/BMI, and Gr/PEEK.

2. In Gr/Ep, Mode I tension interlaminar fracture is characterized by river patterns on the fracture surfaces that are oriented at an angle or parallel to the direction of macroscopic fracture. The river patterns can be used to determine local fracture origins since these would be oriented away from the initiation site, and toward propagating fracture.

3. For pure Mode II shear interlaminar fracture, the characteristic fracture features consist of hackles and scallops that are of different shapes and sizes. These may be oriented toward and away from the local fracture initiation site(s), and therefore, cannot be used to predict initiation site(s) or crack-propagation directions in Mode II shear interlaminar fracture failures.

4. Mixed-mode interlaminar failures are characterized by mixtures of hackles or scallops and river patterns that are generally interspersed between the hackles. The river patterns can again be used to map local fracture origins and direction as for pure Mode I tension.

5. Evaluation of the translaminar fracture results indicate that variations in resin content do not affect fracture characteristics in Mode I tension or Mode I compression failures. Translaminar tension failures can be mapped by the DAF radials on fiber ends, or river patterns on fractured epoxy. In compression failures, there are no indicators of crack-origin or crack-propagation direction in the compression regions; however, these can be determined in tensile failure regions that also form during Mode I compression testing.

6. In-plane shear failure in Gr/Ep is characterized by the occurrence of hackles on fractured resin and tension fracture characteristics on fractured fiber ends. Processing variables do not significantly alter fracture surface characteristics for Gr/Ep tested under in-plane shear.

7. In-plane shear in Gr/Ep can be distinguished from out-of-plane shear failure in Gr/Ep through examination of fractured fiber ends. Out-of-plane shear results in

compressive features on fiber ends, whereas in-plane shear results in tension fracture characteristics on fractured fiber ends.

8. For the systems studied, material form and processing variables (filament winding versus tape) indirectly affect the fracture characteristics in that these may cause localized variations in applied load, thereby altering fractographic features.

9. In fiber-dominated fracture events such as translaminar tension or compression, the type of fiber plays a role in resultant fracture surface characteristics. In pitch base carbon fibers, fracture features such as DAF radials or chop marks occur. These serve as indicators of failure mode (tension, compression), and crack growth direction (DAF radials in tension failures). In organic fibers such as Kevlar 49, defibrillation of the fibers occur, thereby resulting in loss of fracture feature information.

10. Work on Gr/BMI and Gr/PEEK indicates that the resin plays a strong role in controlling the resulting fracture surface characteristics. Fracture in AS4/5250-3 Gr/BMI can be mapped in a manner similar to baseline Gr/Ep. In Gr/PEEK, the fracture surface morphology includes features not observed in baseline Gr/Ep or Gr/BMI.

11. Fractographic evaluation of bolted Gr/Ep joints indicates that varying failure modes occur in these specimens based on applied loads, specimen, and fastener geometries.

12. Evaluation of Gr/Ep and Gr/BMI bonded structures indicates that specimen geometry, lap/strap ratios, and test load play roles in controlling fracture surface characteristics. Fractures can be mapped in under adhesive- or mixed-mode conditions through evaluation of fracture features on the fractured adherends. Crack-direction cannot be easily mapped in pure cohesive joint failures.

13. Environmental variables such as moisture, temperature, or humidity do not significantly affect the fracture surface characteristics in thermoplastic or thermoset composites. The only exception is in elevated temperature failures for situations where pyrolysis of the resin occurs (such as conditioning or testing above Tg). This leads to loss of fracture information from the resin, thereby precluding unequivocal determination of crack-growth directions.

14. Processing variations such as fiber/prepreg variations, or post-consolidation treatments such as holes or impact affect fracture surface characteristics only if these change the local applied load state.

SECTION 5

REFERENCES

1. "Bolted Joints in Composite Structures: Design, Analysis and Verification," Northrop Corporation, Aircraft Division, Air Force Contract F33615-82-C-3217.

2. "Damage Tolerance of Composites," Air Force/Boeing/Northrop Contract No. F33615-82-C-3213.

3. "Failure Analysis for Composite Structure Materials," the Boeing Company, Boeing Military Airplane Division, Air Force Contract F33615-84-C-5010.

4. "Composite Failure Analysis Handbook," the Boeing Company, Boeing Military Airplane Division, Air Force Contract F33615-86-C-5071.

5. "Composite Failure Analysis Handbook," Northrop Corporation, Aircraft Division, Air Force Contract F33615-87-C-5212.

6. Altman, J., et al., "Advanced Composite Serviceability Program," AFWAL TR-80-4092, July 1980.

7. Griffing, C. F., et al., "Standard Tests for Toughened Resin Composites," NASA Reference Publication 1092, 1982, pp. 1-5.

8. Purslow , D., "Some Fundamental Aspects of Composites Fractography," Composites, Volume 12, October 1981.

9. "Test Methods – Graphite/Epoxy Materials and Assemblies," Northrop Process Specification IT-58, November 1978, pp. 1-71.

10. "Fractography and Atlas of Fractographs," Metals Handbook, Volume 5, Eighth Edition, Howard Boyer, Editor; American Society for Metals, Metals Park, Ohio, 1974.

11. "Failure Analysis and Prevention," Metals Handbook, Volume 10, Eighth Edition, Howard Boyer, Editor; American Society for Metals, Metals Park, Ohio, 1975.

12. Ramkumar, R. L., et al., "Handbook: An Engineering Compendium for the Manufacture and Repair of Fiber-Reinforced Composites," Final Technical Report, Contract No. ГTFA03-83-C-0087.

13. "Fabrication of Graphite/Epoxy Laminate Details and Assemblies," Northrop Process Specification MA133, August 1981, pp. 1-17.

14. Grove, R. and Smith, B., "Compendium of Post-Failure Analysis Techniques for Composite Materials," AFWAL TR-86-4137, January 1987.

15. "Advanced Composite Repair Guide," <u>Northrop Report Number NOR 82-60</u>, Air Force Contract F33615-79-C-3217, March, 1982.

16. "General Advanced Composite Repair Processes Manual," <u>USAF TO 1-1-690</u>, August, 1990.

A NEW FAILURE CRITERION

Recently, Christensen (1) has published a failure criterion for continuous fiber composites that is a major departure from the traditional analyses of Hill (2), Tsai and Wu(3) and Hashin (4). This theory developed from an effort to extend conventional laminate theory to thick composite sections. In thick laminate sections, out-of-plane stresses must be considered where as they are usually ignored in thin laminates treated using conventional laminate theory. In order to include out of plane stresses, Christensen postulated certain simplifying assumptions. In doing so, the results led to a failure criteria that separates fiber dominated failure from matrix or fiber-matrix interphase failure. "This new criterion is intended to provide a balance between having a minimum number of parameters to be evaluated from simple experiments while still encompassing the actual physical characteristics of the failure process." (1). In any failure criterion it is necessary to differentiate between fiber and matrix and in general this is accomplished by using separate criteria for these two separate failure events.

A three-dimensional lamination theory was developed in which the usual plane stress assumption of two-dimensional lamination theory is disallowed. Thus, for an individual lamina, the macroscopic properties are those of a *transversely isotropic* *media so that,

$$\sigma_i = C_{ij}\,\varepsilon_j \qquad\qquad [1]$$

where;

$$|C_{ij}| = \begin{bmatrix} C_{11} & C_{12} & C_{12} & 0 & 0 & 0 \\ & C_{22} & C_{23} & 0 & 0 & 0 \\ & & C_{22} & 0 & 0 & 0 \\ & & & \dfrac{C_{22} - C_{23}}{2} & 0 & 0 \\ & & & & C_{66} & 0 \\ & & & & & C_{66} \end{bmatrix} \qquad [2]$$

---

* italics are editorial

There are five independent properties in Eq. 2 which can be related to engineering properties by,

$$C_{11} = E_{11} + 4 v^2{}_{12}K_{23}$$

$$C_{12} = 2K_{23}v_{12}$$

$$C_{22} = \mu_{23} + K_{23}$$

[3]

$$C_{23} = -\mu_{23} + K_{23}$$

$$C_{66} = \mu_{12}$$

where E_{11} is the axial modulus, v_{12} the axial Poisson's ration, μ_{12} the axial shear modulus, μ_{23} the transverse shear modulus and K_{23} the plane strain bulk modulus. The latter can be replaced by the more amenable transverse modulus, E_{22} through.

$$K_{23} = \frac{E_{22}}{4\left(1 - \frac{v^2{}_{12}E_{22}}{E_{11}}\right) - \frac{E_{22}}{\mu_{23}}}$$

[4]

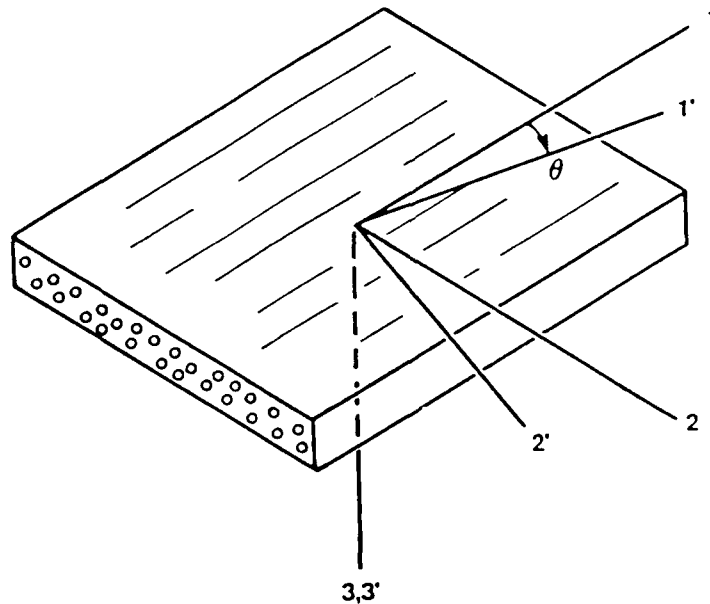Consider a coordinate transformation** as shown in Fig. 1,

Figure A-1. Coordinate Rotation

** note that the coordinate transfromation does not involve the out of plane direction, e.g. 3 = 3'

A-2

so that,

$$[C'_{ij}] = \begin{bmatrix} C'_{11} & C'_{12} & C'_{13} & 0 & 0 & C'_{16} \\ C'_{12} & C'_{12} & C'_{13} & 0 & 0 & C'_{26} \\ C'_{13} & C'_{23} & C'_{33} & 0 & 0 & C'_{36} \\ 0 & 0 & 0 & C'_{44} & C'_{45} & 0 \\ 0 & 0 & 0 & C'_{45} & C'_{55} & 0 \\ C'_{16} & C'_{26} & C'_{36} & 0 & 0 & C'_{44} \end{bmatrix} \qquad [5]$$

Christensen then presents the transformation equations for a rotation in the 1-2 plane, i.e.,

$$C_{11}' = m^4 C_{11'} + 2m^2n^2 (C_{12} + 2C_{66}) = n^4 C_{22}$$

etc

etc

..

..

$$\qquad [6]$$

$$C'_{44} = m^2\left(\frac{C_{11} - C_{23}}{2} + n^2 C_{66}\right)$$

where $m = \cos\theta$ and $n = \cos\theta$

The out of plane terms are bracketed in Eq. (5). The seven coefficients give rise to interlaminar stresses which act between lamina when given a uniform strain. They are functions of the fiber orientation and could be treated as variables from one lamina to the next. This approach would be very formidable. Christensen seeks a simpler solution by identifying any special case in which the out-of plane stresses are *independent of the fiber orientation*. In doing so he sets two restrictions. First,

$$\frac{C_{22} - C_{23}}{2} = C_{66} \qquad [7]$$

The seven out of plane coefficients then become,

$$C'_{13} = m^2 C_{12} + n^2 C_{23}$$

$$C'_{23} = n^2 C_{12} + m^2 C_{23}$$

$$C'_{33} = C_{22} \qquad [8]$$

$$C'_{44} = C'_{55} = C'_{66}$$

$$C'_{45} = 0$$

$$C'_{36} = mn(C_{23} - C_{12})$$

By applying a second restriction,

$$C_{12} = C_{23} \qquad [8]$$

then,

$$C'_{13} = C_{12}$$

$$C'_{23} = C_{12}$$

$$C'_{33} = C_{22} \qquad [9]$$

$$C'_{44} = C'_{55} = C_{66}$$

$$C'_{45} = 0$$

$$C'_{36} = 0$$

Now the out of plane terms in Eq.. 2 are completely independent of fiber orientation in the lamina. Moreover, the same out of plane terms apply for the laminate Eq.5 as for the lamina.

The physical significance of the restrictions imply that,

$$\mu_{12} = \mu_{23} \qquad\qquad [10]$$

i.e. the axial and transverse shear moduli are taken (*assumed*) to be equal. For the second restriction,

$$\nu_{13} = \frac{\nu_{12}\left(1 - \frac{\nu_{12}E_{22}}{E_{11}}\right)}{1 - \nu_{12}} \qquad\qquad [11]$$

Since $E_{11} \gg \nu_{12}E_{22}$, then ν_{13} and ν_{12} take on realistic values, e.g., 0.25 to 0.33.

Christensen gives various examples using published data on epoxy/carbon fiber, aramid/epoxy, glass/epoxy and boron /epoxy data to show that restriction (7) gives reasonable predictions of the measured shear modulus, μ_{12}.

The tensor transformations obtained in this theory are compared to the tensor transformation for an isotropic material with the result that,

$$\sigma_{ij} = \lambda\varepsilon_{kk}\delta_{ij} + 2\mu\varepsilon_{ij} + (E_{11} - E)\delta_{1i}\,\delta_{1j}\varepsilon_{11} \qquad\qquad [12]$$

where

$$\lambda = \frac{\nu_{12}(1 - \nu_{12})E_{22}}{(1 - 2\nu_{12})\left(1 - \nu^2_{12}\frac{E_{22}}{E_{11}}\right)} \qquad\qquad [13]$$

$$\lambda = \frac{2\nu_{12}}{1 - 2\nu_{12}}\mu_{12} \qquad\qquad [14]$$

$$\mu = \frac{(1 - \nu_{12})E_{22}}{2\left(1 - \nu^2_{12}\frac{E_{22}}{E_{11}}\right)} \qquad [15]$$

$$\mu = \mu_{12} \qquad [16]$$

$$E = \frac{(1 - \nu^2_{12})E_{22}}{1 - \frac{\nu^2_{12} \, E_{22}}{E_{11}}} \qquad [17]$$

$$E = 2(1 + \nu_{12})\mu_{12} \qquad [18]$$

and δ_{ij} is the Kronecker Delta.

In effect, Eq. 12 states that the fiber reinforced medium is effectively isotropic except for the presence of the $(E_{11} - E)$ term. Note that all terms in [12] can be obtained from the measurable properties, E_{11}, E_{22} (or μ_{12}) and ν_{12}.

Viewed as a failure criterion, Eq. 12 uncouples fiber failure from fiber/matrix interaction failure. The first terms, λ and μ, are matrix/ interphase dominated whereas the third (RHS) term is dominated by the fiber properties. The fiber/matrix interaction includes the complicated effects of the interface or more generally the fiber/matrix interphase boundary.

Christensen and Swanson (5) applied Eq.12 to the experimental multiaxial failure data obtained by Swanson (6) using bottle and cylindrical specimens .

REFERENCES

1, Christensen, R. M., "Tensor Transformations and Failure Criteria for the Analysis of Fiber Composite Materials," J. Comp. Mat., 22, 874 1989

2. Hill, R. The Mathematical Theory of Plasticity, Oxford Univ. Press, Oxford, 1960

3. Tsai, S. W., Wu, E. M., "A General Theory of Strength for Anisotropic Materials,", J. Comp. Mat., 5 58 1971

4. Hashin, Z. and Rosen, B. W.j, "The Elastic Moduli of Fiber-Reinforced Materials," J. Appl. Mechanics, 47 329 (1980)

5. Christensen, R.M. and Swanson, S.R., "Evaluation of a New Failure Criterion for Fibrous Composite Materials," Proc. Appl. Mech. and Eng. Sci. Conf, 1988

6. Swanson, S.R. and Nelson, M., "Failure Properties of Carbon/Epoxy Laminates Under Tension-Compression Biaxial Stress," Proc. 3rd Japan-US Conf. on Composite Materials, Tokyo, 1986, p279